Modelisation des maisons à ossature en bois et remplissage en terre

Hussein Ali Hussein Al-Gusab

Communauté
UNIVERSITÉ Grenoble Alpes

THÈSE

Pour obtenir le grade de

DOCTEUR DE LA COMMUNAUTE UNIVERSITE GRENOBLE ALPES

Spécialité : **Materials, Mechanics, Civil Engineering, Electrochemistry**

Arrêté ministériel : 7 Novembre 2013

Présentée par

« Hussein Ali Hussein Al-Gusab »

Thèse dirigée par **Laurent Daudeville**, et
codirigée par **Stéphane Grange** et **Yannick Sieffert**

préparée au sein du **Laboratoire Sols, Solides, Structures, Risques 3SR.**
dans **l'École Doctorale Ingénierie – Matériaux, Mécanique, Environnement, Energétique, Procédés, Production (IMEP-2)**

Modélisation des maisons à ossature en bois et remplissage en terre.

Modeling of timber houses structures with infilling of soil.

Thèse soutenue publiquement le **« 20 Avril 2018**,**»**,
devant le jury composé de :

M. Abdelhamid Bouchaïr
Professeur à l'université de Clermont Auvergne, Président.
M. Luc Davenne
Professeur à l'université de Paris Nanterre, Rapporteur.
M. Frédéric Dubois
Professeur à l'université de Limoges, Rapporteur.
M. Edwin Nagy
PhD. Lec. à l'université de Maine (USA), Membre.
M. Yannick Sieffert
Maître de conférences à l'université Grenoble Alpes, co-directeur de thèse.
M. Stéphane Grange
Professeur à l'INSA de Lyon, co-directeur de thèse.
M. Laurent Daudeville
Professeur à l'université Grenoble Alpes, Directeur de thèse.

ABSTRACT

A simplified finite element model was proposed for the analysis of timber-framed structures with infilling of rocks and clay morter by using hysteretic constitutive models for joints and structural elements. Three different scales were defined for the identification and validation of hysteretic models: connection, shear wall and full scale building ; comparisons of numerical and test results were performed at each scale. The calibrated model allowed assessing the earthquake-resistant performance of a traditional Haitian one-storey house and could be used for the design of a two-storey house.

RÉSUMÉ

Un modèle simplifié aux éléments finis a été proposé pour l'analyse des structures à ossature bois avec remplissage en pierres et mortier de terre en utilisant des modèles de comportement hystérétique pour les assemblages et certains éléments structuraux. Trois échelles différentes ont été définies pour l'identification et la validation des modèles hystérétiques: celle de l'assemblage, celle du mur de cisaillement et enfin celle de la structure complète en vraie grandeur. Le modèle calibré a été utilisé pour vérifier la correcte résistance aux séismes d'une maison traditionnelle Haïtienne à un étage ainsi que pour concevoir un exemple de bâtiment à deux étages utilisant les mêmes dispositifs constructifs.

DECLARATION

To my parents the origin and my wife the present and to my children, my future.
To my My old professors the origin.
To my friends the supporters.

ACKNOWLEDGEMENTS

I would like to thank my professors Laurent Daudeville for confidence, Yannick Sieffert for giving advice, Stéphane Grange for fruitful information given to me, thank you very much Sirs, I was lucky and proud to be your student and I will never forget all the pleasant moments spent with you. I also want to thank my friend Florent Vieux-Champagne for all the time that he has spent with me with extremely gentlemanner and for providing the experimental results. Also, of course, i cannot forget my wife and apologize for the very bad situations that she spends with me especially in the beginning and in the last, thank you my better assistant. Despite the absence for four years, i would like to thank the persons which are the reason to be me thank you for every tear of transpiration. Also, i would like to thank all my friends in France as well as in Iraq which they support me all the period that i am in France. Also thanks to all persons which support me in Ministry of higher education in Iraq, and Campus France in France.

ABBREVIATIONS

ACC ..... Acceleration measurment.

ADRS ..... Acceleration displacement response spectrum.

ANR ..... Agence Nationale de la Recherche (French National Research Agency).

ATC ..... Applied Technology Council.

A_m^* ..... Area under V-D curve for pushover calculation.

A_{inf} ..... Area of the masonry infills.

A_{diag} ..... Area of the diagonal timber member.

a ..... acceleration(s) of one or multi degrees of freedom.

ave. ..... Average or mean value.

B(β) ..... Reduction factor for demande cure in pushover analysis.

BWBN ..... Bouc-Wen-Barer-Noori hysteresis model.

C ..... Damping(s) of one or multi degrees of freedom.

CAD ..... Computer aided design.

C_t ..... Contant parameter to find approximate time period of structures.

CLT ..... Cross Laminated Timber.

CHJ ..... Crossing Half Lap Joint.

CMIF ..... Complex Mode Indicating Function.

CSM ..... Capteur à Fil (french terms means wire senser).

CSIRO ..... Commonwealth Scientific and Industrial Research Organisation.

CEN ..... European Committee for Standardisation.

DDDB ..... Direct Displacement Design Based.

DIC ..... Digital Image Correlation.

DVA ..... Displacement, Velocity, Acceleration.

DOF. ..... Degrees of freedom.

DWDS ..... Draw Wire Displacement Sensor

d ..... Displacement.

d_n ..... Top horizontal displacement.

d_s ..... Spectral displacements.

d^*_{et} ..... Target displacement in push over analysis.

d^* ..... Displacement of equivalent SDOF.

d^*_t ..... Displacement of intersection of capacity and demand curves.

d^*_y ..... Yield displacement of equivalent SDOF.

d^*_m ..... Maximum displacement of elasto plastic SDOF system.

d_d ..... Reduced displacement from the spectrum.

EEEP ..... Equivalent Energy of Elasto-Plastic model.

ESTF ..... Equivalent Source Time Functions.

ENV ..... Envelope of cyclic tests.

Eq. ..... Equation.

EVD ..... Equivalent Viscous damping.

EVDR ..... Equivalent Viscous damping ratio.

EGF ..... Empirical Green's Functions.

EMA ..... Experimental Modal Analysis.

E_d ..... Dissipated Energy nonlinear hysteresis loop.

E_p ..... Dissipated Energy of the linear elastic system.

EPP. ..... Elastic perfectly plastic idealized.

EN ..... Euro code.

$EN1998-1$ ... (Eurocode 8) Design of structures for earthquake resistance.

E_E ..... Quadratic combination variable (u, v, a etc.).

E_i ..... Field variable of i^{th} mode.

e.g. ..... Latin term for the sake of an example.

etc. ..... Et cetera (and the rest) Latin term.

FCBA ..... Français Centre de Bois Ameublement or french center of timber building.

FEMA ..... Federal Emergency Management Agency.

Fig. ..... Figure.

F^* ..... Force of equivalent SDOF.

F_y^* ..... Yield force of equivalent SDOF.

F_b ..... Shear force at the base of buiding.

F_i ..... Shear force at level i.

FRF ..... Frequency response function.

$\bar{F_i}$ ..... Normalised shear force.

$\bar{F_n}$ ..... Shear force at each mass for normalized displacements.

GFRP ..... Glass Fibre-Reinforced Polymer.

H ..... Height of the building.

HDC ..... High ductility class.

HL ..... Horizontal Load.

$HHT-\alpha$ ..... Numerical solution method for eq. of motion.

Hz ..... Hertz the unit of cyclic frequency.

ITW ..... Infill timber wall.

i.e. ..... That is to say (used to add explanatory information or to state something in different words).

K ..... Stiffness(s) of one or multi degrees of freedom.

$\hat{K}$ ..... Compacted Global Stiffness vector.

kg ..... kilo grames (mass unit).

LVDT ..... Linear Variable Differential Transformer.

l_{ef} ..... Effective length dimension for calculating compression parallel to grain.

LDC ..... Limited ductility class.

LJ ..... Lap Joint.

M ..... Mass(s) of one or multi degrees of freedom.

MDOF ..... Multi degrees of freedom.

MDC ..... Medium ductility class.

$M\&T$ ..... Mortise and Tenon Joint.

m ..... meter length unit.

m_i ..... mass at level (i) of multi storey building.

m_* ..... Mass of equivalent SDOF.

$\frac{m}{s^2}$ ..... Meter pes square seconds unit of acceleration.

N ..... Newtons the force unit.

NSP ..... Nonlinear static procedure of pushover analysis.

$n_{eq}DOF$ ..... Indication for max rank of MDOF. system.

n ..... number of degrees of freedom.

OSB ..... Oriented strad board.

$p(t)$ ..... force vector in terms of time.

PGA ..... Peak ground acceleration.

$\hat{P}_{n+1}$ ..... Compacted Global Force vector.

QUA4 ..... FE. ANSYS element quadratic with 4 nodes.

q ..... Behaviour factor.

q_d ..... Coefficient of displacement behaviour.

q_u ..... Reduction factor due to ductility.

RTW ..... Reinforced timber wall.

RMS ..... Root mean square.

S_a ..... Pseudo acceleration.

S_d ..... Pseudo displacement.

S_e ..... Elastic spectral response.

s_i ..... Displacement at mass of level (i).

S_e ..... Elastic response spectrum.

ϕ_i ..... Normal modes displacements.S-N

S-N ..... South North direction.

sec ..... Seconds (time unit).

SDOF ..... Single degree of freedom.

T ..... Period.

T_B ..... Minimum period of constant acceleration part in spectrum curve.

T_c ..... period of the end of the flat horizontal line of spectrum curve.

$T_{n_{eq}}$ ..... The period of the highest rank (Nyquest period).

T_1 ..... Approximate time period of building.

T_i ..... Period of $i^{th.}$ mode.

T_j ..... Period of $j^{th.}$ mode.

T^* ..... Period of equivalent SDOF.

t ..... Time.

t_n ..... Temporal instantenous time (at $time = n$).

t_{n+1} ..... Temporal next time (at $time = n + 1$).

UTW ..... Unreinforced timber wall.

u ..... Displacement(s) of one or multi degrees of freedom.

$\ddot{u}$ ..... Acceleration(s) of one or multi degrees of freedom.

$\dot{u}$ ..... Velosity(s) of one or multi degrees of freedom.

v ..... Velosity(s) of one or multi degrees of freedom.

$+ve.$ ..... Positive value.

$-ve.$ ..... Negative value.

V ..... Shear force.

vs. ..... versus (relation between variables).

W-E ..... West East direction.

w.r.t. ..... with respect to.

z_i ..... Heights of the masses.

α ..... Parameter used in the $HHT - \alpha$ integration method.

β ..... Parameter used in the Newmark's integration method.

β_{eff} ..... Effective damping ratio.

γ ..... Parameter used in the Newmark's integration method.

Γ ..... Coeffient of transformation (used in push over method).

γ_{diag} ..... Density of the diagonal timber member.

γ' ..... Equivalent density of the diagonal timber member.

γ_{inf} ..... Density of the masonry infills.

Δt ..... Time step (difference between each successive time records).

ξ ..... Viscous damping ratio.

Δmax ..... Displacement at the peak force of displacement-force curve.

$\Delta failure$ ..... Maximum displacement of displacement-force curve (at failure).

Δy ..... Displacement at yield.

Γ ..... Conversion factor for idelized SDOF system (modal participation factor).

Δt_{cr} ..... time step required for stability of Newmark's method.

η ..... Damping correction factor.

$\tau(t)$ ..... Numerical accuracy function.

$\mathcal{O}$ ..... Indication of order error of numerical problems.

θ ..... Numerical integration method parameter.

λ ..... Correction factor to calculate natural period.

CONTENTS

LIST OF FIGURES

LIST OF TABLES

1. INTRODUCTION

Many countries around the world have some old-style traditional buildings, especially in their rural areas, which are made from simple, locally available and low-cost materials, for example, England, Turkey, Germany, France, Pakistan, Haiti, Portugal, etc. In our case, a basic timber frames filled with pieces of rocks with clay morter are studied, which are cheaper and the most widely available materials in poorer countries like Haiti, Pakistan, India, as well as in rural villages in the developed countries, and also have the benefit that using mud with mortar increases the energy dissipation. After some catastrophic earthquakes around the world many peoples were died and lost many infrastructures, but some of the interesting engineering remarques were obtained, that is the much modern building made by masonry or bad detailed concrete structures were collapsed. On the other hand, some of the traditional old style buildings survived in some countries that suffered from these strong motions, for example, Pakistan, Portugal, and Turkey, Haiti, etc.

As compared to buildings which are made of reinforced concrete with poor reinforcement detailing or masonry buildings, traditional timber buildings show a good performance in terms of earthquake resistance, this observation was remarked after many catastrophic earthquake events. For example it can be seen this performance and the comparison of the damage after the 1999 *Düzce* earthquake in Turkey [48] as shown in the figure (1.1) which shows the level of damage in the reinforced concrete building as compared to that which is construct from traditional style.

Fig. 1.1: Two adjacents buildings concrete and traditional timber in Turkey, [48]

So some experemental programs recently made to investigate the main characteristics of these types of construction so as to implemented in the national building codes especially for the poor countries which most of the people could not be using the expensive modern buildings. To study the main characteristics and the advantages of these types of structures, a quasi-static as well as dynamic shaking tests were performed in the university of Grenoble Alpes in 3-SR laboratory as a part of big program to help Haiti's peoples to reconstruction their houses after the earthquake of January 12, 2010 in this country.

1.1 Navigation in the manuscript

In this thesis, the structural behaviour of the timber frames with braces and infilling of clay and rocks were studied and a numerical model was proposed as a result of experimental tests of three different scales.

- In the second chapter an overview to the modern and traditional timber-framed structures and some types of traditional buildings around the world and reviewing the experimental and numerical recent studies and illustrates some numerical methods of analyzing the traditional timber frame structures as well as modern timber structures for different scale elements.

- In chapter three some approximate and accurate calculation techniques of structural analysis for the buildings subjected to the seismic loading by static and dynamic solution approaches and the modelling of the different structural elements of these structures, some of the hysteretic models were presented and a detailed describtion fot Hysteretic constitutive model.
- In chapter four, some of the experemental results of four scales are presented as connections, elementary unit cell wall, full shear wall scale, and 3D-building full scale that which are tested in (3SR) laboratory in the University of Grenoble Alpes.
- In chapter five, the multiscale nonlinear analysis method was used to analyse the proposed architectural sample of Kay wall and the enhancement configuration of adding two diagonal braces for reconstruction of Haiti after the (10 January 2010 earthquake). It contains the using of Humber's hysteresis law to model the connection scale and the unit panel to be used in the analysis and validated the experimental results of monotonic and cyclic static analysis of the shear wall scale.
- Chapter six introduce the dynamic analysis of the full-scale house by using the connections and unit cell panel elements and compared the numerical results with the shaking table tests. The model also implemented into two storey building, many structural parameters are studied and compared the available data of shaking table test results.
- In chapter seven, the conclusions of the results will be states and recommendations for the future work for the traditional structures of timber frame structures.

1.2 Aim of study

There are many modern techniques for the seismic resistance buildings which is normally suitable for the rich countries but there is a lack in the information of the seismic resistance of the traditional buildings which are suitable for the poorer countries that shows good performance against earthquakes.
This thesis is the first numerical study for a proposed enhancing technical rules for Kay-wall that is used in Haiti which aims to use the experimental data that is obtained by the project of the ANR-Agence Nationale de la Recherche (French National Research Agency) Vieux-Champagne et al. [140] and suggests a suitable numerical FE model to simulate these test results (quasi-static, cyclic test with selected load protocol, multi-scale experimental data, and full-scale shaking table for typical house model) and carries out a comparative study to collect more

information on traditional masonry timber-framed structures in an attempt to assess the behaviour of these types of structures under seismic loadings.

2. LITERATURE REVIEW

2.1 Introduction

Timber-framed structures are widely used in many countries around the world due to their properties of high strength with low mass, which is an economic attraction in static as well as dynamic analysis. The use of wood materials depends on the availability of the material and construction experience, or the need of structure that can withstand sources of loads or disasters like earthquakes, strong wind, etc. As we see in this chapter, different structural configurations have been adopted by people of different countries. To study seismic-resistance of timber buildings, some traditional and modern buildings are investigated in the next sections with experimental and numerical investigations for different scales and elements. The main structural difference between the modern and the traditional structures is that the nonlinearity of the modern building often concentrate in the connections whereas in the different traditional buildings the nonlinearity may be existed also in different parts of structure elements due to different techniques which depend on culture and experience. Actually, there are two types of timber structures, as shown in Fig.(2.1).

- Modern type made usually from oriented strand board (OSB) or plywood.
- Traditional structures which use timber or bamboo and masonry and available mortar material.

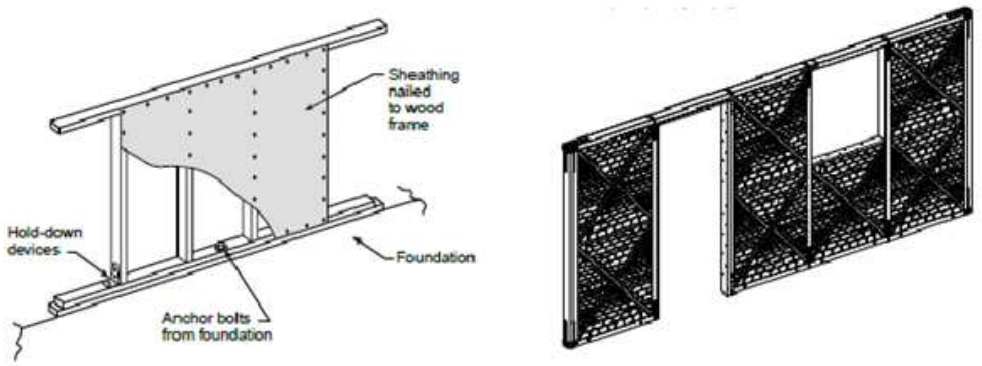

a) Modern timber frame b) Traditional timber frame (with rock and morter)

Fig. 2.1: Main two types of wood frame structures

2.2 Traditional timber-framed buildings

In order to study the behaviour of traditional buildings that were constructed through long periods of history and distributed around the world as in (Fig.2.2), these types of composite structures (basically made of wood and bricks or stones with some type of mortar) are normally shown to have very good performance and an ability to resist earthquake events through numerous seismic disasters (such as Haiti 2010, Vieux-Champagne et al. [140], Kashmir 2005, Ahmad et al. [4], Calabria 1783 (in the south of Italy), Kouris and Kappos [92], etc.).

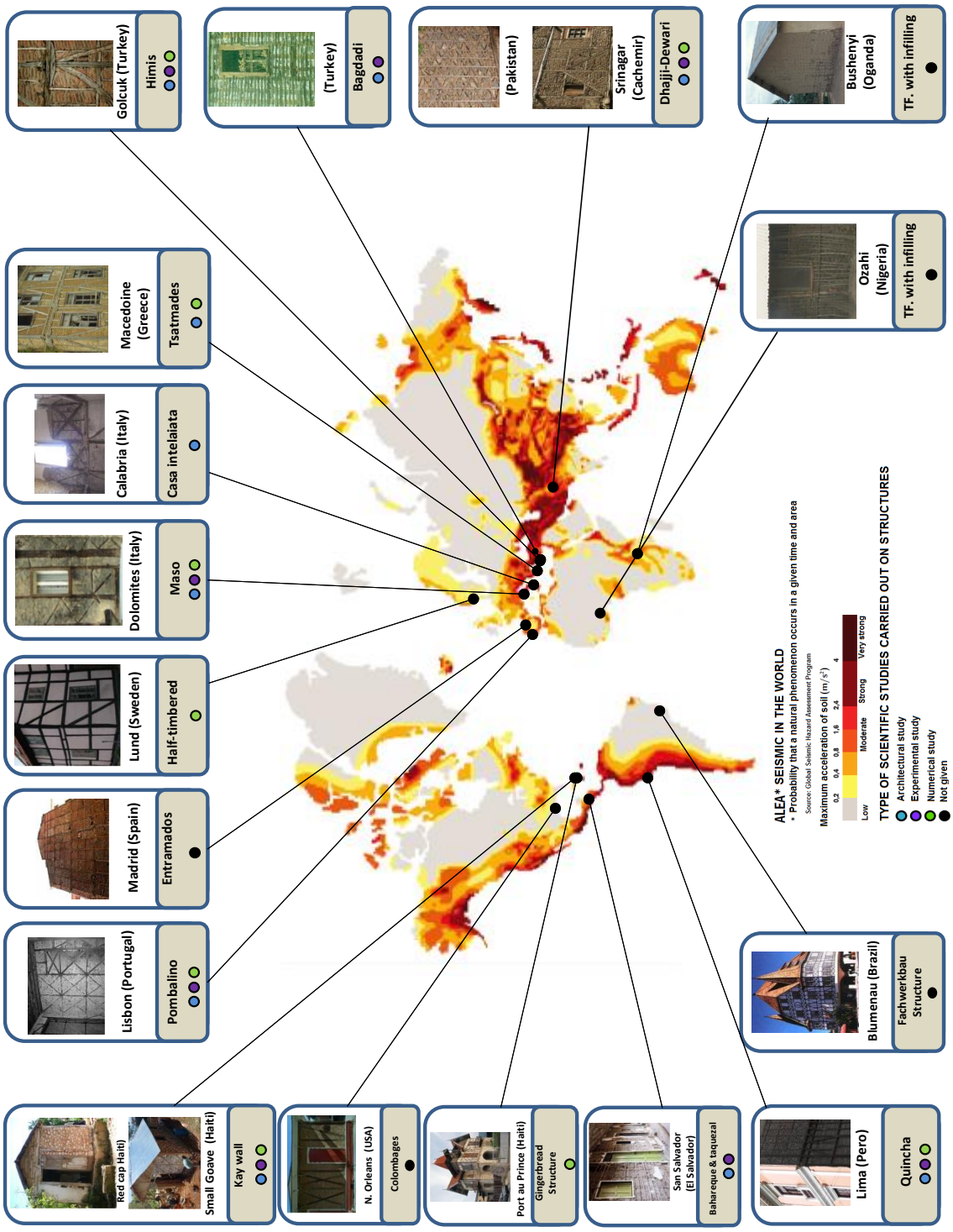

Fig. 2.2: Some Traditional Buildings arround the world [140]

2.3 Behaviour of the timber frame with infilling

Traditional timber-framed constructions with infilling showed a good performance in recent major earthquakes (Turkey 1999, Greece 2003, Kashmir 2005, and Haiti 2010), Langenbach, [96] during which they often suffered some damage. In comparison, the response to earthquakes of new masonry, concrete block or reinforced concrete buildings was bad or disastrous (Haiti 2010), as a result of the poor quality of construction and materials. Indeed, building such a structure, including ensuring that the implementation meets building codes, has a relatively high cost that makes these modern construction techniques inaccessible to the majority of local people (Tobriner , [130] and Makarios and Demosthenous [101], Langenbach, [1], Audefroy [12]). These traditional types have been the subject of many architectural studies and/ or post-seismic analyses to understand and/ or evaluate their seismic behaviour. Here is a description of some types:

2.3.1 The Himis and Baghdadi structures

These types of structures are clearly identified in Turkey [6]. The first, which is depicted in Figs. (2.3-a) and (2.3-c), is composed of a braced framework which can be filled with a mixture of brick, stone or adobe. The latter, shown in (Fig. 2.3-b), consists of a wood frame bracing inner and outer surfaces through a network of strips as a support for a possible ground mortar. The inside of the frame can be filled with a lightweight material such as pieces of wood. The Baghdadi technique is particularly used to produce lighter buildings with greater seismic resistance than those built by the first method. Himis and Baghdadi structures became significantly more widespread between the 15^{th} and the 19^{th} centuries owing to the numerous earthquakes in Turkey. The ductility and damping capacity in Baghdadi type are increased by the use of nails, Dogan [47], AKAN ([6], Gulkan and Langenbach [71] due to the large amount of energy dissipated through the splitting process of nails, whereas most of the energy dissipation in Himis buildings comes from the friction between the rocks and adobe, or between the timber members and the rock pieces or adobe. The structures of these Himis frames have also been studied experimentally and numerically (Aktas et al. [8], and Gubana et al. [70]).

(a) Example of Himis structure, AKAN [6].

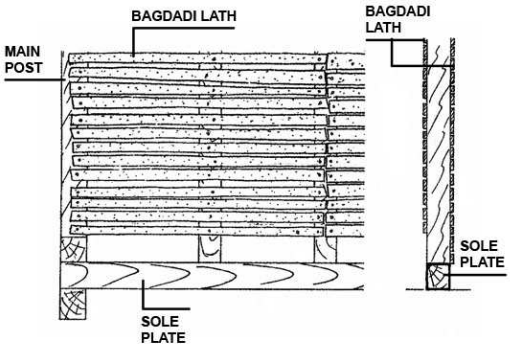

(b) Details of Bagdadi structure, Diskaya [46].

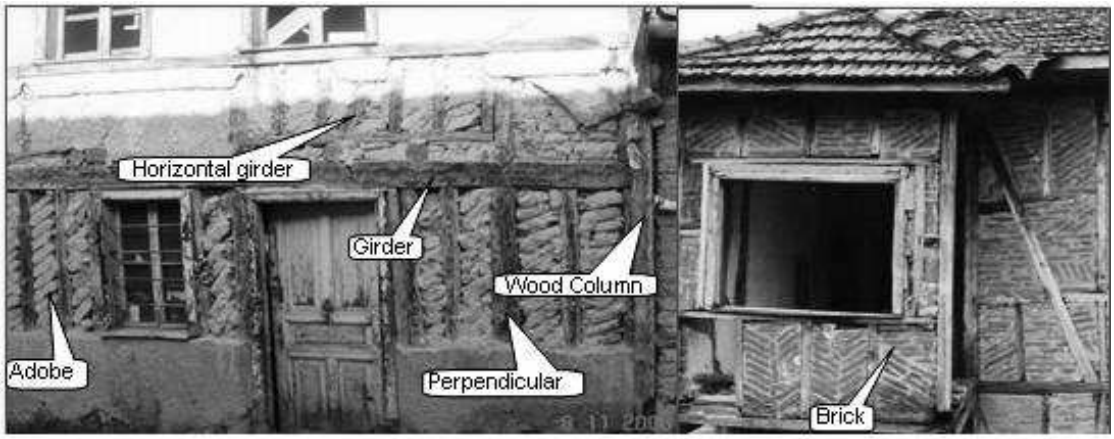

(c) Details of a himis structure, Dogan [47].

Fig. 2.3: Bagdadi and Himis Structures in Turkey

2.3.2 Taq structures

The Taq (shown in Fig. 2.4) is a traditional construction system that was once common in Srinagar (Kashmir), Shah and Tayyibji, [124]. Taq designates a timber-laced masonry building. A Taq building can have several floors and a high structure, but can still withstand earthquakes due to the combined use of masonry and wood. One particularity of Taq walls is that the infill masonry panels are not bonded to the piers. This allows the building to better adapt to differential settlements, which are frequent in the soft soil of Srinagar. Usually, the roofs of buildings in Srinagar were heavy, being covered with clay. Apart from providing thermal insulation, this system also helps to keep the masonry walls together during an earthquake by imparting some amount of pre-compressive strength. The

behaviour of Taq buildings during an earthquake is difficult to model. One of the reasons of seismic performance of Taq buildings, although the walls are brittle, the flexible timber lacings at slab and lintel level, along with the configuration of the interior partitions, seem to be the key to their earthquake resistance. The flexibility of the wooden lacings allows the building components to tolerate slight displacements while dissipating energy, thus preventing the walls from falling. Although some of the individual elements are brittle, the specific configuration of Taq buildings gives the system a certain ductility. According to the observations of Professors Rai and Murty of the earthquake in Kashmir in India, on the old constructions, the timber-laced form with bricks, like Taq, has been studied by Dar and Ahmed [43]. In this type of structure, many parts made of timber material are used as horizontal runners embedded in the heavy walls of timber, adding to the lateral load-resisting ability of the structure. Masonry laced with timber performed satisfactorily as expected, as it arrests destructive cracking, and distributes the deformations, which adds to the energy dissipation capacity of the system, without exposing its structural integrity and vertical load-carrying capacity to danger, Dar and Ahmed [43]. So, it is very interesting to note that this type of structure gives an overall ductility from very brittle materials and this is the advantage of such types of construction. This issue can be seen in Fig. 2.5.

2.3.3 Dhajji-Dewari

Dhajji-Dewari, as shown in Fig.(2.6). Indeed, the bracing can be a network of wooden bars positioned through a random angle, thereby dividing the infilling into a patchwork of masonry. This system is a wood-masonry composite in which the wood plays a structural role in the recovery of horizontal forces. Indeed, the masonry is separated evenly in the vertical direction by horizontal wooden ladders that create an interface to dissipate energy in the case of movement of the masonry subjected to horizontal loads, and thus limits the cracking of masonry. Very little damage was observed of Dhajji-Dewari type buildings after the 2005 earthquake in Kashmir and there were no collapses of such masonry in the regions of higher shaking because of the timber crossing members, which divide the wall into small parts of infill and then arrest the loss of part or all of several infill panels, so resisting progressive destruction of the rest of the wall, Langenbach, [94]. Also, the small distances between braces prevent the propagation of diagonal shear cracks within the single panel and decrease the possibility of out-of-plane failure and the dropping of filling materials, even in higher storeys. These small distances between braces also give a very long path of timber members, as in Fig. 2.6, which increases the friction between the timber and infill and redistributes the loads.

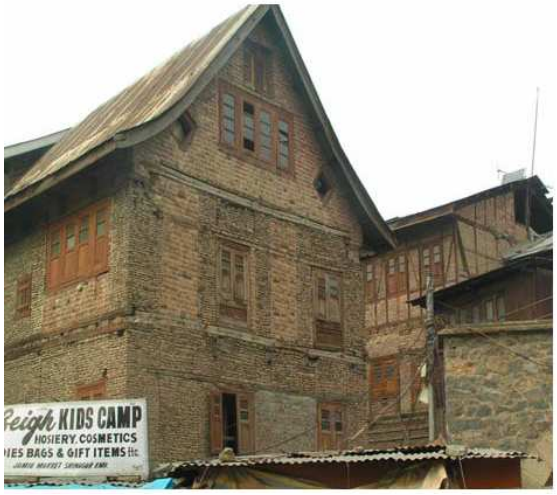

Fig. 2.4: Sample of Taq structural system.[124]

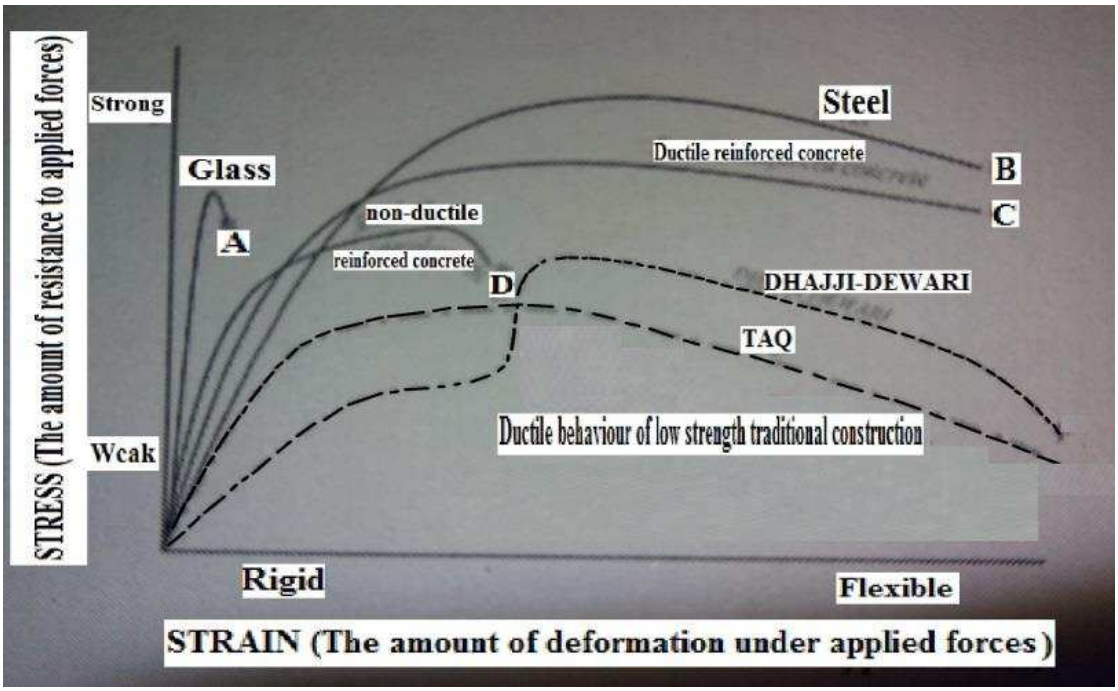

Fig. 2.5: Stress Strain Curves for different materials, Dar and Ahmed, [43].

Fig. 2.6: Sample of Dhajji Dewari system in the north of Pakistan, Ahmad et al. [4].

2.3.4 The Bahareque and Taquezal

These structures are composed of a frame of mixed bamboo and wood Gutierrez [72], and their principle of construction is close to the Baghdadi technique Lopez et al. [98], Gutierrez [73] that is described above. Bamboo slats form a cage around the braced frame. This type of construction has been widely used in rural areas since the colonial era (Ecuador, Colombia, Central America) and still exists in urban areas, in which some buildings are over a 100 years in age. This clearly shows the good performance in serviceability and against earthquakes of the Bahareque style (this is due to the same advantages as the Baghdadi structure mentioned above). These structures have been studied experimentally by Gutierrez [68].

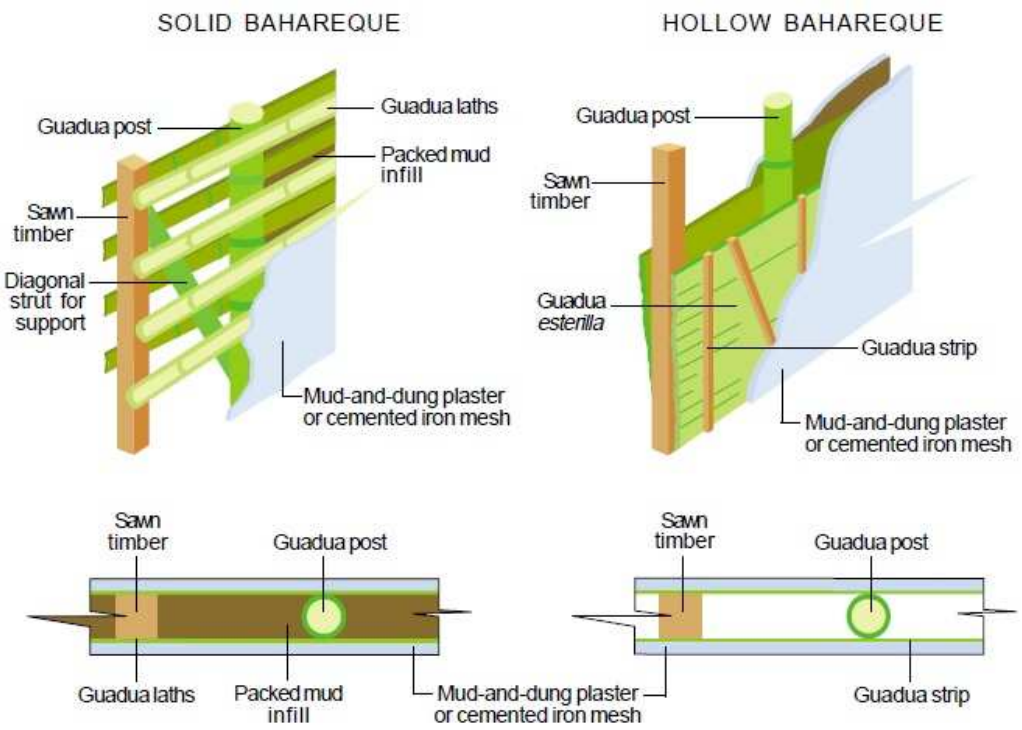

Fig. 2.7: The Bahareque technique, Gutierrez [72].

2.3.5 Adobe-Quincha structures

As seen in Fig.(2.8), in the Quincha structure Cuadra et al. [41], [24], Langenbach [95], Quinn and D'Ayala [45], the ground floor consists of adobe masonry, while the upper floors are made from a system of Quincha that is identifiable by its timber-braced frame filled with brick or covered branches, receiving a mud plaster and gypsum. It is interesting to note that the bracing system was originally Y-shaped structures, which can still be found in some configurations. It is observed that it dissipates a large amount of energy with small cracking in the mud, and a large amount of friction between the mud and frame also by using weak and lightweight materials.

a) Quincha House without finishing with clay

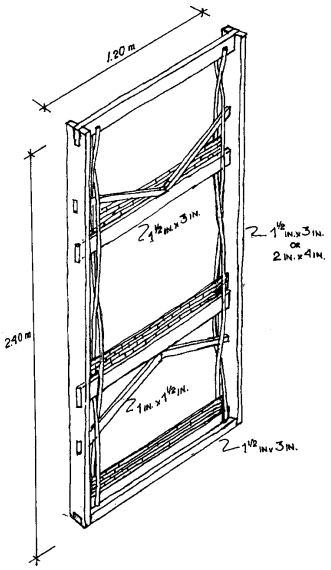

b) Detailed of construction scheme

c) House construct by tree branches

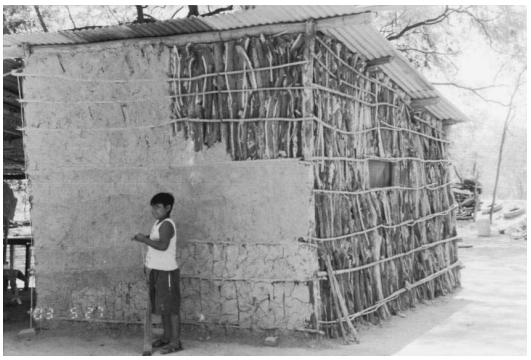

d) House under construction

Fig. 2.8: Some Examples of Quincha construction Techniques [24]

2.3.6 The Gingerbread

This type of structure can be found in Haiti (Fig.2.9), Paz and Leigh [16]) and it contains a timber-framed building with an infilling of stones and natural mortar (clay). This typical hybrid structure which can be recognized in Haiti has existed since the early 20th century. There are three main building techniques, including a timber frame braced without braces or by adding some studs and crosses, or

load-bearing walls made of brick or stone masonry bonded by a mortar of clay or lime.
The Gingerbread style was then prevented by the government in preference to the construction of masonry, reinforced concrete or metal buildings in order to prevent fires, but after the earthquake catastrophe the peoples did not agree to re builed the collapsed concrete structures where killed many peoples througth this disaster. But they were enthusiastics to rebuiled Gingerbread structures for the cultural reasons and also due to the good performance of these buildings, Barbacci et al. [16].

a)Example of Gingerbread construction b) Two survived Buildings

Fig. 2.9: Gingerbread Stucture in Haiiti [16]

2.3.7 The Kay

This type of structure, Curry [42], Joffroy [84], as shown in Fig.(2.10), is a timber portal frames and filled by a rocks and morter, it can be seen in Haiti and is still widely used there due to the poverty of the population as it is cheap and simple to construct. But it provides poor performance against earthquake excitations as compared to the other kinds of traditional construction mentioned in this survey. So an enhancement for this type of building was proposed by ANR (French National Research Agency) in the architectural school in the university of Grenoble

Alpes as shown in the (figure 2.10-c). This modifying structure is to enhance the seismic behaviour of the structure by adding two diagonal braces at each panel and providing additional steel strip connects the foundation (sill plate) and each post. An experimental investigation of these types of construction was performed by Vieux-Champagne et al. [135], [140], [136], [139] with some enhanced properties.

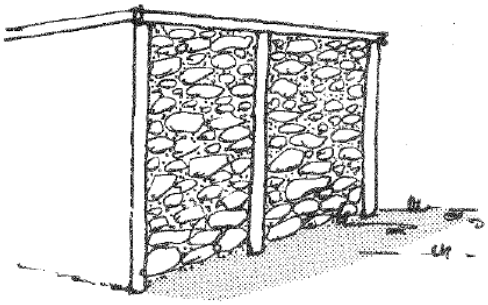

a) Typical Sample of Kay Wall [42]

b) House builed with Kay in Haiiti [84]

a) Enhanced Sample of Kay Wall [85].

Fig. 2.10: Original Kay Wall Structure a, b, and enhanced model c.

2.3.8 The Greek structures bearer dual system

This traditional system Karakostas et al. [90]), Vintzileou and Touliatos [141]), as depicted in Fig.(2.11), developed before the 20^{th} century on the island of Lefkada (the most prone to the seismic hazard), and this type of structure works according to a mechanism whereby in the first level the gravity load is resisted by the masonry wall and there is then a second timber frame wall if the former collapses. The higher levels are composed of a timber frame with infilling. The seismic capacity of this system could not be proven, but could have an interesting potential energy dissipation, which has enabled it to survive several strong earthquakes which occurred over the last 100 years due to the foundation system and good details of the connections in the corners and floors to yield a stiff diaphragm [141].

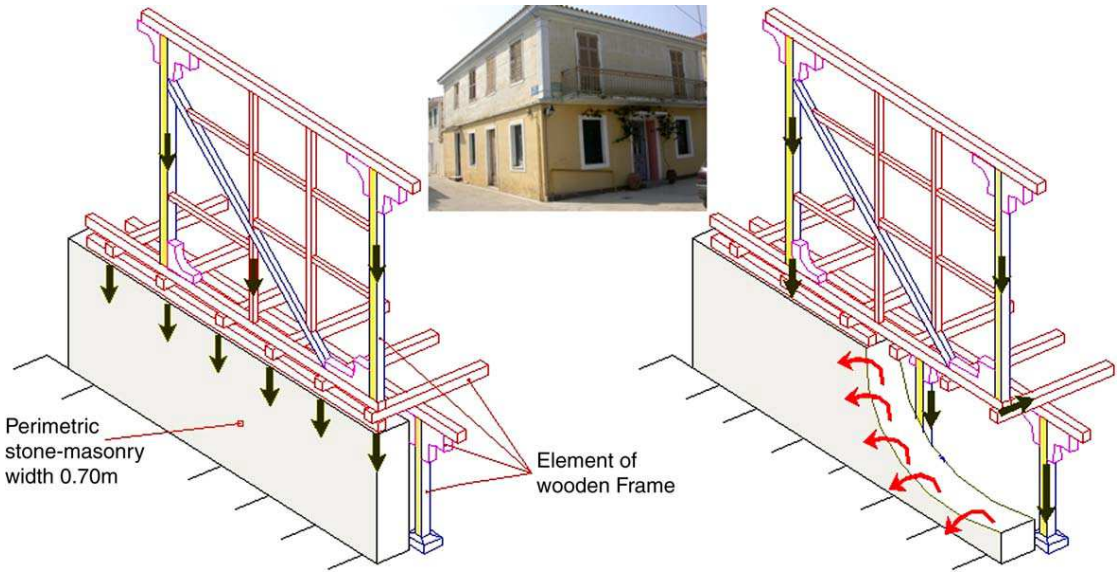

Fig. 2.11: Bearer dual system. [90]

2.3.9 The Pombalino structures

This type was built using mixed timber masonry frames in downtown Lisbon in the 18^{th} century. In 1755 the prime minister delegated to a group of engineers the development of a structural solution that would guarantee the required seismic resistance of the buildings. Based on the experience in this period and according to empirical knowledge collected from the buildings that survived the earthquake, a new type of construction was created, which is now generally referred to as Pombalino construction. The basic aim of Pombalino construction is to provide good resistance to horizontal loads and the capacity to dissipate the earthquake

energy, Ramos and Lourenco [114]. An example of the construction elements that compose a Pombalino building can be seen in Fig. 2.12, [102].

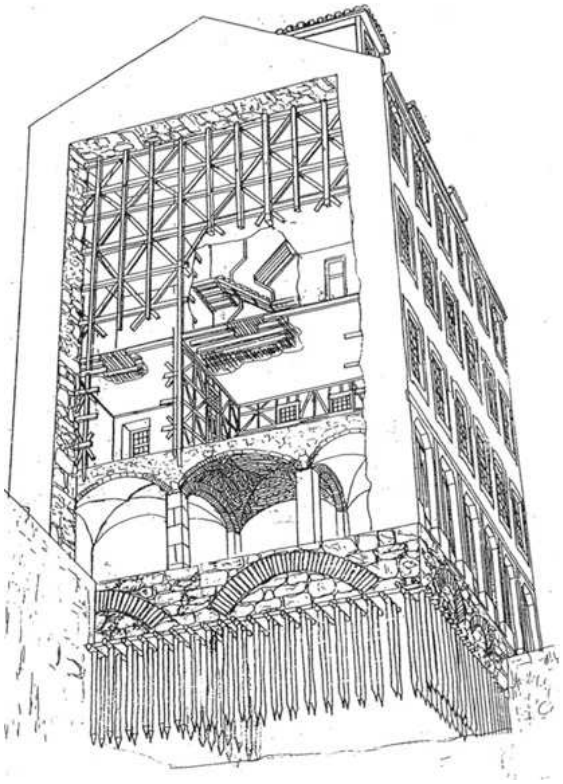

Fig. 2.12: Pombalino building, [102].

2.3.10 Baraccata and intelaiata structures

These structures have been exposed to the earthquake, so a reconstruction projects adopted this type of structures, [119]. They had been incorporated into the building codes as a seismic solution. The priciple behind the seismic resistance is the intersection at which the orthogonal walls are connected for the purpose to obtain a box behaviour of the edifices. This is can be obtained by the timber frame inside the infilling such that the horizontal timber member is the in-plane restrain of the laterally moving due to the infilling parts. Also the second advantage realized to connect the walls of the buildings are the beams of the intermediate floors. These are executed with notches at the end of the member to strengthening the node beam-wooden ring and guarantee, together the latter, a resistance to out-of-plan actions. The timber-framed buildings known as baraccato and intelaiata are braced by Saint Andrew's crosses. Experimental and numerical investigations

were performed by Salerno et al. [120].

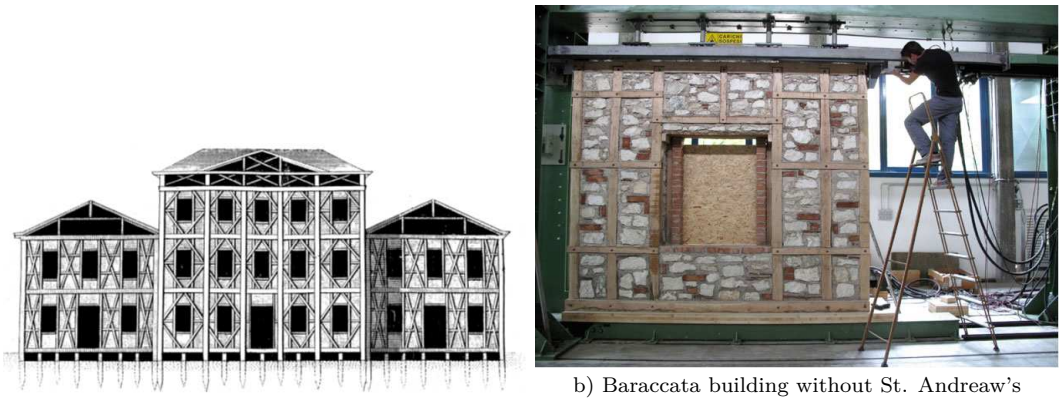

a) Baraccata building, Gubana et al. [70].

b) Baraccata building without St. Andreaw's crosses, Salerno et al. [120].

Fig. 2.13: Baraccata structures.

2.3.11 Summary

Most of the above traditional structures have nails in the connections and showed very good resistance to the earthquake loadings as compared to the modern poorly designed structures in recent earthquake disasters. For each of these buildings, the seismic observations consistently show a remarkable resistance to seismic hazard. This is especially true for areas where modern buildings suffered heavy damage, usually caused by inadequate design and poor implementation. Cases of collapse of these frames are mostly explained by the lack of maintenance, this being responsibility of the owner. These observations usually tend to encourage their use in current construction projects, but these structures, however, are still little used except in rural areas. This can be explained with several reasons according to Vieux-Champagne [135].

- The rare availability of scientific data, with direct consequences.
  - The lack of building code details do not allow safe and secure construction in terms of security.
  - The lack of evidence of the seismic performance of traditional buildings sometimes suffering from an image of "fragility" and poverty.
- The sensitivity of timber frames to fire and insect attacks.

- The maintenance requirements in terms of time for traditional construction (wood, assemblies, coatings, etc.).

Therefore many projects around the world have been established to study in detail the seismic and dynamic characteristics of these types of structures in order to promote the construction of these traditional wooden infilled structures and to remedy the lack of information and permit significant improvements e.g. Vieux-Champagne et al. [140], Ahmad et al. [4], Meireles [104]. Both experimental and properly calibrated proposed models are used to represent the experimental data for multiple scales of modelling for the buildings in order to determine the behaviour of different structural members under different load cases (static, cyclic, and dynamic loading). Some recent experimental investigations about traditional construction techniques are presented below.

2.4 Experimental work

This section presents the state of the art of existing experimental work on the study of the seismic behaviour of timber frames with infilling. According to the available data in the literature, four different scale levels will be discussed below:

2.4.1 Connections

The joints of the timber structures play a significant role in the performance of the behaviour of in the next larger scale (walls and building).

Branco et al. [21]

Branco investigated typical traditional birdsmouth joints without and with three techniques of strengthening, namely stirrup, bolt, and binding stirrup, as shown in Fig. 2.14. The study includes some monotonic (positive (+ve.) and negative (-ve.)) and cyclic tests with a pre-compression force of 1.4 kN or 2.5 kN.

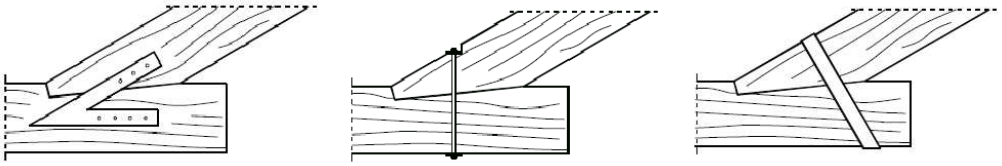

(a) Stirup (b) Bolt (c) Bindiing Stirup

Fig. 2.14: Typical Strengething of Birdsmouth Timber Joints Branco et al. [21]

Yue [149]

In this study there are 13 different ancient wooden joints used in China. These unique types (often mortise and tenon type) have been used for a long time in this country and while the author could not explain cases like earthquakes, the energy dissipation capability has led him to more investigations of traditional timber structures to implement in Chinese codes. These specimens are of different sizes but can be recognized as five types as shown in Fig. 2.15. For the same types of traditional joints, Qing et al. [113] suggest a trilinear moment-rotation relationship and, according to their experimental results, a backbone curve was calibrated and values of stiffness were analysed for these (13) tenon and mortise joints.

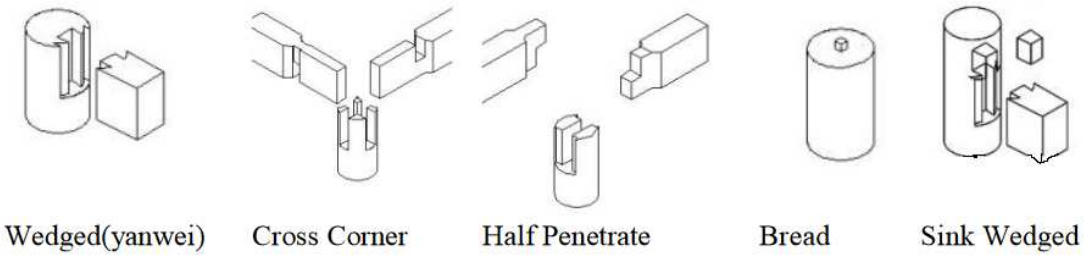

Fig. 2.15: Typical Traditional Joints in China, Yue [149]

2.4.2 Elementary unit wall

This study is performed on the Pombalino structures and for maso structures. The principle is to study the elementary cell to make up the complete wall Ferreira et

al. [57]. The objective, on the other hand, is to provide data to determine the parameters that will lead to the modelling of the structure as accurately as possible.

Ferreira et al. [57]

The dimensions of the cell are shown in Fig.(2.16). The frame is connected by half-wood joints held together by nails measuring about 14 cm long, and has a pyramidal shape which has a base size of $(10 \times 6\,mm^2)$. In addition, a vertical load of (6 kN) has been applied on the frame in order to take into account the presence of the mass existing in situ. In the case of structures with infilling, this loading is (25 kN), since in this case the mass at the top is representative of a filled structure.

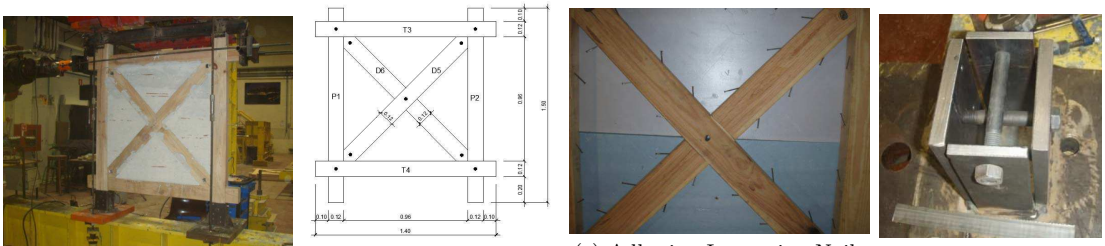

(a) Insitu Wall Cell (b) Dimensions of the Frame (c) Adhesion Improving Nails of the Infilling (d) Fixation System of the Post

Fig. 2.16: Element cell of a frontal wall

2.4.3 Wall

Pombalino structure, reduced scale, Vasconcelos et al. [134]

This work was customised for a real front wall, and its assembly system and the different studied frontal structures are presented in (Fig. 2.17). The small-scale wall, shown in (Fig. 2.17-e), is 90 cm high and (80 cm) wide. The wood studs have the same cross-section equal to $7 \times 5\,cm^2$. The studs have a section $2 \times 4\,cm^2$ and a height of (3 cm). Two types of nails were used: one with a square section of (2.1 cm) and a length of (4 cm), and the other with 3.1 cm and a length of (7 cm). The shortest nail was fixed transversely to the frame in order to improve the effectiveness of the mortise and tenon joints. As for the long nails, they were set in the plane framework of the frame to strengthen the contact between the diagonals and the frame. Filling is carried out with bricks of (6 cm) thickness related to the timber structure by a cement mortar composed of sand and lime in the ratio

2 : 6 : 3. This study includes new experimental tests to analyse the influence on the behaviour of the wall:

- of structural reinforcement.
- of the infilling.
- of vertical load.

The tested configurations are as follows:

- Empty wall: (UTW) three tests varying the vertical load each time (25, 43 and 70 kN).
- Wall with infilling: (ITW) three tests varying the vertical loading each time (70, 80 and 100 kN).
- Empty wall strengthened with Glass Fibre-Reinforced Polymer (GFRP): (RTW): three tests varying the vertical loading each time (43, 70, and 80 kN).

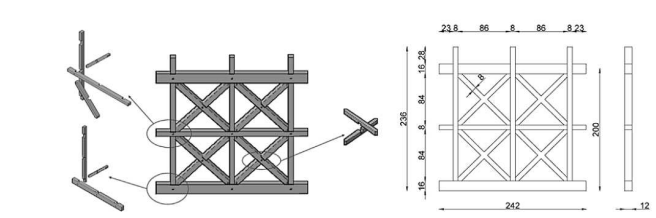

(a) Connections and dimensions of the Wall [111]

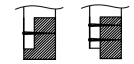

(b) Beam-Post Connections Right:[102] Left:[111]

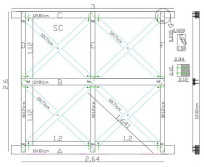

(c) Dimensions of Tested Wall with filling [102]

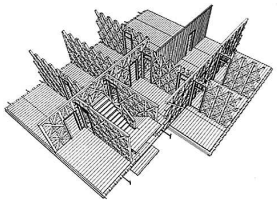

(d) Wall in situ [111]

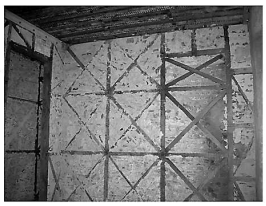

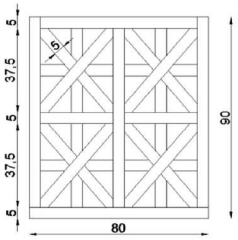

(e) Tested Wall with reduced scale [134]

(f) Wall with infill[134]

Fig. 2.17: Frontal Shear Wall

Pombalino Structure, Meireles et al. [102]

The front wall, which will be called "wall 1" for the sake of simplicity, is shown in (Fig. 2.17-c). It consists of continuous beams and columns connected together by joints as a half-lap in the timber members depicted in (Fig. 2.17-a). This frame is braced by a Saint Andrew's cross and filled with brick masonry and broken tiles connected by a mortar lime. The sections of the timber studs are: $16 \times 8\,cm^2$, $12 \times 8\,cm^2$, and $7 \times 10\,cm^2$. Nails with a length of (12.5 cm) have a pyramidal shape with base $6 \times 10\,mm^2$. These nails were used to connect the diagonals together and are of the same type, measuring $7.5cm$ long with a cross-section of $5 \times 5\,mm^2$. A hole of (7.5 mm) was pre-drilled in the horizontal elements in order to be able to join the connections. A vertical weight of (30 kN/m) was applied to the wall to take into account the weight of the floors and the roof in the actual constructions.

Pombalino Structure, Poletti and Vasconcelos [111].

The front wall, which will be called "wall 2", is shown in (Fig. 2.17-a). Although it seems very similar to the above, various technical details have a significant influence on the response of the walls, as discussed in paragraph 2.5. The half-lap joints connecting the horizontal and vertical members differ between wall 1 and wall 2 (see Fig. 2.17-c). We see that for the first level the post is placed outside the horizontal sill plate and is attached there by two nails. For the second level, the same post is fixed in the section of the bottom plate and is held with only a point whose dimensions are unknown. Another important difference in wall 1 is that the braces have low inertia ($7 \times 10\,cm^2$) in the direction out of the wall plane, while for wall 2, they have high inertia in the right direction ($8 \times 12\,cm^2$). The dimensions of the other figures are also different, as seen in (Fig. 2.17-a) and (Fig. 2.17-c).

Wall Dhajji-Dewari, Ali et al. [9]

For the Dhajji-Dewari type of wall, the frame and assembly system are presented in (Fig. 2.18). Three walls were constructed for three different dimensions of timber beams: $10 \times 10\,cm^2$, $5 \times 10\,cm^2$, and $2.5 \times 10\,cm^2$. The nails that were used to connect the horizontal top and bottom beams are $75\,mm$ long, while other nails are $50\,mm$. All of them are made of mild steel. The horizontal beams are connected to the posts by mortise and tenon joints. The composition of the filling (ratio of stone/mortar) varies according to the tested configurations as: 9:1, 7:3 and without filling. A vertical weight (2 kN) was applied to the wall to take into account the actual weight of the roof construction.

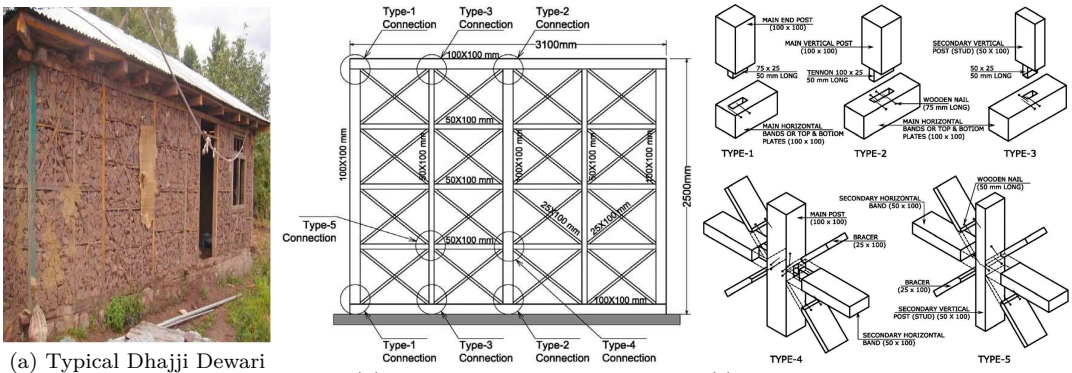

(a) Typical Dhajji Dewari House

(b) Plan of the tested Wall

(c) Some Details of the Connections

Fig. 2.18: Dhajji Dewari Wall [9].

Wall Maso Ceccotti et al. [28]

The maso type wall, its frame and its assembly system are shown in (Fig.2.19). The posts of this structure have a section of $16 \times 16\,cm^2$ and are connected together by lap joints and held by two wooden anchors instead of the traditional pyramidal nails. The bracing members have a cross-section of $7 \times 16\,cm^2$ and are simply placed inside the frame without connection. The filling is composed of masonry of crushed stones linked by a mortar composed of lime, clay and sand.

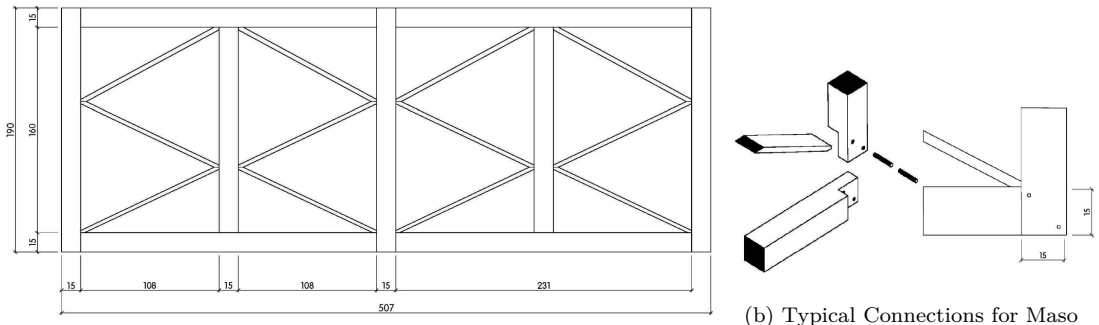

(a) Maso Wall Structure

(b) Typical Connections for Maso Wall

Fig. 2.19: Maso Structure in Italy [28].

2.5 Results of the experimental work

From the data available in the literature, this section describes the results of quasi-static tests performed on the three types of above mentioned structures. In each case, when it is possible to estimate the necessary parameters, the seismic performance of these frames is compared. These parameters are ductility, energy dissipation, the equivalent viscous damping ratio (EVDR), the maximum force, drift and the influence of the infilling on the behaviour of the wall. The methods for calculating these values are described below.

Ductility (μ): Ductility is the ability of the material/assembly/component/structure to deform without breaking. This gives an estimate of the ability of the structure to deform nonlinearly without significant loss of strength or stiffness. So, classically, the ductility of a structure is defined as the ratio of displacement at the peak (Δ_{max}) or at the rupture ($\Delta_{failure}$) and the elastic displacement (Δ_y) obtained from force–displacement relationships of the structure (Eq. 2.1).

$$\mu = \frac{\Delta_{max}}{\Delta_y} \qquad or \qquad \mu = \frac{\Delta_{failure}}{\Delta_y} \tag{2.1}$$

The calculation of μ does not appear to be trivial because the choice of the yield displacement limit causes important differences, meaning that accurate determination of Δ_y is often difficult from the experimental curve. Thus, there are several methods for calculating this coefficient, using Δ_{max} or $\Delta_{failure}$ and indicating how to obtain the elastic displacement. These methods are illustrated in (Fig. 2.20) and summarized in Munoz et al.[105] and Jorissen and Fragiacomo [86].

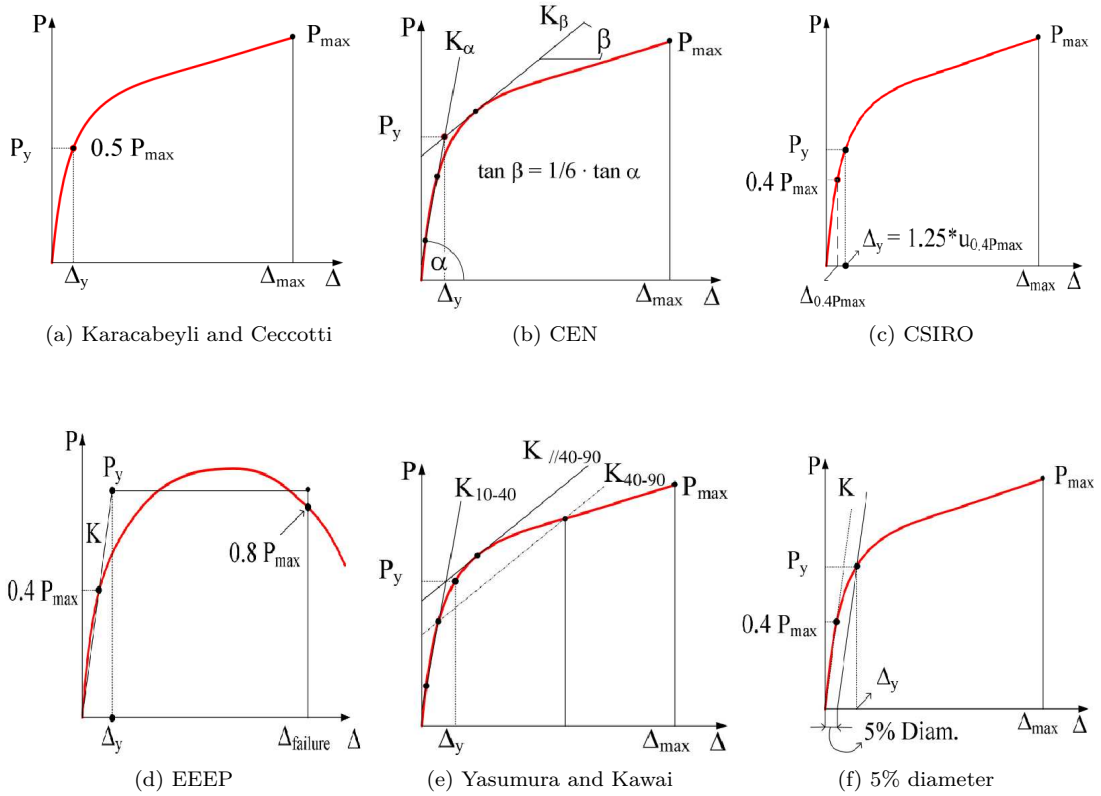

(a) Karacabeyli and Ceccotti (b) CEN (c) CSIRO

(d) EEEP (e) Yasumura and Kawai (f) 5% diameter

Fig. 2.20: Methods of classical analysis used to determine the displacement elastic, Munoz et al. [105], Jorissen and Fragiacomo [86]

Munoz et al. [105] calculated ductility according to these six methods, based on test results from 60 assemblies (several configurations) and 18 walls. They conclude that each method can be difficult to estimate a realistic value or determine the ductility depending on the experimental analysis of behaviour. The method of Yasumura and Kawai seems to give more consistent values. Despite the many cases of overestimation obtained from the EEEP (Equivalent Energy Elastic-Plastic method (Fig. 2.20-d)), it is defined as the reference in some building codes (e.g. [65]), which makes it a tool widely used in the literature. It therefore seems appropriate to use the latter and to emphasize the calculated results by the additional use of one of the methods described above. It is interesting to refer to Jorissen and Fragiacomo [86], who conclude that it is better to express the concept of the ductility parameter as an absolute value and not a relative one, i.e. ($\mu = \Delta_{failure}$) or the difference between them ($\mu = \Delta_{failure} - \Delta_y$).

Energy dissipation and EVDR: As an evaluation goal of the ability of the structure to dissipate the energy, the equivalent viscous damping ratio (EVDR) is calculated from hysteresis loops of the force–displacement curve (as in Fig. 3.9) according to Equation 2.2.

$$\xi eq = \frac{E_d}{2\pi E_p} \tag{2.2}$$

Where:
E_d: is the energy dissipated. It is equal to the area of the hysteresis loop.
E_p: is the elastic (or potential) energy equal to half the product of the maximum force by the corresponding displacement.
The average value of (ξ) is calculated for positive and negative displacements.
Maximum force: As the name indicates, the maximum force (F_{max}) noted is the force corresponding to the peak of the constitutive law expressed from the force applied to the structure.
Drift: In the case of quasi-static tests to the scale of the wall, the drift is the ratio of displacement at the top divided by the height of the wall. Normally it is expressed as a percentage ratio. The relative magnitude compares walls of different heights.
Influence of the filling ratio on the wood: This may relate to the initial stiffness, vertical and lateral strength of the structure. The impact on the stiffness and vertical strength (better load distribution) is true in most cases. The influence on the lateral resistance depends on the behaviour of the timber frame: if the lattice formed by the timber frame is undeformable, then the filling does not play any role. On the contrary, if the braces of this lattice are not fixed to the frame, as is the case for maso walls, filling is essential to ensure the confinement of the frame. In most cases, the behaviour of the structure is intermediate to these two situations. The ratio of wood then seems to be a relevant indicator to understand this influence. This is explained by the fact that the buildings are normally designed with structural consistency. For example, the size of the connectors logically depends on that of the timber frame. So if this is massive, the connections will be as illustrated by the structure of frontal walls. However, this cannot be generalized, as illustrated by the large dimensions of the sections of beams and columns used for construction and tested in Himis structures by Aktas et al. [8]. Indeed, these beams and posts are connected by only a few points (1 to 5). Some examples of the experimental results in the literature are in the next section:

2.5.1 Results of the elementary unit cell wall

Experiments on the unit cell were carried out by Ferreira et al. [57] is listed as example as below:

Ferreira et al.

Experiments by Ferreira et al. [57] allow us to infer the effect of the infilling on the behaviour of the structure subjected to vertical and horizontal loads. (Fig. 2.21) shows the different failure modes for the tested specimens. The brittle rupture of wood allows us to note that the boundary conditions play an important role in the response of the structure. Indeed, fixation of the posts in this way (Fig. 2.21-f) induces a significant shearing of these elements, which does not exist in reality, since there is a continuity of the braces at the level of the assemblies. In addition, explaining the increase in stiffness and strength by the presence of only infilling is questionable, since a non-negligible part of this increase comes from the vertical load (see, for example, Vasconcelos et al. [134] and Poletti and Vasconcelos [111]), which is significantly higher for a configuration with infilling (25 kN against 6 kN for an empty frame according to Ferreira et al. [57]). On the other hand, the infilling seems to contribute to the decreasing of the instability for out of planes of the braces.

(a) SR1: Breaking of out of plane for braces

(b) SR2: Breaking in the post member dut to tensile force

(c) SR3:Breaking in connections between column and braces

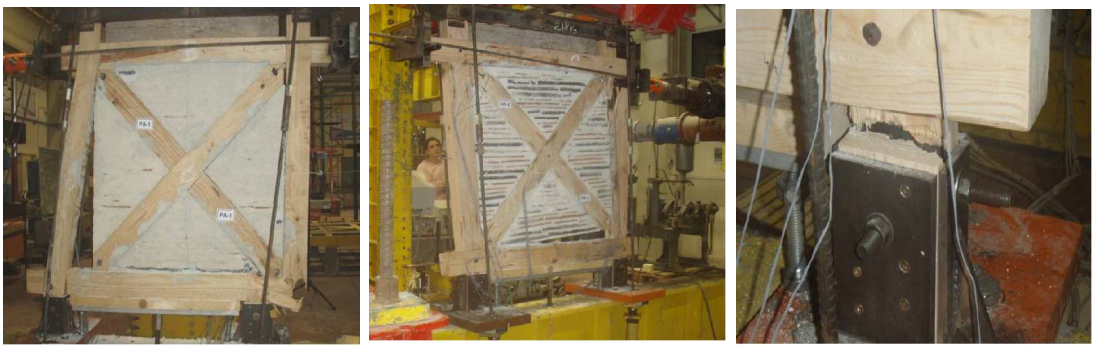

(d) R1: shear failure of timber post in the connection level

(e) R2: Rupture in tension for timber post

(f) R3: Rupture in timber post due to tension at connection

Fig. 2.21: Locations of Failure of Elementary Cell Wall by Ferreira et al. [57], Fonseca [64]

2.5.2 Some results of scale wall

The basic values and observations of these tests are presented in (table 4.4), which lists the types of connections that were used in the structures and the element types in which rupture occurred. When data are available, it is also summarizes the values of vertical loading, drift, the ductility of EVRD, energy dissipation, and the maximum force (F_{max}). The values of (F_{max}) are different and no direct comparison can be made between them due to geometric differences on the one hand and the technical details of the structures on the other. Finally, this table provides information on the influence or not of infilling on the structural behaviour. The following observations can be concluded from these comparisons:

- **Vertical Loading**: Vasconcelos et al. [134] and Poletti and Vasconcelos [111] show that its influence on the behaviour of the wall as well as on the rest of the seismic characteristics presented above can be significant. The main conclusions drawn from these trials for the vertical loading influences are as follows:
  - *The mode of failure of the wall*: For small values of loading, the wall tends to deform in rigid body motion instead of deforming in shear, as is normally intended during its design. Increasing the vertical load allows the wall to be more shear-stressed by reducing the uplift forces from the lateral load on the connections, thus reducing the tensile stress in the connections and so increasing the overall strength of the structure, as shown in (Fig.2.22-a).
  - *The initial stiffness*: (Fig.2.22-b) shows the variation of the initial stiffness as a function of the value of the vertical load. From this figure we cannot draw clear conclusions regarding the configuration of the infilled frame, and this parameter is less obvious.
  - *Energy dissipation*: (Fig.2.22-c) shows that when the vertical load increases, the energy dissipation increases.
- **Drift**: For each studied frame, the value reached for the displacement corresponding to peak force varies from (1.0 to 2.6%). The low value obtained for the Dhajji-Dewari walls can be explained by the mode of failure visible in (Fig. 2.23). Indeed, the short tearing distance of the tenon and mortise joint, which causes a tearing failure of the pin joint, does not allow the use of the potential ductility of the metal connectors.
- **EVDR**: (Table 4.4) shows consistent values between each infilled timber-framed configuration. These values are also consistent with those of modern timber frames in terms of (ξ), which is (15%) (Filiatrault et al. [58]). On the other hand, for configurations without infilling, Ali et al. [9] obtained a value of ($EVDR$) about (7%), while the work of Vasconcelos et al. [134] suggests that the presence of infilling does not appear to have a clear effect on the ($EVDR$). Moreover, in these two works, the authors observe that the infilling has little or no influence on the overall behaviour of the structure.
- **Influence of filling**: (Table 4.4) summarizes the observations and assumptions of the influence of the filling on the initial stiffness and the maximum force. According to Vasconcelos et al. [134], Ali et al. [9], and Meireles et al. [102], the infilling has little or no effect on the shear resistance of the wall. On Dhajji-Dewari structures, this can be explained by the dimensions

of a unit cell of the wall. It measures (53.8 cm) high and (67.5cm) wide, which corresponds to a relatively small cell size compared to others of the same family of structures, which are studied in (chapter 5) of this document. Its ratio of (29%) of the wood material is moderate compared to the frontal wall where ratios of (43%, 82%, and 54%) may be a good indicator of the influence of the infilling. It is necessary to complete this indicator with an accurate observation of the timber frames. The elementary cells of frontal walls have relatively large dimensions ($1.2 \times 1.2\,m$), but their structure is constructed from continuous elements of assembled wood members, which makes it possible to ensure the behaviour of the truss for the cells. As discussed above, despite the wood ratio of the maso walls (39%), the infilling is essential in this case, since it allows confining of the braces simply placed inside the wooden frame and decreasing of the p-delta effect of the braces.

These observations show that, in spite of these similarities of infilling timber frames and their overall good behaviour under quasi-static loading, the geometry and technical details of their assembly mean that they have different structural responses.

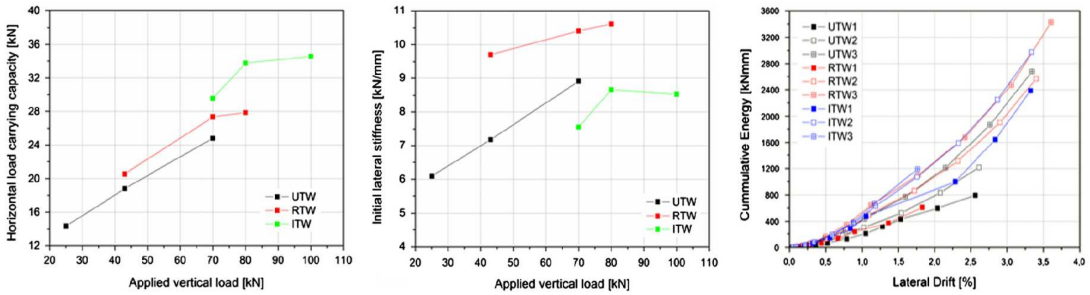

(a) The Total Shear Resistance of The Walls in terms of Vertical Loading

(b) The Initial Stiffness of The Walls in terms of Vertical Applied Loading

(c) Comulative Energy of The Walls in terms of Drift for different amount of Vertical Loading

Fig. 2.22: Effect of Vertical Loading on the Lateral Resistance of Shear Walls, Vasconcelos et al. [134]

(a) Failure in the corner bottom support of post (b) Detachment between braces and infilling

Fig. 2.23: Modes of failure for Dhajji-Dewari, Ali et al. [9]

(a) Schematic Shape of Deformed Shape (b) Tension Failure in the joint of tenon (c) Little Damage in the Central Joint

Fig. 2.24: Failure Modes in the Frontal Wall, Vasconcelos et al. [102]

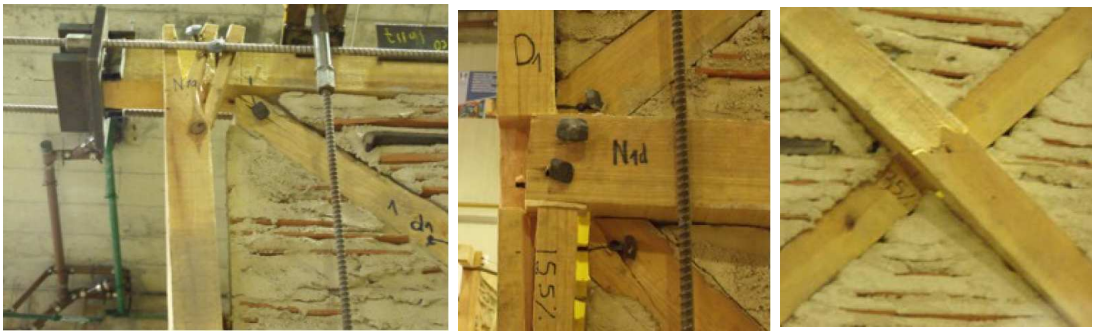

(a) Failure in the Top corner Lap Joint of Post

(b) Failure in the Lap Joint of Extreme Post

(c) Out of Plane Failure after Reinforcing the Joints

Fig. 2.25: Modes of Failures for the Wall studied by Meireles et al. [102] befor and after Reinforcing Joints

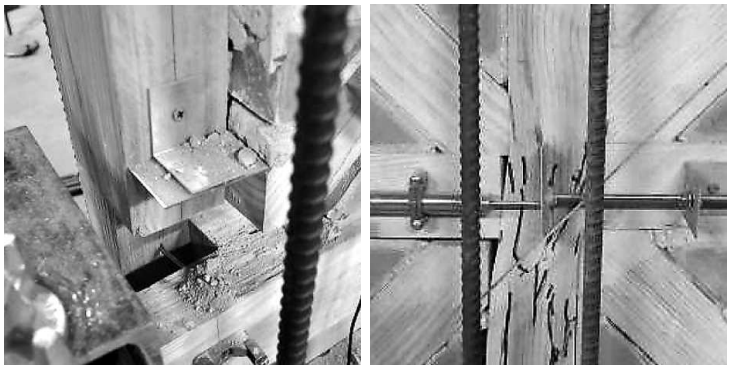

(a) Uplifting Failure of terminal Post

(b) Shear Failure in middle Connection of Post

Fig. 2.26: Modes of Damage for the Wall of Poletti and Vasconcelos [111]

(a) Out of plane Slip for infilling due to lack of braces

(b) High deformation of the infilling in the bottom Support

(c) Slipping of the bricks and detachment at the top of the post due to the confinement

Fig. 2.27: Modes of Failure of Maso Wall by Ceccotti et al. [27], [135]

2.5.3 Some conclusions for experimental works

From the different tests in the literature, we can discover some common remarks about the behaviour of the traditional timber frames with and without infilling, these are:

- The effect of applying vertical forces is very important almost in all the cases of the tested shear walls and this raised in the strength and ductility as well as stiffnesses reffering to the prestressing effect and confinement which decrease the detachment effects in the case of tension for joints.
- They proves the importance of connections in the middle, top, and bottom and the last one plays an important role in ductility behaviour and premature failure and failure modes of the structures.
- The effects of infilling are not clear if we compared between different tests, this factor gives no crucial effects, of course, the confinement due to infilling gives a good energy amount of dissipation but their effect on strength not proved definitely and further investigation must be performed for this factor.
- In term of damping, it is proved a good energy dissipation for different types of walls with equivalent viscous damping between $(10 - 20\,\%)$ which represents the very good performance of structural damping.

- The drift value for all specimens is roughly about (3%) except the case of Kay wall which gives a double value with respect the other types, this lead to increase the ductility of this type as compared to others.

Therefore, it is still a lack of information about the structural behaviour of timber-framed with infilling and more experimental as well as numerical investigations are needed to use in the building codes for construction these types of structures as an alternative solution for the seismic loads.

2.6 Modern timber-framed structures

In addition to the traditional timber structures, many types of modern-style timber structures (e.g. cross-laminated timber (CLT) or X-Lam, oriented strand board (OSB), plywood, etc.) were studied in numerical and experimental investigations due to the high strength to mass ratio, and some further investigations were established for the connections, wall, and building scales. Some of experimental studies are stated below.

2.6.1 connections

The connections in modern timber structures play a significant role (especially in metallic joints) in the total behaviour of the static and dynamic loading conditions due to their ductile nature and the easy use of these connections.

Experimental work, Tomasi and Sartori [131]

In this study, some hold-down connection types and shear connections connecting the building with the foundation as well connecting multiple storeys to each other and connecting to OSB panels were used in an experimental campaign to investigate some commercial connection types and it was found that these connections are not convenient to use in modern platforms. There were 16 different tests for lateral shear connection systems, 9 for monotonic tests and 7 for cyclic, while for hold-down systems there was a total of 16 tests, 11 for monotonic and 5 for cyclic tests. The results of the study suggest that, according to these investigations, newly designed types of shear connections should be used, namely NEW120, NEW150, and SCREW.

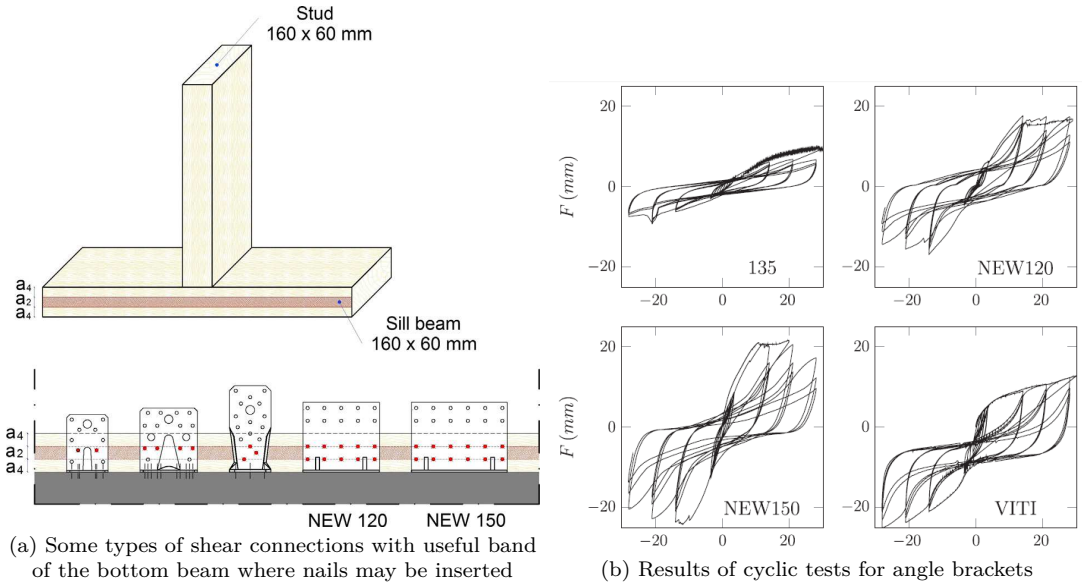

(a) Some types of shear connections with useful band of the bottom beam where nails may be inserted

(b) Results of cyclic tests for angle brackets

Fig. 2.28: Experimental campagne of metalic Connections, Tomasi and Sartori [131]

Experimental and Numerical, Humbert et al. [83]

A versatile FE model is used by Humbert et al. [83] to calibrate about 300 experimental tests of different types of fastners (nails, screws, staples, bracket-type 3D connectors, punched shear plates) to this FE joint model. This model used a *Bézier* curves, [82] instead of exponential function as in the previous studies (see for example Richard et al. [118], Dolan and Foschi [50]) to define the backbone curve of hysteresis model and the comparison between the experimental results of shear wall test and numerical model proposed by implementing this Humbert's model into each fastner. Only axial tension test was performed in this study but there is no tangential shear test.

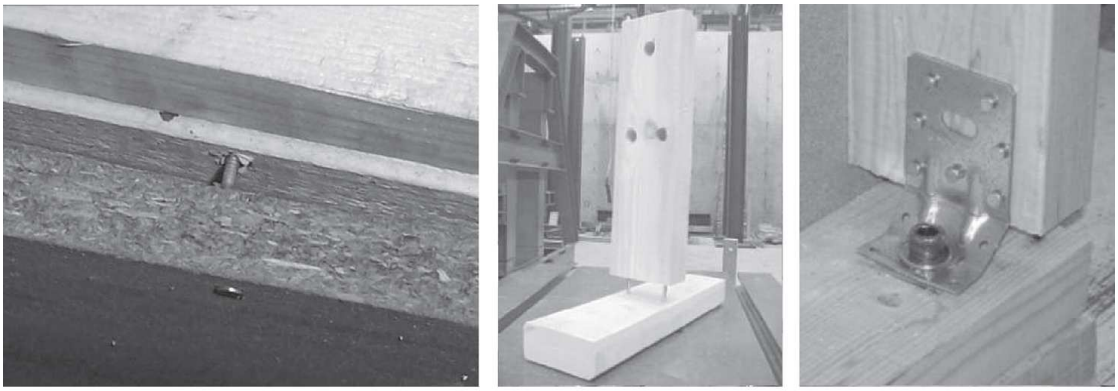

Fig. 2.29: Three joints with metal fasteners used in a shear wall, Humbert et al. [83]

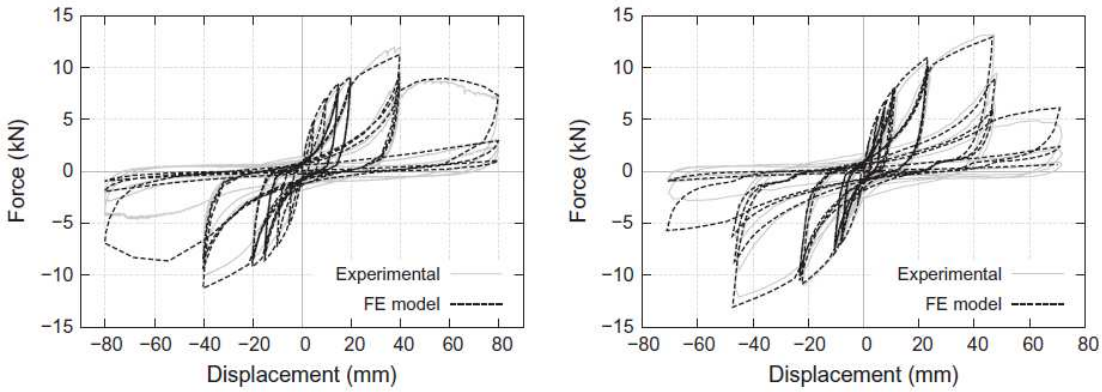

Fig. 2.30: Force–displacement curves of shear walls: comparisons of experimental results and FE model predictions, Humbert et al. [83]

2.6.2 Shear wall

Some of the numerical models were proposed for the analysis of modern shear walls subjected to lateral forces in the literature, where all the structural components

were idealised as a macroelement with 1-DOF as in Richard et al. [117].

Yasumura et al. [146]

Pseudodynamic tests were conducted on a two-storey building of plywood-sheathed shear walls with openings of different configurations. The lateral loading was applied step by step at the top of the timber frames using a computer-controlled actuator, and the displacement response for the next step was computed on the basis of the input accelerogram of the 1940 El Centro earthquake, scaled up to (0.4g). The test results were compared with those of the lumped mass time-history earthquake response analysis using the hysteresis model with pinching defined by Yasumura and Yasui [147], (Fig.2.31) and the required parameters were calibrated according to $3 \times 3\,m^2$ tested level 1 walls. A plywood sheath walls connected to the frame by nails from one side. Each storey has a mass of (2,500 kg) and a total mass approximation was used in the analysis. The numerical results show that the maximum displacements for the first storey matched the experimental values, but they were underestimated by half for the second floor.

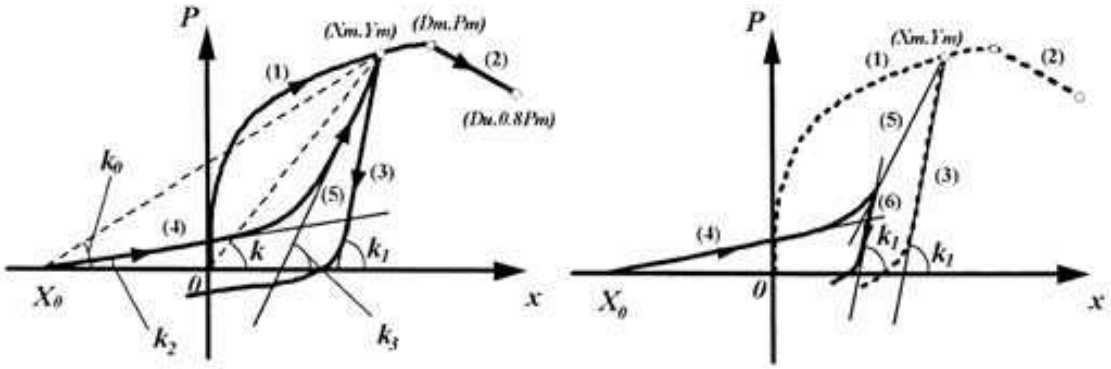

Fig. 2.31: Hysteresis model of wall system for Yasumura and Yasui, Yasumura and Yasui [147]

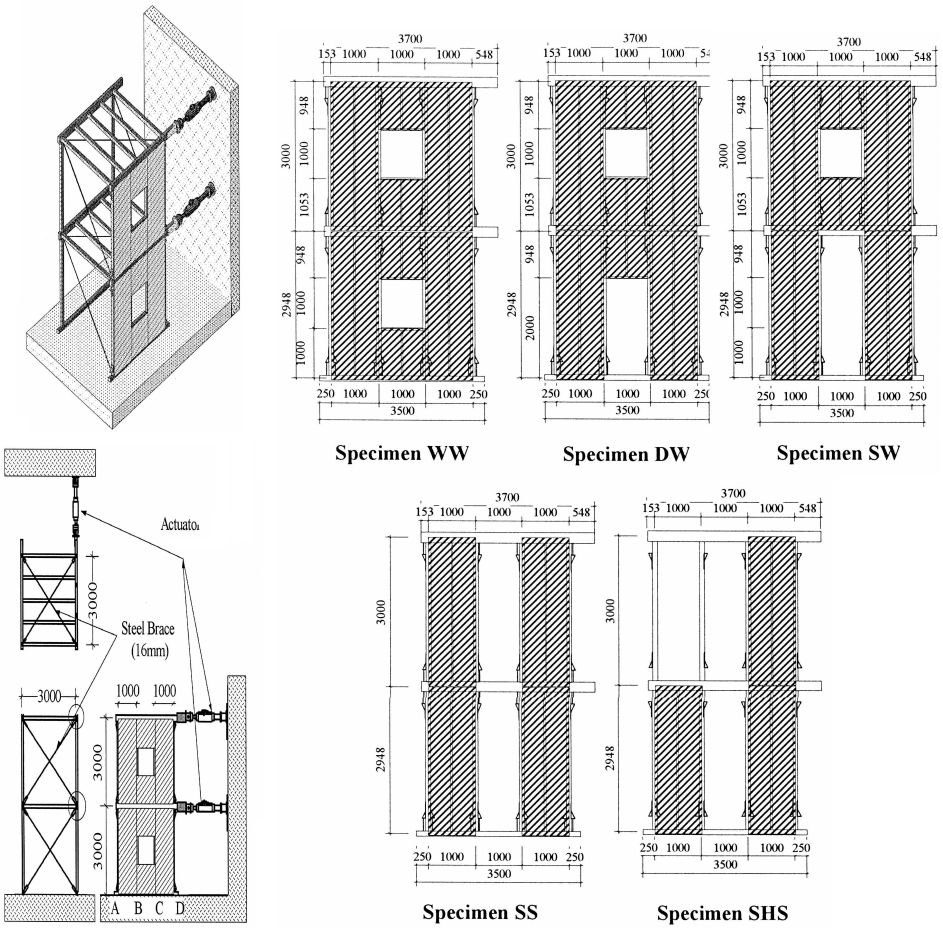

(a) Test Setup

(b) Configurations of specimens

Fig. 2.32: Pseudodynamic Test of Shear Wall Frames by Yasumura et al. Model, Yasumura et al. [146]

2.6.3 Building scale

The building scale is the last step of multi-scale analysis and the modelling of such structures depends on the previous definition of the smaller scale. One example of a multi-storey building will be considered for this scale, as performed by Ceccotti et al. [32] below.

Ceccotti et al. [32]

A cross-laminated (CLT) or (X-Lam) structure was studied by Ceccotti et al. [32] to investigate the seismic characteristics and make a comparison with the EC8 code. A shaking table test was performed for three- and seven-storey buildings with dimensions of 7.5× 13.5 m×23 m height. This shaking table test aims to evaluate the seismic performance of multi-storey CLT buildings and to determine the required parameters, such as force reduction factors, in order to design these buildings in earthquake regions. For the three-storey building, the thickness of the panels was 85 mm for the wall panels and 142 mm for the floor panels, while for the seven-storey building the thickness of both was constant at 142 mm for the two lower storeys, 125 mm for storeys 2 and 3 and 85 mm for storeys 4,5 and 6. The connections were calibrated according to monotonic and cyclic loads. The tests showed that the near collapse PGA value of the three-storey building is $1.2g$ for the Nocera Umbra record signal, a value which gives a behaviour factor of $q = 1.2g/0.35g = 3.4$, whereas for the seven-storey building the use of a behaviour factor of $q = 3$ and importance factor $\lambda_I = 1.5$ for strategic buildings shows no permanent deformation for all the listed signals, according to Ceccotti et al. [32]).

(a) Three Storey X-Lam Building (b) Seven Storey X-Lam Building

Fig. 2.33: Multi Storey Shaking Table Tests by Ceccoti et al. [32]

2.7 Conclusions

The seismic analysis of traditional and modern timber-framed structures has been investigated in different studies of experimental tests. The different tests show that the nonlinear behaviour of traditional buildings can be seen in differnt parts of the structure where as in the modern buildings the nonlinearity can be seen often in the connections. The experiments also show the good performance of traditional timber buildings in terms of energy dissipation, ductility, the redistribution load patterns throw differnt structural elements and the effects of the existence of vertical loads on the strength of these structures. Hysteresis curves provide an effective way to calculate the amount of dissipated energy in the system by drawing a cyclic load deformation diagram, and the monotonic curve is also important to give knowledge about the maximum resistance and deformations of different element scales of the structure.

3. STRUCTURAL DYNAMIC ANALYSIS

3.1 Introduction

Many ways have been used for the analysis of different loading sources according to the nature of loading. Seismic analysis can be performed by some approximate and more accurate methods, some of the static and dynamic methods will be explained in this chapter for the seismic analysis of structures. This chapter deals with a type of approach to numerical modelling of timber-framed buildings for the purpose of seismic analysis. The need for sufficiently detailed numerical models (to reproduce the local behaviours), however, with an affordable capacity in terms of conventional calculation, was highlighted in the previous chapter. The literature shows that multi-scale approaches help address this issue and that the laws of behaviour used for connections are essential for modelling timber-framed structures. The first part of this chapter will discuss the approximate analysis methods and the second part deals with the multi-scale approach and the third part deals with modelling the behaviour of metallic connections, which can be generalized to the studies of other levels. Some applications of this method of analysis for the traditional and modern building will be stated.

3.2 Dynamic structural analysis

In seismic engineering the distributed loads exerted by an earthquake are translated from the soil to the structure by foundation supports, in contrast to the other sources of loads that are translated from structural members to the earth. The general equation of motion (Eq.3.1) can be written as :

$$M.a(t) + C.v(t) + K.u(t) = p(t) \tag{3.1}$$

- The term $K.u(t)$ models the internal forces (or restoring forces), which are directed opposite to the motion. In the general case of nonlinear systems, the stiffness matrix is not constant and depends on $u(t)$. This is particularly the case for wood-framed structures, where it will be seen that the behaviour

is nonlinear and hysteretic. In the case of linear systems, the stiffness matrix is constant, which greatly simplifies the resolution equation .

- The term $C.v(t)$ models the viscous damping forces, which oppose the speed. For a linear system, the overall damping of the system is only due to this term. This is no longer the case for a nonlinear system, because the nonlinearity is associated with a dissipation energy, thus damping, commonly called structural or hysteretic. The overall damping of the structure is the sum of depreciation and viscous hysteresis.

- The term $M.a(t)$ models the inertial forces which oppose the acceleration. Although the timber-framed structure is light, the forces of inertia are not proved negligible. The masses are primarily at the roof and floors.

- The vector $p(t)$ is defined for each DOF of the biasing force due to the earthquake. The terms $p(t)$ are calculated from the accelerogram records of the earthquake and masses associated with each DOF.

When a model with a large number of DOF, time-history analysis (time-dependent) is necessary. This application has a significant means of calculations. This was involved in the development of simplified analysis methods. They make it more affordable to calculate the idealised behaviour of a structure, linear or bilinear, as well as calculating a particular response, typically the maximum displacement or stress, rather than the full-time response. Linear methods take into account the nonlinearity by multiplying appropriate factors. These approaches do not provide information on local behaviours. Three simplified calculation methods are generally used. The first method, particularly suitable for wood-framed structures, is the analysis of lateral forces. This is a special case of the second method, which is spectral modal analysis. Both methods are linear. The third method is pushover analysis, which is nonlinear.

3.2.1 Direct time integration methods

Newmark's integration method

In 1959, N. M. Newmark developed a family of time-stepping methods based on the following equations 3.2, 3.3 (Chopra)[34]. Their application to systems with multiple DOF can be carried out easily by extending the scalar equations linking displacements, velocities, and accelerations at times t_n and t_{n+1} into matrix equations (Paultre) [109].

$$\dot{u}_{n+1} = \dot{u}_n + [(1-\gamma)\Delta t]\ddot{u}_n + (\gamma\Delta t)\ddot{u}_{n+1} \tag{3.2}$$

$$u_{n+1} = u_n + (\Delta t)\dot{u}_n + [(0.5-\beta)(\Delta t)^2]\ddot{u}_n + [\beta(\Delta t)^2]\ddot{u}_{n+1} \tag{3.3}$$

The parameters β and γ define the variation of acceleration over a time step and determine the stability and accuracy characteristics of the method. A typical selection of γ is $\frac{1}{2}$ and $\frac{1}{6} \leqslant \beta \leqslant \frac{1}{4}$ is satisfactory from all points of view, including that of accuracy. Actually, where the constants γ and β are the usual parameters of the Newmark methods, with average acceleration ($\gamma = \frac{1}{2}$ and $\beta = \frac{1}{4}$) and with linear acceleration ($\gamma = \frac{1}{2}$ and $\beta = \frac{1}{6}$). These two equations combined with the equilibrium equation Eq. 3.1 at the end of the time step, provide the basis for computing u_{n+1}, $\dot{u}_{n+1}$, $\ddot{u}_{n+1}$ at time $n+1$ from the known u_n, $\dot{u}_n$, $\ddot{u}_n$ at time i. Iteration is required to implement these calculations because the unknown $\ddot{u}_{n+1}$ appears in the right side of the equations 3.2 and 3.3.
Expressing the equations of dynamic equilibrium 3.1 at time t_{n+1} yields Eq.3.4:

$$M\ddot{u}_{n+1} + C\dot{u}_{n+1} + Ku_{n+1} = p_{n+1} \tag{3.4}$$

Equations 3.2, 3.3, and 3.4 are used to determine the state of the system at time t_{n+1} by iteration. This iteration can be avoided as follows. Let us express the acceleration at time t_{n+1} from Eq. (3.3).

$$\ddot{u}_{n+1} = \frac{1}{\beta(\Delta t)^2}(u_{n+1} - u_n) - \frac{1}{\beta(\Delta t)}\dot{u}_n - (\frac{1}{2\beta} - 1)\ddot{u}_n \tag{3.5}$$

Replacing $\ddot{u}_{n+1}$ into Eq. 3.2, we obtain:

$$\dot{u}_{n+1} = \frac{\gamma}{\beta(\Delta t)}(u_{n+1} - u_n) - (\frac{\gamma}{\beta} - 1)\dot{u}_n - (\frac{\gamma}{2\beta} - 1)\Delta t\ddot{u}_n \tag{3.6}$$

Substituting Eqs. (3.5) and (3.6) into Eq. (3.4), we have:

$$\hat{K}u_{n+1} = \hat{P}_{n+1} \tag{3.7}$$

where

$$\hat{K} = K + \frac{1}{\beta(\Delta t)^2}M + \frac{\gamma}{\beta(\Delta t)}C \tag{3.8}$$

and

$$\begin{aligned}\hat{P}_{n+1} = P_{n+1} &\\ &+ M[\frac{1}{\beta(\Delta t)^2}u_n + \frac{1}{\beta(\Delta t)}\dot{u}_n + (\frac{1}{2\beta} - 1)\ddot{u}_n] \\ &+ C[\frac{\gamma}{\beta(\Delta t)}u_n + (\frac{\gamma}{\beta} - 1)\dot{u}_n + (\frac{\gamma}{2\beta} - 1)\Delta t\ddot{u}_n]\end{aligned} \tag{3.9}$$

The algorithm describing the Newmark integration methods applied to MDOF systems is illustrated in detail in many textbooks of structural dynamics e.g. [34], [109], [17], etc. We note that when we use linear analysis, the factorization of the effective stiffness matrix $\hat{K}$, which is the most costly operation in computing time, is carried out only once in the Newmark methods algorithm. It is interesting to know that the Newmark method with average acceleration is unconditionally stable, while the method with linear acceleration is conditionally stable, requiring a time step not exceeding a critical value Δt_{cr} given by:

$$\Delta t \leq \Delta t_{cr} = \frac{T_{n_{eq}}}{2\pi\sqrt{\frac{\gamma}{2} - \beta}} = 0.551 T_{n_{eq}} \tag{3.10}$$

where $T_{n_{eq}}$ is the period of the highest rank, i.e. the smallest period of the system with $n_{eq}DOF$. For a time step satisfying the stability limit, the Newmark method with linear acceleration is more accurate than the method with average acceleration. For finite-element models with a very large number of DOF, the period of the highest mode can be very small, requiring the selection of a very short time step when the method with linear acceleration is to be used. The computing time of the response of systems with a very large number of DOF can thus become extremely long. Consequently, we would generally prefer to adopt the unconditionally stable Newmark method with average acceleration rather than the method with linear acceleration, even though it is more accurate. Some recent researches suggest some modifications for Newmark's linear acceleration to be unconditionally stable, e.g. θ-Wilson method, and Hilber, Hughes, and Taylor ($HHT - \alpha$) (Hughes [81], Paultre [109]).

HHT-α integration method

Numerical damping cannot be introduced to Newmark's method without degrading the order of accuracy. Spurious high frequencies due to finite element modelling have to be filtered out. In fact, a certain amount of numerical damping can be used to control these spurious vibrations. We will see that the local truncation error of the Newmark method has the form $\tau(t) = \mathcal{O}(\Delta t^m)$, where m is the convergence rate. For the Newmark method, we have m = 2 when $\gamma = \frac{1}{2}$. We then say that the method has a second-order accuracy, and when m = 1 for any other value of γ the method has a first-order accuracy. We will also see that the Newmark method does not produce numerical damping for $\gamma = \frac{1}{2}$. Introducing numerical damping affects the accuracy of the Newmark method. Hilber, Hughes, and Taylor (Hughes[81], and Paultre [109]) proposed a method that produces numerical damping for higher modes while conserving a second-order convergence rate. This technique is known as the $\alpha - method$, but we will designate it as the $HHT - \alpha$ method. It uses the

Newmark difference equations 3.2 and 3.3 but modifies the equations of dynamic equilibrium as follows:

$$M\ddot{u}_{n+1}+(1+\alpha)C\dot{u}_{n+1}-\alpha C\dot{u}_n+(1+\alpha)Ku_{n+1}-\alpha Ku_n=(1+\alpha)P_{n+1}-\alpha P_n \quad (3.11)$$

The integration scheme uses the approach of the Newmark method. We substitute Eqs. 3.5 and 3.6 into Eq. 3.11 to get:

$$\hat{K}u_{n+1}=\hat{P}_{n+1} \quad (3.12)$$

where

$$\hat{K}=(1+\alpha)K+(1+\alpha)\frac{\gamma}{\beta(\Delta t)}C+\frac{1}{\beta(\Delta t)^2}M \quad (3.13)$$

and

$$\begin{aligned}\hat{P}_{n+1}=(1+\alpha)P_{n+1}-\alpha P_n+M[&\frac{1}{\beta(\Delta t)^2}u_n\\&+\frac{1}{\beta(\Delta t)}\dot{u}_n+(\frac{1}{2\beta}-1)\ddot{u}_n]\\&+C[(1+\alpha)\frac{\gamma}{\beta(\Delta t)}u_n+(1+\alpha)(\frac{\gamma}{\beta}-1)\dot{u}_n\\&+(1+\alpha)(\frac{\gamma}{2\beta}-1)\Delta t\ddot{u}_n]+C\alpha\dot{u}_n\\&+K\alpha u_n\end{aligned} \quad (3.14)$$

where we note that, for $\alpha=0$, the $HHT-\alpha$ method corresponds to the Newmark method. If $(-\frac{1}{3}\leq\alpha\leq 0)$, $(\gamma=\frac{1-2\alpha}{2})$, and $(\beta=\frac{(1-\alpha)^2}{4})$, we obtain an unconditionally stable second-order integration scheme [81]. Lower values of α, which is a negative value, lead to an increase of numerical energy dissipation. The algorithm of the $HHT-\alpha$ method is similar to that of Newmark's methods.

3.2.2 Approximate analysis methods

Lateral loads analysis method

We are in need of some simple methods to separate the analysis in each principal direction of the structure to reduce the computational effort. Another criterion for the use of this method is that the response of the structure must not be significantly

affected by the vibration modes other than the fundamental mode. This point is checked if the fundamental period is less than ($(4T_c)$ or 2.0 sec) (remember that T_c is the period of the end of the flat horizontal line of the spectrum curve). The fundamental period can be obtained in several ways, [65]

1. As a function of the height of the building (when the height of the building H $\leqslant$ 40 m), with ($T_1 = C_t H^{\frac{3}{4}}$), with the height H of the building in (m) and ($C_t = 0.05$) for wooden structures.

2. As a function of the displacement under gravity loads applied horizontally ($T_1 = 2\sqrt{d}$).

3. By using a more sophisticated or complicated method such as the Rayleigh method.

The seismic shear in the base of the structure (F_b) is equivalent to the static force at the dynamic loading expected. It is calculated for each main direction of the spectral product of the mass and acceleration. A corrective term λ appears to take account of the fact that in a building with at least three storeys with degrees of translational freedom in each main direction, the modal mass of the fundamental mode may not exceed 85% of the total mass of the building.

$$F_b = S_d(T_1)m\lambda \qquad \text{Or} \qquad F_b = \frac{S_e(T_1)}{q}m\lambda \qquad \text{for} \qquad T_1 \geq T_B \tag{3.15}$$

$S_d(T_1)$: acceleration spectrum for calculating the fundamental period $T_1(\frac{m}{s^2})$
S_e : the elastic response spectrum $(\frac{m}{s^2})$
m : the total building mass (kg)
q : behavior factor
λ : Correction coefficient $\lambda = 0.85$ if $T_1 \leq 2T_c$ and if the structure is more than two stories, otherwise $\lambda = 1.0$
In the case of multi-storey buildings, the force F_b is to be distributed on each level. The general formula is to calculate the distribution of shear force at each storey from F_b, modal displacements and modal masses.

$$F_i = \frac{s_i m_i}{\sum s_j m_j} F_b \tag{3.16}$$

F_i : Shear at level i (N)
m_i, m_j : Masses levels i and j (kg)
s_i, s_j : Displacements of masses m_i and m_j in the fundamental mode.

In cases where a linear distribution along the height of the building is assumed, this simple formula is proposed (Eq.3.17).

$$F_i = \frac{z_i m_i}{\sum z_j m_j} F_b \tag{3.17}$$

z_i, z_j : heights of the masses m_i and m_j (m)

Displacements are calculated linearly from the bias provided by the spectrum calculation. This spectrum is reduced by a factor of behaviour, the displacements d_s of a point on the structure is given by $d_s = q_d \, .d_d$ and d_d is the displacement of the point which is calculated linearly from the spectrum and q_d is the coefficient of displacement behaviour.

General method of modal spectral analysis

For the buildings whose response is affected not only by the first modes but also by the effects of several modes of vibration, and therefore do not satisfy the criteria for the use of the analysis of lateral force method, in this case, the modal analysis method is used. The model of the structure is linearly elastic and the design spectrum serves as a reference for stresses. As for the equivalent force analysis, the nonlinearity of the structure is therefore taken into account in the spectrum S_d by using the behaviour factor q. To ensure the answers for all significant modes are taken into account, it is necessary to verify that the sum of n modal masses exceeds 90% of the total mass, or that all the modes for which the modal mass is greater than 5% of the total mass are considered. The independence of two successive modes is verified by the relation (Eq. 3.18).

$$T_j \leq 0.9 \times T_i \quad \text{with} \qquad T_j < T_i \quad \text{and} \qquad (i,j) \in [1,n]^2 \tag{3.18}$$

If all the modes are considered independent of each other, the value of the variable considered E_E is calculated by a quadratic combination (Eq.3.19). If all modes are not independent, it is then necessary to make a complete quadratic combination that includes a correlation coefficient between the dependent modes [135].

$$E_E = \sqrt{\sum E_{E_i}^2} \tag{3.19}$$

Method of pushover analysis

The pushover method is composed of two separate phases: First, a **capacity curve** is calculated by a nonlinear static analysis under constant gravity loads and horizontal loads increasing monotonically. Then a **demand seismic curve** is

calculated by reducing the elastic response spectrum. The capacity curve can be obtained from both planes of the model (one in each principal direction) in the case where correctness criteria are met. Otherwise, a spatial model should be used and studied independently in two directions. The capacity curve represents the shear force in the base of the structure according to the displacement control, typically that of the roof of the structure. The choice of the vertical distribution of lateral loads is a crucial aspect of the method. Indeed, each mode of the structure is a vertical distribution of lateral loads. Thus, the vertical distribution corresponding to the fundamental mode will be equal to the distribution of forces during an earthquake in a structure having an imaginary straight only proper mode. The vertical load distribution is an approximation. Eurocode 8 ($EN1998-1$ [65]) has two vertical distributions that are considered to envelop the result. The first is a uniform distribution (Eq.3.20), where the force at i is proportional to the weight of level i and independent of the height. The second is a modal distribution (Eq.3.21) corresponding to the distribution of the lateral forces, determined by linear analysis for the first mode(s) of the structure.

$$F_i = s_i m_i \tag{3.20}$$

$$F_i = \frac{s_i m_i}{\sum s_j m_j} F_b \tag{3.21}$$

F_i : shear at level i (N)
m_i, m_j : mass levels i and j (kg)
s_i, s_j : displacementts of masses m_i and m_j in the fundamental mode
F_b : The shearing force to the base structure (N).
The force–displacement curves can be written in the form of Equation (3.22), with $\bar{F_i}$ ($\bar{F_i} \in [0,1]$), where the lateral forces are normalized and ϕ_i ($\phi_i \in [0,1]$) the displacements are normalized too ($1 \leq i \leq n$). This relationship models the behaviour of a system with n degrees of freedom (DOF).

$$\bar{F_i} = m_i \phi_i \tag{3.22}$$

The capacity curve defined by the relation (Eq.3.22) should be compared to the demand curve, which is obtained from the elastic response spectrum S_d. It is therefore necessary to transform the model with n degrees of freedom of the structure to a model with a $SDOF$ system. The mass of an equivalent $SDOF$ system m^* is given by the summation of Eq.3.23, the displacements ϕ_i are normalized, and actually we have $\bar{F_n} = m_n$.

$$m^* = \sum m_i \phi_i \tag{3.23}$$

The force F^* and displacement d^* of the system is equivalent to a system with a single degree of freedom ($SDOF$) and are respectively calculated from the shear force at the base of the structure F_b (Eq.3.25) and the displacement head d_n (Eq.3.26), and a conversion factor (Γ) (Eq.3.24).

$$\Gamma = \frac{m^*}{\sum m_i \phi_i^2} \tag{3.24}$$

$$F^* = \frac{F_b}{\Gamma} \tag{3.25}$$

$$d^* = \frac{d_n}{\Gamma} \tag{3.26}$$

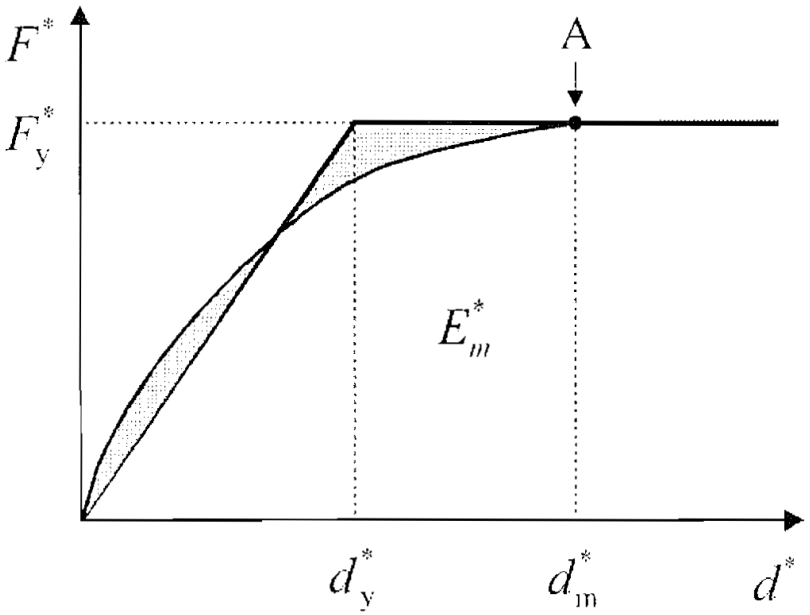

Fig. 3.1: Elasto Plastic Force Displacemnet relatioonship of SDOF.[65]

On the curve (Fig.3.1) $F^* = F(d_*)$ can obtained, marking a point on the curve (d_m^*, F_y^*) which lies on the behaviour of pure plasticity. The equivalent purely

elastic-plastic curve is calculated by equal energies in the interval $[0, d_m^*]$ (Fig.3.1). The displacement of the yield of d_y^* is given by the equation (Eq.3.27), noting E_m^* the area under the curve ($F^* = F(d^*)$). In the interval $[0, d_m^*]$. The natural period T^* of the system to an idealized DOF can then be calculated (Eq.3.28). Note that the choice of displacement d_m^* may be important to the final result, particularly in cases where the level of plasticity is not clearly defined. A correction method (iterative procedure) of d_m^* can be used where this approximation is considered too high. The details are given at the end of this part.

$$d_y^* = 2[d_m^* - \frac{E_m^*}{F_y^*}] \tag{3.27}$$

$$T^* = 2\pi\sqrt{\frac{m^* d_y^*}{F_y^*}} \tag{3.28}$$

The expressions established above define a system with SDOF equivalent to the nonlinear model of the structure. For the natural period T^* of this system, it can be establish the displacement demand d_{et}^* from the elastic response spectrum S_e. It can be looked then for the displacement target of d_t^* for which the curves of capacity and demand (inelastic spectrum S^i) are equal. The calculation of the inelastic spectrum is differentiated according to time periods, as shown in (Fiq. 3.2). For medium and long periods ($T^* \geq T_C$), which correspond to the zone of the spectrum where the velocity is constant, it can be used the principle of equivalence of maximum displacements (Fig.3.2-b). So it can be obtained $d_t^* = d_{et}$. For short periods ($T^* \leq T_C$), which correspond to the region of the spectrum where the acceleration is constant, d_t^* follows the principle of energy equivalence (Fig.3.2-(a)). For the cases where the capacity curve is greater in terms of the elastic spectrum $[\frac{F_y^*}{m^*} \geq S_e(T^*)]$, a direct equivalent displacement can be used, $d_t^* = d_{et}^*$. In the opposite case, energy equivalence means that, for the same loading, the elastic system undergoes a displacement d_{et}^* that is less than the elastic-plastic system d_t^*. The calculation of the target displacement d_t^* is given by (Eq.3.29).

$$d_t^* = \frac{d_{et}^*}{q_u}[1 + (q_u - 1)\frac{T_c}{T^*}] \quad \text{with} \quad q_u = \frac{S_e(T^*)m^*}{F_y^*} \tag{3.29}$$

To convert the standard spectral curve (T-S_a) to the (S_d-S_a) curve, we use (Eq. 3.30).

$$S_d = \frac{T^2}{4\pi^2} S_a \tag{3.30}$$

Where,
S_a is the psseudo acceleration,
S_d is the spectral displacement,
T is the period.

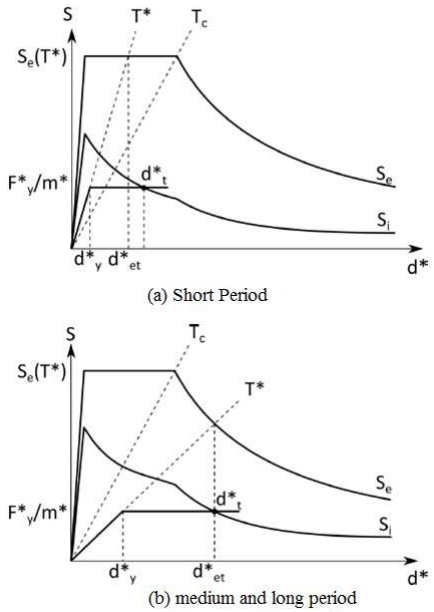

Fig. 3.2: Determination of the target displacement for the equivalent SDOF system.[65]

The value of d_t^* obtained by the pushover method lets us know the state of the structure for the loading under consideration. If the displacement d_t^* is very different from displacement d_m^*, an iterative procedure can be carried out to reduce the approximation induced by idealizing the nonlinear behaviour by a perfect elastic-plastic curve (sometimes with stress hardening or softening). It is simply repeating the method on the basis of computing d_y^* (Eq.3.27), replacing d_m^* by d_t^* (and the corresponding value F_y^*). Knowing that d_t^* must not exceed $(3 \times d_{et}^*)$.

3.2.3 Values of the behaviour factor

This section deals with the values of the behaviour factor (q) provided for wooden structures. Eurocode 8 defines two principles of the design of structures, the behaviour of dissipative or weakly dissipative structures. In addition, the ductility of the structures is classified into three categories as LDC, MDC, and HDC, meaning respectively Limited, Medium and High. The weakly dissipative design is used for structures in the LDC class. Structures classified as MDC or HDC can be

sized taking account of the dissipation of energy (Table. 3.1). Ceccotti and Sandhaas, [31] suggested a simplified approach to calculate the (q) factor for selected buildings by performing shaking tests, and estimated the (q) factor by dividing the near-collapse PGA to the designed PGA. The structure is classified as a class of ductility by means of rules or criteria of experimental resistance. The rules are a set of prescriptions for including the mechanical properties of materials and dimensions. The criteria of experimental resistance defines a maximum allowable loss in strength in a low cycle of quasi-static test. Finally, note that in cases where the building is non-regular in elevation, the behaviour factor given above should be underestimated by 20% in the lower limit of $q = 1.5$.
The existing of steel fastners increases the ductility class of timber elements and then increase (q), this is due to the high ductility of steel material. As shown in the table (3.1) that the maximum behaviour factor is (5) and this is small value as compared to steel which may reach in EC8 to (8) in the case when the value of (α_u/α_1[1]=1.6) knowing that (α_u/α_1) can be calculated by pushover analysis. The using of (q) factor is suitable for the calculations of the engineers in the site or office but it is conservative solution, so to benefit of all the strength of the the materials and for the application of limit state solutions which is more accurate and economic nonlinear analysis must be used as in the next section.

Tab. 3.1: Behaviour factor for the timber structures for the three ductility classes EC8 [65].

design concepts and ductility class	q	Examples of structures
Low capacity to dissipate energy DCL	1.5	Cantilever, Beams, Arches with two or three pinned joints, Trusses joints with connections
Medium capacity to dissipate energy DCM	2	Glued Wall pannels with glued diaphrams connected with nails and bolts, Trusses with doweld and bolted joints, Mixed structures consisting of timber framing (resisting the horizontal forces) and non load bearing infill
	2.5	Hyperstatic portal frames with doweled and bolted joints
High capacity to dissipative energy DCH	3	Nailed wall pannels with glued diaphragms, connected with nails and bolts, Trusses with nailed joints
	4	Hyperstatic portal frames with doweled and bolted joints
	5	Nailed wall pannels with nailed diaphragms, connected with nails and bolts

3.3 Advanced modelling of timber frames

The development in the world helps us to discover new materials, new technique and the need of decreasing the cost of construction techniques and due to huge developement in the computers makes the possibility to benefit of the full resistance of the materials by studying the behaviour of construction materials in the range

[1] α_u/α_1 is the ratio of the multiplier of the horizontal seismic design action at formation of global plastic to that of the first plastic hinge in the system.

away from elastic deformation, so many mathematical models were developed and nowadays it is easy to perform many complicated physical phenomenon and benefits of full resistance of the materials and reduced the costs, multi scale analysis method is a good tool which can be used to study different scales of structural elements with acceptable accuracy.

3.3.1 Multi-scale technique

In a numerical finite element method (FEM), the scale of discretization is a key parameter. It depends on the size of the modelled element, the type of results expected (global, local, or both) and computing resources available. For example, nailed connections can be finely modelled, representing the wood tip and interaction phenomena between them (Fig. 3.3).

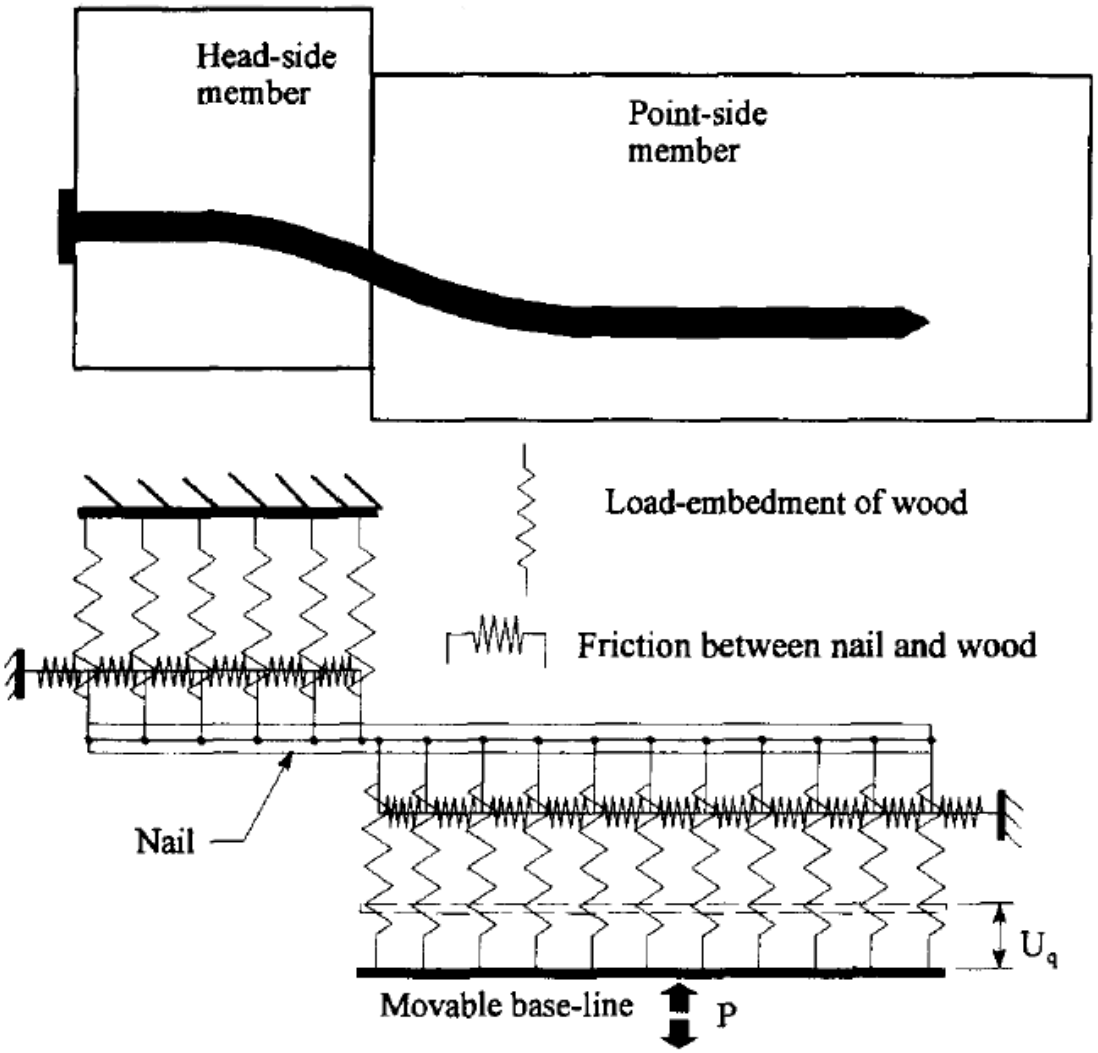

Fig. 3.3: Finite Element assemblage of naild wood joint.[38]

The global behaviour, as well as the local behaviour of the joints (embedment of wood, and plasticity in steel) can then be calculated. Such a scale of discretization does not, however, make it possible to study a structure of these assemblies. The development of the model and the need for calculations would make it difficult to overcome the constraints. The multi-scale approach is used to overcome this type of compromise and combine the benefits of modelling at each scale. The connections are modelled in a very simplified way by a two-node element. The constituted behaviour law is adopted to reproduce finely the hysteresis phenomena associated with it (see section 3.5). This law is calibrated according to the experimental

results. At the scale of the structure, the behaviour of the assemblies is thus represented finely through a macroscopic law that is much more "light" numerically. The quality of a multi-scale modelling is mainly given by two points:

- Behaviour law: The law used in the model is able to reproduce most of the actual behaviour of the elements.
- Simplified element: At each new level, the behaviour of the lower level is reproduced by a simplified element, with a limited number of DOFs. These DOFs must nevertheless allow this element to reproduce the actual deformation. For example, a system deformed under the combined effect of stress in compression and bending cannot be modelled by a unidirectional element (1-DOF) unless it is shown that the deformation due to one of the two is negligible compared to the other.

The multi-scale approaches are adapted for various fields, such as reinforced concrete structures [125], soil–structure interaction [69] or connections in semi-rigid steel structures [80]. Wooden frames are another area of study particularly suited to this type of approach [116], [63], [107] and [143]). This is illustrated by the behaviour of a cyclic experiment for three different scales (Fig. 3.4). It shows the behaviour of a nailed panel-framed joint connected in the tangential direction, a braced wall and a house under horizontal loads. At each level (scale), the behaviour is strongly nonlinear. It has pinched hysteresis loops and degradation resistance cycles with constant amplitude. These similarities in the behaviour highlight the importance of metal connectors in the overall behaviour of the structure, which shows the relevance of the multi-scale approach. This also shows that the ductility and energy dissipation in the wood-framed structures under seismic loading is largely related to these properties at the metal connectors. The identified three scales are metallic connectors, the elements of the structure, and the buildings. These similarities also show that a single law of behaviour must be able to reproduce the behaviour at each scale.
The same behaviour is observed for traditional timber frames with infilling across a wall, as shown in Figure (3.5). This suggests that for similar reasons, a multi-scale approach would effectively study the behaviour of the frames with infilling. This remark is further supported by observations in the next sections.
It can be concluded that this section by addressing the simplified elements techniques:

- Scale 1 - Metal connectors elements: A simplified model of connectors can be used by modelling a two-node element. This type of element has a maximum of 6 DOF (3 translations DX, DY, DZ and 3 rotations DRX, DRY,

DRZ). The selected DOFs depend on the type of connector and the needs of the model (the plane model (2D) limits the number of DOFs by neglecting the third direction effects). The most studied connections are nailed connections between the bracing panels and the wall framing members. These connections can be modelled by 3 DOF, 2 translations (DX and DY) for shear (orthogonally to the nail cross-section) and one translation (DRZ) in pullout-axial force (parallel to the nail length) (Collins et al. [39], Li et al. [97]).

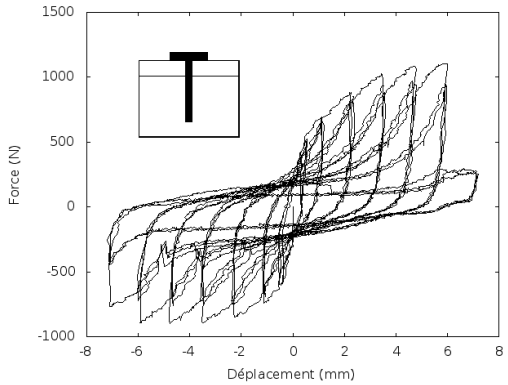

a) Nail

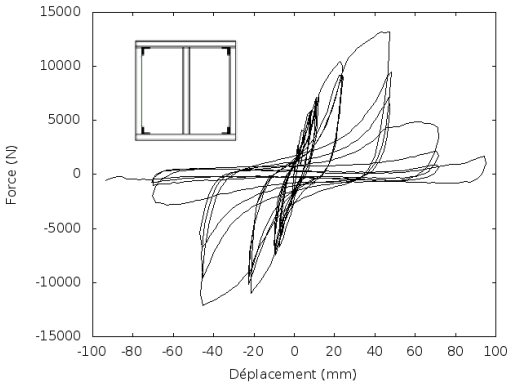

b) Shear wall

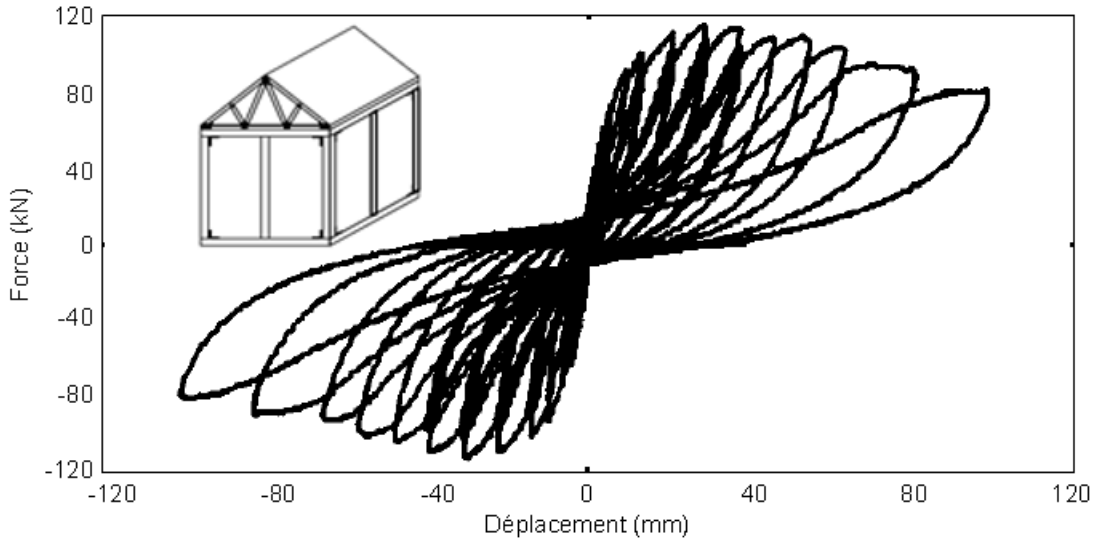

c) House [106]

Fig. 3.4: Different cyclic force-displacement experimental results at different studied scales modern wood frame, [18]

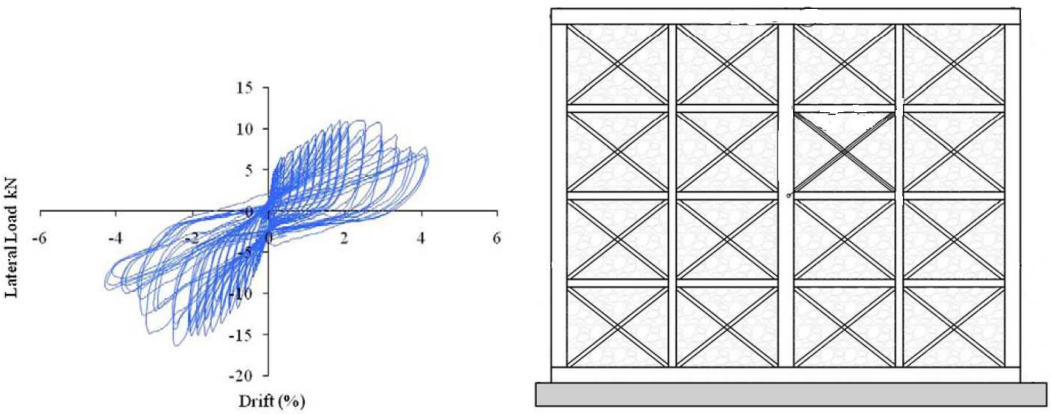

a) Lateral Force Drift relation b) Wall specimen

Fig. 3.5: Cyclic force-displacement experimental results of Dhajji-Dewari, [9]

On the other hand, for the cases where there are no sheathing elements, as in the case of traditional buildings where the connections connect the basic structural members, for instance the connections that were tested by Vieux-Champagne et al. [140], the model collects the shear resistance of the nails in addition to the steel strip device by an equivalent 2D element (see chapter 5). In most cases, the walls are drawings and models only for 2DOF. In the case of 2D problems, the translations DOF come from the shear resistance of the nails considered (Richard [116], Xu and Dolan [143], Christovasilis and Filiatrault [37], Folz and Filiatrault [63]). The literature includes work with other types of connectors (angles, hold-down, traditional, hybrids), but the principle is the same for the modelling.

- Scale 2 - Elements of the structure, unit cell: while modern structures are provided with bracing panels with a size suitable for the walls, traditional timber frames are braced by diagonal or inclined members. In most cases, even within the main structures formed by the beams and columns, it is observed that they contain groups of repeating elements in the structural form, which will be called a "unit cell or unit wall or elementary unit wall/unit cell" in this document. An example of the latter is illustrated in (Fig. 3.5) by a wooden frame braced by a St. Andrew's cross. Their behaviour is similar at each part in a wall, which is described for scale 3.

- Scale 3 - Elements of the structure wall: experimental tests show that under horizontal stresses, several phenomena can be observed:

- Rigid body motion of translation (Fig.3.6-(a)) which is especially seen when the stiffness of the bottom supports in shear is low compared with that of the wooden frame.
- Rigid body motion of rotation (Fig.3.6-(b)) which is especially seen when the anchor's stiffness with the foundation is low compared with that of the wooden frame.
- Pure shear (Fig.3.6-(c)) which is the dominant behaviour in modern frames.
- Bending of the wall (Fig.3.6-(d)), which is generally considered the second order at least for low-rise buildings.

The elements of simplified modelling of shear walls are generally composed of four linear bars with hinged joints that construct a frame. These elements often have one horizontal degree of freedom (Folz and Filiatrault [63], and Ceccotti and Karacabeyli [29], Richard [117], and Dujic Zarnic [53], Foliente [59], Ayoub [13]). The effect of the vertical degree of freedom is also studied to clarify the behaviour of the structure e.g. (Xu and Dolan [143] Van de Lindt et al. [133], Christovasilis and Filiatrault [37]). The constitutive law of the horizontal DOF is keyed from a force–displacement curve of experimental or numerical results for the shear wall. The latter can be obtained from the strength and the horizontal displacement (or drift) of the top corner, and the rigid body motion and bending and shear are taken into account in the simplified component.

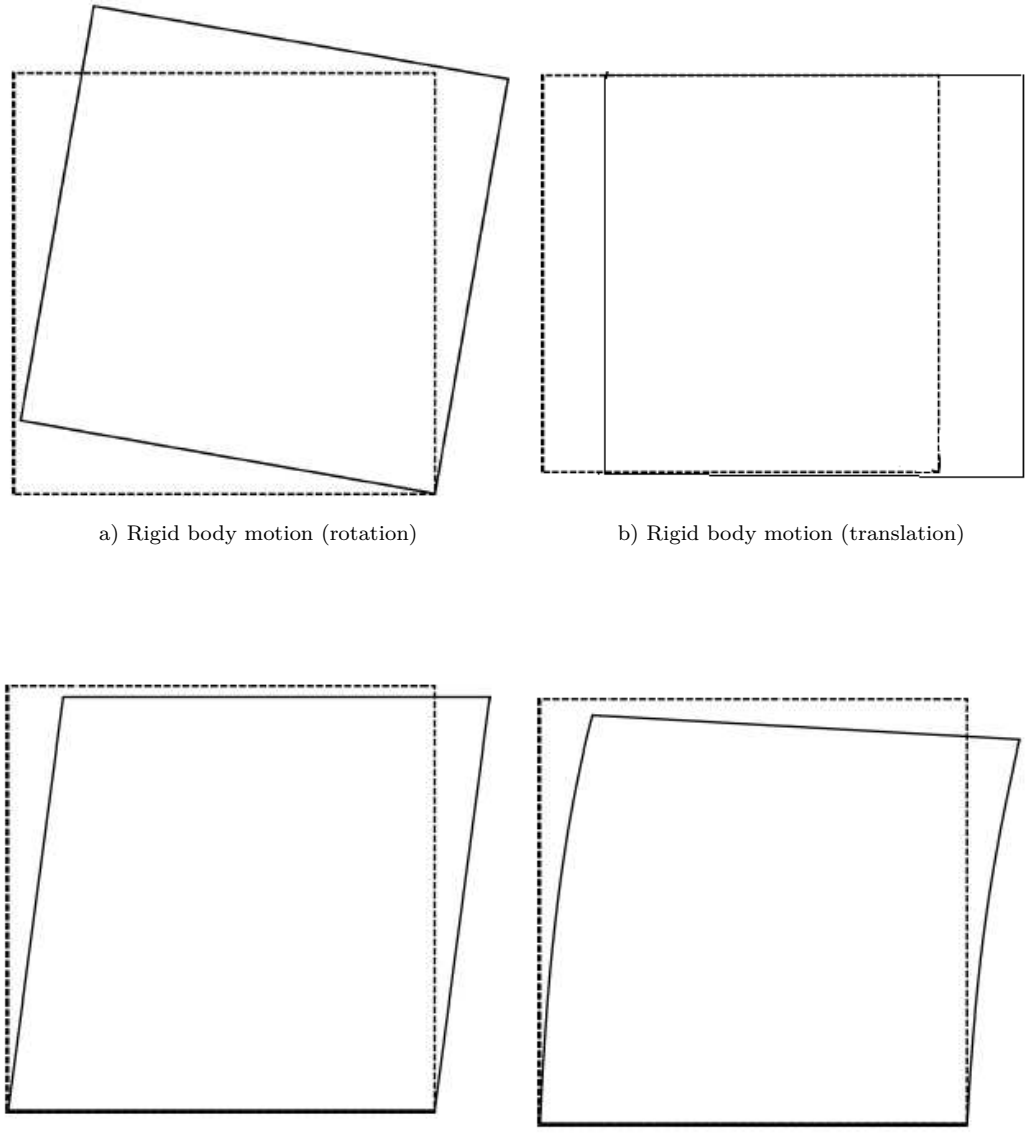

a) Rigid body motion (rotation)

b) Rigid body motion (translation)

c) Shear deformation

d) Bending deformation

Fig. 3.6: Failure modes of shear walls [18]

3.4 Hysteresis models

In timber structures many types of fasteners are used to connect the different wood members to ensure structural compatibility between them. These include nails, bolts, shear connectors or fasteners stiffened by steel strips (see for example [20], [92], [82], [83], [140]).

In earthquake engineering, loads are repeated frequently in both positive and negative directions, hence we need a constitutive model to account for these loading types and to assess the behaviour of the structures in both tension and compression periodically. Most of materials have nonlinear constitutive laws as well as some structural configurations like connections, and timber is one such material. So to perform an accurate modelling of the structural behaviour of these configurations a suitable hysteresis model must be designed to evaluate some important parameters in order to define as accurately as possible the real behaviour of such connections. These parameters which can be calibrated and estimated from the hysteresis curve are as follows:

- Ductility can be calculated if the curve reaches the damage level.
- Equivalent viscous damping (EVD) of the system Fig.(3.9):
- Degradation in the strength after each loop.
- Pinching that occurs at successive loops.

The hysteretic behaviour of elements reflects their ability to dissipate seismic energy. This behaviour is explained by the phenomenon of lamination of steel metal connectors and can be illustrated as follows.

- The cumulative damage explains the difference between the envelope curve of hysteresis loops and the monotonic curve. Indeed, each cycle causes damage in the wood and metal that adds to the damage already present (Fig.(3.7-a)). With more cycles of loading, the envelope curve moves away from the monotonic curve, resulting in a shift of displacement (d_m) away from the maximum force (Fig.(3.7-b)), called cap degradation in the literature, Ayoub [13]. However, this is only true to a certain extent, because for repeated constant amplitude cycles, the damage reaches its maximum after three to five cycles, Karacabeyli and Ceccotti [89]. This maximum damage will not be exceeded until the loading reaches cycles of higher amplitude.
- The degradation of the stiffness of load K_5 corresponds to the fact that as the amplitudes increase, there is a loss in the stiffness of the cyclic load. Fig.(3.7-c) shows the stiffness of the loading phase (i^{th}) cycle ($K_{5,i}$) to highlight this phenomenon.

- The degradation of stiffness discharge (reloading) (K_4) is the fact that over the amplitudes, the stiffness of a discharge cycle will decrease. Fig.(3.7-d) shows the stiffness of the reloading phase (i^{th}) cycle ($K_{4,i}$) to highlight this phenomenon.

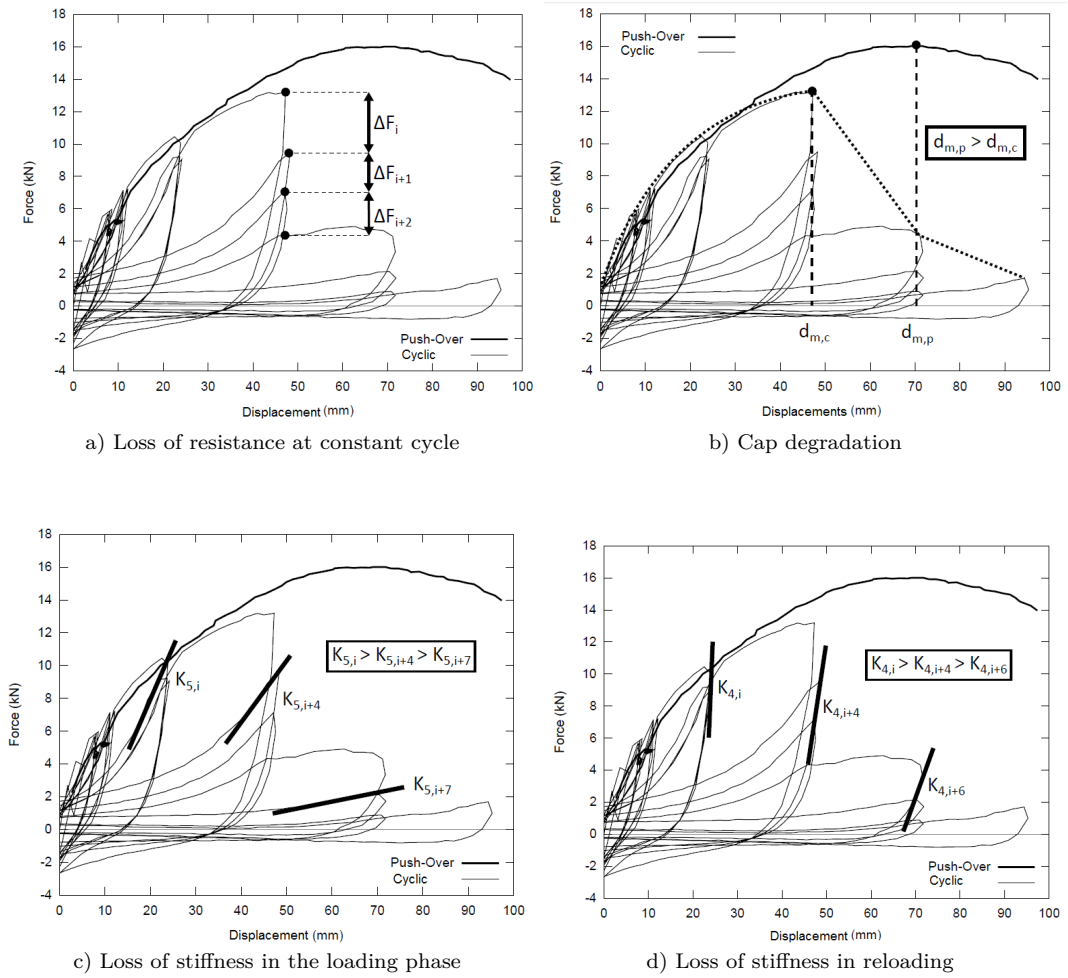

a) Loss of resistance at constant cycle

b) Cap degradation

c) Loss of stiffness in the loading phase

d) Loss of stiffness in reloading

Fig. 3.7: Effects of damage on the behavior of a structural elements of Wood frame, [18]

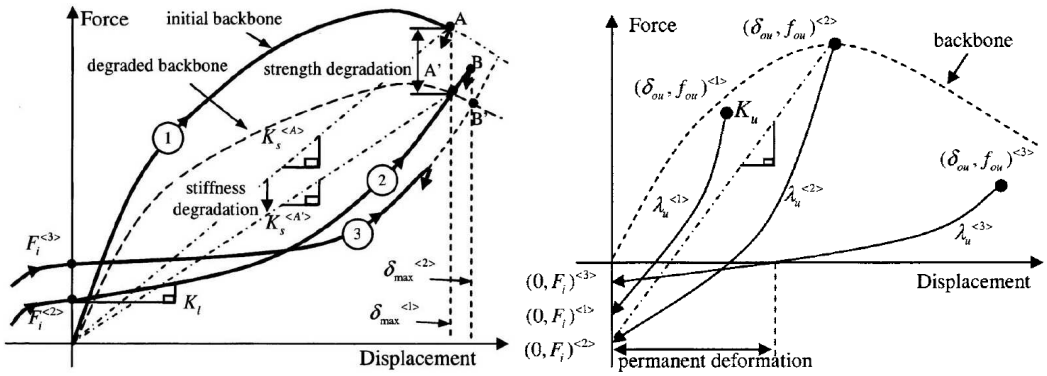

a) Loading curve model b) Unloading curve model

Fig. 3.8: Hysteresis parameters of Peng model [108]

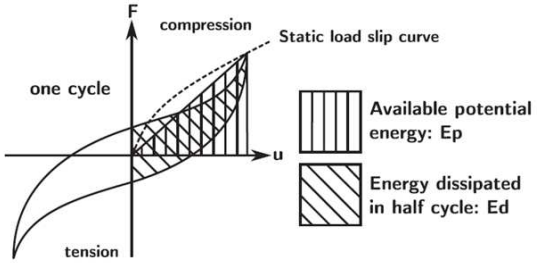

Fig. 3.9: Definition of Ed and Ep in determining the equivalent viscous damping ratio for one cycle.[139]

Many hysteresis models have been proposed in the literature, and there are also laws for monotonic nonlinear behaviour. In the following, we distinguish the phenomenological laws from mechanical laws.

- **Phenomenological laws**: Empirical Laws developed to reproduce a known behaviour (e.g. force–displacement relationships). Most phenomenological laws are formulated by input parameters and a set of rules determining the loading and unloading paths. Nevertheless, analytical approaches exist. They are formulated by input parameters and mathematical equations whose resolution generally provides the resisting force for a given displacement. The principle of these laws is to calibrate the input parameters in order

to reproduce the behaviour desired. It will be noted that ***phenomenological laws*** are by far the most widely used for the study of timber-framed structures under seismic loadings.

- **Mechanical laws**: Theoretical laws which attempt to model causes in order to reproduce the effects. In the case of wooden structures, this involves, for example, modelling a nail and taking into account the characteristics of the steel and all the mechanical phenomena occurring in the connection (crushing of the wood, pulling out of the connector, bending of the connector, etc.). Effective modelling of all these phenomena, based on strictly physical parameters, then allows the prediction of the behaviour of the connection.

3.4.1 Existing laws

Here we have a list of some examples of the principal hysteresis laws and their main characteristics, taken from the literature, to help understanding. The graphs which describe these laws are summarized in Appendix A.

Foschi (2000)

The Foschi model (2000) [66] is, to our knowledge, the only case of a hysteretic mechanical law listed in the field of earthquake resistance (we might mention the model of Chui et al. [38] which adopts a similar approach, but some of its parameters have to be calibrated in the same way as for a phenomenological model). A nail assembly is modelled, where the point is represented by an elastic-plastic beam which follows a law of hysteretic behaviour specific to steel. The wood has a nonlinear behaviour in compression, thus allowing spaces to be created between the tip and the wood in tension. The input parameters are the only physical quantities (y, E, etc.), enabling the laws of behaviour of the materials. The overall behaviour of the bond is obtained by calculating, for a given load, the deformation of the tip and of the elements. The difficulty of this type of law is to take into account all the phenomena observed during the tests. These include the crushing of wood, the localization at one or more points of the point, tearing of the tip and the friction thus created, or the passage of the head of the tip through the panel.

Ayoub (2007)

The model of Ayoub (2007) [13] is an evolution of the model of Clough (1966). The Clough model is identified by a trilinear envelope curve. The hysteresis loops are modelled by linear loading and reloading paths. This model does not allows to take into account the damage occurring with repetition of the cycles. Moreover, it should be noted that the quadrilateral shape of the hysteresis loops produced

by this model cannot accurately account for the energy dissipated during a test. Ayoub has introduced many improvements to the Clough model. First, the loading branch is bilinear, rather than linear as in the original model. Also the damage is modelled by taking into account the same factors as in the manner that is illustrated above in the (Fig.3.7).

EPHM (2007)

The Evolutionary Parameter Hysteretic Model (EPHM) of Pang et al. (2007), [108] is an evolution of the model of Folz and Filiatrault (2004) [62], itself based on the Stewart model (1987) [127]. Stewart's model takes a trilinear envelope curve and bilinear hysteresis loops in linear loading and reloading. Folz and Filiatrault have proposed a definite envelope curve by an exponential function, to model the rise in load better. The EPHM improves this model by adding the following points:

- The degradation in force works such that for a maximum amplitude of each loading cycle, the retained force is that of the envelope curve. For the next loading which has this amplitude, the returned force will be that of a degraded envelope curve. Since the degraded envelope curve is unique, the damage is not cumulative, because this implies that $\Delta F_i \neq 0$ and $\Delta F_{i+1} = \Delta F_{i+2} = ... = 0$ (see Fig. 3.7-a).
- The degradation of the stiffness of the reloading (Figure 3.7-d) is a function of the amplitude of the cycle.
- From the variation of the force, which has zero displacement, it is observed that in fact it is the hysteresis loops intersecting the axis of the ordinates of a force–displacement diagram, at varying levels of force (first increasing and then decreasing).
- The envelope curve is defined by two exponential functions, one modelling the pre-peak part and the other the post-peak part. The hysteresis loops are modelled by exponential functions, one for the loading branches and the other for the reloading branches.

Q-Pinch (2005)

The Q-Pinch model proposed by Judd (2005)[87] is a combination of the Q-Hyst of Balendra et al. (2013)[15] (an evolution of the Clough model (1966) [18]) for small displacements and the model of Folz and Filiatrault (2004)[62]) in large displacements. The envelope curve is defined by an exponential function in both cases. The idea of combining two models is related to the following observation:
For small displacements, the hysteresis loops are not pinched, and a rise in linear

load (Q-Hyst) represents this behaviour well. For large displacements, however, the hysteresis loops are pinched, and a rise in bilinear load (Folz and Filiatrault) makes it possible to represent it well. In addition, the degradation of reloading stiffness is added. Its consideration is inspired by Takeda et al. (1971)[128], such that the reloading stiffness is a variable fraction of the initial stiffness.

Ceccotti (1989)

The model of Ceccotti and Vignoli (1989)[33] is also known as the Florence model, Ceccotti and Nart [30]. It is based on a trilinear envelope curve. The loading and unloading branches of the hysteresis loops are bilinear. This model does not take into account the damage.

Collins (2005)

The model of Collins et al. (2005)[39] is an evolution of the models of Dolan (1989)[49] and Kasal and Xu (1997)[39]. The first evolution of Dolan's model was introduced by the author himself in 1991 [50]. Historically, the Dolan model is the first to define the force–displacement evolution by exponential functions, rather than by a succession of straight lines of stiffness. The envelope curve is constituted by an exponential curve up to the peak of force and the post-peak part is linear. The loading and reloading branches of the hysteresis loops are exponential functions. The use of these functions allows more precise modelling of the behaviour of wood structures. Nevertheless, this type of definition can give rise to problems of continuity between the branches of the model for certain sets of parameters. Moreover, it should be noted that the Dolan model does not propose to take account of the damage, the ends of the peaks of the hysteresis loops being in each case placed on the envelope curve of the model. The Collins model takes account of the damage as a function of the loading history, while the degradation of the force at each peak is a fraction of the previous peak force.

Humbert (2010)

The model of Humbert (2010)[82] is an evolution of the model of Daudeville et al. (1998), [44], Richard (2001) [117]. The latter relies on the models of Dolan (1989)[49] and Yasumura (2001)[82]. The model of Yasumura defines the branches of the hysteresis loops in a linear manner, but with stiffness dependent on the displacement reached. This makes it possible to model the deterioration of stiffness of loading and reloading. The damage in strength is not modelled. Richard's model combines this approach with the Dolan model, in which the branches of the hysteresis loops are exponential functions. The stiffnesses that evolve from the displacement are the stiffnesses of the asymptotes to the exponential curves.

The other principle is that Richard's model is concerned with the modelling of damage. Degradation in force is modelled such that the peaks of the hysteresis loops are lower than the envelope curve. The calculation of the force at the peak of a hysteresis loop is based on the value of the force of the envelope curves at the same displacement and a coefficient of damage. This coefficient is calculated from the previously achieved forces as well as from the damage parameters. The Humbert model replaces the exponential functions with *Bézier* polynomials. This makes it possible to ensure the continuity between the different branches of the representative curve of the model. In addition, the damage taken into account is modified. In fact, in Richard's model, the damage is calculated from the force reached in the opposite direction. This does not make it possible to correctly model the response to a very clearly asymmetric loading, which may be the case during earthquakes. Humbert's law therefore calculates the damage in one direction, depending on the loading history in that direction. In addition, this damage is cumulative. Whenever the force changes sign, the amount of damage due to the last cycle is calculated and added to the overall damage of the model.

BWBN (1985)

The updated version of the BWBN (Bouc, Wen, Baber, and Noori) model [14] was presented by Xu and Dolan [144] for the study of vibrations in mechanical systems. It is an analytical hysteretic model taking into account energy dissipation, degradation of force resistance and stiffness, as well as pinching of the hysteresis curves. The principle of the model is that the element is to be modelled with an oscillator with one degree of freedom and then it was generalized to MDOF. [74] . This oscillator consists of a mass, an elastic spring, a hysteretic spring and a damper. The behaviour of the hysteretic spring is defined by a function which comes from the solution of a differential equation involving several parameters of the model (including parameters of the degradation of force and stiffness of reloading), as well as a function of pinching. The solution of the equation of motion of the oscillator at each instant makes it possible to determine the force as a function of the loading imposed. This model was improved by Foliente (1995) [59] and [60] to adapt it to the study of timber structures. Evolutions are new formulas for calculating the degradations in strength and stiffness. More recently, as mentioned above, it was Xu and Dolan (2009) [144] who evolved this model, replacing a coefficient by a function in order to enhance the modelling of the post-peak part. The other modifications are more theoretical and allow the numerical stability of the model to be improved.

Synthesis

Table 3.2 provides a synthetic comparison of the laws of behaviour. It is observed that for the different quality models, of course, there are also differences in the complexity of the implementation. The choice of a law for the realization of a study depends on these two parameters. The simplest laws in terms of implementation, such as in Ceccotti and Vignoli [33], which do not take into account the phenomena of damage, are used for studies when the provided quality of the modelling is sufficient and when the calculations are long and numerous (Ceccotti and Sandhaas, [31]), (Schadle and Blass, [122]). The two models which give the best results (BWBN and Humbert) are also the most complex to implement. The main difference between these two models is the ability of Humbert's law to model non-symmetric behaviours, such as assemblies by square or tooth, and strip plates. The last case cannot be achieved by the BWBN model, so in our study we used Humbert's model which will be called Hysteretic constitutive law.

3.5 Hysteretic constitutive (Humbert's law)

Hysteretic constitutive law [83] has been developed with the aim of modelling any assembly of wood and metal connectors under quasi-static and dynamic loads. Most laws in the literature do not satisfy this condition by not taking into account damage or asymmetric behaviour. It is for this reason that this law was chosen for the numerical modelling of the structures referred to in this study. So in this part, the behaviour of the law will be described in detail.

3.5.1 Description of Hysteretic constitutive law

Figure (3.10) shows the unidimensional behaviour law as a force–displacement curve. It consists of a curve modelling the behaviour under monotonic loading and hysteresis loops. The monotonic curve has a linear elastic branch (0) followed by a polynomial arm (1) (modelled in the present study according to Bezier's curves [83]) extending to the peak force, followed by a softening behaviour which is modelled by two consecutive losses of rigidity, corresponding respectively to two rectilinear branches (2) and (3). The mechanical disruption of the modeled system occurs for displacements extending beyond the branch (3).
The hysteresis loops are described by two numbered arms (4) and (5) and limited firstly by the envelope curve (derived from the monotonic curve) and secondly by the abscissa axis. These boundaries between different branches of the law are indicated by dots in Fig.(3.10). Maintaining a versatile behaviour in both tension (positive) and compression (negative) is assumed to be different, so the parameters

Tab. 3.2: Synthetic Comparison between some types of hysteresis models [18].

	Envelope Curve	**Hysteresis Curve**	**Damage**
Foschi	Non linear behaviour for timber and hysteresis for steel		Damage to steel and wood modeling by a Mechanical representation phenomena
Q-Pinch	Exponential function	Bilinear or trilinear according to amplitude	Damage not consider
Ceccotti	Trilinear	Trilinear	Damage not consider
Ayoub	Trilinear Curve	Trilinear Curve	Damage in force, stiffness and reloading of position of peak of force in function of dissipated energy
EPHM	Two exponential functions	Two exponential functions	Damage not cumulative
Collins	Exponential function and Linear for post peak	Two exponential functions	Damage in force in function of force at the previous peak
Humbert	Linear and Polynomial and Bilinear for post peak	Polynomial	Cumulative Damage forces and stiffnesses in function of loading history in terms of displacements or forces
BWBN	Exponential form of the solution of analytical problem	Exponential form of the solution of analytical problem	Damage in force based on dissipated energy

of the monotonic curve are duplicated in two sets reported by the exhibitors (+ve) (tension) and (-ve) (compression). In the absence of an explicit index, reference is made indifferently to the two directions of loading. As illustrated below, there are five main stages, through the propagation of the loading, unloading, and reloading stages as follows:

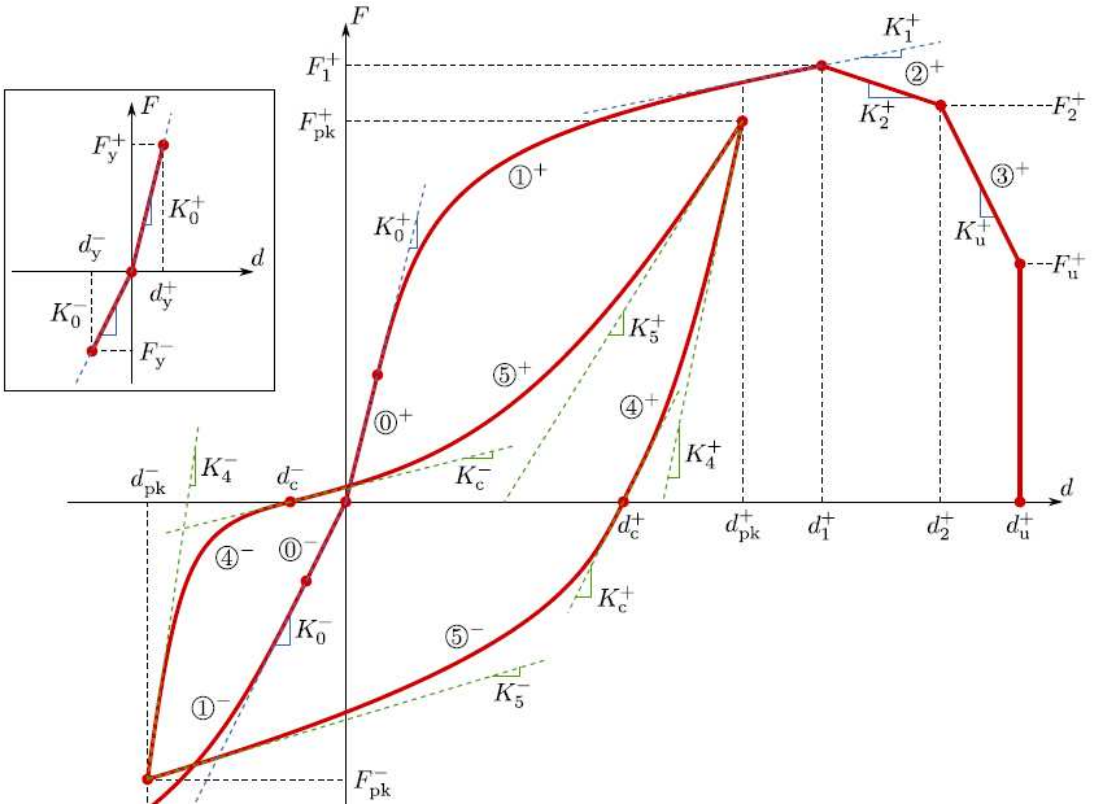

a) Main definitions of Hysteretic constitutive law

$$d_c^+ = \begin{cases} C_4^+ \cdot d_0^+ & (C_4^+ \geqslant 0) \\ d_{pk}^+ - \dfrac{F_{pk}^+}{|C_4^+| \cdot K_4^+} & (C_4^+ < 0) \end{cases}$$

$$K_5^- = \begin{cases} C_2^- \cdot \left| \dfrac{F_{pk}^-}{d_{pk}^-} \right| & (C_2^- > 0) \\ |C_2^-| \cdot K_0^- & (C_2^- \leqslant 0) \end{cases}$$

$$K_4^+ = \begin{cases} C_1^+ \cdot \left| \dfrac{F_{pk}^+}{d_{pk}^+} \right| & (C_1^+ > 0) \\ |C_1^+| \cdot K_0^+ & (C_1^+ \leqslant 0) \end{cases}$$

$$K_c^+ = \min\left(K_0^+ \; ; \; C_3^+ \cdot \left| \frac{F_{pk}^-}{d_c^+ - d_{pk}^-} \right| \right)$$

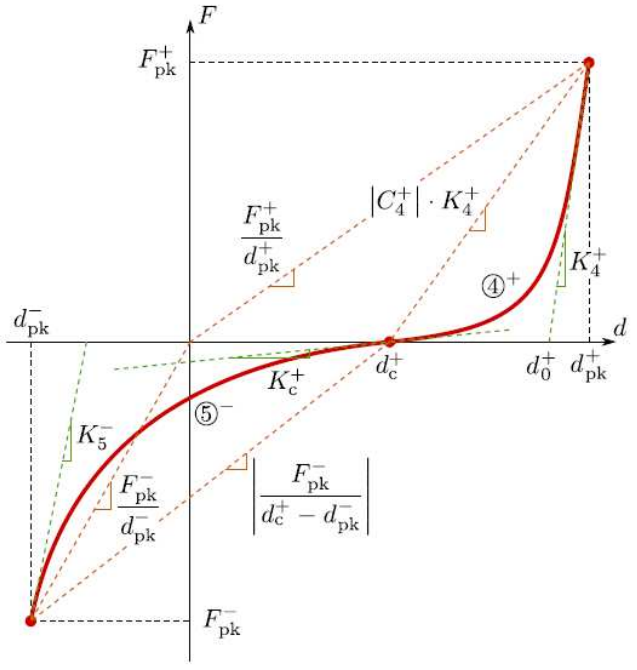

b) Definition of hysteresis loops

Fig. 3.10: Hysteretic constitutive law of semi rigid connection for 1D [83]

Branch(0):Initial linear elasticity

Initial linear elasticity is necessary when we have very small displacements and to ensure the rapid convergence of the calculation, the linear elastic leg is limited by the displacement $d < d_{y^+}$ for tensile and $d > d_{y^-}$ for compression. It can be traversed in two directions, but once this branch has been left (for $d > min|d_{y^-}, d_{y^+}|$), it is not possible to return. Generally, d_y is limited to values that are very low because the extent of the linear elastic behaviour of metallic connectors in wood structures is difficult to quantify in the experimental tests, and the behaviour quickly becomes nonlinear (no free boundary between linear and nonlinear).

Branch (1): Loading until peak point

This Branch can be activated in tension and compression, only in the direction of load (increased displacement and force). It is activated from the branch (0) (exceeding the elastic limit in motion: d_y). It is also activated during a recharge exceeding the maximum previous from branch (5). Loading to peak force activates the branch in tension and compression only in the load direction (increased displacement and force). It is activated from the leg (0) (the limit is exceeded the elastic displacement: d_y). It is also activated when a refill surpasses the previous maximum from the leg (5).

Branch (2): First loss of stiffness

It is activated from branch (1) during loading greater than d_1, or at a charging exceeding the maximum from the previous branch (5).

Branch (3): Second loss of stiffness

This branch starts from branch (2) during loading greater than d_2, or during a recharge exceeding the previous maximum from the leg (5).

Branch (4): Nonlinear elastic unloading

The arm (4) models a nonlinear elastic hysteresis loop unloading. (Fig.3.10). For unloading initiated from one of the branches (1), (2), (3) or (5), we defined d_{pk} as the maximum displacement (absolute value) reached in time step t^n before the initiation of this discharge. It is the displacement to the peak, but it is not necessarily the maximum displacement d_{max} under all loading history. The unloading branch (4)(which is activated at t^{n+1}) then extends from the last peak (at abscissa $d = d_{pk}$) till the intersection with the abscissa axis at $d = d_c$. The value of the force at $d = d_{pk}$ is denoted as F_{pk}. The initial stiffness K_4 can be obtained as

illustrated in (Fig. 3.10) by using parameter C_1 multiplied by either effective stiffness at point (d_{pk}, F_{pk}) or initial stiffness of loading. It is determined during the preceding load on one of the branches (1), (2), (3), or (5), by a homothety of the monotone curve, (eqn.3.31).

$$F_{pk} = (1 - D)F_{mono} \tag{3.31}$$

F_{mono} is calculated from the current displacement on the monotonic strength curve (curve composed of branches (0), (1), (2) and (3)), and D is a scalar coefficient for damage to the relevant (tension or compression) part. This coefficient, initially equal to 0, is set to update only at the first time step t^{n+1}, for which a change in direction is detected (sign change of force), using the following formula:

$$\Delta D = D^n - D^{n+1} = \eta(D^n - D^\infty) \tag{3.32}$$

D^{n+1} is the new damage coefficient from time step t^{n+1} for which there is now an unloading ($\Delta d < 0$), D^n of the previous coefficient until time step t^n for which there was still loading ($\Delta d > 0$), and the theoretical damage to D^∞ is an infinite number of cycles, and η is a coefficient controlling the effect on the damage of cycles. The damage limit D^∞ is calculated from the force or displacement maximum depending on the desired pattern of damage. In general, we prefer the displacements of the model. It is thus found that each cycle of the current hysteresis loop damage (reducing in the absolute value of maximum force) compared to the previous one was a cumulative damage to all loops. The value of η is determined from the experimental tests. The model of the damage occurring assumes that the evolution of D infinity is linked to the F_{max} maximum force reached during the loading history by a power law AC and AR parameters. The model is a similar in terms of displacement and assumes that this trend is linked to a maximum displacement by d_{max} power law parameters BC and BR.

$$D^\infty = AC(F_{max})^{AR} \quad \text{or} \qquad D^\infty = BC(d_{max})^{BR} \tag{3.33}$$

Branch (5): Nonlinear reloading

Branch (5) is a rational Bezier curve [82] from $(d_c, 0)$ to (d_{pk}, F_{pk}). By continuity, the tangent at the origin is K_c. The slope of the peak corresponds to K_5 stiffness, calculated in the same manner used to calculate K_4 but with a coefficient C_2 instead of C_1. When loading exceeds d_{pk}, we go on next load branches (1), (2) or (3) according to the value of the displacement current d.

3.5.2 Synthesis parameters

A complete listing of the input parameters of the model is presented below. There are three categories of parameters. The parameters used to calibrate the monotonic curve, called "monotonous" parameters for simplicity, forces, displacements and stiffness are the main parameters that define the monotonous curve model. The parameters used to calibrate the curve cycles, called "cyclical", also for simplification, are coefficients that define the shape of the hysteresis loop. Finally, the damage parameters are coefficients defining the power law and the increment of damage at each new cycle.

Monotonous parameters

- d_y: Yield point.
- d_1: Displacement of maximum force of monotone curve.
- d_2: Displacement limit of the first post-peak stage
- d_u: Ultimate displacement of monotonous curve.
- K_0: Initial stiffness of the monotonous curve.
- F_1: Force Maximum in the monotonous curve.
- K_1: Tangent stiffness at the point (d_1, F_1).
- K_2: First post-peak stiffness.
- K_u: Second post-peak stiffness.
- V_1: First factor of *Bézier* weights for the branch (1).
- W_1: Second factor of *Bézier* weights for the branch (1).

Cyclical parameters

- C_1: Coefficient defining stiffness discharge K_4.
- C_2: Factor for the load stiffness K_5.
- C_3: Factor for the stiffness to zero force K_c.
- C_4: Coefficient defining the x-zero dc power.

- V_4: First factor of *Bézier* weights for unloading branch.
- W_4: Second factor *Bézier* weights for unloading branch.
- V_5: First factor *Bézier* weights for the branch load.
- W_5: Second factor *Bézier* weights for the branch load.

Damage parameters

- AC: Multiplier law damage strength.
- AR: Power Law of damage strength.
- BC: Multiplier law of damage on the displacement.
- BR: Power Law of damage on the displacement.
- η: Coefficient acting on the increment of damage between each cycle.

The number of parameters are (24), as presented above, is high. However, the processing of the law is relatively simple and quick. Indeed, the *Bézier* weights (V_1, W_1, V_4, W_4, V_5, and W_5), set to 1 by default, do not usually need to be changed. The damage is based on either the strengths (AC and AR) or displacements (BC and BR). It is therefore necessary to calibrate only one of the two pairs of parameters. This leaves 16 parameters, including 9 (monotonic parameters) that are identified directly on an experimental monotonic curve. The cyclic parameters (C_1, C_2, C_3 and C_4) can be estimated, in a first approach, from the experimental observation of a cyclical pattern. The remaining parameters are identified by comparison of the experimental and numerical results, and changing settings until a satisfactory match is obtained.

Limitations of the law

The Hysteretic constitutive law (2010) is used for numerical modelling by according to its versatility and its modelling quality, particularly in terms of the cumulative damage. However, it should be noted that this law is unidirectional, otherwise, it can be modelled in two or three dimensions. Depending on the case, different kinds of hypotheses are possible to ensure correct modelling.

3.6 Numerical investigations of timber frame with infilling

The timber-frame structures developed in largely populated areas of the world many years ago, e.g. Britain, France, Germany, Central America, South America, Turkey, Portugal, etc., are known as half-timber, colombage, Fachwerk, taquezal or bahareque, Himis and Gaiola, respectively [79]. These were used due to reasons such as the availability and relatively cheap price of the material in nature and its ease of use, with some interesting properties like light weight which reduces the inertia forces and gives a reasonable tension strength. On other hand, they have low compression strength and a brittle nature in failure [92], [86]. The latter property is not desirable in general and especially in seismic settings, but this behaviour can be improved by adding steel nails in the joints to increase the ductility of these types of structure. These traditional timber-framed structures with infilling of rocks (and/or brick) and locally obtained mortar are distributed all around the world, with different structural details according to the culture of each region.
From the data available in the literature, this section describes the different methods which were used for numerical analysis of the seismic behaviour of infilled timber-framed structures. These methods can be applied to four scales of connection, unit cell, wall, and building and are divided into two different types:

- The detailed methods used for carrying out the modelling of the structure.
- The simplified approach of modelling the overall behaviour of a structure by a combination of individual elements describing the behaviour of the substructures that compose it. Several techniques are used to describe the modelling: the localized plasticity model (lumped plasticity approach) method, the equivalent frame method or the wide-column analogy [91], [88], [100], and [7].

In this thesis, for each of these studies, the relevant observations regarding the development of the approach (see chapter 4) were analyzed and are summarized in the next items.

3.6.1 Detailed modelling

A detailed modeling is defined as any numerical work aimed at modelling accurately the reality, where each element of the structure (connections, timber members, infilling, mortar, etc.) has a more or less complex law of behaviour. The compromise is usually use to make a balance between time and the required accuracy. The work of both Kouris and Kappos [92] and Hicyilmaz et al. [79] on timber frames with infilling was analysed in detail. Indeed, the results of these detailed models are the only validated tests from experimental work for the scale of the

wall. In addition, other detailed models have been developed for these structures with infilling, almost all based on the case of an elastic analysis. This research focuses on Pombalino buildings which are mainly available in the centre of Lisbon (Portugal) [114], [25], and those of the same type located in Greece on the island of Lefkada ([101], [141]), but also in Athens ([129]).

Wall scale

Kouris and Kappos [92]
This study aims to predict the behaviour of a timber structure with infilling from pushover analysis. The study has two stages: the first is to model accurately the wall of the experimental test, from which the results are used to validate the model. The second stage is to suggest a simplified approach to reproduce the behaviour of the wall (discussed in section 3.6.2). The timber members are modelled in tension and compression by a trilinear behaviour (σ, ϵ) whose last straight portion is a plateau (flat), which is highly disputable in light of the brittle behaviour of the materials. Wood anisotropy is taken into account according to the Hill criterion. The authors define the material parameters based on the standard [55], as in general it is not possible to carry out destructive tests on historic structures. Finite elements for four nodes (QUA4), as shown in (Fig. 3.11), with each node having two degrees of freedom, were used in plane stress. The infilling is not modelled, but its mass is taken into account indirectly in each of the timber diagonals by reflecting the equivalent wood mass using (Eq. 3.34).

$$A_{inf} * \gamma_{inf} + A_{diag} * \gamma_{diag} = A_{diag} * \gamma' \tag{3.34}$$

where:
A is the area and γ the weighted density.

In addition, the uniaxial timber members working indirectly takes into account the effects of containing of the infilling in the timber frame, which neglects the risk of buckling. The timber-to-timber contact in the case of old buildings often has corroded steel fasteners (oxidation and defects over time), which then do not play their role. For this reason, they are not taken into account in this study. And timber-to-timber contact as modelled by the Mohr–Coulomb contact law, with c=0 and $\mu = 0.5$, can only transmit compressive forces and shear. This amounts to the basic Coulomb's law friction (an analogy with sand-like structures). The model reproduces a monotonic test which is compared to cyclic testing of the frontal walls. The mechanical class of timber is C24, but the mechanical properties taken into account are degraded to consider the effect of the loading time and the effect of moisture on the strength of the structure. The detailed model correctly estimates the initial stiffness and ultimate strength of the structure. However, the tri-linear

shape of the curve is unable to follow the cyclical envelope curve of the experimental testing results. It is interesting to note that the maximum resistance is achieved because the internal force in the wood has reached the maximum stress of the material model with a flat line. The timber has reached its maximum strength and can be deformed to a value three times greater than its elastic displacement. No information is given on the nature of the stress (shear or compression). This study does not seem relevant from the point of view of the difficulty of its implementation and the overall results. However, it can be seen in (section 3.6.2) that it allows the building of a simplified model that is used for the wall scale and then the complete building.

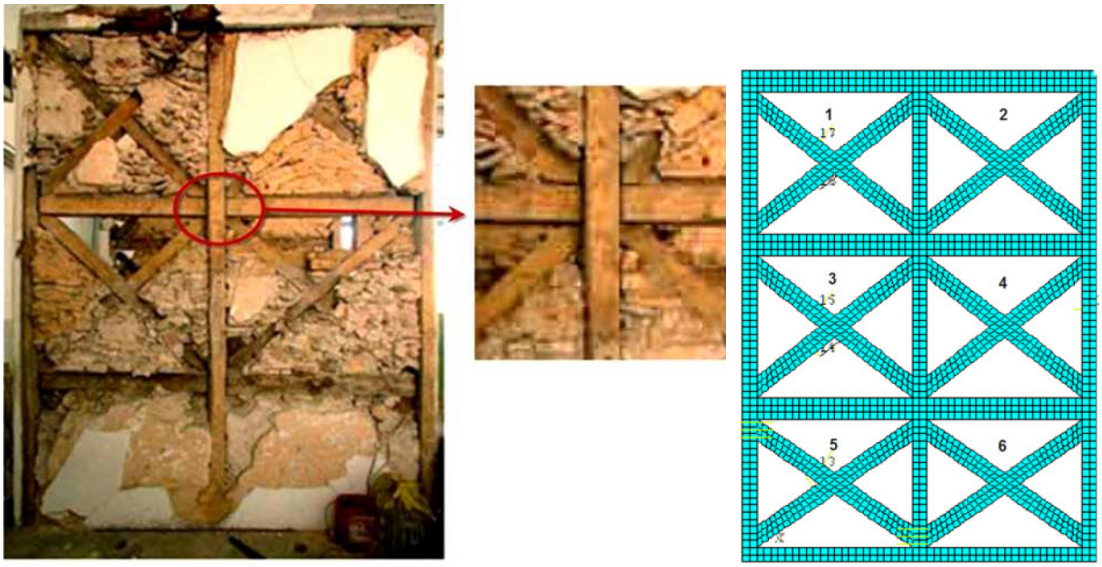

(a) Real Tested Wall (b) Non Deformed Wall

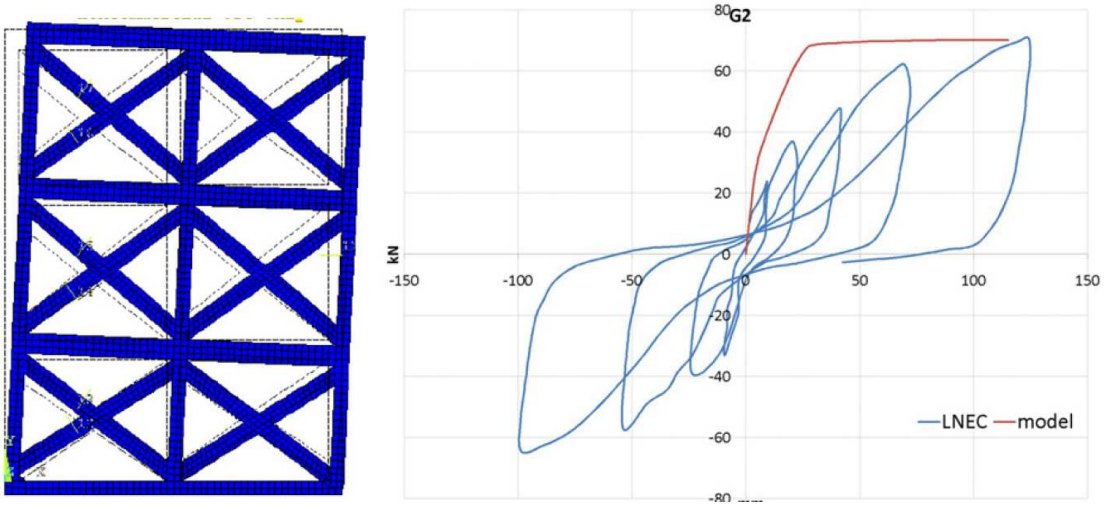

(a) Deformed Wall (b) Comparison of Experimental and Numerical Results

Fig. 3.11: Detailed Modeling of of Frontal Wall and Comparison with the Experimental Results, Kouris and Kappos. [92]

Hicyilmaz et al. [79]

The work of Hicyilmaz et al. [79] concerns the study of the seismic behaviour of a real Dhajji-Dewari building. It is divided into two parts:

- The first is a detailed scale modelling of the wall, in which a benchmark is produced from the tests of Ali et al. [79], and a parametric study analysing the effect of vertical loading and the influence of the change in the length of the bracing.
- The second is the detailed modelling of the entire structure.

The modelling takes into account some sources of nonlinearities such as:

- The mortise and tenon connections (Fig. 3.12-a) by an elastic-plastic law.
- Connections of the nails (Fig. 3.12-b) and (Fig. 3.12-e) present in the whole structure (wall and roof) by a perfect elastic-plastic law in the axial and shear directions. The characteristics of the tip are derived from the British Standard BS 5268-2(2002) [23].
- The friction due to infilling and the timber frame in the contact zones (Fig. 3.12-d).

The infilling (Fig. 3.12-c) is modelled by connections of rigid blocks linked together by the friction interface described above. The result of the benchmark on the wall is shown in (Fig. 3.13-b). The initial stiffness and the ductility of the shear wall seem to be well predicted. However, the overall resistance of the pattern obtained is about 50% below the expected value. However, this is the only study that attempts to reproduce the cyclic behaviour of the wall. Moreover, having been performed before testing, the modelling has important differences as below:

- Geometry: The clearest remark is that the number of unit cells (three) considered and the height of each one is adapted by Hicyilmaz et al. [79] from the walls actually built by Ali et al. [79]) but with four cells in this direction (see Fig. 2.18-b).
- Number of nails: The tensile tests on the connections made by Ali et al. [79] assessed the overall behaviour of the nails, which differs between the connections of type 1, 2 and 3. The results in terms of stiffness and strength show that Hicyilmaz et al. [79] largely underestimated the values.

Nevertheless, the actual failure modes obtained by modelling (Fig. 3.14-c) are remarkable. We find that, as has been observed experimentally, there is damage to the connections of type 1 (tenon-mortise foot of the corner post) and type 5 (assembly nailed centrally) shown in (Figs. 3.14-a) and 3.14-b).

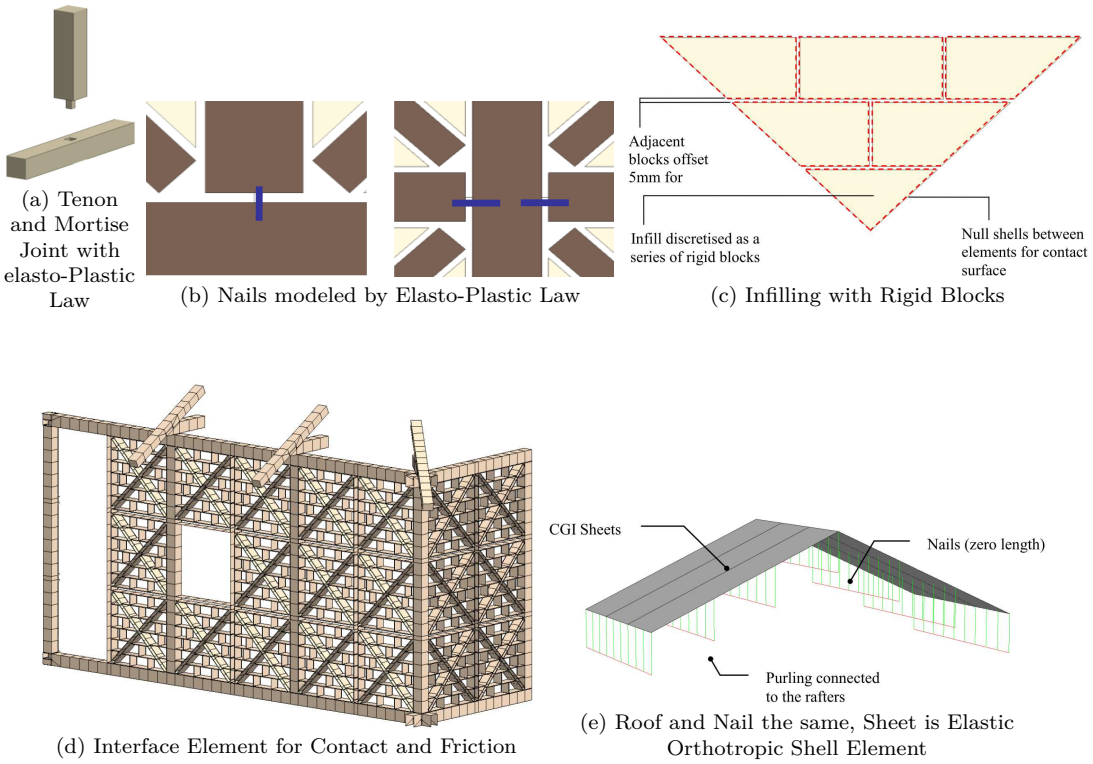

(a) Tenon and Mortise Joint with elasto-Plastic Law

(b) Nails modeled by Elasto-Plastic Law

(c) Infilling with Rigid Blocks

(d) Interface Element for Contact and Friction

(e) Roof and Nail the same, Sheet is Elastic Orthotropic Shell Element

Fig. 3.12: Constitutive Law for Different parts of Dhajji-Dewari Modeling by Hicyilmaz et al. [79]

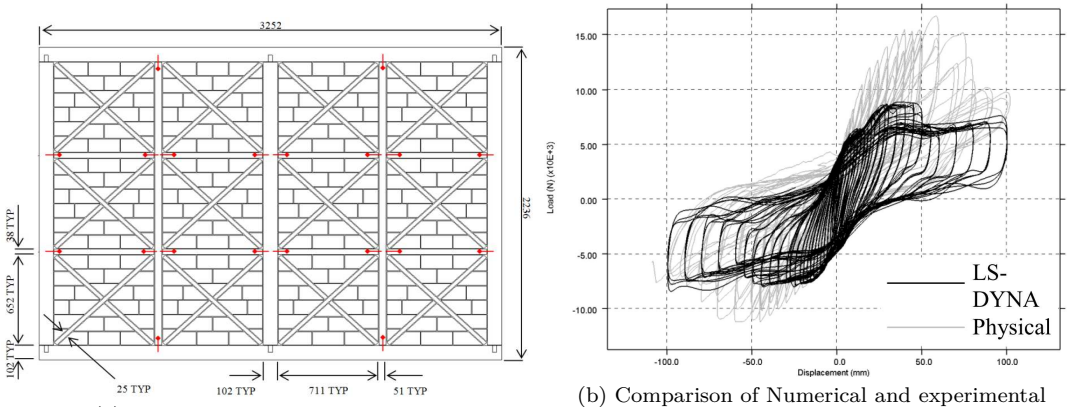

(a)Dimension of The Modeled Wall

(b) Comparison of Numerical and experimental Results of DW-2 Wall

Fig. 3.13: Modeling of the Wall, Dhajji-Dewari Hicyilmaz et al. [79]

(a) Experimental Damage in the Connection Type (5), [79]

(b) Experimental Damage in the Connection Type (1), [79]

(c) Experimental Damage in the Connections Type (1), (5), [79]

Fig. 3.14: Experimental and Numerical Comparison of the Failure modes of Dhajji-Dewari Hicyilmaz et al. [79]

The consistent failure modes between the experimental and numerical results show that the model correctly reproduces the behaviour of a Dhajji-Dewari structure and that differences in the results can be explained by the poor definition

of the elastic-plastic laws of connections of types 1, 2 and 3. Then, a parametric study was carried out at the scale of the wall in order to estimate:

- The influence of the vertical force on the structure. This analysis was performed by experimental trials across the wall (see section 2.5, by Vasconcelos et al. [134] and Poletti and Vasconcelos [111])
- The influence of the length of braces.

The first parameter of the study supports the conclusions already presented in section 2.5. For the second parameter, the analysis leads to find that there is little influence on the overall response of the wall in terms of either stiffness or resistance. These experimental tests are in contrast with the experimental results of the elementary cells presented by Vieux-Champagne et al. [137] (see section 4.3). This may be explained by the different conditions of the experiments of both, in terms of the infilling material, dimensions of cells and aspect ratio, types of connections, existing vertical forces, etc. As an alternative option to an experiment for the wall-scale test, this model seems to be interesting to validate a simplified approach. Indeed, as discussed in next paragraph 3.6.1, the scale of the building when using this method becomes very complicated to develop.

Building Scale

At this level, only the study performed by Hicyilmaz et al. [79] is described (briefly) here, with the aim of investigating the seismic behaviour of traditional buildings with a case study of a one-storey building.

Hicyilmaz et al. [79]

It consists in analyzing a complete building made with the same accuracy and the same type of mesh as on the wall scale, for two different configurations, one with nails between the vertical and horizontal members, as shown in (Fig.3.15). The other case is without these nailed connections. The structure is subjected to a seismic signal based on an elastic response spectrum of the universal building code UBC 97 [132]. The result clearly shows the importance of the nails in the connections. Indeed, even if the shear behaviour of a wall without these nailed assemblies has an interesting seismic performance like that observed for the maso walls in section 2.5, it remains very vulnerable to seismic loading in the out-of-plane direction. (Fig.3.15-b) illustrates the collapse of an external wall stressed out of its plane in the nail-less configuration, while (Fig. 3.15-a) shows that the nail configuration only experienced a few drops of bricks. Pushover analysis was performed for the two lateral directions with nails, and the force applied at the top of the ring beam and displacements were recorded to draw force–displacement curves as illustrated below in (Fig. 3.16). The lateral displacement was applied

for a value of more than (1 m) until failure in each direction, and we can see that the drift is very high as compared to the expected value of a maximum earthquake in the UBC97, where the Zone 4 peak ground displacement at a building period of 1 second is approximately 200 mm. The application of vertical loads increases the energy dissipation, which increases when the braces length is decreasing, although increasing the vertical overburden force did not give the same results. On the other hand, when these two variables change together at the same time, the amount of dissipated energy is greater than the algebraic addition of each case separately, and this phenomenon remains valid till a specified value of overburden and when this value of force increases, this relation will be reflected. Table (3.3) shows the dissipation energy for these two variables.

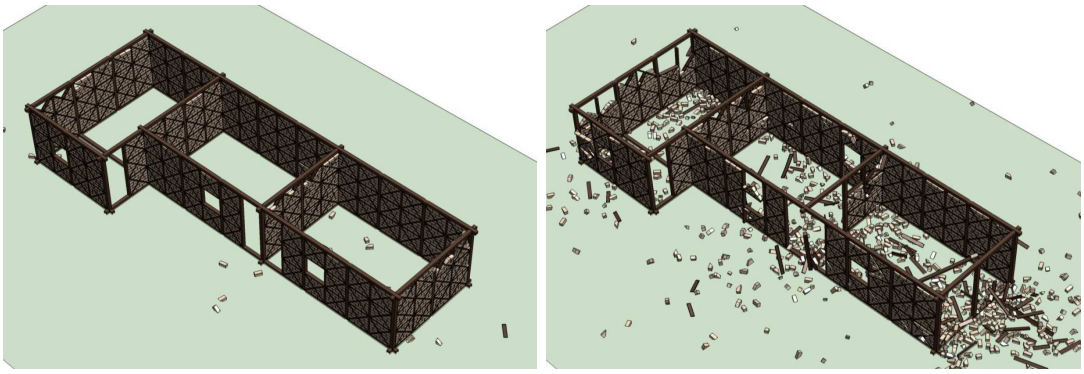

(a) with nailed connections (b) without nailed connections

Fig. 3.15: Damage of walls of Dhajji with nailed connections at joints and without, Hicyilmaz et al. [79]

Finally, this study tries to take into account the real behaviour of the structure (deformation, stiffness, modes of failure, and energy dissipation). However, a study in greater depth is required, taking into account the actual behaviour of the connections and the infilling, which would no doubt make it possible to approach more closely the actual behaviour of the structure. However, the difficulty of modelling such a structure, the difficulty of making modifications to the model and the calculation time, which was $68 hours$ for the complete building, collectively make this modelling method difficult and uneconomic.

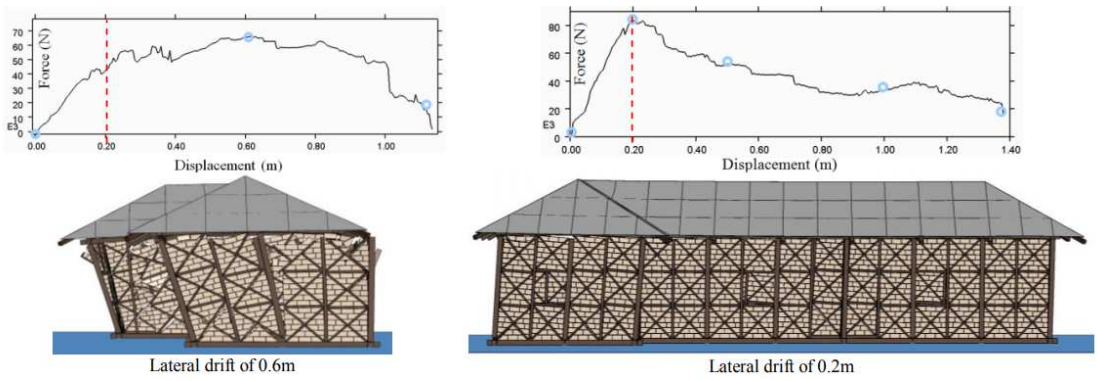

Fig. 3.16: Force displacement curves and images of the two orthogonal building directions with nails, Hicyilmaz et al. [79]

Tab. 3.3: Comparison of the Energy Dissipation with different values of Vertical forces, Hicyilmaz et al. [79].

Model description	Work Done (Joules)	Normalised work done
Original model	$5.07 * 10^4$	1.00
Brace lack of fit by 15 mm	$5.54 * 10^4$	1.09
Overburden of 4.6 kN/m	$7.56 * 10^4$	1.49
Brace lack of fit by 25 mm	$6.09 * 10^4$	1.20
Overburden of 9.2 kN/m	$1.09 * 10^5$	2.16
Brace lack of fit by 50 mm	$6.13 * 10^4$	1.21
Overburden of 18.3 kN/m	$1.51 * 10^5$	2.99
Brace lack of fit by 25 mm with overburden of 4.6 kN/m	$9.29 * 10^4$	1.83
Overburden of 4.6kN/m without nails	$7.22 * 10^4$	7.22
Brace lack of fit by 25 mm with overburden of 9.2 kN/m	$1.36 * 10^5$	2.68
Overburden of 9.2 kN/m without nails	$8.03 * 10^4$	1.58
Brace lack of fit by 25 mm with overburden of 18.3 kN/m	$1.41 * 10^5$	2.78
Overburden of 18.3 kN/m without nails	$8.27 * 10^4$	1.63

3.6.2 Simplified approach

The following section describes the simplified approaches used for the modelling of wood frames with infilling to the scale of a wall or building.

Wall scale

At this scale, the modelling of the structure allows us to predict or to reproduce its hysteretic behaviour, which has several levels of simplification of which two main levels are used:

- Level 1: very simple modelling (frame, beam or bar with plastic hinges), allowing the association of a law of nonlinear behaviour, whose objective is simply to calibrate the overall response of the structure (Ahmad et al. [4], Ceccotti and Sandhaas [31], Meireles et al. [104] and Kouris and Kappos [92]).

- Level 2: based on the hypothesis that most of the energy dissipation comes from the deformation of certain sources (metal connectors, infilling), the wall is modelled by a system of beams or elastic bars and the behaviour of the dissipative elements is described by nonlinear springs (Ahmad et al [4], and Hicyilmaz et al. [79]). Unlike the previous method, it attempts to describe a structural reality (geometry, components, mechanical properties, etc).

Maso wall, Ceccotti and Sandhaas [31]

The aim of this study is to model the buildings from macroelements (a simplified model of a wall) in order to study their seismic behaviour. Models have been made of the behaviour of maso walls and X-Lam walls (modern timber construction composed of planks glued and laminated in perpendicular layers). While the former, under cyclic loading, deform more in pure shear, the latter, given their very great stiffness with respect to their metallic connections, deform in a rigid body mode. This difference in response leads to the creation of distinct simplified elements:

- The macroelement for representing the shear wall is shown in Fig. (3.17-a) and corresponds to the "level 1" modelling described above. The force applied by the actuator, expressed as a displacement control applied at the top of the corner of the wall, defines the overall response of the wall. It is used to calibrate a hysteretic law (see Appendix 7.2.2, Fig. A.9), which is then expressed as a global relation of the moment rotation and divided by the number of nonlinear (rotational) springs, (Fig. 3.17-a) to obtain the relations of each one.

- The macroelement representing the X-Lam wall is illustrated in (Fig. 3.17-b). It represents the degree of accuracy of the "level 2" modelling type described above to obtain an overall behaviour which is modelled by:

  - Vertical hysteretic springs: their behaviour is described by the relation between the overall force and the vertical displacement of the hold on connections.

– Horizontal hysteretic spring: its behaviour is expressed by the relation between the overall force and the displacements in the same direction.

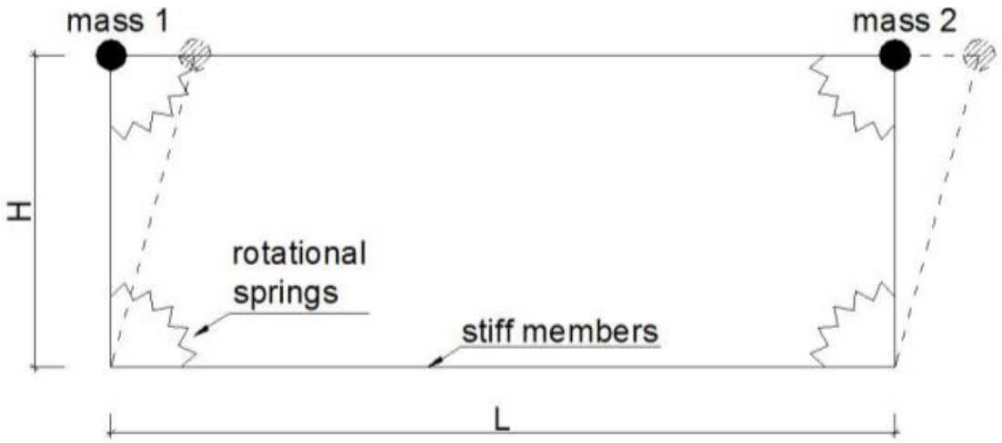

(a) Example of the Maso Wall

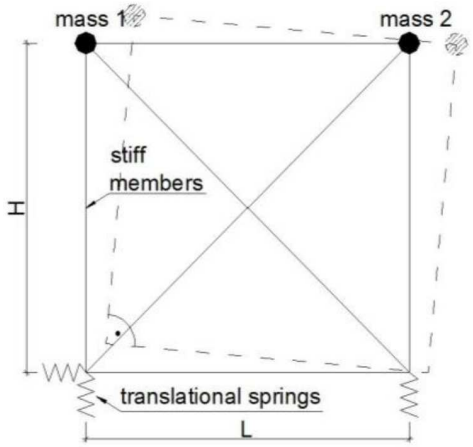

(b) Example of the X-Lam Wall

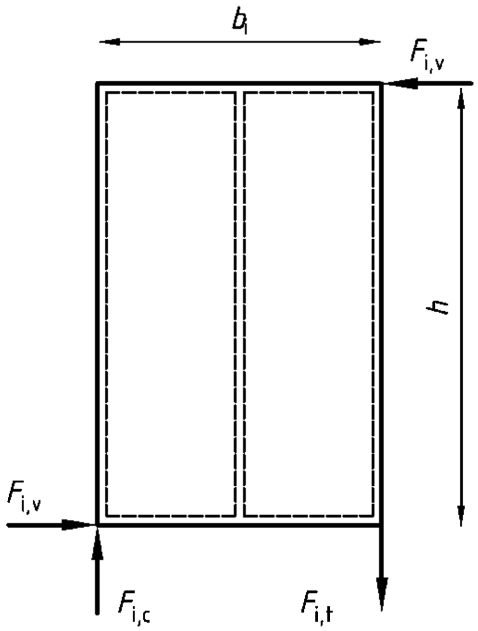

(c) Equilibrium of the X-Lam Wall

Fig. 3.17: Simplified Model of Maso and X-Lam Walls which are modeled by Model of Ceccotti and Vignoli, [33]

The internal forces in these springs are obtained by equilibrium of the wall, as shown in (Fig. 3.17-c) and Eq. 3.35).

$$F_{i,c} = F_{i,t} = \frac{F_{i,v} * h}{b_i} \tag{3.35}$$

Frontal wall, Kouris et Kappos [92]
In this simplified model, a localized plasticity (level 2) approach takes into account any source of nonlinearities of the elementary cell in an axial spring in the centre of the St. Andrew's crosses in the bars of the bracing elements modelling, as shown in (Fig. 3.18-a). The vertical and horizontal timber elements are modelled by linear elastic beam elements.

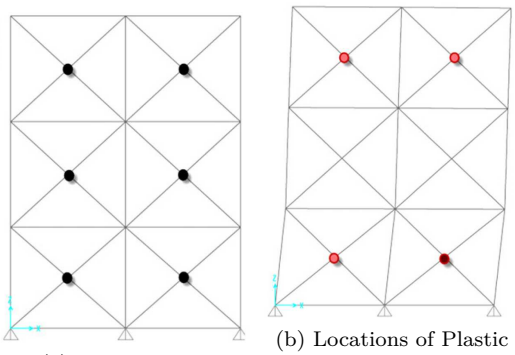

(a) Simple Model

(b) Locations of Plastic Hinges

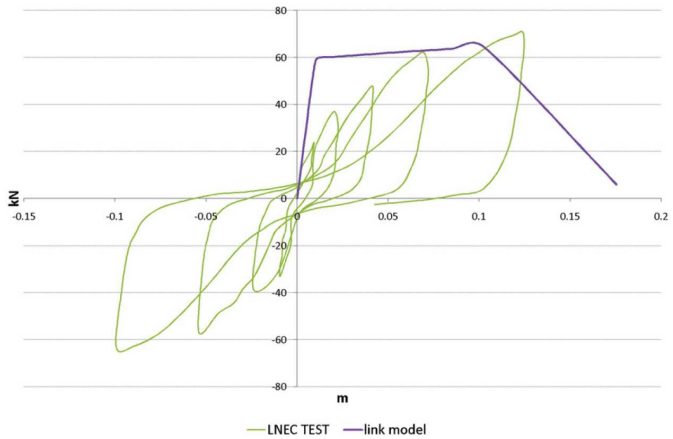

(b) Numerical and Experimental Comparison of Force Deformation of shear Wall

Fig. 3.18: Simple Modeling of Shear Walls, Kouris et Kappos [92]

In order to obtain a bilinear law for each plastic hinge, a pushover analysis was performed on a unit wall size, modelled in detail by the same method for the wall, (section 3.6.1, and Alexandros et al. [93]). The obtained pushover curve is thus idealized by the bilinear law using the method of equal areas. Furthermore, in order to take into account the infilling materials which are present at the beginning of the experimental test, which influence some characteristics like displacement and thrust in the braces, a correction factor is respectively used based on the geometrical parameters for each field variable, and calculated for each individual cell. Finally, the post-peak curve is obtained according to the recommendations made in section (FEMA-356 [3]).
This study makes some interesting remarks such as on the behaviour of the timber, the connections approach, the correction factor, and the post-peak behaviour as described by values from recommendations. However, given the repetition of elementary cells across the shear wall, decomposition of the behaviour of the shear wall in the form of the combination of the behaviour of individual cells is a relevant choice. Moreover, this method facilitates detailed modelling and gets satisfactory results from the maximum strength viewpoint and the initial stiffness.

Dhajji-Dewari wall, Ahmad et al. [4]

The approach used by Ahmad et al. [4] is to provthat ide a mathematical tool for engineers such that the dimensions of the Dhajji-Dewari walls structures is according to the rules of building codes. To do this, a pushover analysis is carried out using a simplified modelling that tests experimentally the wall (level 2) shown in (Fig. 3.19-a). The vertical and horizontal timber members are modelled by beam elements while bracings are modelled by bar elements for which only the compressive strength is taken into account. To introduce nonlinearities, each beam has two end-nodes with plastic hinge joint that are associated with constitutive elastic-plastic moment–rotation laws and force–displacement calibrated from the experimental tests of Ali et al. [9]. The result of this pushover analysis is shown in (Fig. 3.19-b).

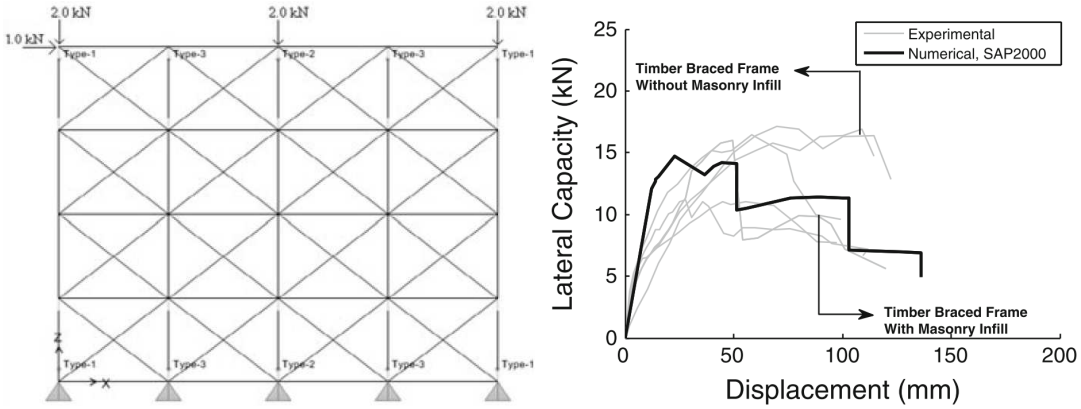

(a) Simple Model of Dhajji-Dewari Wall (b) Pushover Analysis Experimental and Numerical

Fig. 3.19: Pushover Analysis of Dhajji-Dewari Wall, Ahmad et al. [4]

The initial stiffness as well as the maximum resistance are well predicted by the model, with an error of (7%) and (27%) respectively. These parameters were also well predicted by Kouris and Kappos [92]. The displacement limit of the elastic zone is underestimated by (50%). The additional contribution of Ahmad et al.[4] is the consideration of the behaviour of the connections for the calibration of the constitutive laws associated with plastic hinges, allowing us to obtain a satisfactory post-peak behaviour. Then a seismic analysis is carried out using a simplified element equivalent to the shear wall (wide column analogy), or (level 1), as illustrated in (Fig. 3.20-a). This rigid bar has at each end two rigid elements and a plastic hinge joint. The first represents the horizontal and vertical degrees of freedom, while the second describes the trilinear moment–rotation law presented in (Fig. 3.20-b). The beam element is connected at the top to a rigid, horizontally translated bi-supported element subjected to static or dynamic excitation. This macroelement constitutes a simplified tool for carrying out a seismic analysis of one- or multi-storey buildings, as was done in Ahmad et al. [5] and shown in (Fig. 3.23) in section 3.6.2.

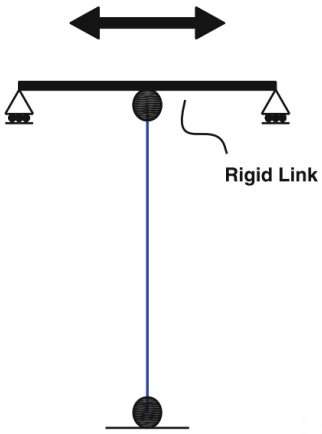

(a) Representation of Macrelement

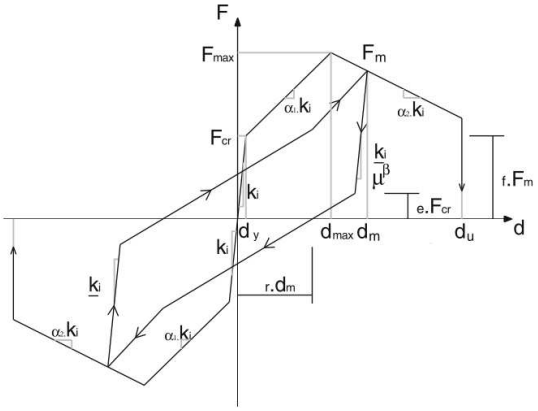

(b) Trilinear Hysteresis law

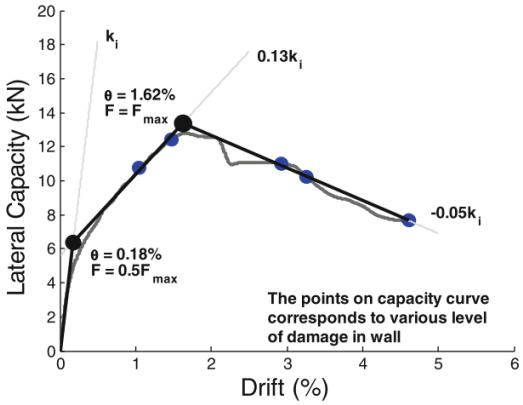

(a) Monotonic Calibrated Curve

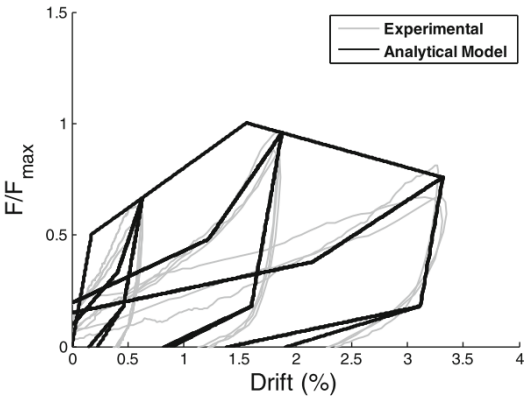

(b) Cyclic Calibrated Curve

Fig. 3.20: Seismic analysis of Dhajji-dewari walls represented by a beam with plastic end-joints whose behavior is described by a tri-linear law, Ahmad et al. [4]

Meireles et al. [104]

In the same way used by Ahmad et al. [4], Meireles et al. [104] have created a simplified frontal wall element (equivalent wall, level 1), by using the experimental response of the wall under cyclic loading (Fig. 3.21-c), [102]), and according to the hysteretic model shown in (Fig. 3.21-b) to develop a constitutive law of the equivalent wall. This additional example shows again that the use of simplified elements (level 1 modelling) is platform-routine for nonlinear seismic analysis of buildings with infilled timber frames. Indeed, as shown by Hicyilmaz [78], the time

calculation for performing temporal analysis from a detailed model is relatively long and complicated to implement.

However, the creation of a macroelement across the wall does not take into account local phenomena and does not allow changes to the parameters, such as the type of connectors, the dimensions of the structure, etc. This makes the model developed hard to re-use for other structures.

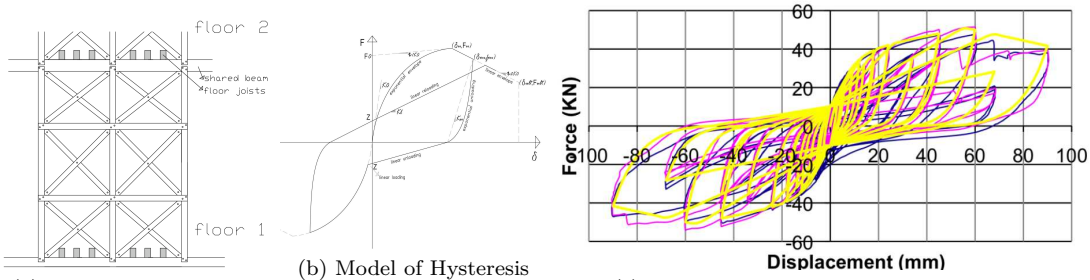

(a) Simulated Shear Wall

(b) Model of Hysteresis Law

(c) Calibration of Model of Cyclic Loading

Fig. 3.21: Siumplified Modeling of Frontal Wall by using Macroelement Concept, Meireles et al. [104]

The multi-scale approach which takes into account the behaviour of the joints to predict the behaviour of the wall is very interesting and provides consistent and conservative results. The lack of connection between the simplified modelling of the wall and the creation of the macroelements remains an area for improvement. In addition, it is interesting to note that the authors reported the small effect of the moment–rotation relationships of the joints on the overall behaviour of the wall for moderate dimensions of the timber element sections.

Scale of building

This section illustrates the implementation of the simplified approaches presented above for the modelling of complete buildings as shown in Figures (3.22) to (3.25). The purpose of each one is to analyse the timber-framed buildings with infilling for seismic excitations. Two types of approach are used:

- The temporal approach (see section 3.2.1), by Ahmad et al. [4], Ceccotti and Sandhaas [31] and Meireles et al. [103] allows to conduct probabilistic analyses for the establishment of fragility curves. This method gives an

estimate of the probability of damage of the structure as a function of the peak ground acceleration (PGA) of the soil or to establish a behaviour factor value (EC8, [65]).

- The simplified approach of the pushover method (see Section 3.2.2) by Kouris and Kappos [92] and Meireles et al. [103] are used to analyse the level of damage to the structure to determine appropriate strategies for strengthening.

However, none of these studies can be compared to a real experimental test scale. For this reason, the comparison between the experimental and numerical study by Ceccotti and Sandhaas [31] performed for buildings constructed from panels of X-Lam (Fig. 3.24-b) is briefly presented. This shows that the simplified approach using the association of macroelements predicted an acceptable response of the structures (acceleration in terms of time), as shown in (Fig. 3.24-c).

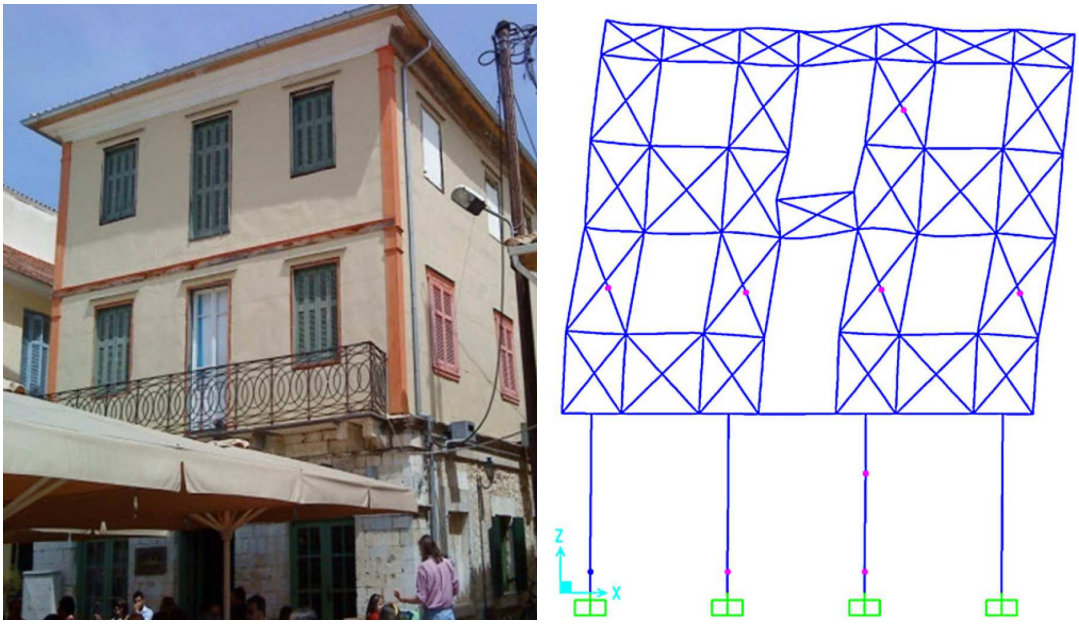

(a) Real Building (b) Plastic Hinges Locations

Fig. 3.22: Simplified Modeling of Full Building, Kouris and Kappos [92]

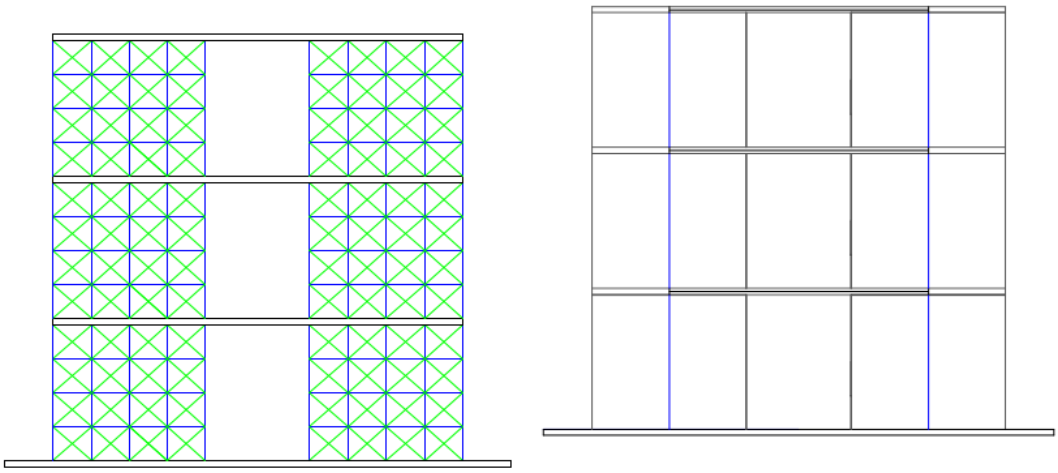

(a) Multi Storeys Dhajji-Dewari Bulding

(b) Modeling of Building by Macroelement (Blue Lines)

Fig. 3.23: Modeling of Multi Storeys Building of Dhajji-Dewari structures, Ahmad et al. [5]

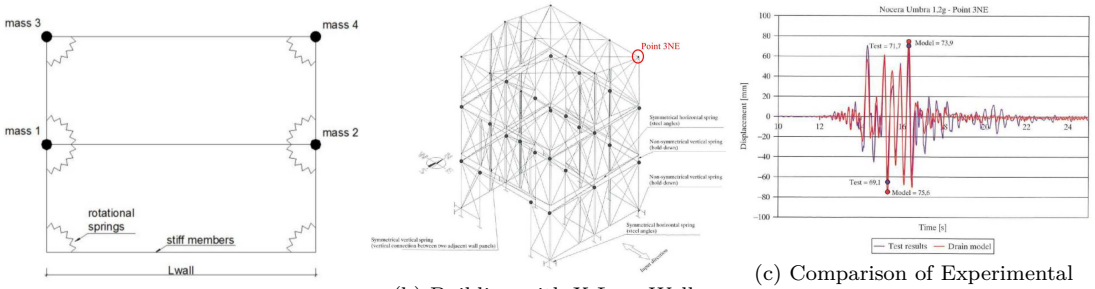

(a) Two Storey Building with Maso Walls

(b) Building with X-Lam Walls with specified Node 3NE

(c) Comparison of Experimental and Numerical Displacement at Node 3NE

Fig. 3.24: Simplified Model of Building from Maso Walls and X-Lam Timber Structure, Ceccotti and Sandhaas [31]

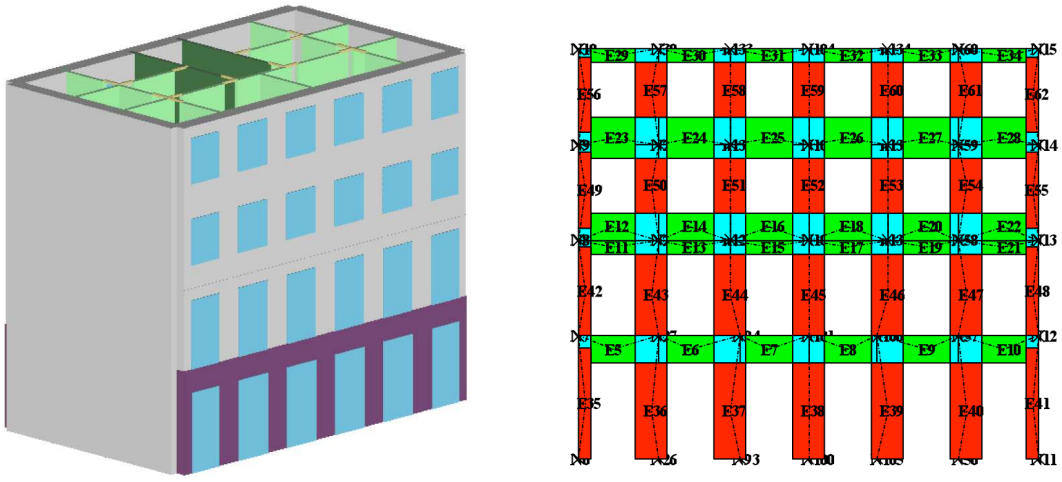

(a) Pombalino Building (b) Equivalent Frame Model

Fig. 3.25: Effect of Vertical Loading on the Lateral Resistance of Shear Walls, Meireles et al. [103]

3.7 Numerical analysis of modern timber frame structures

3.7.1 Connections

Xu and Dolan [144]

Due to the lack of general hysteresis elements in the commercial structural software, Xu and Dolan [144] proposed a modification to the Bouc–Wen–Baber–Noori (BWBN) model for a nailed joint by solving some ordinary differential equations, and the model can represent the degradation of strength, stiffness and pinching well. The modifications to the BWBN model change some of the parameters of the first trial use of BWBN by Foliente [61] in timber structures to overcome some of the difficulties of previous works. The orientations of nails deformations are treated in the same way as in the oriented spring pair model that was proposed by Judd [87]. (Fig. 3.26) shows the validated curves of some specified nails according to the experimental results.

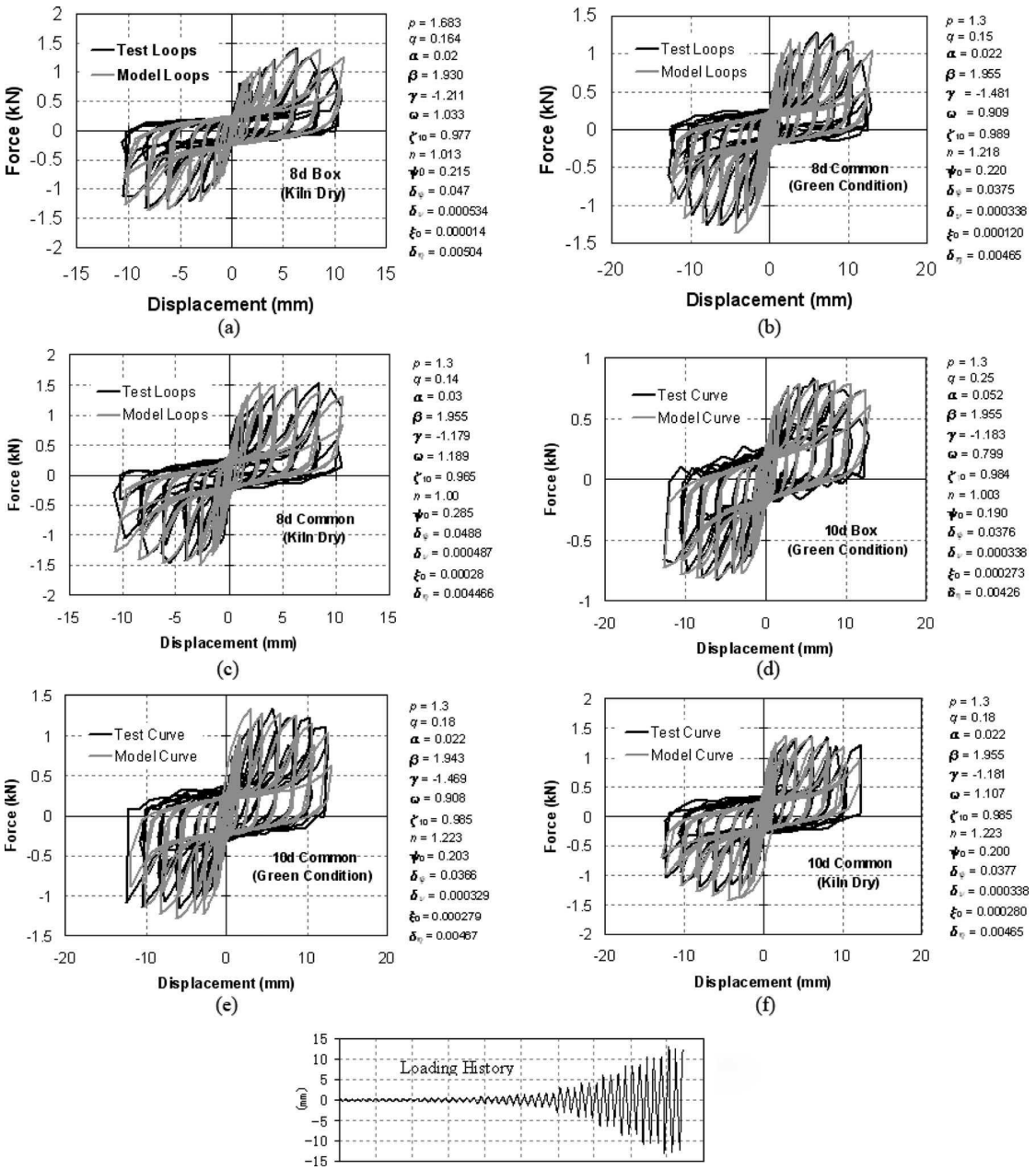

Fig. 3.26: Validation of Selected Nail Joints, Xu and Dolan [144]

The numerical modeling of Richard et al. [118]

Richard et al. [118] developed a finite element code for connections of timber-framed structures to study the nonlinear response of monotonic, cyclic and dynamic loading conditions of multi-storey buildings. The nonlinearity is considered only in the connections, but the other structural components are linear elastic. Dowel-type connections were used and a backbone curve was proposed according to Dolan and Foschi's [50] model, but the hysteresis law for nails and hold-on connections is different. The hysteresis model is represented by 4 equations and 13 parameters to define the law. The use of an exponential function gives acceptable values of the maximum force but inaccurate values of stiffness due to the mathematical nature of the exponential function, so a modification was performed by Humbert et al. [83] in the next section.

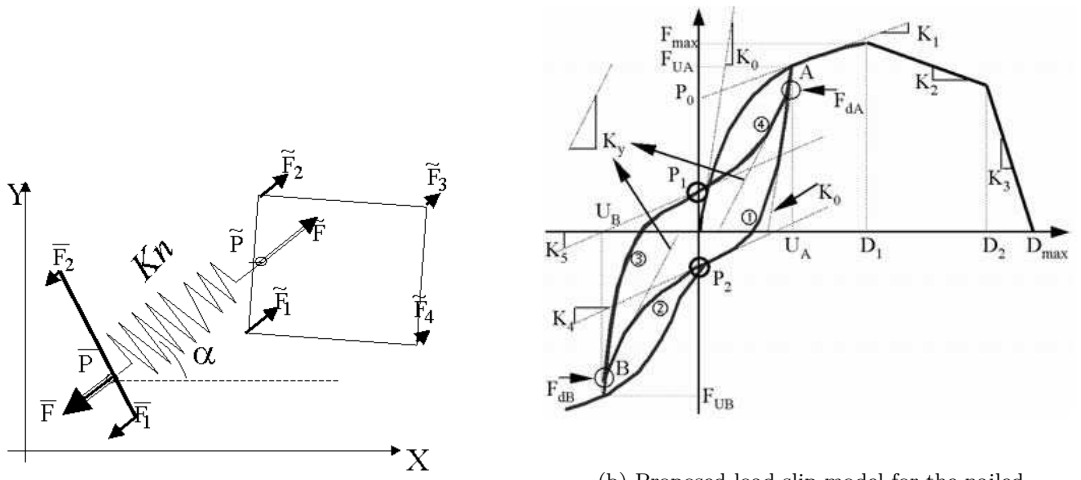

(a) Proposed joint element

(b) Proposed load slip model for the nailed connections

Fig. 3.27: Proposed load slip model for the nailed connections, Richard et al. [118]

3.7.2 Shear wall scale

Xu and Dolan [143]

Some modifications for the hysteresis law of the BWBN model of Xu and Dolan [144] were added to idealise a macroelement for the wall scale according to some experimental results on shear walls and the results were verified by comparing a 3D timber two-storey building model containing these macroelements of walls with the experimental results for the same scale. This paper was the first attempt to

use two diagonal springs to represent the shear wall scale by using the BWBN hysteresis model. (Fig. 3.28-c) shows the 3D building idealisation and (Figs. 3.28-a,b) show a comparison of the results obtained by using the proposed model and the tested results of the 4^{th} and 5^{th}[2] design level for the middle roof point of the first storey. The numerical model was more flexible than the actual specimen.

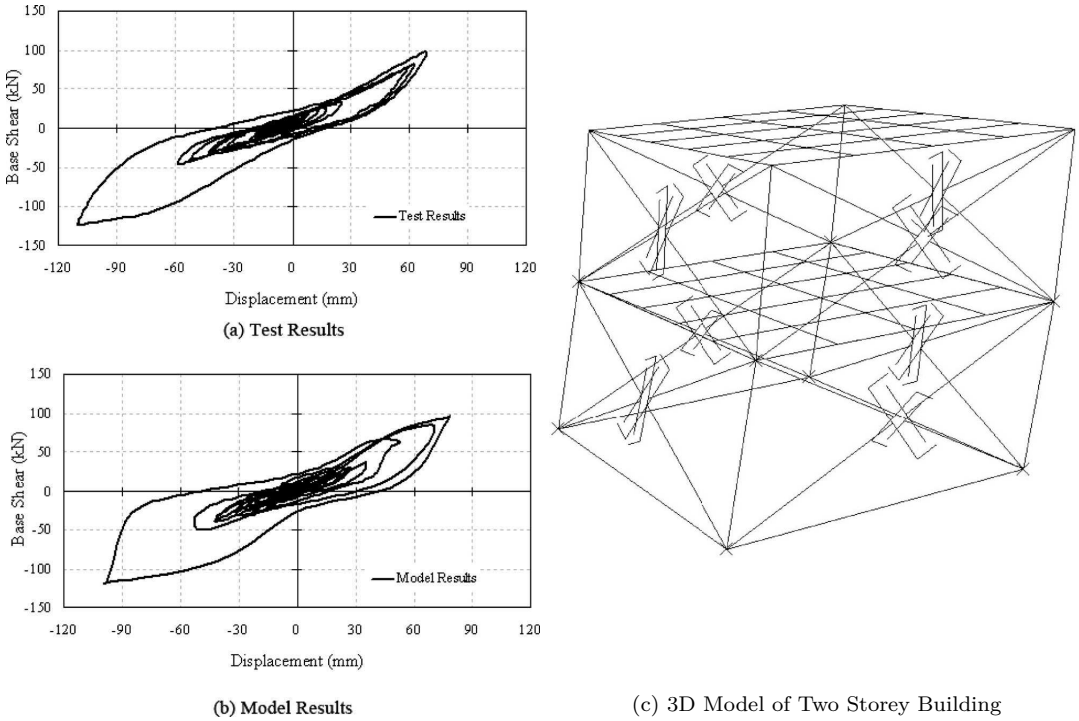

Fig. 3.28: Modeling of Shear Wall Frames by BWBN Model, Xu and Dolan [143]

Hold-down connection and OSB panel, Richard et al. [117]

Richard et al. [117] studied a finite element model for a shear wall with a large opening by using a lineal elastic sheathing and framing elements and nonlinear connections according to the hysteresis spring element, which was defined previously by Humbert et al. [83], (Fig. 3.27). This study includes OSB panels connected by nails of different lengths under monotonic and cyclic lateral loads, and many parametric tests were performed, such as the number of hold-downs, the shape of

[2] There are 6 different acceleration levels to study accomulated failure

the panel, the distribution of the nails, the braces, and the existence of washers to reinforce the nails. The results for monotonic and cyclic tests were compared and good results are obtained. The results for different nail lengths show that reinforcement by adding washers does not have a major effect when using short nails (51 mm) in the case of cyclic loading, but gives a significant improvement for longer nails (76 mm). The latter were able to provide good anchorage, so they tested the advantages of reinforcement by washers. No great effects for the washers were observed for the resistance to monotonic and cyclic loading, but for a high number of cycles an increase in the energy dissipation was noticed for shear walls with washers by 50% as compared to those without washer reinforcement. In addition, increasing the number of hold-downs or changing the shape[3] of the OSB increased the initial stiffness but led to sudden failures as the panels were torn or buckled.

[3] rectangular or L-shape

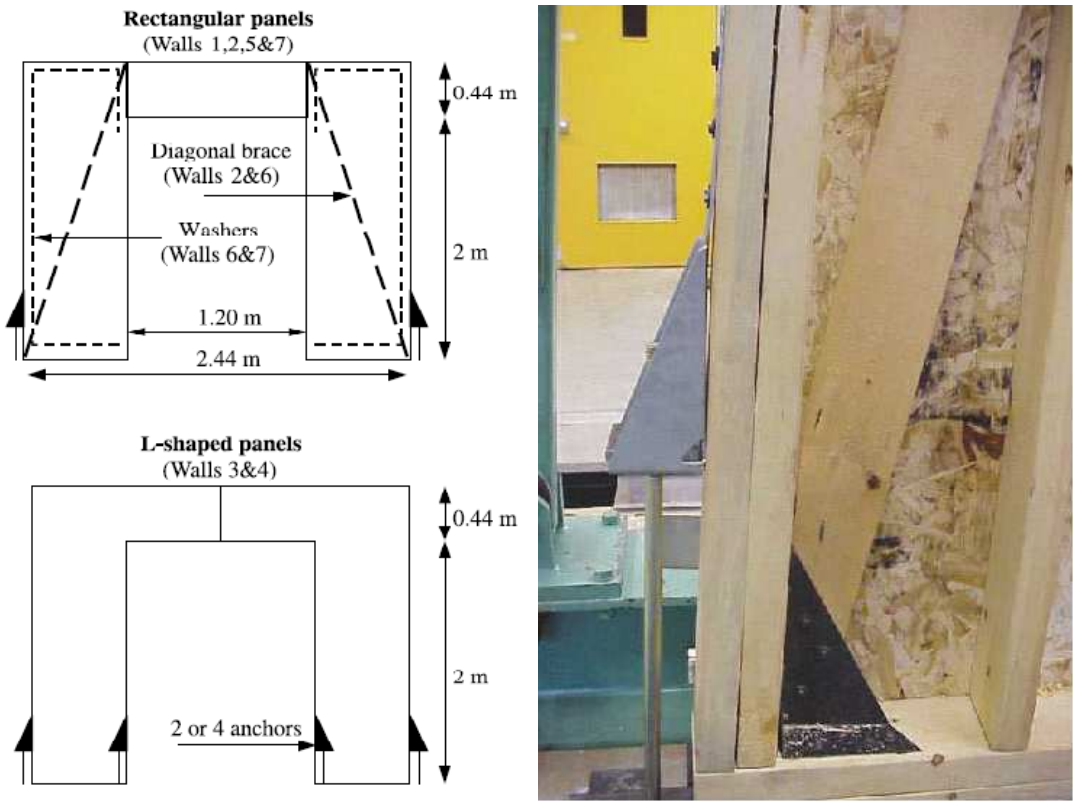

(a) Details of the walls configurations.

(b) Hold-down Device and Braces of Shear Wall

Fig. 3.29: Modeling of Shear Wall Frames by Richards's Joint Model, Richard et al. [117]

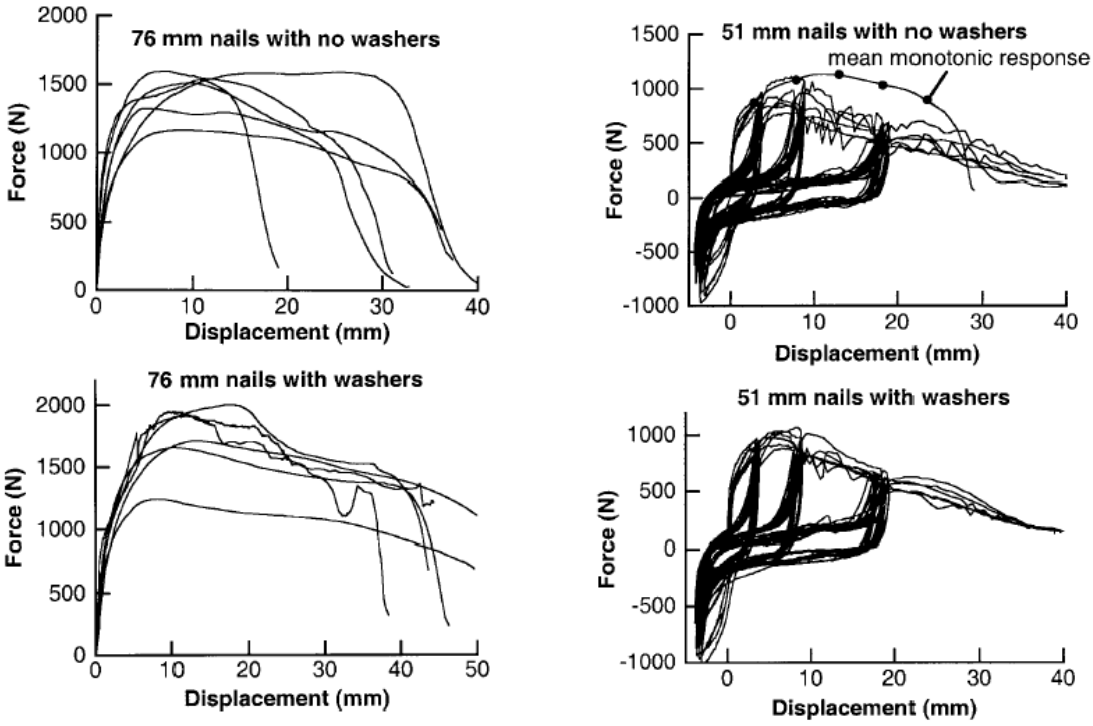

Fig. 3.30: Monotonic and Cyclic Force Displacement for Two different Nails Lengths, Richard et al. [117]

Multi-scale analysis method, Boudaud et al. [19]

A multi-scale analysis technique was proposed by Boudaud et al. [19] to analyse timber shear walls on one-storey 3D building scales according to the macroelements for each shear wall by using a simplified macroelement approach. This macroelement constitutive law could be obtained by using the Hysteretic constitutive nonlinear hysteresis law (see Richard et al. [117], and Humbert [82]), according to experimental tests of different types of connections (nails, hold-down, etc.), and the shear walls were subjected to monotonic and cyclic tests to define the nonlinear law of the macroelements. Openings can be modelled either by a simplified FE model which contains adjacent shear walls, or by a specific simplified FE model limited to the opening area (see Richard et al. [117]). The second choice is selected due its simplicity, and the shear wall tests showed that the maximal force is proportional to the length of the wall. Each macroelement wall was mod-

elled by four rigid members with a one-directional spring element. The latter were implemented for a 3D ($6 * 6m^2$) timber-framed house as shown in (Fig. 3.31-a) to perform dynamic time history analysis, and the results are shown in (Fig. 3.31-b).

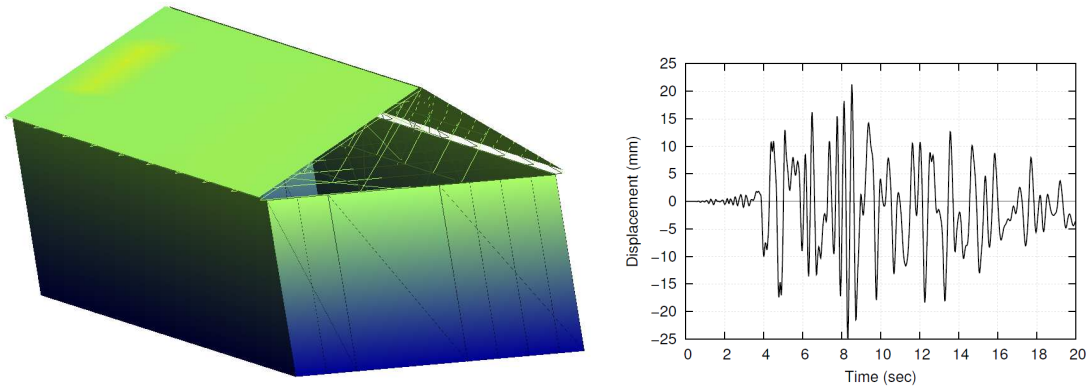

(a) 3D House Model

(b) Displacement time History of a Wall

Fig. 3.31: 3D House Modeled by Multi Scale Approach, Boudaud et al. [19]

Folz and Filiatrault [62]

In 2004 Folz and Filiatrault [62] proposed a simplified finite element model to find the response of a building to seismic and other horizontal loading conditions. This model basically contains a rigid horizontal diaphragm, and nonlinear springs represent the lateral shear wall resistance. The 3D model of the frame is degenerated into a 2D plane model with zero height zero element members connected between adjacent diaphragms or the foundations, and the hysteresis law of each spring wall model can be derived from the experimental results. The greatest advantage of this approach is that the response of the building is defined in terms of only three degrees of freedom per floor (two translations and one rotation) as shown in (Fig. 3.32-b). The idea is to collect the strength of all walls in the orthogonal axes (rigidity centre) according to the transmissibility concept. The authors suggest a procedure for pushover analysis by applying a timed pushover by setting the restriction that the monotonic loading rate is sinusoidal with a frequency 100 times slower than the fundamental frequency of the system, in order to minimize the contribution from inertia and the damping effects of the equation of motion.

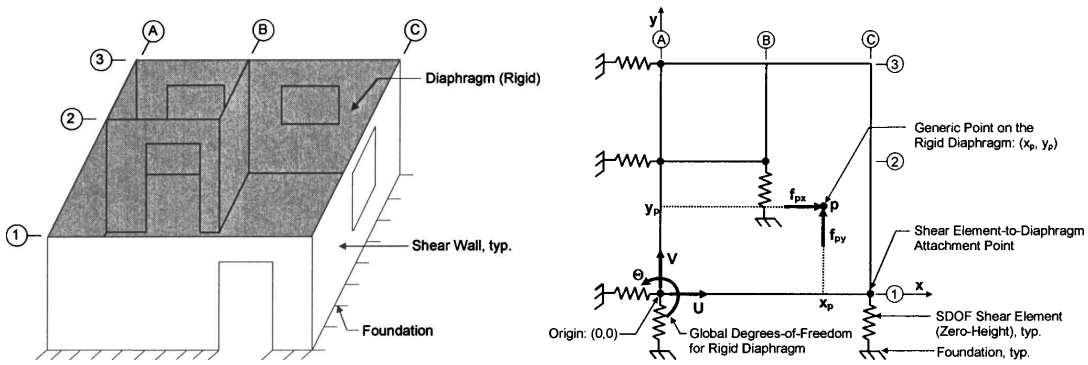

(a) Components of one Story Timber Frame Structure (b) Model of One Story Timber Frame Structure

Fig. 3.32: Simplified 3D Model of One Storey Building by Folz and Filiatrault [62]

3.8 Conclusions

Some of the approximated linear and nonlinear analysis methods as well as dynamic calculation techniques for analyzing structures subjected to an earthquake with some examples of traditional and modern timber framed structures. The multi-step analysis technique is selected to find the response of timber frame analysis for each size or selected scale to reduce the time required for large-scale structures. Some of the hysteretic models were presented and a description of the Hysteretic constitutive model for joint elements with different types of fasteners. There are many simplified methods to calculate the dynamic response of buildings and these can be chosen according to the required details and accuracy according to design codes. For the non-linear analysis, a direct integration method is used to find the response of structures for earthquake loading conditions, and Newmark's implicit time integration method is widely used in the calculations. The stability of the solution and the time step is crucial for these analyses. The stability of numerical calculations can be enhanced by using some mathematical techniques like $\alpha - HHT$ or $\theta - Wilson$ method.

4. PREVIOUS EXPERIMENTAL WORK

4.1 Introduction

In this chapter the experimental tests of Kay wall structure type which is used as a traditional houses in Haiti had been investigated, this experimental program was performed by Vieux-Champagne et al. [140]. These tests were performed for four different scales, these are joints, elementary unit wall, shear wall, and one storey building.

4.2 Scale one: Connections

In this scale the bottom connections only were tested and some parameters were investigated.
The behaviour of steel strip connections was established by Vieux-Champagne [135], some of the parametrs were studied as the connecting of a sill plate to a post by different types of nails (smooth and serrated) and two types of steel strip were used (French standard section of (1.5 mm) thickness, and a weaker one that is used in Haiti with a thickness of 0.64 mm) for monotonic and cyclic tests [135] to derive the parameters of the Hysteretic constitutive law spring element in the directions of axial hold-down and tangential shear tests for these connections. Many tests were carried out by Vieux-Champagne et al. [140] using different numbers of nails per connection for the two types of steel strip, and calibrating the experimental analysis to develop a 3D-FEM joint model and then use it in the next level of their multi-scale analysis technique. The experimental tests show that the mean shear force resistance of one nail is (1.3 kN). These parametric studies can be seen in (Fig. 4.1), where A represents the average values and ENV are the envelope of cyclic tests.

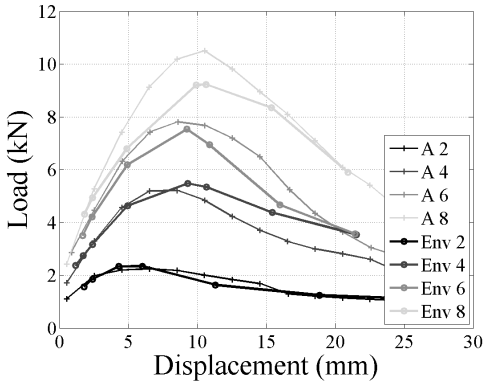

(a)Effect of No. of Nails for Uplift Deformation

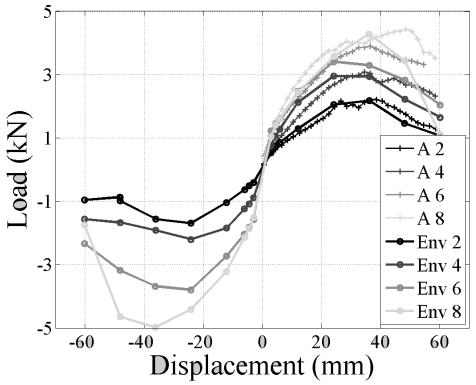

(b) Effect of No. of Nails for Shear Deformation

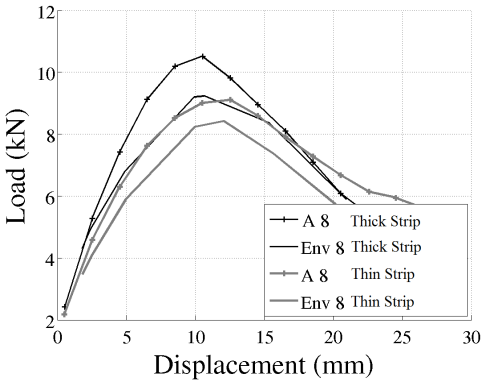

(c) Effect of Type of Steel Strip for Uplift Deformation

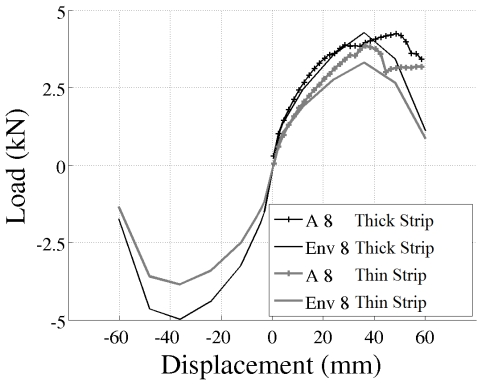

(d) Effect of Type of Steel Strip for Shear Deformation

Fig. 4.1: Effect of number of Nails and Type of Steel Strip for Connections between Sill plate and Posts, Vieux-Champagne et al. [135]

The constitutive laws of the connections in uplift tension and compression and the calibrated FE model according to Hysteretic constitutive model can be shown in figure (4.2) and all the parameters required in the model for tension, compression, and shear deformations can be seen in table (4.1).

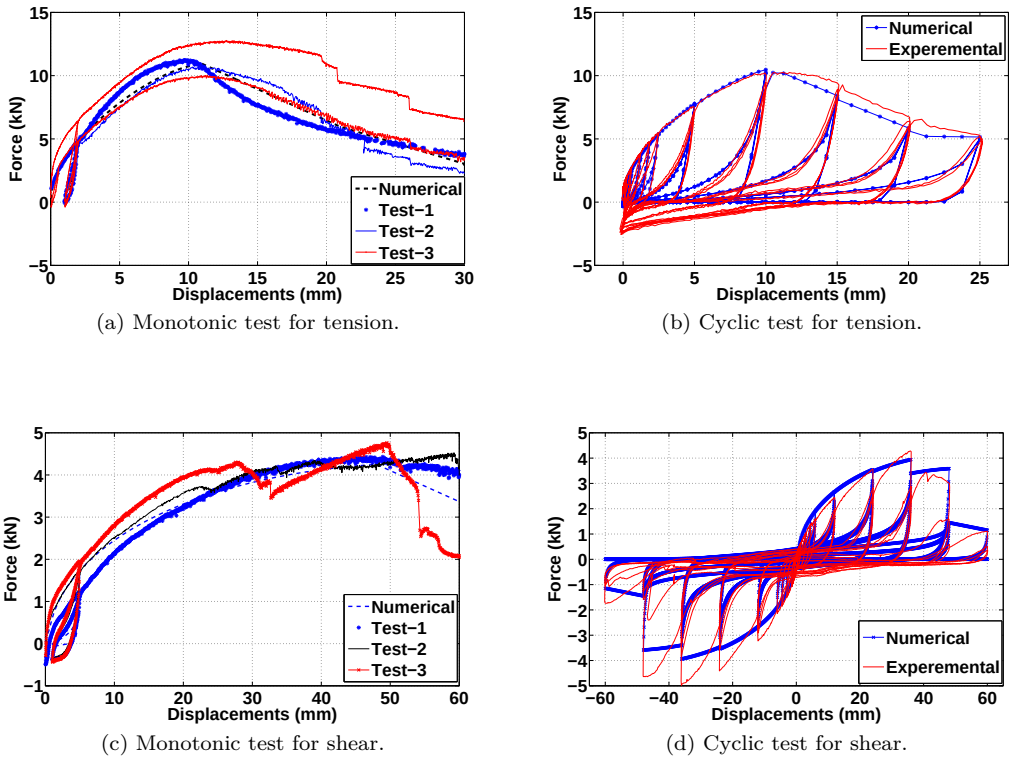

(a) Monotonic test for tension.

(b) Cyclic test for tension.

(c) Monotonic test for shear.

(d) Cyclic test for shear.

Fig. 4.2: Constitutive laws for tension and shear deformation of steel strip connections.

4.3 Scale 2: Elementary unit cell wall

In this scale, a monotonic and cyclic tests were used for some parametric studies like effect of infilling, type of infilling, and the existing braces ($0.97 \times 0.97\, m^2$), as in (Fig. 4.3) and 6 nails were used in the connection (of type 1[1]) which connects the sill plate and the post (see section 4.2). The infilling is made from natural stones or adobe or daub with in-situ clay as a mortar or limestone. The tests were performed four times without crosses (rocks, adobe, daub, and empty), along with some other tests with Saint Andrew's crosses (3 tests for rocks infill, including 1 monotonic and 2 cyclic, 5 tests for adobe infilling, including 1 monotonic and 4 cyclic, and 3 tests for empty frame, 1 monotonic and 2 cyclic loading). This scale was not used in the calibrated of FE model because it is not possible to separate

[1] Type 1 represent the connection in the bottom according to Ali et al. [9] and shown in Fig.2.18-b, c

Tab. 4.1: Calibrated parameters of Hysteretic constitutive law for sttel strip connection supports.

Parameter	**Axial Tension**	**Axial Compression**	**Shear**
d_y (mm)	0.1	0.005	0.9
F_y (kN)	1.0	0.4	0.55
d_1 (mm)	11.0	0.5	48.0
F_1 (kN)	11.0	39	4.25
d_2 (mm)	21.0	20	65
F_2 (kN)	6.0	20	3.0
d_u (mm)	39.0	25	90.0
F_u (kN)	0.1	0.1	0.5
η	0.5	0.7	0.5
AC	0	0	0
AR	1	1	1.0
BC	0.12	0.1	0.25
BR	1	0.1	1.5
C_1	-1	-2	-10
C_2	-0.5	-1	-10
C_3	0.01	0.1	0.2
C_4	0.9	0.5	0.75

the effects of boundary conditions (see figure 4.3-c) and the behaviour of the cell in the test of this case and can not obtain accurate model due to this essential factor.

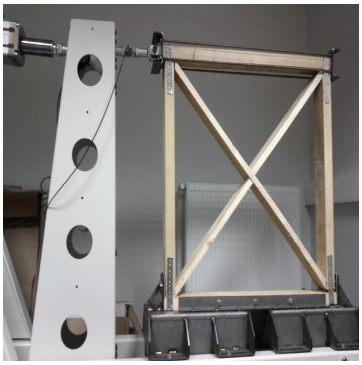

(a) Specimen and tested machine

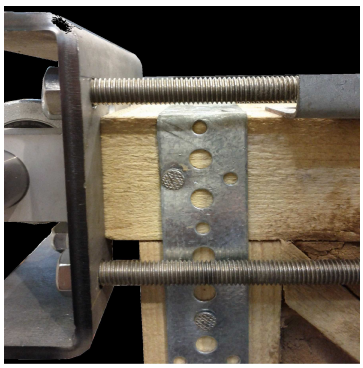

(b) Actuator and applied loads

(c) Side support of post bottom

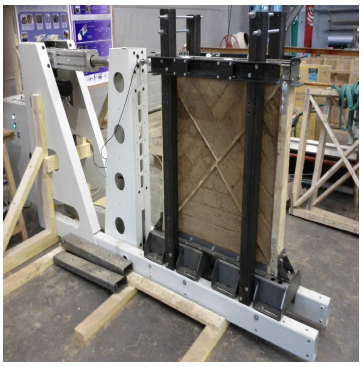

(d) Tested specimen wit infilling

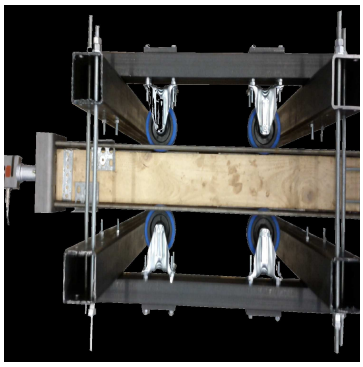

(a) Top view of Test

(b) Miniwall with Rock Infill

(c) Miniwall with Adobe Infill

(d) Miniwall without Infill

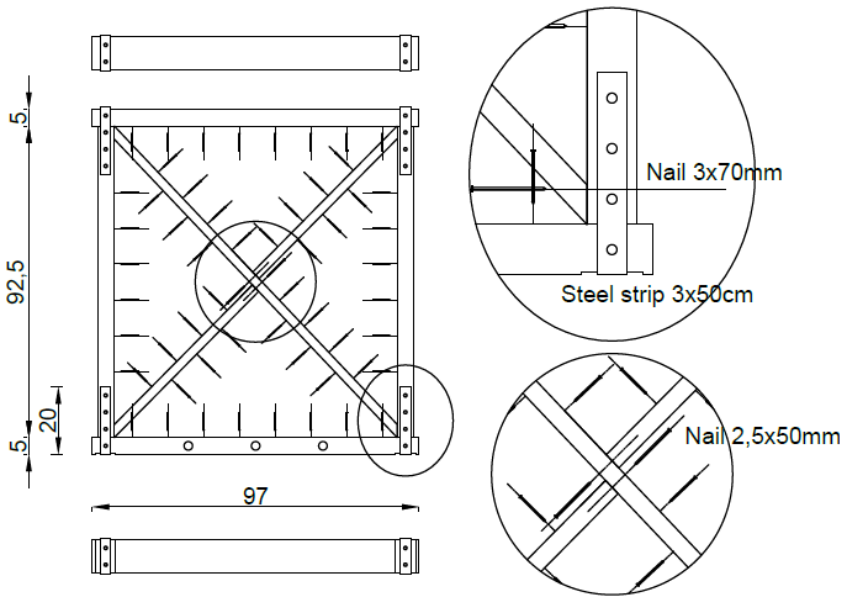

(d) Dimensions of unit Scale Wall

Fig. 4.3: Element Cell of a Wall [140], [135]

Some configurations of $(97 \times 97\,cm^2)$ were be tested for elementary unit wall for different types of infilling as shown in (Fig. 4.3). The wall was subjected to quasi static monotonic, and cyclic loads. model, (Fig. 4.4) shows the load drift relationships for different cases of existing of infilling or not for differnt types of infilling, for all these tests, no vertical forces were applied and the only vertical loads is the self weight, so no big difference recognized in the maximum load capacity of the wall for all (11) tests, it is also observed that the existance of braces (St. Andrew's) raised the resistance of wall for all cases (except empty) from 5 kN to 15 kN). The ratio of timber per m^3 is (0.28) which is less than the timber ratio of unit cell adopted by Ferreira et al. [57] that is equal to (0.59). The initial stiffness in the case of infilling is little bit larger than that in the case of empty for existing braces specimens, but it is more clear for the case of frames without braces because of the infilling is responsable on resting diagonal compressive forces. The amount of dissipated energy EVDR is larger in the case of infilled than the empty. The average value of $(\xi_{eq} = 12.3\%)$ is consistent with the values in the literature for timber frames with and without infilling (see Ali et al. [9], Vasconcelos et al. [134], and Filiatrault et al. [58]). The average ductility was $(+2.28$ and $-2.75)$ which is equivalent to value of Ali et al. [9] but it is moderate value as compared to some authors (Vasconcelos et al. [134], Poletti and Vasconcelos [111] and Munoz et al. [105]). No influence of infilling on the ductility, but the type of infilling is an important facter that effect on ductility in the case of non-braced frames. Table 4.2 summarised the results of braced specimens, while table 4.3 gives the results for the case of frames without St. Andrew's braces.

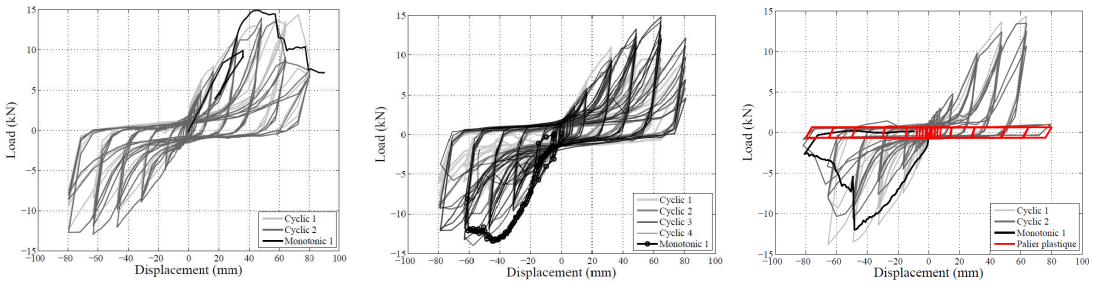

(a) Infilled with rocks (b) Infilled with Adobes (c) Without Infilling

Fig. 4.4: Lateral Force Resistance of Mini wall with St. Andrew's croses. Vieux-Champagne [135]

4.4 Scale 3: Shear wall

The elementary wall scale that is derived from the experemental results of elementary unit cell (section 4.3) by Vieux-Champagne et al. [137] is used to model the shear wall scale by distributing as a matrix form the mentioned elementary unit wall in order to construct the shear wall by assuming that the dimensions of each bay in the shear wall are identical to the elementary cell dimensions.

The wall contains 8 bays as shown in (Fig. 4.5). The vertical posts and the lintel top beam and columns were modelled as beam elements, the nonlinearities were lumped in the elementary wall, and all the joints were taken to be hinges.

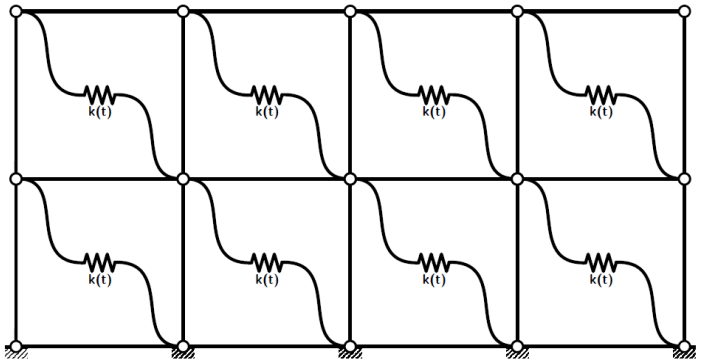

(a) Simplified FE. model for Shear Wall

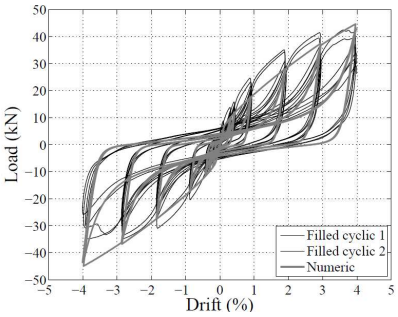

(b) Drift-Force Diagram of Filled and Empty Shear Wall

Fig. 4.5: Modeling of Shear Wall of Eight Identical Bays, Vieux-Champagne et al. [137]

Tab. 4.2: Experimental Results of Unit Wall Scale for Lateral Load at Top Corner With Braces of St. Andrew's. Vieux-Champagne [135].

Type of Infill -	Loading -	F_{min} (kN)	F_{max} kN	$Drift_{min}$ (%)	$Drift_{max}$ (%)	$K_0,-$ $(\frac{kN}{mm})$	$K_0,+$ $(\frac{kN}{mm})$	ξ %	μ_- -	μ_+ -	E_c $(kN.mm)$
Rocks	Cyclic1	-12.6	12.8	-7.95	8.6	0.45	0.89	11.8	2.02	4.74	4040
	Cyclic2	-12.8	12.8	-6.35	4.85	0.5	0.73	12.7	2.14	2.75	4196
	Monotone	-	14.3	-	4.48	-	-	-	-	-	-
Adobes	Cyclic1	-9.1	10.2	-6.35	3.25	0.57	0.63	13.8	3.51	4.77	38.71
	Cyclic2	-10.7	10.7	-4.75	4.85	0.9	0.58	13.1	2.75	2.74	3791
	Cyclic3	-12.7	14.1	-6.32	6.49	0.81	0.53	12.0	1.46	2.11	4309
	Cyclic4	-13.3	13.6	-6.31	6.49	0.49	0.58	12.8	2.3	2.04	5344
	Monotonic	-12.9	-	-4.47	-	0.64	-	-	2.46	-	-
Empty	Cyclic1	-13.0	14.0	-6.55	6.37	0.54	0.48	10.6	2.52	1.39	-
	Cyclic2	-10.2	12.5	-4.94	6.37	0.35	0.15	11.5	2.23	1.48	3127
	Monotonic	-12.0	-	-4.83	-	1.69	-	-	1.39	-	-
F_{max}		-11.9	12.8	-5.88	5.69	0.69	0.62	12.3	2.28	2.75	-
σ_d		-1.4	1.4	-1.04	1.36	0.37	0.13	0.95	0.58	1.25	-

Tab. 4.3: Experimental Results of Unit Wall Scale for Lateral Load at Top Corner Without Braces. Vieux-Champagne [135].

type of Infill -	F_{min} kN	F_{max} (kN)	$Drift_{min}$ %	$Drift_{max}$ (%)	$K_0,-$ $\frac{kN}{m}$	$K_0,+$ $\frac{kN}{m}$	ξ (%)	$\mu-$ -	$\mu+$ -
Rocks	-4.9	4.9	-4.73	3.26	0.57	0.75	16.8	6.05	8.92
Adobes	-4.5	4.3	-7.89	8.09	0.27	0.29	17.1	3.86	3.97
Daub	-4.3	5.0	-7.90	6.49	0.21	0.25	13.4	2.15	2.52
Empty	-1.3	0.5	-8.17	7.94	-	-	-	-	-

Tab. 4.4: Parametric Comparison for Shearwalls with Infill, Important values and general notes Vieux-Champagne [135].

Tested wall -	Dimensions m^2	Vertical Loading (kN)	Type of Joints -	$\lvert F_{max} \rvert$ (kN)	Drift (%)	μ -	E_d $(kN.mm)$	ξ %	Failure Location -	Wood ratio per m^2 (%)	Infill Impact $K_{initial}$	F_{max}
Kay mur [135]	3.6*2.0	0	Steel Strip	42.5	3.0	3.11	11022	15	Joint	18	Yes	Yes
Pombalino [102]	3.0*2.6	90	LJ, CHJ	50.0	2.3	9.5	26886	19.5	CHJ	43	Yes	No
Pombalino [134]	0.8*0.9	70	$M\&T$[2], CHJ	25.0	2.8	15.3	2200	16.0	LJ	82	No	No
Pombalino [111]	1.9*1.9	75	$M\&T$, CHJ	65.0	3.1	6.5	2500	-	LJ	54	-	-
Pombalino[3] [57]	1.2*1.2	25	LJ[4], CHJ[5]	60.0	3.5	-	-	-	Wood	59	Yes	Yes
Dhajji [9]	3.1*2.5	6	$M\&T$	13.7	2.2	4.8	10305	15	$M\&T$	29	Yes	No
Maso [27]	5.1*1.9	$\propto HL$[6]	$LJscrewed$	74.4	2.1	8.3	3060	18	Bracing	39	Yes	Yes

1) $M\&T$: Mortise and Tenon with nail
2) Elementary cell wall
3) LJ : Lap Joint
4) CHJ : Cross Half Lap Joint
5) $\propto HL$: Proportional to Horizontal Load

4.5 Building scale

There are two different signals for the shaking table tests, one of them is a synthetic signal called Haiti signal which can be evaluated by a proccedudre explained in chapter 6. The temporal input data and response spectrum of the the yield signal is shown in (Fig. 4.6)

The second is a distant signal called Guadaloupe signal, as shown in (Fig. 4.7) and section 6.2.2

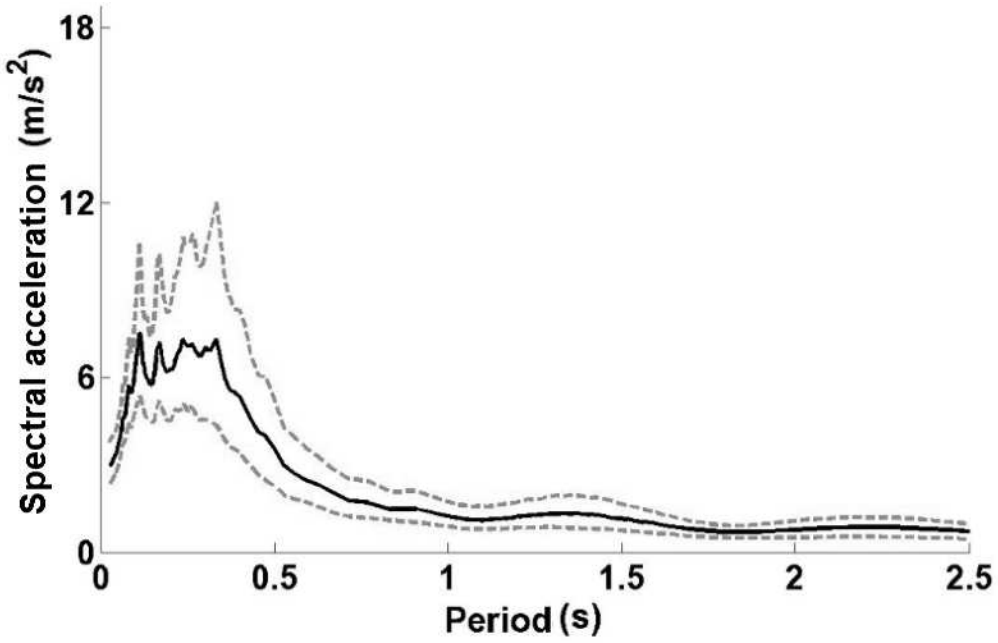

a) Elastic response spectrum of signal (5% damping) obtained from the earthquake simulation (HVPR station). 500 simulations were realized. (Average curve in bold and curves of signal limits in dotted line).

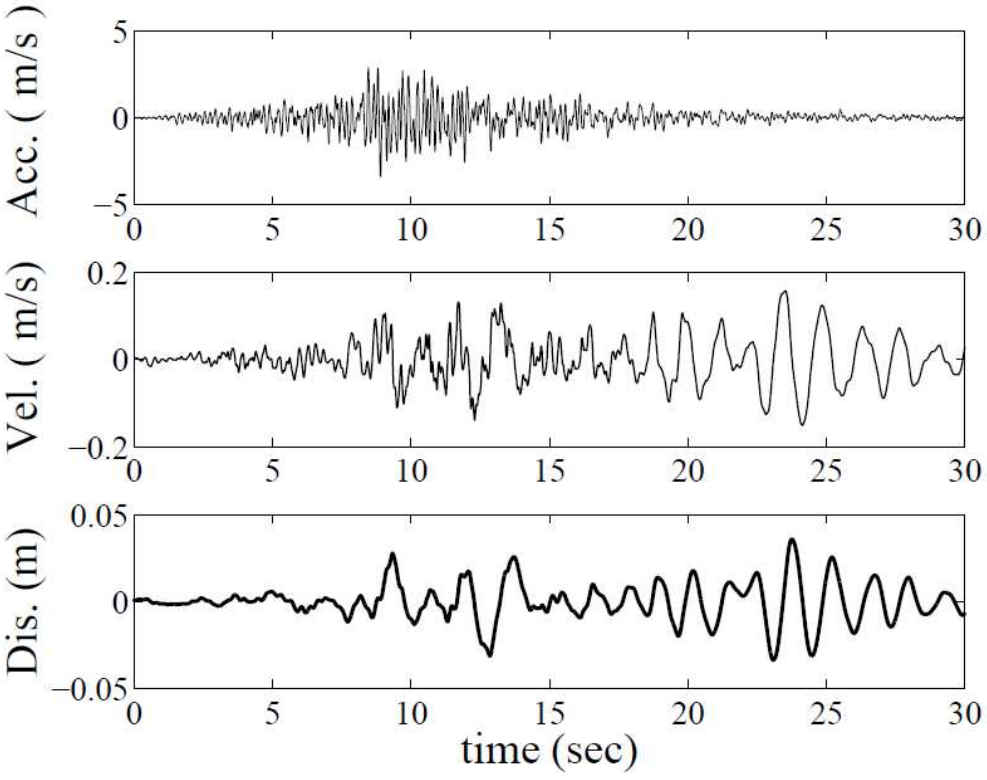

b) Temperal input data of HVPR station (horizontal component of North-South)

Fig. 4.6: Frequency and temporal input data of the signal of Haiti.

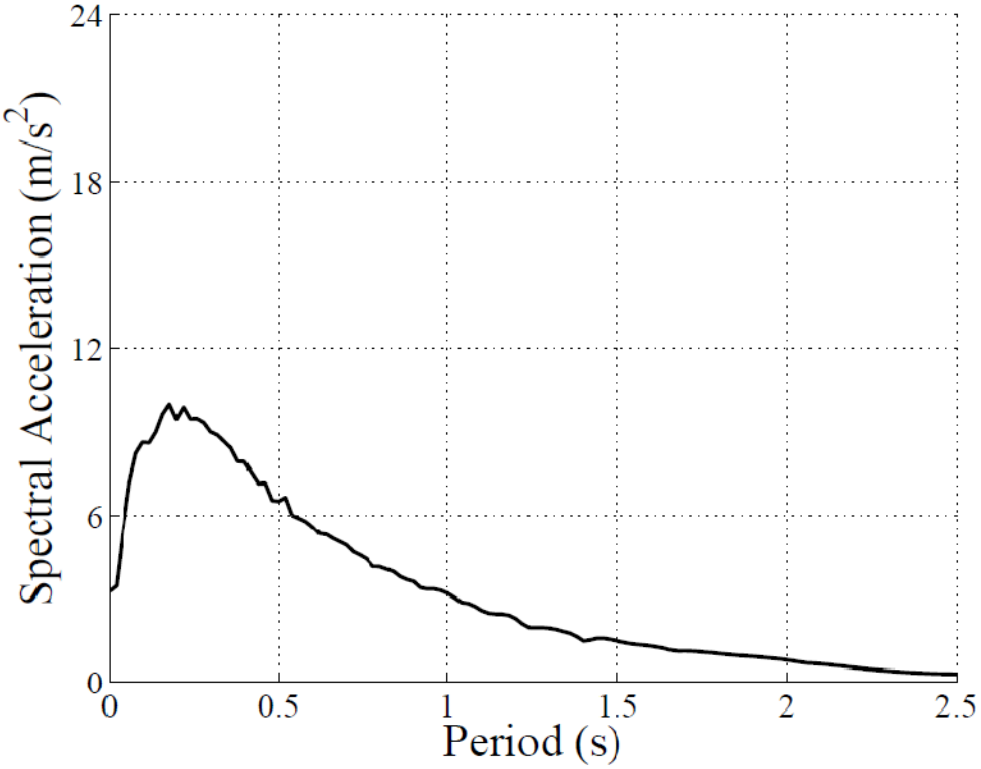

a) Elastic response spectrum of the signal (5% damping)

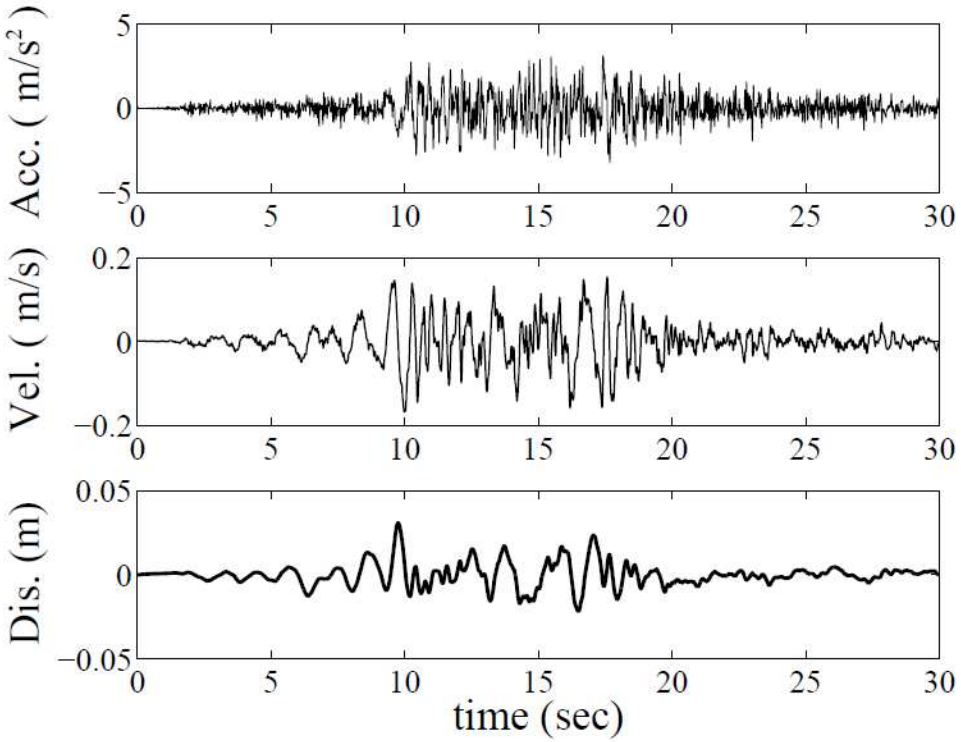

b) Input time history

Fig. 4.7: Frequency and temporal data of the distant signal of Guadeloupe Shaking test

4.6 Conclusions

IN this chapter the experemental tests which are performed by Vieux-Champagne et al. [140] are presented for three different scales and the main results for each scale were stated. Some of these results were used in present study to propose a nummerical FE model to be used in the analysis of traditional timber frame buildings and to enhancing the macroelement model which is based on one horizontal spring element by using multi scale analysis method which will be discussed in the next chapter.

5. MULTI STEP NON-LINEAR ANALYSIS METHOD

5.1 Introduction

As mentioned above, the timber structures have different structural elements connected usually by one or more fastener types into the different parts of the frames. Timber elements have a nonlinear behaviour as well as the metallic fasteners which gives the system an additional nonlinearity behaviour. To make a good understanding of these different behaviours, a multi-scale analysis technique may be a good choice for calculating the response of one or more compound structural elements in deep. In this chapter, a study of shear wall scale with the help of connection scale results will be used to derive two diagonal hysteresis elements which can be used to the analysis of any house and multi-storey building scale.
In the multi-step analysis method the procedure is normally the specimens of each scale are tested and proposed a mathematical model with some parameters for each scale must be selected efficiently. The idea of this proccedure is the testing a certain part and proposed a corresponding numerical model according to these tests and then used this model in the next bigger scale consequently till arriving to total structure size. This approach was used recently by Richard in 2001, [116], Boudaud in 2012, [18], and Vieux-Champagne in 2013, [135] for timber structures. But in our study some manipulation in the order will be used to take the analysis and design of proposed structures more flexibility. This modification can be performed by using the connection level model in the analysis of full scale shear wall test to derive one panel wall scale model, this model can be used subsequently in the real wall scale and compared the experimental results with full numerical model of full wall scale and finally suggests a mini-wall FE model which can be used for the final scale of buildings. This technique proposed can be illustrated as shown in (Fig. 5.1).

5.2 Connections at the Supports

For each physical system boundary conditions are essential to find out the specified solution. In structural analysis, the boundary conditions or connections play an important role in the mode of failures, strength, and stiffness for these structures.

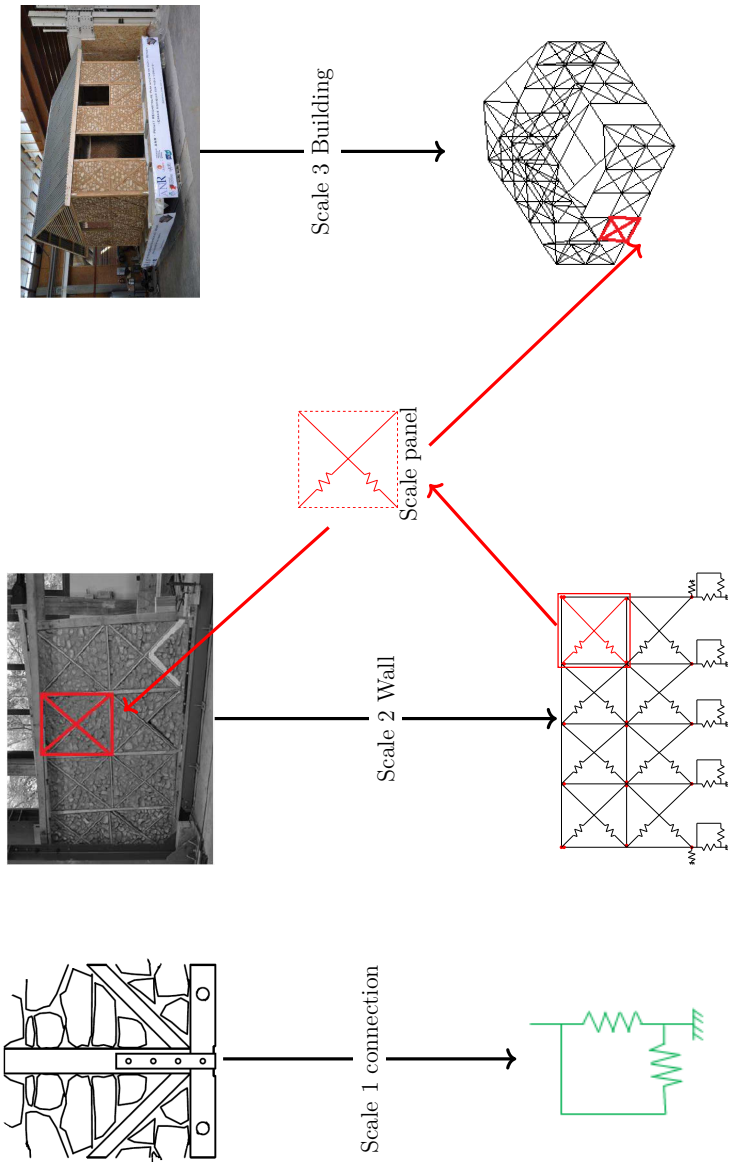

Fig. 5.1: Steps of multi scale analysis method.

In the timber-framed structures, all the different elements (beams, columns, roofs, etc.) made from timber are connected by metal fasteners to increase the ductility except some rare cases in some old buildings around the world (e.g. 2.4.1). Many metallic configurations are used to connect the brittle timber material to enhance the ductility of the joint system, (e.g. holding up [116], punching plate [82], bracket, nails [18], etc.).

The link between the sill plate and the post of the wall is a steel strip connection, the force-slip relationships test for axial pull out as well as tangential shear tests are illustrated in the Fig. (5.2). So only translation uplift and shear deformations were tested and the moment-rotation relationships were neglected due to hinge like behaviour of the bottom joints [135] and therefore, it was considered these connections as hinges.

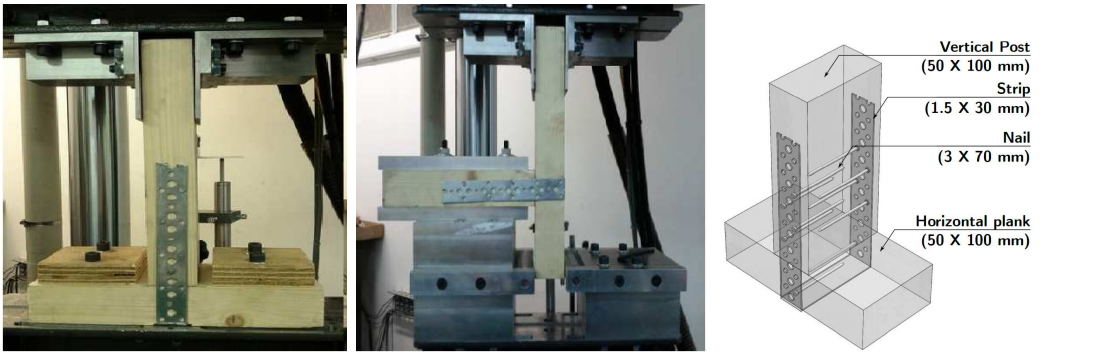

(a) Axial Deformation Test. (b) Shear Deformation Test. (a) Scheme of Connection in the Base.

Fig. 5.2: Tested of Connections of Steel Strip Connections, Vieux-Champagne et al. [136]

This constitutive laws of connections between the sill plate and the post which is depicted in Fig.(5.2-c) with 4 nails at each side of the steel plate for uplifting tension (small stiffness) and compression (higner stiffness value) in the vertical direction as in Fig.(5.2-a) and for the shear symmetric law direction in the orthogonal horizontal direction in the direction of the plane of steel strip (which is normally the plane of the shear wall) as in (Fig.5.2-b).

5.2.1 Loading protocole

The choice of protocols for these two types of loading can have a significant influence on the response of the assembly or on the structure, mainly due to the speed control of the test, Yamaguchi et al. [145] and history of loading (Gatto and

Uang, [67]. According to these authors and the observations made by Boudaud [18], it is difficult to rid or neglect these parameters during the quasi-static test. However, the magnitudes and the observed phenomena are consistent by properly choosing the loading protocols (compromise case of moderate speed with a number of cycles not too low nor too high). Most frequently available historical literature in standards: CEN EN 12512, ISO 16670, and CUREE SPD (ASTM E 2126 [2]). In this work (scale 1 and 2), the loading described in EN 12512 (see Fig. 5.4) was chosen because it takes into account the above remarks, Ceccotti and Nart, [30], [135]. All loading protocols that used in the connection tests are illustrated in (Fig. 5.5), He et al. [77], [30].

5.2.2 Behaviour of bottom connections, Uplift and Shear Deformations

The axial or parallel to post tension and compression deformations laws for the steel strip joint that is shown in Fig.(5.2-a), was tested by fixing the sill plate by two bolted plywood pieces at each side of the post with two bolts for each one, the post is connected to the actuator to applying displacement control loading protocols. The force-slip relationships for the tension law is shown below in (Fig. 4.2-a) for monotonic loading and shows a good agreement with FE model result. The last figure was calibrated according to the experiments of six different tests (4 monotonic and 2 cyclic) with factored average maximum force value equals to (11 kN), [135]. This last term is the average of maximum force at each tension test taking into account the different densities of wood specimens acording on equation (8.15), in the EC5 [54] which shows the effect of the characteristic timber density (ρ_k), so the resistance force for each specimen must be factored to an equivalent C18 timber class [55], Dorn et al. [51] (which has characteristic density ρ_k of 320 kg/m^3). The compression resistance of the joint is much more as compared to tension in terms of maximum force resistance as well as stiffness. The maximum resistance of compression is selected according to Vieux-Champagne et al., [140] equal to (39 kN). A schematic shape which illustrates Hysteretic constitutive law for the bi-axial and symmetric shear deformation in the bottom joints is depicted in (Fig. 5.3).

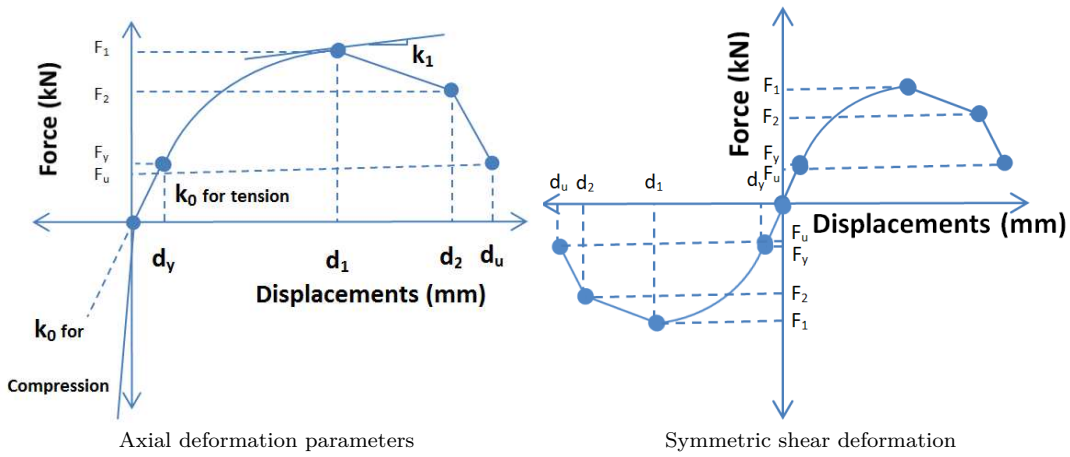

Fig. 5.3: Backbone curve of Humbert's law for connections

The initial stiffness of the connection in compression is (80 kN/mm) according to Vieux-Champagne [135], all other parameters were taken from the last reference. The calibrated FE model of the connection for tension and the experimental cyclic test with peak force resistance equal to mean value (11 kN) is shown in (Fig.4.2-b), it can be seen a good agreement between the experimental and numerical model based on these parameters results in terms of stiffness, force resistance, damage, and energy dissipation.

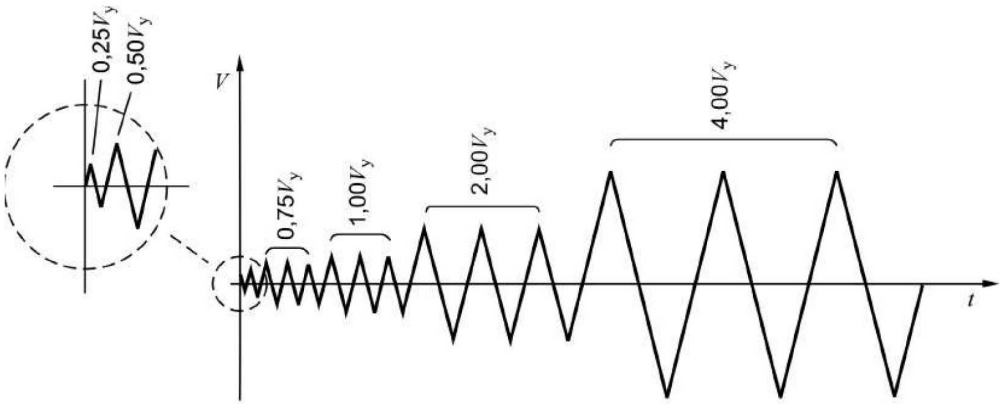

Fig. 5.4: Cyclic loading protocole according to EN 12512 [30].

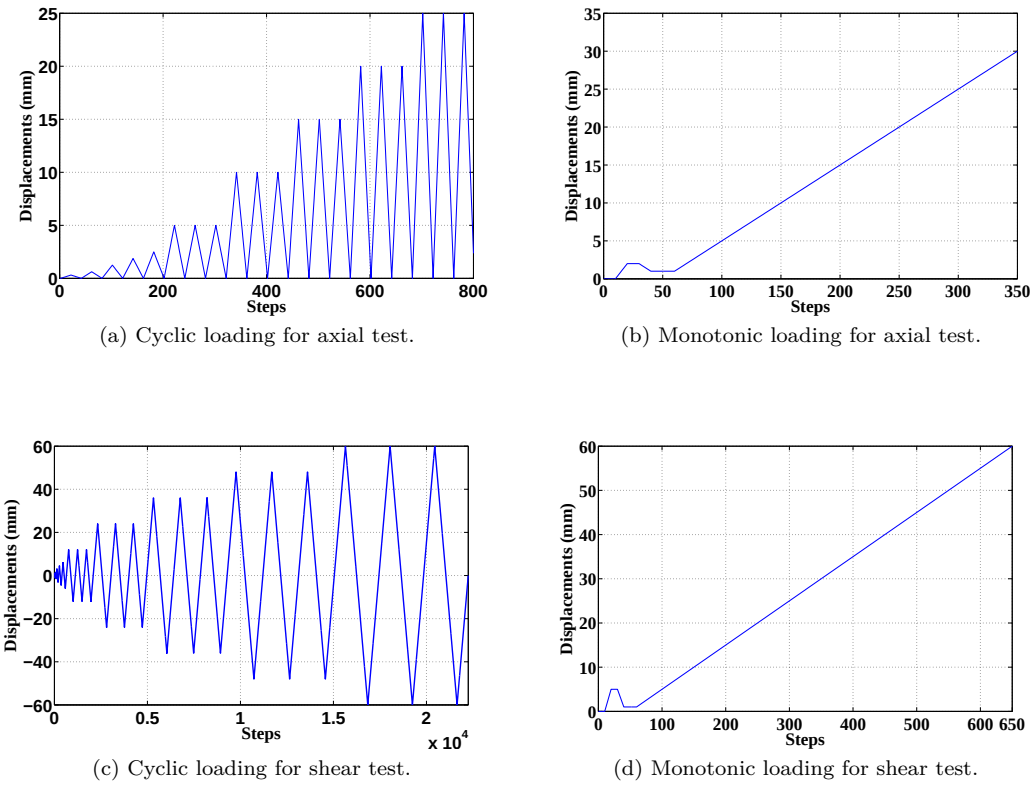

(a) Cyclic loading for axial test.

(b) Monotonic loading for axial test.

(c) Cyclic loading for shear test.

(d) Monotonic loading for shear test.

Fig. 5.5: Displacement loading protocols, EN 12512, EN26891 [30], [135].

In addition to the axial tension test, a tangential shear test was performed to the joints as shown in (Fig.5.2-b) for 4 nails at each side of the steel plate. The force-slip curve shown in (Fig. 4.2-c, d) for monotonic and cyclic tests respectively. It is evident that the shear resistance of the joint which is the perpendicular to the vertical post is symmetric, so the positive and negative parameters in table 4.1) are identicals, this table listed also all the parameters required for tension and compression behaviour of the connections. All the parameters were calibrated and optimised according to Hysteretic constitutive law model (section 3.5) by using trial and error method. The dotted curve of calibrated monotonic response, (Fig. 4.2-c) shows the average path of the numerical result as compared to the other tests which are factored according to the density of each specimen. Also, we can see good agreement between numerical cyclic response and cyclic test for shear direction. There are some little differences in the values of peak forces at the cyclic experimental curve in the end of each loading loop in the positive and

negative sides, this differences is due to fixing the actuator in one side (the metal two inverted L letter shape at (fig. 5.2-b)), so the full symmetry of the compression force (downward vertical) in the actuator and tension force (upward vertical) are not exactly symmetric, so the parameters of the model are selected depending on positive direction.

5.2.3 *Energy dissipations in the connections*

The phenomenon of energy dissipation in both types of loading in the connection system is taking place with the splitting of the connecting nails, this process may occur mainly in our case due to the shear forces subjected in the plane of cross sections of the nails, but the high rigidity of the steel strips and nails cause the nails to pulling out of the wooden body which is the weakest part. Figure (5.6) shows the energy dissipation of the joints for the cyclic loading in tension and shear tests and it illustrates a good agreement for the cases of experimental and numerical model calculated by finding out the area inside each hysteresis loop. So this comparison proves the ability of the FE model of the joint to dissipate the same amount of energy in addition to the previous mention parameters.

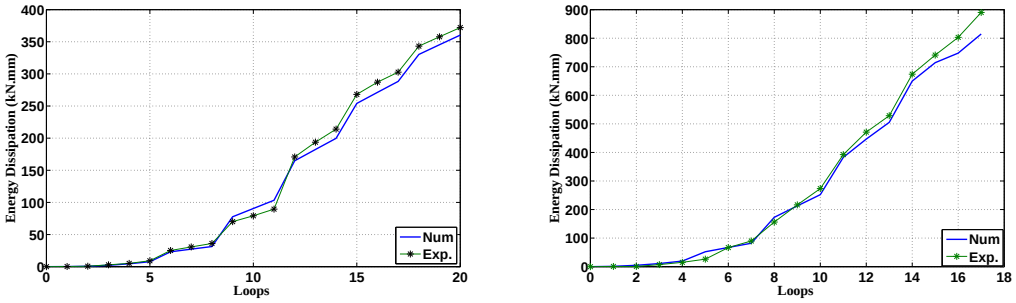

Axial deformation test

Shear deformation test

Fig. 5.6: Energy dissipations in the connections.

5.3 *Scale two: Shear wall*

In our study, the second scale used is the timber shear wall scale, this structure is compound of main timber frame infilled with in-situ rocks and mortar of clay or any available cheap mortar, this composite materials structure was tested for a quasi-static monotonic and cyclic tests to study its structural behaviour and discover it's ability to undergo the seismic loading conditions. The experimental program

has been performed at the CNR-Ivalsa (Trento, Italy) by Vieux-Champagne [135] and the testing machine with the wall installation can be shown in (Fig. 5.7). The dimensions of the wall knowing that the normal to plane thickness is constant and equal to (100 mm) can be found in (Fig. 5.8).

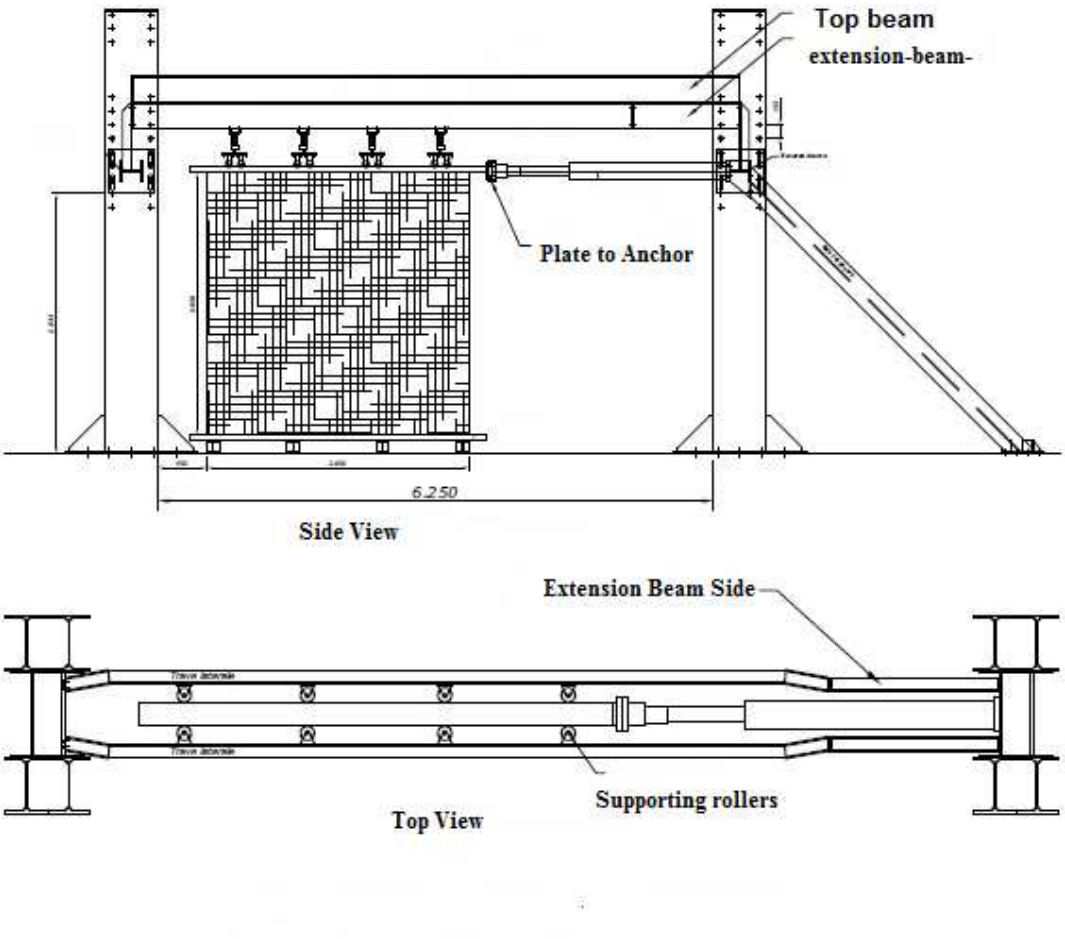

Fig. 5.7: Testing apparatus with the shear wall specimen [30]

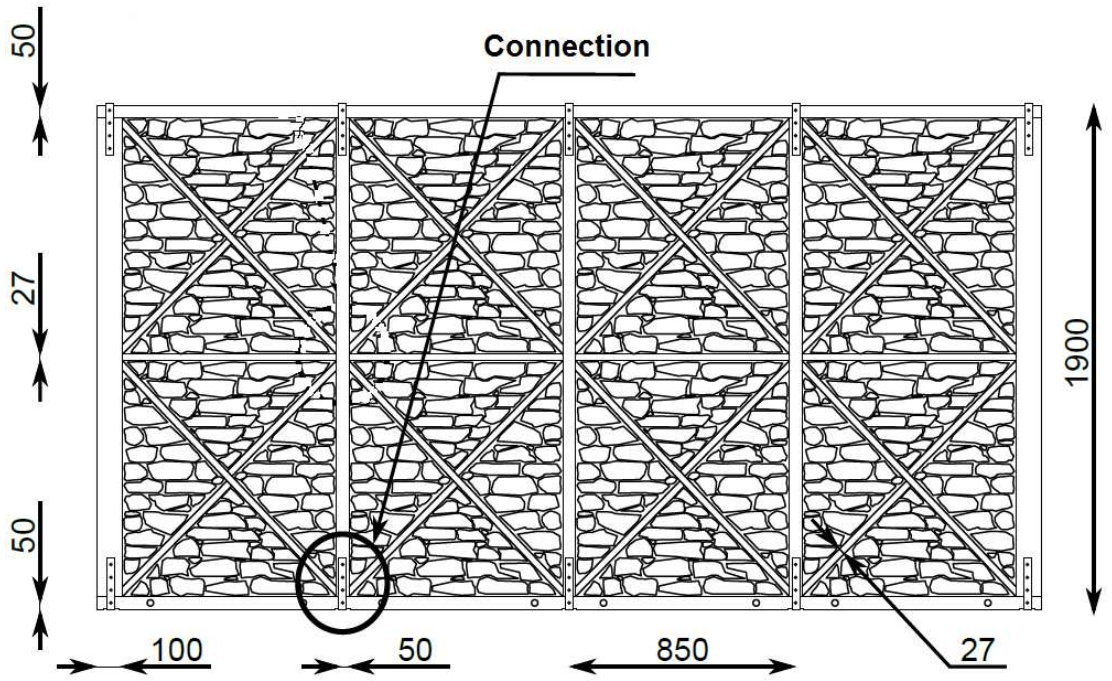

Fig. 5.8: Dimensions of the timber shear wall with infilling.

5.3.1 Simplified modeling of timber frame structures

As mensioned above the objective of this thesis is to propose a simplified finite element model to be used in the analysis and design of timber frame structures infilled with any available cheap materials subjected to severe earthquake excitation and this technique may be used effictivelly as in the poor countries which proved to be safe in many recently earthquakes, one of these examples is the two neighbor buildings after the 1999 *Düzce* earthquake in Turkey [48], in this type of composite structures the analysis is difficult to do with many complicated interactions between the different materials and the connection among them, so to decrese the calculation time and implemented a suitable analysis method for the practical engineers and building codes a simple numerical model needed for this objective.

5.3.2 Main frame

This simplified model is an integration of main timber frame with five columns. The two terminal columns as shown in (Fig. 5.8) above is doubled in width as compared to the middle columns, the last have the same dimensions with the top continuous beam. The mid-height horizontal timber braces are modelled as linear bar elements with axial forces only and no moment resistance. The (2×4) identical cells which are compound of two diagonal timber braces and infilling materials. The basic idea of our model is to model this compound system (infilling and the two diagonal timber braces) by two nonlinear diagonal elements as shown in (Fig. 5.11). This two identical springs display nonlinear backbone force displacement behaviour follows Hysteretic constitutive law model according to Bézier's curve, (see appendix B) Prautzsch et al. [112], the reason to choosing Bézier's curves instead of exponential functions as usually in the timber structures, (eg. White et al. [142], Foschi, [66]) is due to the flexibility of calculating analytically the stiffness of the back bone curve at any point when we use Bézier's curves whereas the experimental and simulated results do not give the values especially in the region arround peak force reistance because of the nature of exponential function, Humbert [82]. The thick red points in the (Fig. 5.11) represents the modeling of the structural hinges in the shear wall where there is no bending moment, these locations of the hinges will still in the full house scale (see chapter 6) at the corresponding points in the house scale. The free rotations in these points can be assumed because of we do not have moment-rotation relationships for these specified joints and also if we take a look at (Fig. 5.9) which shows the ability of the joints to rotate relatively freely in the plane of the shear wall.

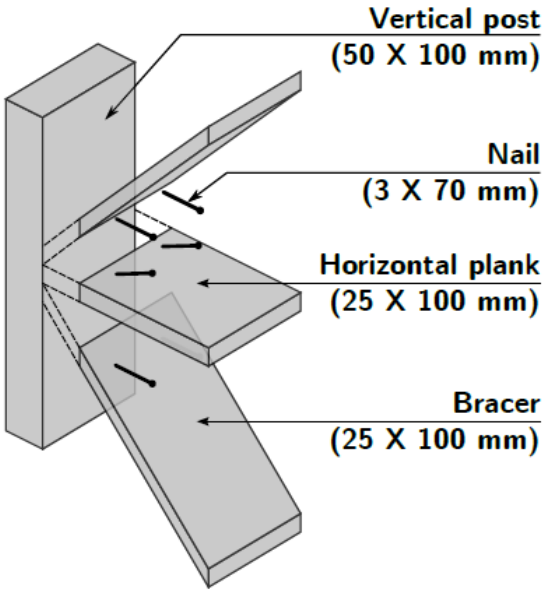

Fig. 5.9: Joints in the mid height of shear wall, [135].

5.3.3 Unit cell model

The parameters of these springs are different for compression and tension deformations. These bi-nonlinear behaviours come due to the fact that the compression in the timber crosses and the surround infilling materials is stronger in the compression than in the tension deformation case. The two identical diagonal springs were used instead of one horizontal macroelement. Most of the timber shear walls macroelement used the one dimensional horizontal springs, e.g. Boudaud 2012, [18], and Vieux-Champagne 2013, [135] but this approach of inclined two braces FE. was also proposed in the literature by Dujic and Zarnic, [53] which propose a transformation equations for the deformations of lateral horizontal displacement to the displacements in the directions of each diagonal spring and it was used by Xu and Dolan, [143] which used it for OSB modern building.

It should be noted that the analytical equations of two diagonals that are used by Dujic and Zarnic, [53] and also almost same equations was used by Xu and Dolan, [143], but these equations can be used only as a sub-element with specified dimensions and materials and not valid for full shear wall because the assumption of truss modeling leads to making the forces in the springs as axial thrust, consequently the external forces can not be concurrent and aditional moment resisting

devices are required. In our case, this condition was applied but for idealised shear walls models for modern and traditional applications it must be carefully modelled. For the walls at which modelled as one superelement a second optional solution can be used by adding transverse DOF at each node in the hysteresis spring element which is removed in our study (see table 5.1), (i.e. modelling the spring as beam instead of the truss).

The choice of the two diagonal springs comes from two reasons:

- To maintain the symmetry of the structures for the symmetrical sub structures or uniform repeated elements and then to make sure that the load distribution will approach as accurate as possible.
- For the case of numerical modelling, some of the structures modeled as a truss, the using of one horizontal spring transmits the horizontal loads but not the vertical and these calculations may lead us to lack in the design of some elements effectively.

For the sake of illustrating these different behaviours, and the modelling of the wall according to the lateral force in the left up corner in the shear wall (Fig. 5.11) as follows:

- **Compression force**: The behaviour of the diagonal part at each cell wall which contains of an infilling materials of clay and rocks and two diagonal timber braces can be consider as like as the behaviour of concrete structures with strut (in the compression zone) and tie (in the other diagonal direction) under tension. That means the diagonal zone of timber braces and (surrounding infill which is parallel to braceed bar) can be considered as a strut in the compression zone and tie in the other diagonal direction, Reineck [115]. This analogy of the traditional buildings with the concrete structures come from the nature of the similarity of the material behaviour of infilling materials of clays and plain concrete specimens, (i.e. high compression concrete and very weak strength in tension). This compression strength in each cell is also due to timber bracing member which represent the main element of each one of the eight-unit cell as shown in the (Fig. 5.8). So the diagonal compressive force in each cell inside the walls is resisted by these timber braces and the surrounding infilling by the same way in the case of a concrete strut, see (Fig. 5.10) In spite of that, the equivalent nonlinear spring elements proposed to have a maximum force resistance which is equivalent to the C18 timber allowable compression and the cross-sectional area of these timber braces which is equal to (48.6 kN). This value could be justified by the experimental results of shear wall tests and the physical fact that in the

compression region of the strut model in the traditional buildings especially that when they used clays as a cheap mortar material, the adhesion forces between wood and clay is very weak so the participation or the increasing of the infilling in the compression resistance is small due to the lateral tension force in this diagonal compression zone or (strut prism).

- **Tension force**: The resistance of tension force in the diagonal spring at each panel is weak in terms of strength and stiffness as compared to the compression even in the timber brace due to the pulling out the nails at the corners which separate the diagonal from its original position. In the case of lateral loads on shear walls like monotonic or cyclic tests as well as earthquake excitations, half numbers of the FE. braces subjected to compression forces and transmitted to the base whereas the second half of the other diagonals direction subjected to tension, this sign convention of the forces will be reflected in the reverse direction of the loading. So the parameters in the springs which define the behaviour of the numerical bracing spring elements and the surrounding infilling are different for tension and compression deformations.

- **Shear force**: The design of each diagonal spring according to Hysteretic constitutive law model is considered by neglecting the shear and flexural resistance so it is a link-like element. The physical justification of the bar element type is the existing of the confinement due to infilling prevents the timber braces to buckle and no bending will occur and then the loading transfer as an axial force only, so all parameters of Hysteretic constitutive law in this case will be vanishing.

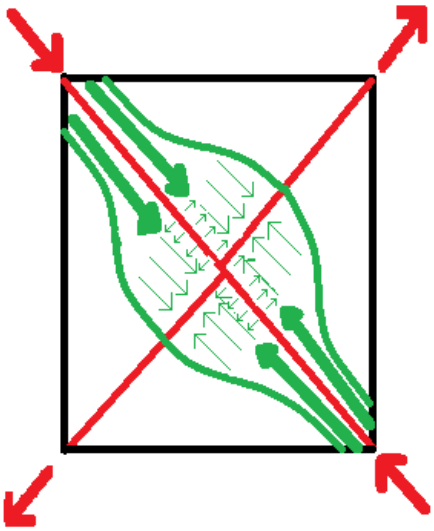

Fig. 5.10: Schematic Strut and tie model in the elementary wall.

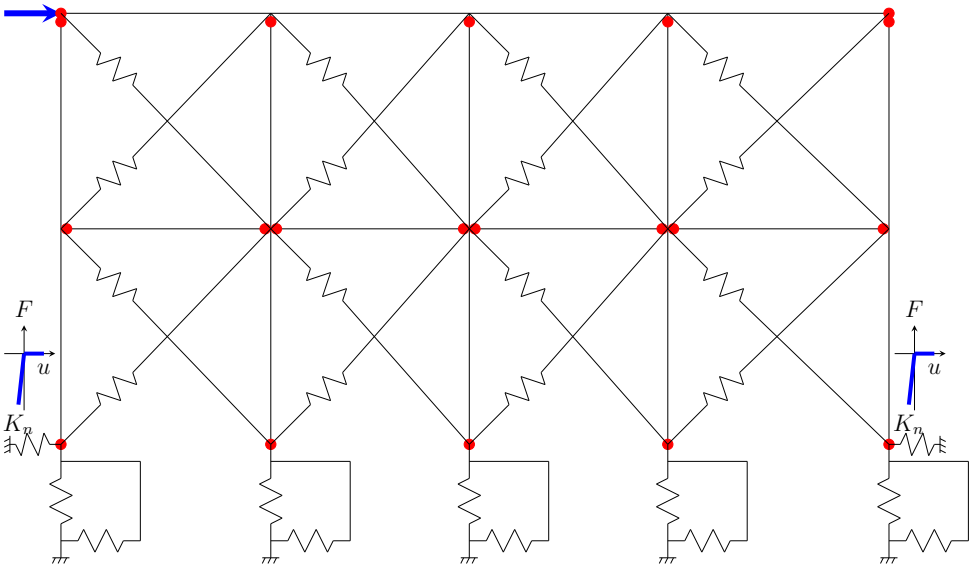

Fig. 5.11: Finite element modeling of the shear wall.

5.3.4 Side supports modeling

In the experimental test, there are two side supports in each end of the shear wall, one of them can be shown in (Fig. 5.12). The purpose of this fixation device is to increase the stability of the wall and this will force the wall to fail in racking (shear) and overturning mode, so as to make the failure of the connections is due to the exceeding the tension resistance in the bottom joints. This support prevents the bottom side of the post to slip outside, it's clear from the figure that it resists the compression force which comes from inside direction of the wall to outside and no tension resistance due to this device because when the post displaces away from the support there is no contact between them. Thus the side support was modelled as a spring with no resistance for the tension deformation but with compression resistance with a stiffness of (lets called $K_n = 1\,\mathrm{kN/mm}$) in each side as shown in the (Fig. 5.11).

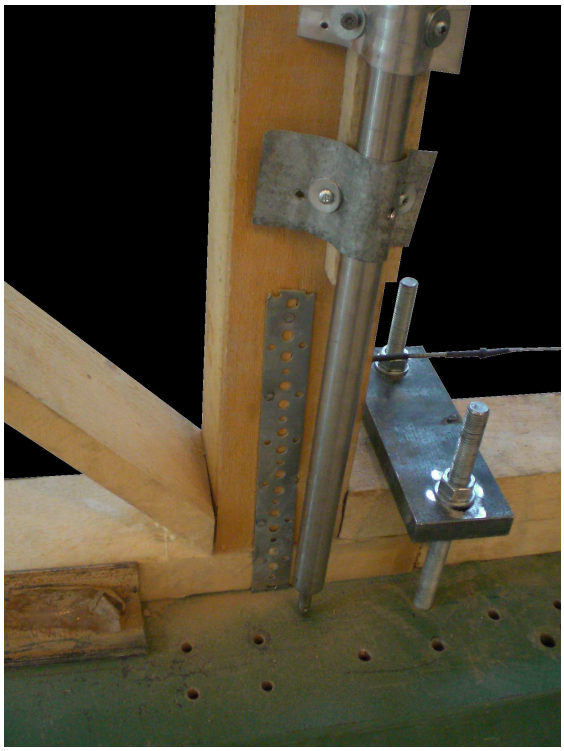

Fig. 5.12: Side suppoting of the shear wall.

5.3.5 Joint bottom supports

Under each vertical post, there is a connection support connects the post with the foundation of sill plate with properties calibrated from scale 1 (see section 5.2). In our study, the objective work is to validate and calibrate the structural elements according to the experiments in the laboratory, so the real in situ practical behaviours of soil structure interaction will be neglected because of the foundation of the frame in the laboratory is rigid and no relative displacements occur between foundation and sill plate. The sill plate itself was fixed rigidly to the foundation (floor of the lab.) by strong steel bolts and the only relative deformations occur between the fixed sill plate and the bottom part of the vertical post.

For the calibrated parameters of the tested joints for uplifting tension test it will be used as mentioned above according to mean values, but for the shear deformation it is not the case but we will increase the force values and then the corresponding stiffnesses in the law by (10 %), this increase can be explained logically by taking into account the existing of infilling in the physical model and removing in the numerical knowing that the tested shear for joints was without taking account for the infilling. The existing of the infilling inside each panel will gives an additional big confinement to the posts and prevent or at least decrease the horizontal slip of the bottom node of the post, the values of the forces in the table (4.1) for the case of shear deformations was increased by (10 %) for the specified case of infilling of rocks and clay mortar. Also this increasing comes from (but with less effect) the two braced bars which can absorbe some amount of the horizontal force energy and redistributed to the mid-height nodes of the two adjacents posts.

5.3.6 Self weight

Timber structures are the lightest structures but with some cases of traditional heavy timber-infilled structures, the weight plays a more significant role in the behaviour of such structures. As a conclusion from (section 2), the existing of vertical force of the walls has a significant effect on the behaviour of shear walls. Actually, there are no applied vertical loads on the wall but the self-weight of the wall can be considered as a concentrated vertical loads on each node in the discretization of the FE mesh. Each cell has a weight of (150 kg), so each node has a quarter part from each panel. (Fig.5.13) shows the distribution of self-weight at each node, the red rectangles represent the shared part of weight for each node, the nodes are located by the blue circles.

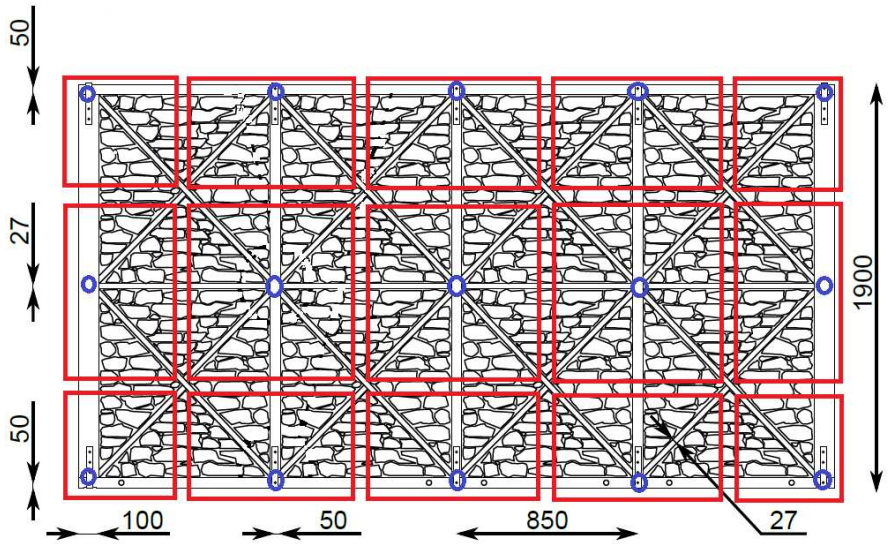

Fig. 5.13: Distribution of the self weight participation at each node.

5.3.7 Shear wall tests and calibration of FE model

The experimental results of force-drift relationships of full scale shear wall monotonic and cyclic tests were used to develope a mini-wall size FE model. This model represents the dimensions of one panel in the full size of shear wall which constructed by two diagonal timber braces and infilling of natural rocks and morter of clay. This FE model can be evaluated by using multi-step analysis technique by using Hysteretic constitutive model but with manipulated proccess as stated above by deriving the properties and parameters of the model from the wall results.

The advantages of our technique as compared to the previous studies are:

- Decreasing the experimental efforts and reduced the cost of tests by using three level tests instead of four.
- This way gives more flexible and more accurate results in the designing traditional timber frames because the model removes the effect of the stiffnesses and strengths of the main frame elements and consider only the effect of timber braces and infilling inside it.
- Each panel of them can be used for the design requirements if it has a properties of the same materials of infilling and the same dimensions of timber

braces members and the same dimensions of panel, so this way could simplify the design of buildings with the identical parts (say panels) which reduced the cost by using available in situ economic materials and simple efforts for the labours by reducing the complexity of construction processes.

5.3.8 Monotonic shear wall test

To study the behaviour of the shear wall for lateral loading and to define the backbone curve of force drift, the tested specimens of the shear wall give a good performance in terms of strength and ductility with a moderate level of damage and according to the pseudo-static tests of pushover loading. The test was performed by applying the actuator in the left top corner by displacement control according to the same way that was used in the connection scale, (section 5.2) and is shown in (Fig. 5.14). The drift can be used as a dimensionless parameter to assess the deformation which is the ratio between the lateral displacement at the top corner of the wall to the height of wall for one-storey building and the difference in the lateral deflection of two successive storeys to the different height between them. The monotonic curve for tested wall and numerical model can be shown in (Fig. 5.15).
One of the simplified methods to study the nonlinear behaviour of elements is the elastic-plastic behaviour that is the constitutive law is a compound of two linear elastic part follows by a perfect plastic plateau with constant force value, Munoz et al. [105]. This method called equivalent energy elastic plastic (EEEP) which is at the first used for the concrete and steel structures but it can be used for the timber or timber steel connections. This bilinear relationship can be derived by equating the strain energy of the real behaviour constitutive law with that the same amount of energy of elastic-plastic law (see (Fig. 2.20-d) in section (2.5)) and according to the Eq. (5.1) below:

$$P_y = K \times [\Delta_{failure} - \sqrt{\Delta_{failure}^2 - \frac{2.w_{failure}}{K}}] \tag{5.1}$$

Where: P_y: Yield force, K: Equivalent elastic plastic stiffness,
$\Delta_{failure}$: Deformation at failure, $w_{failure}$: Energy dissipated until failure (failure defined at the displacement of the 80% of the peak force after peak in the original constitutive law), Munoz et al. [105].

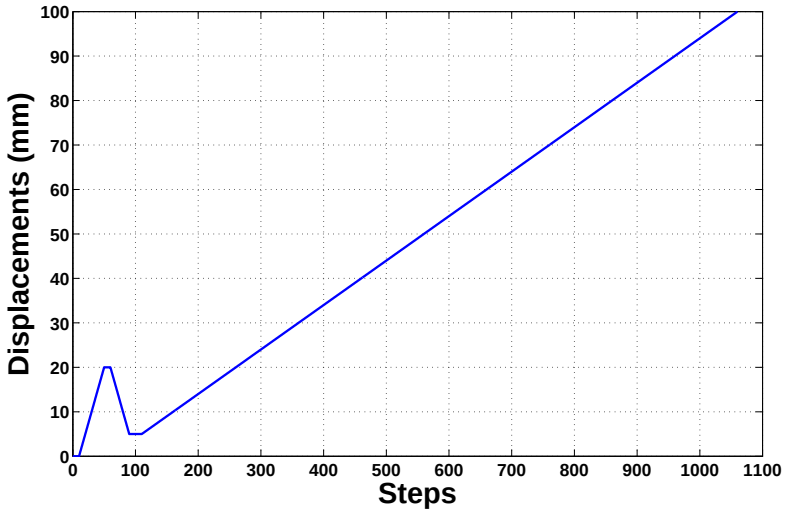

Fig. 5.14: Monotonic displacement control loading protocol.

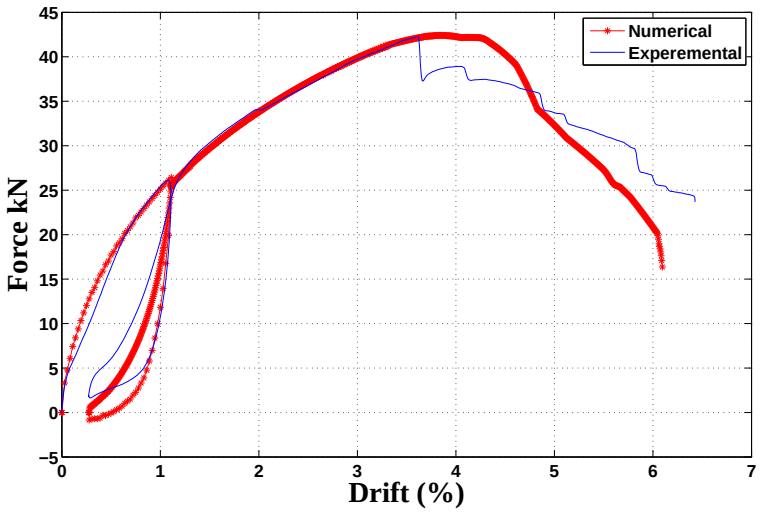

Fig. 5.15: Monotonic force displacement relation of shear wall.

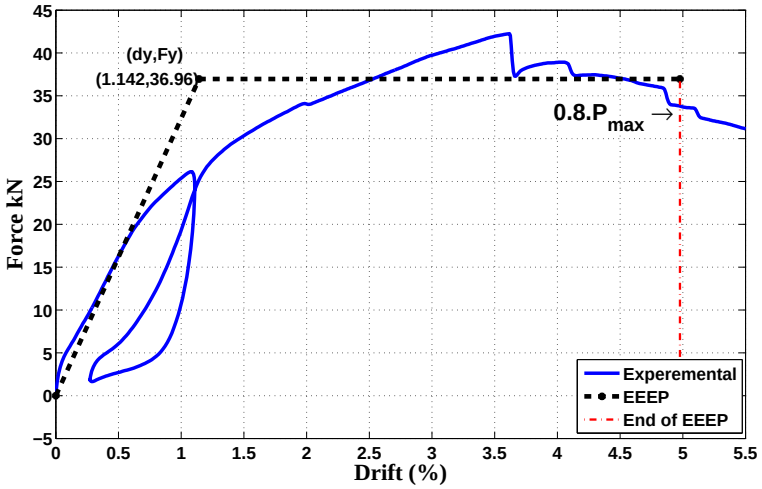

Fig. 5.16: Equivalent energy elastic plastic (EEEP) representation of the shear wall.

We can recognise from the above curve in the (Fig. 5.15) the good agreement of the results in terms of maximum strength, initial and followed hardening stiffnesses until peak force, the sudden decreasing in the force at a value of drift (3.64%) is due to the sudden splitting in one or more of the eight nails in one of the connections which not the case in the numerical model. We can recognize also the gradual softening of the tested values and a more steep degradation in the response of the model, this little differences may be logically explained by the role of infilling materials to decrease the steepest softening phenomenon. This may be an emphasis by the fast dropping in the resistance of numerical results after a value of drifting of (6.0%) because the model does not include the infilling directly whereas the experimental values continue softening at a moderate rate. This behaviour prove the good performance of the timber buildings with infilling and shows us the effect of infilling in the incresing the high ductility of this structures and this may be also emphasis by the big value of drift of more than (6%). The difference in the behaviour at the unloading stage of monotonic loading protocol is due to existing of the infilling materials which reduce the negative displacements by the friction effects between the timber members and the infilling materials and this friction is obeyed to the general mohr-colomb theory (dry friction contact for rocks materials and cohesion for morter) and this effect was neglected into our simplified model. Knowing that the energy dissipation in the two cases (numerical and experimental) as shown in the monotonic figure (5.15) are identical according to the equal area

enclosed by the elliptical loop of the figure above.

5.3.9 Cyclic shear wall test

In addition to the monotonic test, two cyclic tests were performed to the shear wall to study the other information of the behaviour in the case of reversed loading conditions. The main reasons for the cyclic tests are to estimate the response of the multi-scale structures (joints, columns, beams, walls, etc.) to the successive difference in the directions of loading sources (force, displacement, velocity, acceleration, etc.) like seismic excitation. The displacement loading control of the two cyclic loading is shown in (Fig. 5.17), this protocol is based on EN 12512 (2002), with a maximum displacement of (80 mm) and a slip limit of (20 mm). The tests are driven by an LVDT at a speed of (2.2 mm/s), Vieux-Champagne [135].

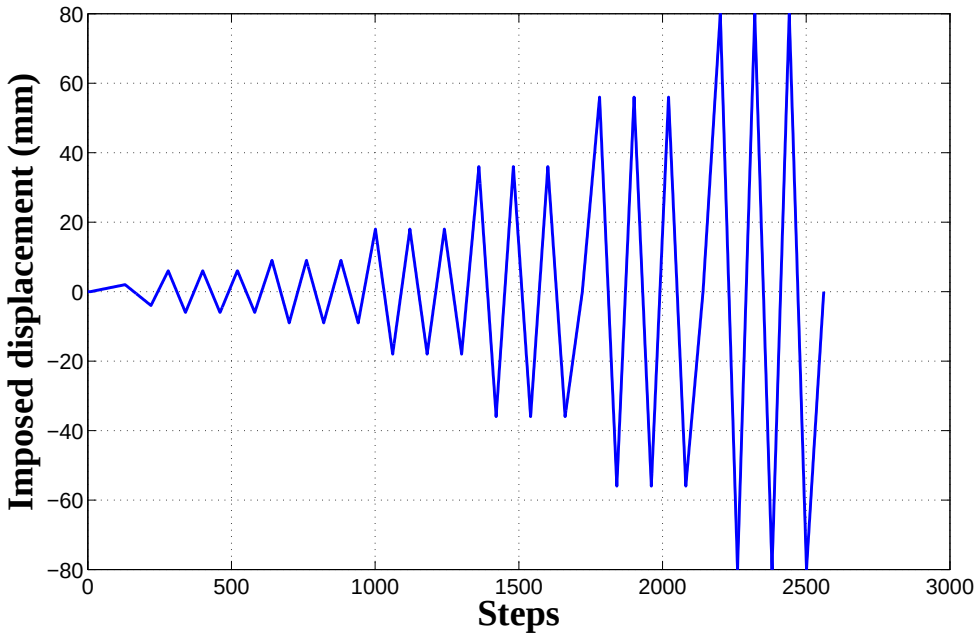

Fig. 5.17: Applied displacements of shear wall.

The response of the cyclic loading of shear wall for two cyclic tests and numerical response can be shown in the (Fig. 5.18), it can be shown that there is no full symmetry of the negative and positive force resistance especially for the first

test (cyclic 1) it may be due to the the construction method of the timber braces which is not exactly symmetric because one of the two oriented timber braces were partioned and installed such that it will not aligned any more and there is a shifting a way in the center of the frame by a distance equal to the thickness of timber braces in the plane (27 mm) as shown in (Fig. 5.8) so as to be possible to knocks the nails in each part of timber braces to fix it to the other oriented aligned one. The numerical model results were symmetric and gives an acceptable increase in the strength to the experimental results. In the other hand there is also some difference in the results between the two tests. We can see the good agreement between the response of the numerical model and the tested results with some bigger difference in the negative part which is accumulated due to the little differences in the positive part and the non symmetric experimental curve as mensioned recently. It can be shown also that the initial stiffness are the same for all cases.

5.3.10 Calibration and estimating Hysteretic constitutive law parameters

The cyclic curve is followed the backbone monotonic curve with some degradation throw the successive cycles and the cyclic behaviour helps us with the basic monotonic cureve to define the other parameters of the panel scale FE model based on the depicted scheme in (Fig. 5.11). These all required parameters of the panel scale FE model from monotonic and cyclic tests are listed in the table (5.1). It is intrested to know that the strength of the unit cell system in the tension is law as compared to the resistance of compression as mensioned due to premature losse in tension strength at the corner connections an the unit wall panel, this choice was adopted also by Kouris et al. [92] and, so the parameters are differents in each case.

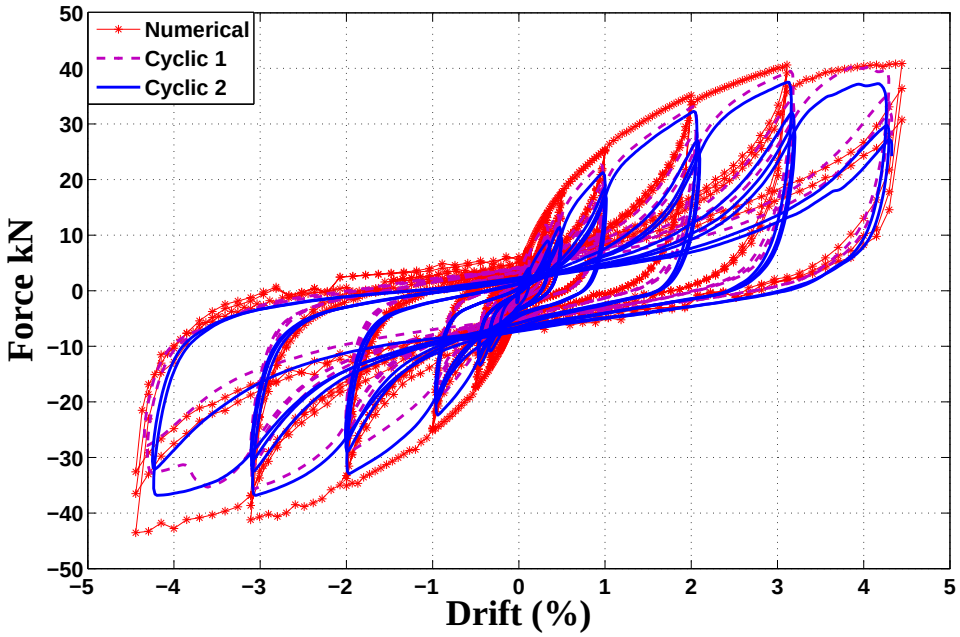

Fig. 5.18: Cyclic force displacement relation of shear wall.

5.3.11 Energy dissipation and equivalent damping ratio

In the structural analysis the energy consumption and dissipation have an improtant role in the distribution of forces and deformations with all parts of the structures. One of the important sources of the resistance forces to the dynamic loading effects is the damping force which is modeled conventionally by a viscous fluid damper analogy and one of the main energy dissipation sources is the hysteresis energy and can be evaluated from the cyclic curve. When the strain level pass the yield point, plastic deformations will occur and the reloading state curve does not return back to the original displacement point, this phenomenon leads to permenant deformation and the force-displacement curve makes a series of loops and the area enclosed by these loops represents the energy dissipation and mathematically it is simply to reflect these amount of energy to an equivalent viscous damping to be used in the general dynamic equation of motion (Eqn. (3.1)) in the damping force term. The strain energy of the shear wall which can be obtained by calculating the area monotonic curve till a value of drift (6%) are

Tab. 5.1: Actual parameters of Humbrt's law for unit cell panel.

Parameter	**Axial Tension**	**Axial Compression**
d_y (mm)	0.005	0.003
F_y (kN)	0.0193	0.084
d_1 (mm)	330.0	170.0
F_1 (kN)	2.0	48.6
d_2 (mm)	340.0	180
F_2 (kN)	1.0	40.0
d_u (mm)	350.0	190
F_u (kN)	0.5	35.0
η	0.2	0.3
AC	0	0
AR	1	1.0
BC	35	35.0
BR	2.6	2.6
C_1	-3.0	-3
C_2	-1.0	-1
C_3	0.1	0.1
C_4	0.5	0.5

equal to (**3504 kN.mm** for the experimental monotonic test) and a value of (**3479 kN.mm** for the Finite element wall model), that is the percentage error is (0.72%) which prove the efficiency of the our simplified modeling method. The equivalent viscous damping ratio (EVDR) value of the tested shear wall can be calculated according to (Eqn. (2.2)), which can be re-written as (Eq. (5.2)):

$$\xi eq = \frac{E_d}{2\pi(E_s^+ + E_s^-)} \tag{5.2}$$

It is very important to know that the value of E_s is the linear strain energy in both the positive and negative displacement axis, (Vasconcelos et al. [134], and Magenes and Calvi [99]), this last shape equation can be clarified by the (Fig. 5.19) below.

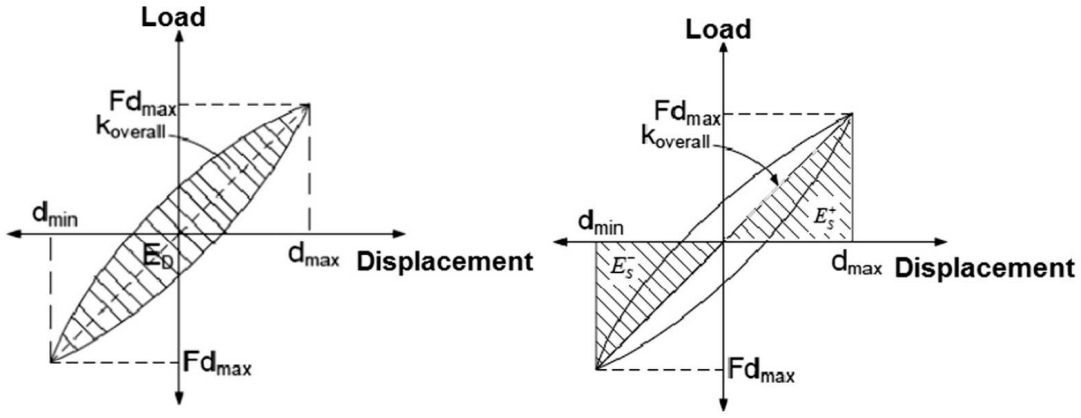

a) Hysteresis damping energy dissipation. b)Linear potential energy.

Fig. 5.19: Scheme drawing shows the definition of Equivalent viscous damping ratio (EVDR), Vasconcelos et al. [134].

The energy dissipation in the successive cycles of shear wall cyclic tests are illustrated in (Fig.5.20) for two tests and comared to the energy that dissipated by the numerical model, from these graphs we can see that the energy dissipation of the model is little bit more than that consumed by the real case, and these errors are (12.5% and 15.24% for the two tests), this percentage error not all coming due to the difference in behaviour of the experimental and numerical models but also due to the cummulative error between the real experimental data which have alredy some perturbations and rough curve values especially at small values of forces and displacements and also when the loading changing its direction.

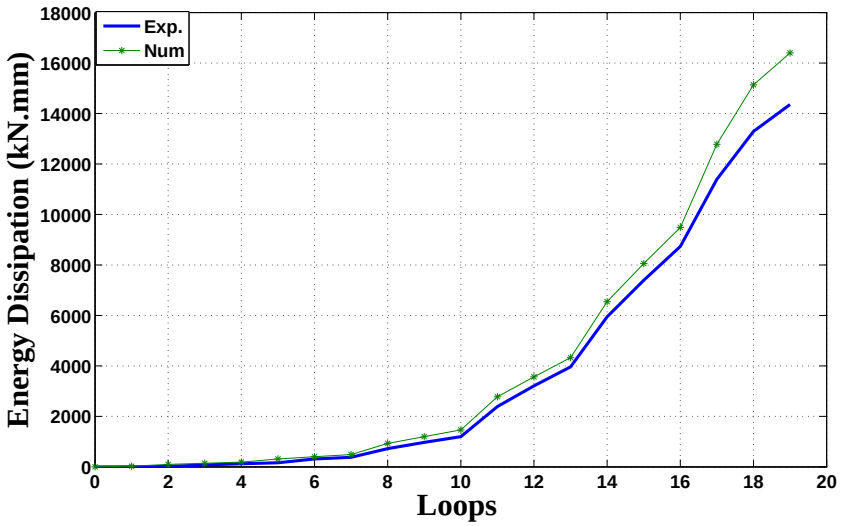

a) Comparison with cyclic 1.

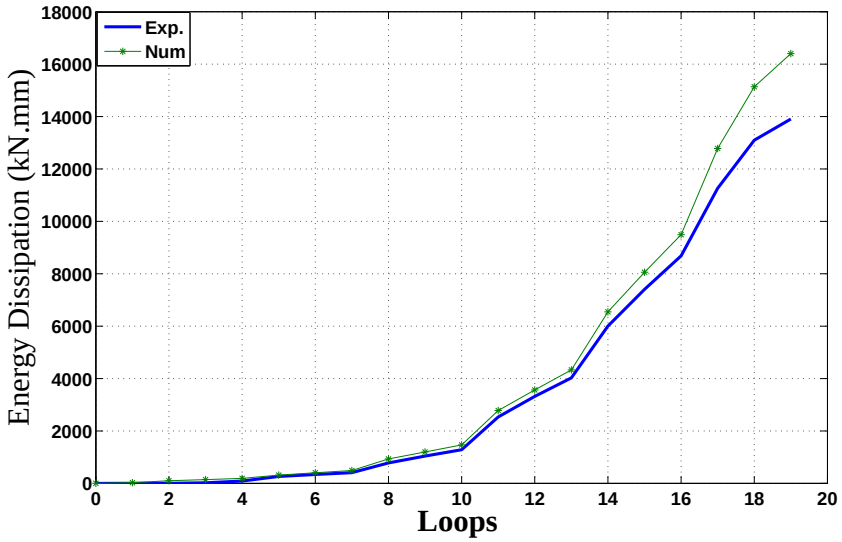

b) Comparison with cyclic 2.

Fig. 5.20: Comparison of the energy dissipation for the shear wall test.

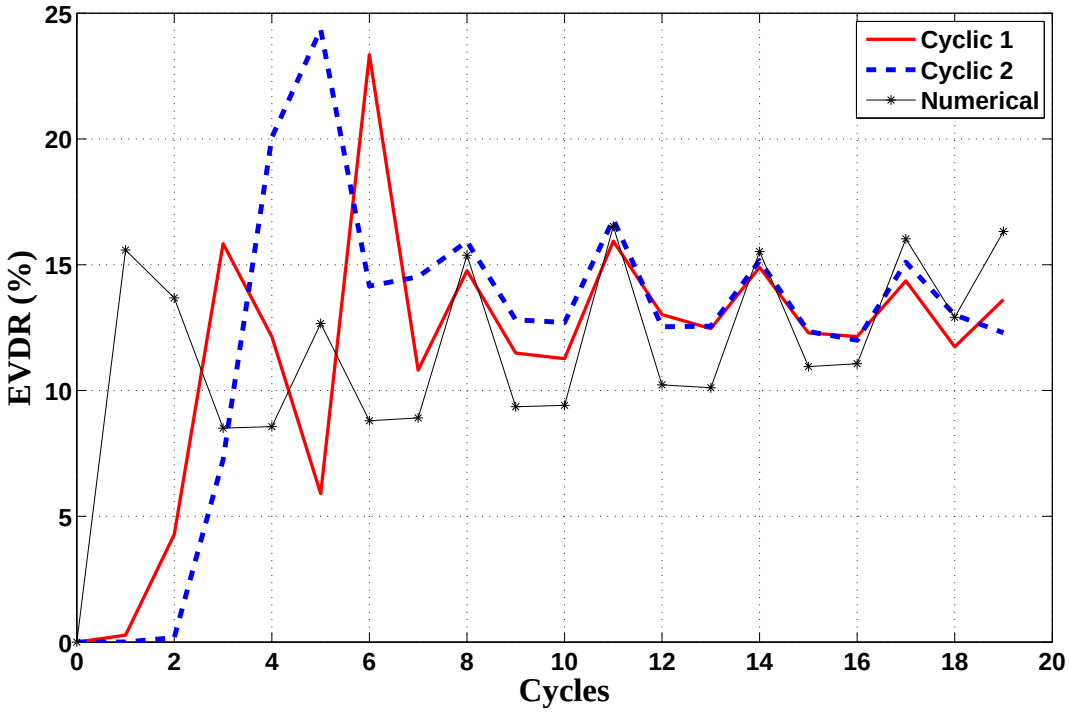

a) Equivalent damping ratio with each hysteretic cyles.

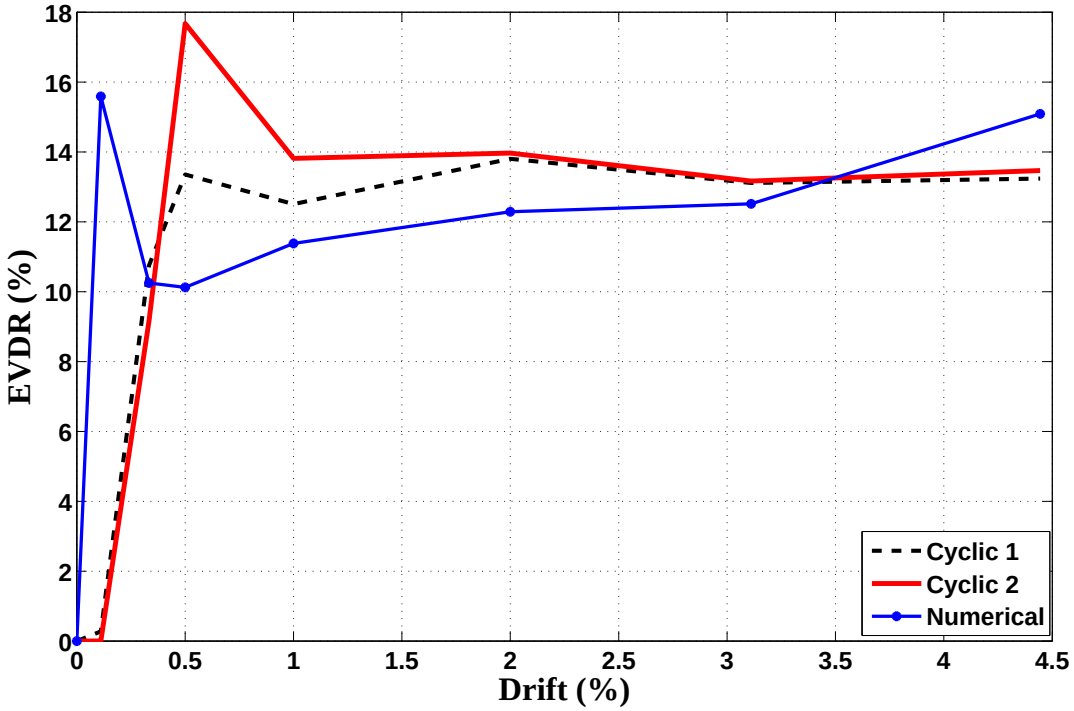

b) Average damping ratio for each drift value.

Fig. 5.21: Equivalent viscous energy dissipation ratio (EVDR) of cyclic shear wall.

The equivalent viscous damping ratio (EVDR) can be calculated for each hysteretic cycle, these values are shown in (Fig. 5.21-a, b) in terms of cycles and drift respectively and compared to the result of numerical model, which shows the perturbation in the value at the beginning cycles and then a relative stability for big cyclic loops was remarked. The values for each cycle are listed in the table (5.2) and shows that the average value of equivalent viscous value for numerical (11.9%) is less then the energy dissipated by the two wall tests of (12.05% and 12.86% for cyclic 1 and cyclic 2 respectively) and these differences of (1.24% and 7.5% respectively), it is clear that the error with respect to (cyclic 1) test is very little as compared to (cyclic 2) value and the reason may be due to the fact that the calibrated model and especially for the cyclic parameters are based on (cyclic 1) test, this issue was due to the nature of numerical values of the experimental tests was not uniform in the number of values and the accuracy of tests and also no smooth curve can be obtained (which is a crucial in the determining the good parameters) from averaging the values, this numerical difficulties forced us to build the model on the more logical test.

In the cyclic test behaviour it can be recognise that the effects of degradation of the strength, stiffness as well as pinching, the last one caused by the permenant or gap deformation in the nail-wood body such that in one cycle there is a permenant deformation and in the next cycle when reloading occurs, the zone of pastic deformation does no more reflect a big value of force due to loss the required contact in the previous cycle which is less than the ordinary case due to this gap, or in other words, the area of hysteretic curve decreases and so decreasing the ability of structure to dissipate energy, Vasconcelos et al. [134], Meireles et al. [102].
The degradations of the stiffness in the successive cycles are shown in the (Fig. 5.22) for both positive and negative directions of displacements for each cycle knowing that the first cycle of bigger Stiffness value had been chosen and for each cycle for comparison in this figure. Knowing that the initial positive side stiffness for each tested cyclic case (1 or 2) are listed in the end of the table (5.2) which illustrate the differences in the values of initial stiffness with the numerical model are (9%, 17.6% respectively). These differences in the initial stiffness is due to the disturbation in the experimental records at the small displacements and the required calibrated value to follow the monotonic and also cyclic curves.

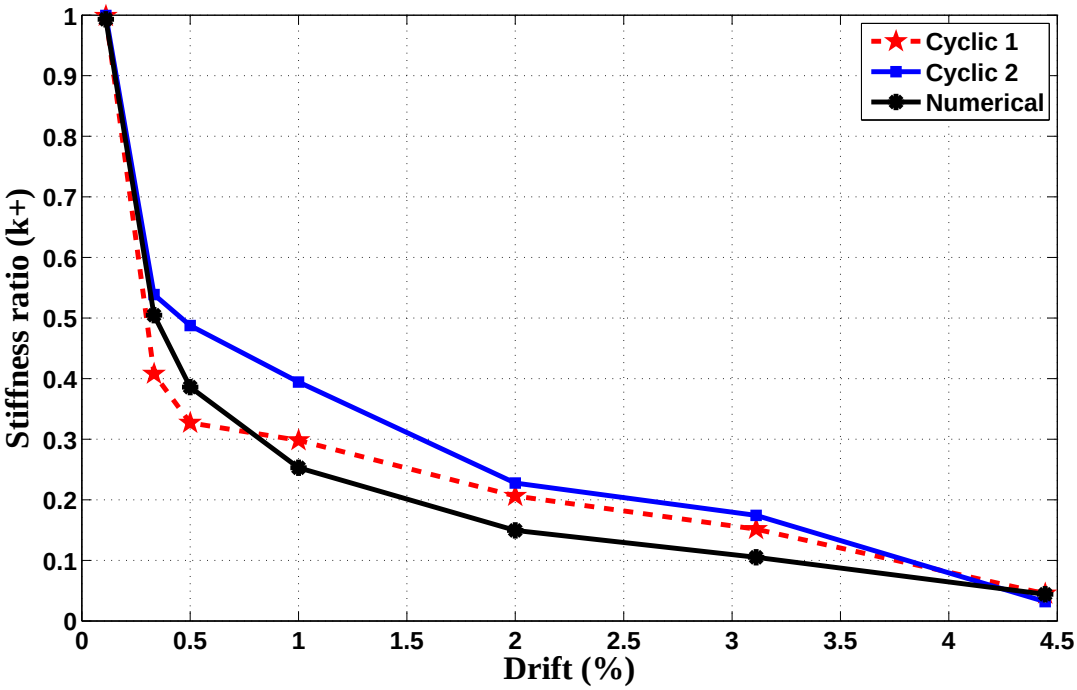

a) Degradation for positive part.

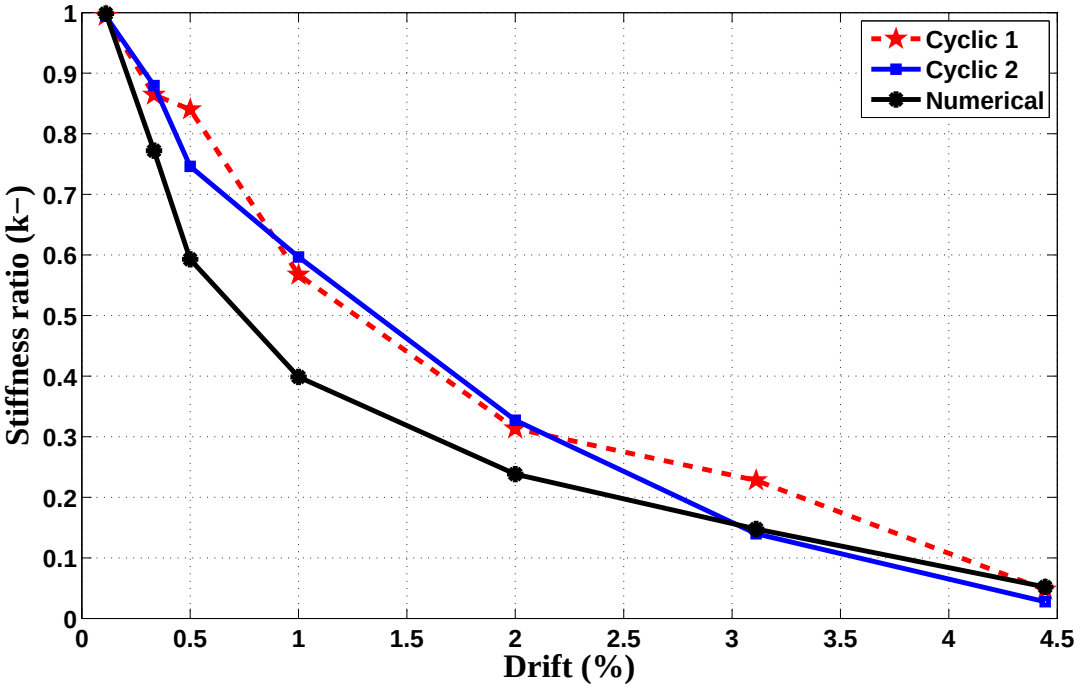

b) Degradation for negative part.

Fig. 5.22: Degradation of the stiffness with evolution of cycles.

Tab. 5.2: Equivalent viscous damping and stiffness of cyclic shear wall.

Drift	Cyclic 1	Cyclic 2	Numerical
0	0	0	0
0.11	0.27	0.24	15.59
0.33	4.28	0.18	13.68
0.33	15.84	7.25	8.50
0.33	12.14	20.06	8.57
0.5	5.90	24.35	12.66
0.5	23.34	14.15	8.80
0.5	10.81	14.52	8.91
1.0	14.77	15.93	15.38
1.0	11.49	12.81	9.36
1.0	11.27	12.70	9.41
2.0	15.93	16.81	16.53
2.0	13.02	12.53	10.22
2.0	12.46	12.56	10.11
3.11	14.90	15.16	15.52
3.11	12.29	12.34	10.95
3.11	12.15	12.00	11.07
4.44	14.36	15.10	16.03
4.44	11.74	13.00	12.91
4.44	13.62	12.30	16.32
Average (Mean)	12.05	12.86	11.9
Standard deviation	4.8	5.7	3.0
Initial cyclic stiffness (kN/mm)	2.64	2.39	2.90

5.4 Nonlinear static analysis (pushover)

In the seismic analysis and design of structures, the linear and non-linear dynamic time history analysis is a good and accurate choice for the engineering judgement but these are taking a long time and not practical in use for the engineers, so a compromise choice between linear static and nonlinear dynamic can be performed by using a nonlinear static analysis or pushover to estimate the direct displacement-based performance which is an alternative technique to conventional direct force methods and can be used economically and practically for engineering practice. Nowadays the direct displacement design based (DDDB) methods are used widely, (eg. Shah et al. [123] and Ahmed et al. [4]), these methods are used normally

Tab. 5.3: Initial stiffness of monotonic behaviour of unit cell panel.

	Monotonic test	Numerical
Initial stiffness (kN/mm)	2.31	2.68

pushover to estimate the performance point of displacement by this static nonlinear method, gives an accurate and fast method of analysis. There are many ways to estimate the performance but the most commonly used are:

- The nonlinear static procedure (NSP method) which can be found in (FEMA 356 American provisions), [3] or it is called also coefficients method, in this approach the target displacement can be evaluated by multiplying the displacement spectrum of the (acceleration displacement response spectrum) (ADRS) format by 4 coefficients (C_0, C_1, C_2, C_3). The capacity curve (nonlinear relation between base shear and top displacements of the height storey) is idealised as a bilinear relation. The coefficients (C_i) are:

  - C_0: Related to spectral displacement of an equivalent SDOF system to the roof displacement of the building MDOF system.
  - C_1: Expected maximum inelastic deformation to that calculated for the linear elastic response.
  - C_2: The effect of pinched hysteretic shape, stiffness degradation and strength deterioration on the maximum value of displacement response.
  - C_3: The increasing of the displacements due to dynamic P-Δ effects.

  All of these factors can be found tabulated in FEMA-356 standard, [3].

- The capacity spectrum method (CSM) which is adobted by (ATC-40 American provisions, [11]) and proposed by Chopra and Goel, [36]. The basic idea of this methods is to convert the ADRS curve to a new one by a modifying factor for demand curve called [B(β) as in method A] in terms of effective damping β_{eff}), then using another multiplication factor (M) to modify the curve of ADRS to another called (MADRS) by using secant period (T_{sec}) instead of effective period (T_{eff}) for the acceleration ordinate of (ADRS) only, (Method B) to (MADRS) depending on the ductility of the idealized bilinear curve (in our study this bilinear curve will be used as elato-perfectly plastic curve, i.e. the coefficient of post elastic stiffness $\alpha = zero$), this assumptrion has been taken for two reasons first to simplify the analysis and because the value of α is more than (20%) and in this case there is a lack of the constants (A to L) that used for calculating β_{eff}, and T_{eff}, FEMA-440, [40]. The details of this approach can be found in three main proccedures (A, B, C) and

an additional approximated method in FEMA-440 provisions, [40]. In this standard, both demand spectrum and capacity curve must be converted to ADRS format and iterations are required to evaluated performance point.

- N2 method which was developed by Fajfar, [56] and adopted for the design of structures for earthquake resistance by (Eurocode 8), [65], all the required information for this method is descripted in section 3.2.2.

5.4.1 Pushover analysis by EC8 method

The monotonic curve of the tested shear wall in the section 5.3.7 has already a relationship between the base shear force and the drift in the top corner which is represents the control point that is construct the capacity curve. The first mode of vibration represents the sway mode with a frequency of (10.2 Hz). This fundamental mode corresponds a maximum value of the normal mode for this control point (the point of application of displacements as shown in Fig. 5.11) and then it can be considered as the control DOF., therefore, this (V-Δ) curve can be used directly without assuming a distribution law for the forces as usual in the different approches of distributing the forces at each DOF. The demand curve can be derived from response spectrum according to eurocode EC8 and some parameters (important class II ($\gamma_1 = 1.0$) with corresponding initial damping ratio 5%, correction factor $\eta = 1.0$, and ground type C with values of type 1 as (S, T_B, T_C, T_D equal to 1.15, 0.2, 0.6, 2.0 respectively) with different values of acceleration (a_g) for seven different signals of PGA values (2.65, 5.27, 7.56, 3.09 12.36, 13.95, and 15.85 m/s^2, the first five signals have the same PGA values for signals of Haiti, 100, 200, 300% and Guadaloupe 100, 390% respectively that will be used in shaking table in ection 6.3). The fundamental mode can be shown in the (Fig. 5.23). The performance point of ADRS format are shown in (Fig. 5.24). It is observed that the wall remain in the elastic range for the first five signals and the plasticity appears in the two last signals (PGA=13.95, 14.85 m/s^2), (Fig. 5.24-f, g). The proccedure of calculation can be illustrate in the (table 5.4) and all the details are already stated in (3.2.2). It can be seen also from the figures that the performance points is very far from the maximum capacity of the structure and the elastic demand curve in the five small signals have an acceleration demand of idelized plastic perfectly plastic (EPP.) is less than the corresponding in the capacity curve, that is ($F_y^* > S_e$) and these cases occurs due to the low height of shear wall and a good prove for the resistance of shear walls for the seismic loading. Also it can be remarked that the abscissa coordinate in the ADRS is less than the corresponding value of (T_b). Itteration process was required for the two last bigger signals, so there are two capacity curves for linear ($\mu = 1$) and nonlinear reduced for ($\mu = 1.53$ and $\mu = 1.62$), the deduced capacity spectrums was drawn according

to Fajfar, [56] mathod, (Eqs. (5.3)), (5.6)).

$$S_a = \frac{S_{ae}}{q_u} \tag{5.3}$$

$$S_d = \frac{\mu}{q_u} S_{de} \tag{5.4}$$

If $T < T_c$, then:

$$q_u = (\mu - 1)\frac{T}{T_c} \tag{5.5}$$

or if $T \geqslant T_c$, then:

$$q_u = \mu \tag{5.6}$$

Where, μ: The ductility factor (max. displacement to yield.),

T_c: Maximum of period (T) value of the plateau for demande curve,
q_u: Reduction factor due to ductility,
S_{de}, S_{ae}: Elastic spectral displacement and acceleration,
S_d, S_a: Inelastic spectral displacement and acceleration.

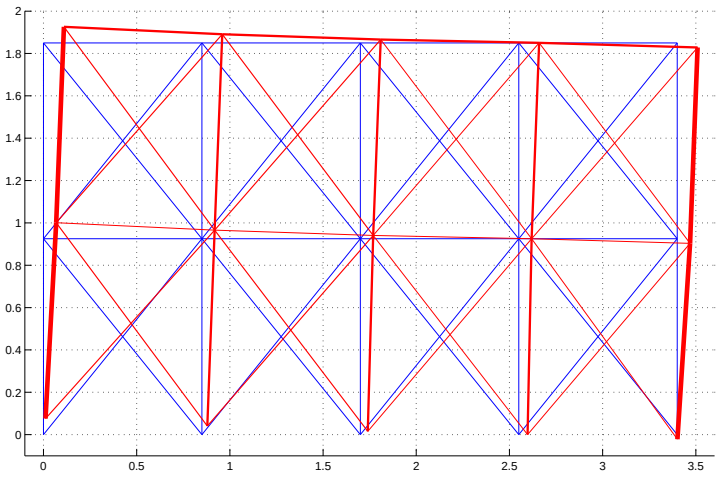

Fig. 5.23: Fundamental mode deformation, f_1=10.2 Hz.

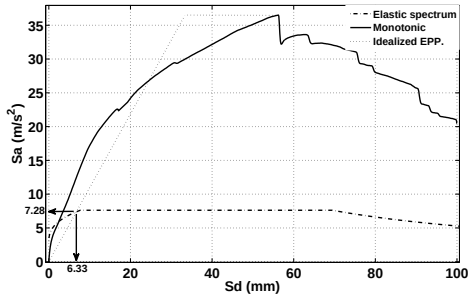

a) PGA=2.65 m/s^2.

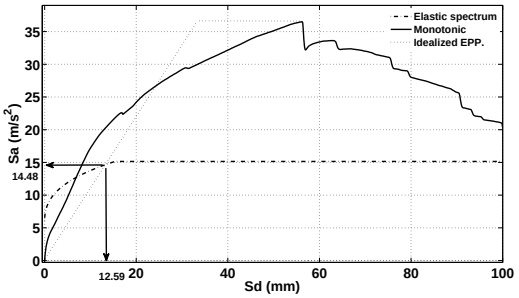

b) PGA=5.27 m/s^2.

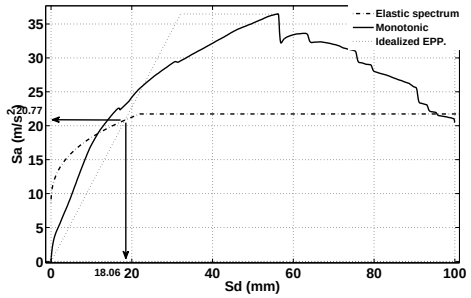

c) PGA=7.56 m/s^2.

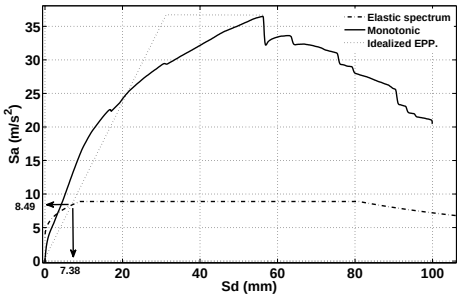

d) PGA=3.09 m/s^2.

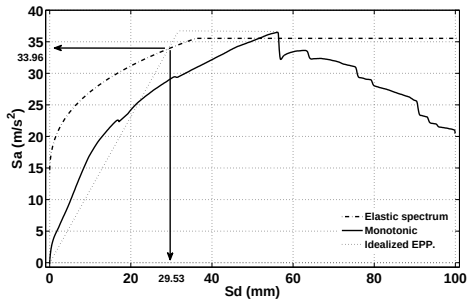

e) PGA=12.36 m/s^2.

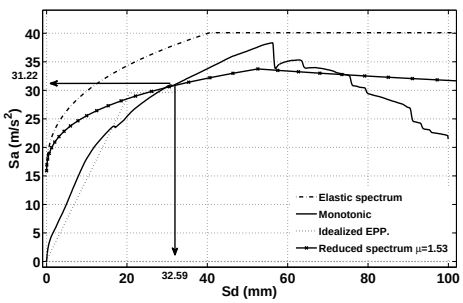

f) PGA=13.95 m/s^2.

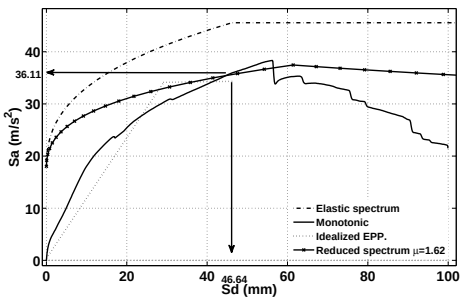

g) PGA=15.85 m/s^2.

Fig. 5.24: Pushover analysis by N2 method.

Tab. 5.4: Parameters of pushover analysis by N2 method of code EC8.

PGA m/s^2	m^* (kg)	Γ	A_m^* (N.m)	d_m^* (mm)	F_y^* (kN)	d_y^* (mm)	T^* (sec)	S_e m/s^2	F_y^*/m^* m/s^2	d_{et}^* (mm)	μ	q_u	d_t (mm)
2.65	953	1.16	1446	56.25	36.50	33.3	0.185	7.28	38.30	6.33	1.69	0.19	6.33
5.27	953	1.16	1446	56.25	36.50	33.3	0.185	14.48	38.30	12.59	1.69	0.38	12.59
7.56	953	1.16	1446	56.25	36.50	33.3	0.185	20.77	38.30	18.06	1.69	0.54	18.06
3.09	953	1.16	1446	56.25	36.50	33.3	0.185	8.49	38.30	7.38	1.69	0.22	7.38
12.36	953	1.16	1446	56.25	36.50	33.3	0.185	33.96	38.30	29.53	1.69	0.89	29.53
	953	1.16	1446	56.25	36.50	33.3	0.185	43.55	38.30	37.87	1.69	1.14	48.10
15.85	953	1.16	1154	48.10	34.66	29.6	0.179	42.74	36.37	34.84	1.62	1.18	47.02
	953	1.16	1118	47.02	34.41	29.1	0.178	42.59	36.11	34.29	1.69	1.62	46.64
	953	1.16	1446	56.25	36.50	33.3	0.185	38.33	38.30	33.34	1.69	1.00	33.39
13.95	953	1.16	676.9	33.39	29.97	21.6	0.165	35.86	31.45	24.66	1.55	1.14	32.68
	953	1.16	656.1	32.68	29.75	21.3	0.164	35.76	31.22	24.36	1.53	1.15	32.59

5.4.2 Pushover analysis by capacity spectrum method (CSM)

The characterestic response spectrum of the (EC8) is smooth and evaluated by imperical equations. The performance point was in the range of periods less than T_b as we've seen by N2 method in the previous section and to verify the performance of the shear wall by a real signal of Guadaloupe 390% with PGA=1.25g by using the method (C) of the capacity spectrum method (CSM) in the (FEMA-440) which is called also (MADRS Locus of Possible Performance Points), [40]. The main difference of this method from the others that it is a graphical solution method. The method can be explained simply by drawing many arrays from the origin which represents different time periods (each one corresponds to specified ductility value (μ), and then pointed out the intersection points of these arrows for each value of ductility (μ) and by using reduced spectrum curves with the ADRS format of demand spectrum curve by using the two reduction factors [M and B(β_{eff})] as.

- B(β_{eff}) can be calculated to reduce the ADRS capacity curve by using spectral reduction for effective damping according to the damping in terms of the value of ductility μ and post-elastic stiffness value (α) but in our study the latter factor will be vanish and elastic perfectly plastic idealized (EPP.) relation has been used. knowing that β_{eff} can be calculated by using μ, α=0, and some imperical equations and constants (A, B,...,F) for each value of α, these equations and constants can be seen in FEMA-440, [40].

$$(S_a)_\beta = \frac{(S_a)_0}{B(\beta_{eff})} \tag{5.7}$$

$$B = \frac{4}{5.6 - ln(\beta_{eff})} \tag{5.8}$$

Where β_{eff}: Effective damping (%).

- M is factor of multiplication at which it can be use the secant period T_{sec} instead of effective period T_{eff}, the latter can be calculated in the same way of β_{eff} but with different constants (G, H,...,L) and different equations, see FEMA-440, [40]. The effective acceleration, a_{eff}, is not meaningful since the actual maximum acceleration, a_{max} must lie on the capacity curve and coincide with the maximum displacement, d_{max}, see (figure 5.25). So this factor convert the ADRS curve to MADRS by multiplying the acceleration ordinate only by this factor M as:

$$M = \frac{a_{max}}{a_{eff}} \tag{5.9}$$

$$M = (\frac{T_{eff}}{T_{sec}})^2 = (\frac{T_{eff}}{T_0})^2(\frac{T_0}{T_{sec}})^2 \tag{5.10}$$

$$(\frac{T_0}{T_{sec}})^2 = \frac{1 + \alpha(\mu - 1)}{\mu} \tag{5.11}$$

Where α is the post-elastic stiffness.

The Graphical proccedure of CSM-menthod (c) can be illustrated briefly by assuming different values of ductilities, for each ductility, it can be calculate a corresponding secant period and the latter will intersect the demand curve (in MADRS format) by a point, the curve of connecting these points (called MADRS locus of possible performance points) will intersect the capacity curve in a point which represents the performance point, the ordered steps of the proccedure is illustrated in the table (5.5) and the graph can be shown in (Fig. 5.26).

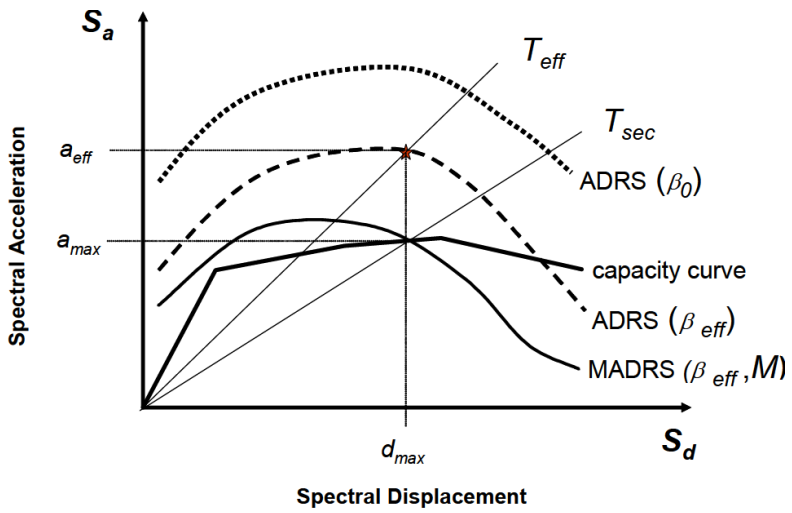

Fig. 5.25: Capacity spectrum method showing modified acceleration-displacement response spectrum (MADRS) for use with secant period, T_{sec}., FEMA-440, [40]

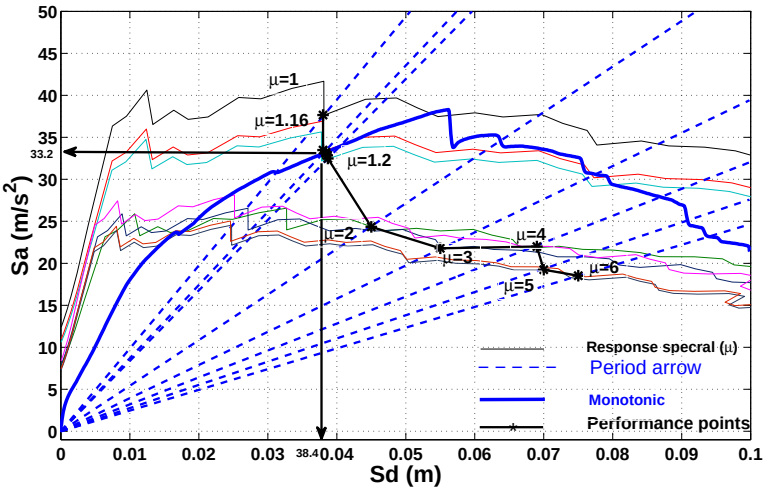

Fig. 5.26: ADRS by the ATC-440 (CSM method-C) for Guadaloupe 390% registered signal.

Tab. 5.5: Iterated parameters for pushover analysis by CSM method (c).

μ	S_d (m)	S_a (m/s^2)	T_{sec}	T_{eff}	$\beta_{eff}\%$	$B(\beta_{eff})$	M
1.00	0.038	37.65	0.200	0.200	5.000	1.002	1.000
2.00	0.045	24.34	0.270	0.232	8.80	1.168	0.743
3.00	0.055	21.79	0.316	0.299	15.80	1.409	0.895
4.00	0.069	22.00	0.351	0.355	19.40	1.518	1.023
5.00	0.070	19.24	0.378	0.360	20.28	1.544	0.907
6.00	0.075	18.53	0.400	0.386	20.60	1.554	0.931
1.20	0.039	32.48	0.220	0.201	5.19	1.012	0.863
1.18	0.039	32.85	0.215	0.201	5.15	1.010	0.874
1.15	0.038	33.48	0.213	0.201	5.11	1.008	0.890
1.17	0.0384	33.09	0.214	0.201	5.13	1.009	0.882
1.16	0.0384	33.22	0.214	0.201	5.12	1.008	0.885

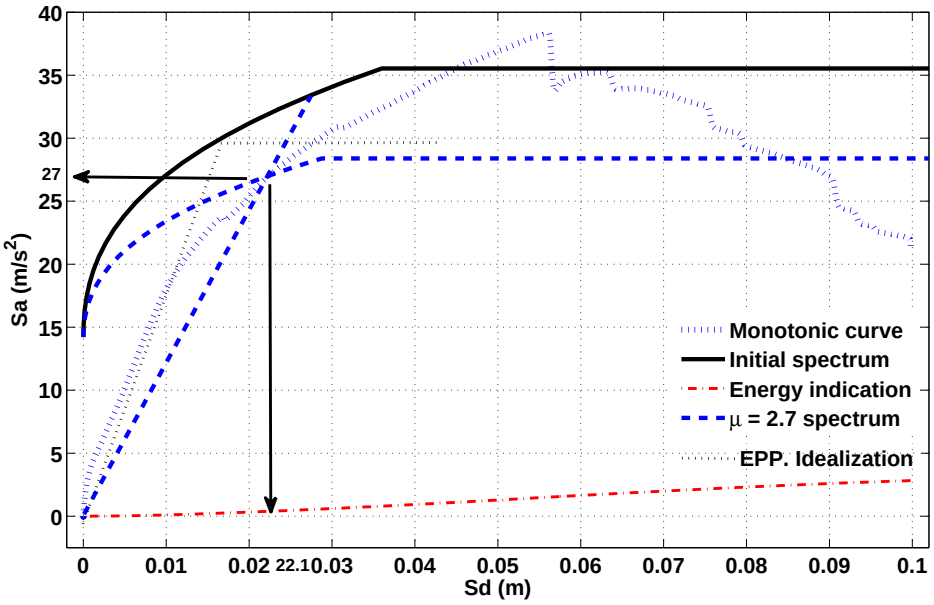

Fig. 5.27: ADRS by the ATC-440 (CSM method-A) for EC8 assigned spectrum for (PGA=1.25g).

To make a comparison between the methods of calculating performance points an example of the signal equivalent to the PGA=12.36% was used as shown in (Fig. 5.24-e) in terms of N2 method, the spectral displacement of performance point is (29.53 mm) as compared to the value of (CSM-C) method which yields (38.43 mm), this big difference (23%) comes from many reasons such as the perturbation of the rouph natural signal of the latter case and the different mathematical rules of each approach and that the graphical solution is a personally accurate solution, so to verify the more accurate method, the method (A) of the capacity spectrum method (CSM) was added to verify the results. The performance point can be found by using the (EPP.) curve with value of α=0 and by assuming an initial point of performance and then calculating the ductility value according to well-known rule of equal area (EPP.), then it can be calculate β_{eff} by the same equations of CSM-C method and then by finding out B(β_{eff}) and converting ADRS curve by using the latter factor to a new $(\text{ADRS})_{\beta_{eff}}$, Eqn. (5.7), the new point is the point of intersection of T_{eff} and the new reduced $(\text{ADRS})_{\beta_{eff}}$ curve, so this point compared to the initial point or previous one within specified precision, the last point is the performance point, if not, the process must be repeated by choosing the last point and new (EPP.) curve and calculate a new μ value until arriving to required accuracy.

This pushover analysis method by CSM-A method can be shown in (Fig. 5.27), in this figure the continous line represents the original demande curve and the dotted one represents the reduced demand for ductility value $\mu = 2.7$ and the μ value is calculated according to EPP. curve (which represents the light dotted line) idealization of the original capacity curve (pushover) which represent the dotted points curve.

The value of spectral displacement is (22.14 mm) and this is also far from the value found by graphical (CSM-C) method of (38.43 mm), (difference=42%) but it is more approach to the value of N2 method of (29.53 mm), (difference=25%), the latter point by N2 method is near the average value of the left two values (error=2.5%) and this may be make the method of EC8 is more efficient for our case due to last accuracy and also simplicity. It was also taken into account that the obtained results by the procedures of ATC-40 are sometimes not converging and different solutions can be obtained when real spectra are used, Causevic and Mitrovic [26]. Unfortunately, the results of ATC-40 procedures are deficient for even the elastic spectrum in the periods of the acceleration and velocity sensitive regions (in our cases we are in the acceleration sensitive region), and this is may be one of the reasons of different values obtained, Chopra and Goel [36], [35].

Also according to Paultre, [109], the effective modal mass which is used for converting the V-Δ capacity to ADRS format can be used effectively for the buildings of multi-storey where the big masses are distributed vertically. The summary of

the results of pushover analysis for the three methods shown in figures above are listed in the table (5.6) knowing that the effective damping ratio of method N2 or the EC8 method was evaluated by reflecting the equation (3.6) of the damping correction factor η in the (EC8 standard, clause 3.2.2.2), [65], (Eq.(5.12)) below.

$$\eta = \sqrt{\frac{10}{5+\xi}} \tag{5.12}$$

This (Eqn. (5.12)) can be used for finding out the corresponding nonlinear damping for ductility (μ) value.

$$\xi = \frac{10}{\eta^2} - 5 \tag{5.13}$$

For the sake of substitution of η, it represents the behaviour factor (q_μ) but due to very small ductility μ, it can be substitute instead of q and the error for this case is (8.3%).

Tab. 5.6: Summary of some results of pushover analysis

Method	**Sd (mm)**	**Sa** (m/s^2)	μ	β_{eff}	T_{eff}
CSM-A	22.14	27.00	2.70	11.06	0.18
CSM-C	38.43	33.22	1.16	10.12	0.20
N2	29.53	33.96	1.69	9.83	–

5.5 Conclusions

In this chapter, both the scales one for the connections and the shear wall second scale are used to develop a FE. model to be used for specific dimensions and materials of traditional timber with infilling wall panel. A nonlinear spring model was suggested for the connections by using Hysteretic constitutive law for the bottom supports according to experimental tests for both axial and tangential directions. Also, a second law of Hysteretic constitutive model with different parameters was used of two identical diagonal springs was selected to model the behaviour of each unit panel in the tested shearwall frame. This proposed element was calibrated for the fixed dimension panel and good results obtained in terms of strength, ductility, and energy dissipation, this model was calibrated according to monotonic and reversed cyclic pseudo static tests. Also applications of pushover analysis for the shear wall according to experimental shear-top displacement curve

by three different methods. The N2 method that adopted by EC8 gives results near the average values of the CSM-A, B in FEMA-440 American provision. The proposed FE model of two diagonal nonlinear springs can be used to represent the nonlinear behaviour of a specified dimensions of panels made by rocks and clays as a morters with two diagonal timber braces which can be used for any building scale made by the same materials and same dimensions as we will see in next chapter 6.

6. DYNAMIC ANALYSIS AND SHAKING TABLE TEST

6.1 Introduction

In the previous chapter, it had been seen that the good performance of the timber frame structures according to quasi-static tests for the scale of connections and the wall. As stated before the objective of using multi-scale analysis technique is to study the main characteristics of the different scales or elements which are representing the partitions of full building scale and they can be used to design of bigger structures of multi-storey structures. The third scale in our study is the full building scale, so shaking table were derived two different types of acceleration signals for house specimen to investigate the main dynamic characteristics of the full house scale to validate the proposed model and applied the model to the analysis of two storey building. These tests were conducted at the FCBA (Français Centre de Bois Ameublement: French center of timber building) in Technological Institute in Bordeaux in April 2013 as part of ReparH project.

6.2 Records and seismic signals

6.2.1 Synthetic signal of Haiti

The structure studied in this manuscript results from the improvement of a constructive typology for Haitian tradition motivated by several reconstruction projects in this country. The objective is to performing the seismic tests to prove the resistance of these timber frames with infilling at a load of intensity greater than or equal to that occurring during the Earthquake of January 12, 2010, in Haiti. The problem is that there is no recording station existing in this country before the mentioned earthquake. A collaboration was therefore set up between the 3SR laboratory of Grenoble Alpes University and Nice's CEREMA in Nice in order to generate a representative accelerogram of the hazard concerned.

To predict the movements of the ground over a wide frequency band, an empirical approach based on the technique of Empirical Green's Functions (EGF) was used, Hartzell [76]. This method is based on the assumption of similarities between earthquakes in the same area, with low and high intensity, dependent on a scale factor. The idea is to simulate an important event from a magnitude

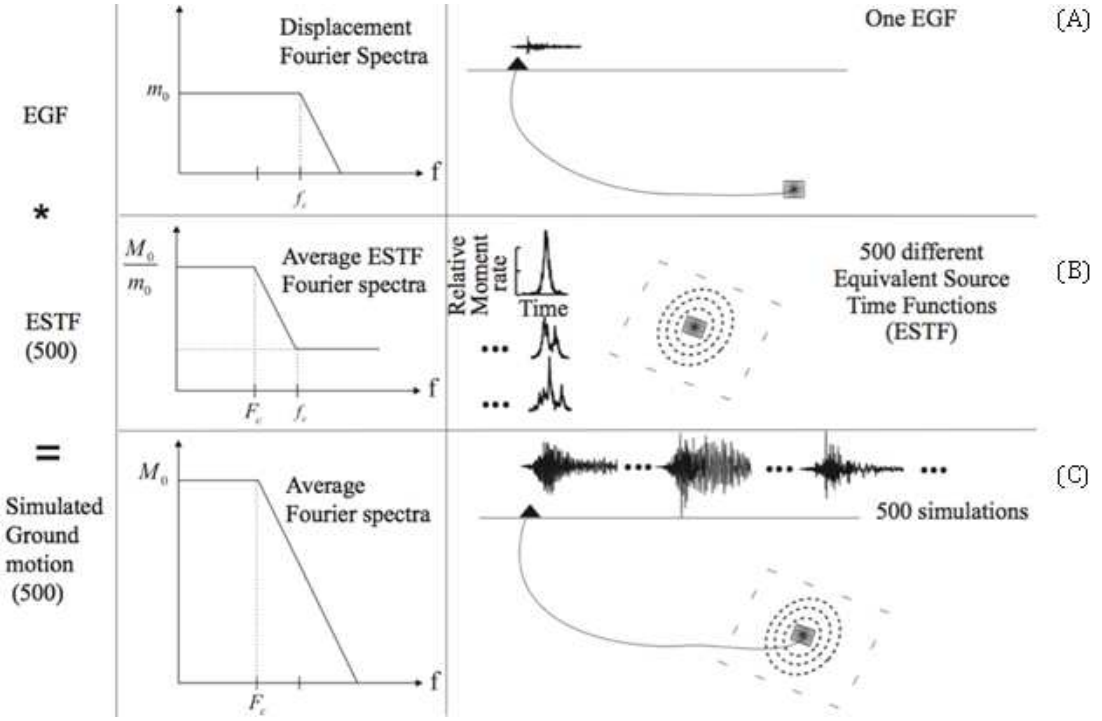

Fig. 6.1: Schematic of the EGF summation method, [135].

less strong containing other information necessary for the path and site effects. There are 500 accelerograms (Equivalent Source Time Functions (ESTF)) were generated, representing the history of the release of Energy for the fault below the cutoff frequency of the (small) event frequencies taken into account (see Fig. 6.1). All details of this approach are available in the work of Sansorny et al. [121].

The summarised steps of the method:

(A) The Green function corresponds to the (small) recorded event. The source is modelled by a spectrum of (Brune ω^2, [22]).

(B) 500 ESTF were generated taking into account different fracture process on an event of high intensity.

(C) The convolution of each ESTF is performed with the Green function to obtain the 500 simulated acceleration.

For the simulation, HVPR station northwest of Port-au-Prince has been selected. Green's function corresponds to the signal of the most powerful aftershocks measured occurred on 3 May 2010 at 19:21. The moment magnitude (Hanks and Kanamori [75]) was recorded 4.4 and the epicenter located near Leogane

(18.538° N, 72.643° W). The North-South axis of the aftershock has been selected for the simulation of 500 signals magnitude 6.8 M_w equivalent to the hazard of January 12, 2010, with the elastic response spectrum is shown in (Fig. 4.6-a). To take into account the variability of the results, the signal inducing greater demand in a structure has been selected on the frequency band (2-10 Hz). This range has been identified in order to contain the natural frequency of the prior tested structure through modal analysis (see section 6.3). Temporal data (acceleration, velocity and displacement) of the selected signal can be shown in (Fig. 4.6-b).

6.2.2 Guadaloupe signal

The synthetic signal of Haiti in the form of time acceleration relation-ships showed in the last paragraph was applied to a vibration table by the help of FCBA engineers who have an experience of testing of timber structures for example, roofs, Humbert, [82] or shear walls, Boudaud, [19], and house, Vieux-Champagne, [135] on more severe criteria of the new French regulations earthquake. The second signal which was used by generation a modified natural accelerogram from the earthquake in Miyagi in Japan, measured from the K-Net station and fixed on a spectrum of the relationship with earthquake Youngs et al. [148] (scenario Guadeloupe, distant subduction earthquake) to improve the representation of the spectrum. It is very specific scenario hazard, by using soil B of Eurocode 8 [65] and based on probabilistic 475-year return period calculations. This corresponds to an exceedance probability of 10% over 50 years, is the probability associated with the requirement of non-collapse in Eurocode 8. A distant earthquake, corresponding to a spectrum rich in low frequencies (<3 Hz) with a long signal duration. The temporal and frequency input data of earthquake, obtained by the method described above for the distant scenario Guadeloupe (PGA =0.33g) are depicted in Fig. 4.7.

6.3 Shaking table test

As a reminder, one of the main objectives was to bring structure to the signal 100% of Haiti to reveal its behaviour under load equivalent to the January 12 earthquake 2010. To study the main characteristics of the house structure, Haiti seismic signal was factored to a 2 and 3 times to investigate the level of damage in the different elements in the house scale. It was expected, due to a geometrical dimension (low height) and the position of the significant mass of infilling distribution (low mass wall head), that the house would stand well 100% signal. Thus, the increase in the power of the earthquake was multiplied, between each test, by a factor expressed as a percentage. For example, a factor 2, applying to the three temporal magnitudes

of the signal (a(t), v(t), d(t)), will then correspond to the 200% of the latter. All the tested signals cases are listed in the table (6.1).

Tab. 6.1: Maximum values of selected seismic signals, Vieux-Champagne, [135].

Signal -	Factor -	Displacement mm	Velocity m/s	Acceleration m/s^2
Haiti	1	35.7	0.158	2.65
	2	71.4	0.316	5.27
	3	107.1	0.474	7.56
Guadeloupe	1	30.9	0.168	3.09
	3.9	117.3	0.637	12.36

An experimental modal analysis (EMA) was performed at the initial state of the house and between each two earthquake scales loading. It consisted of subjecting the structure to a white noise (signal covering a wide range of frequencies with the same amplitude) of low intensity so as not to fail the house due to resonant frequency. Thus, the structure naturally resonates with its different modes.
EMA can analyze and obtain various important issues such as:

- The development of normal frequencies of the structure, revealing its process of damage characterized by the lower stiffness.
- The eigenmodes.
- The equivalent viscous damping of the structure and the overall system (Machine + structure).

The experimental modal analysis of the house scale is shown in (Fig. 6.2).

6.3.1 Description of the shaking table

The tests were carried out on a horizontal uniaxial seismic table whose characteristics and performances are defined as below and there are some notes about the shaking table test.

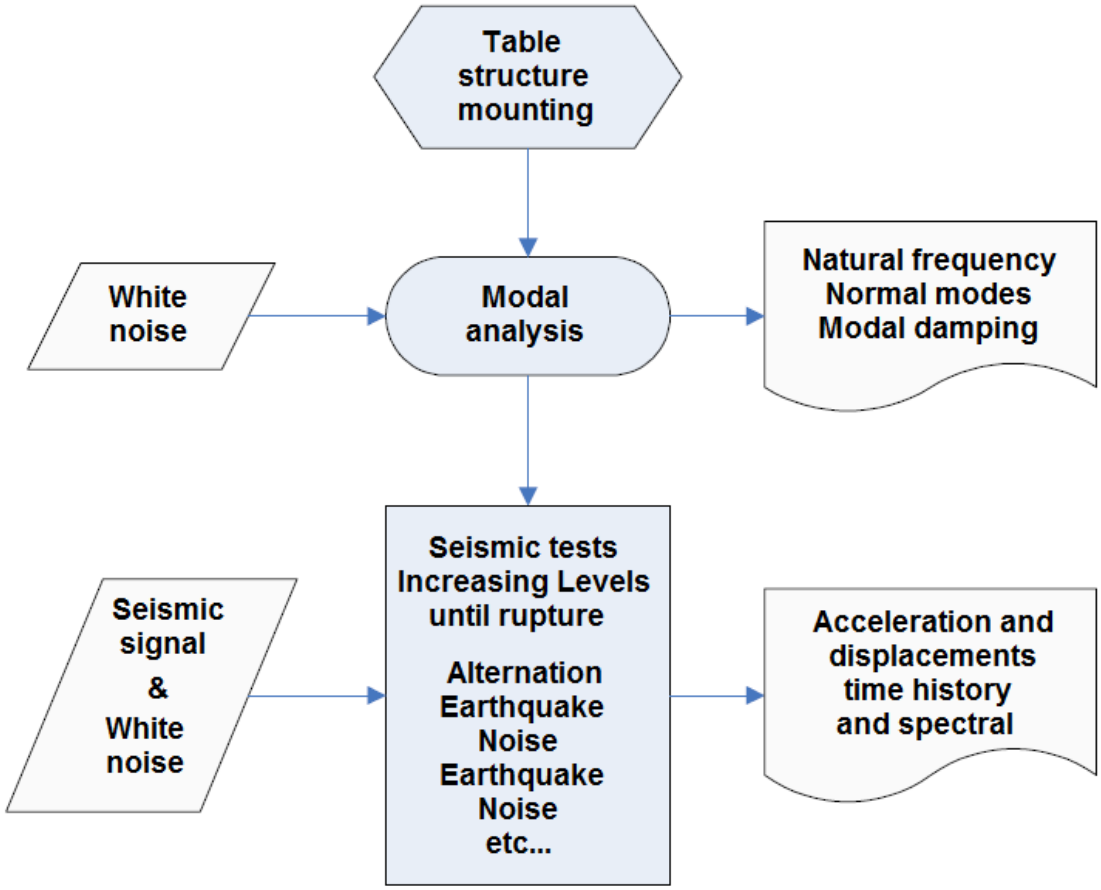

Fig. 6.2: Flow chart for the proccedure of shaking table test, Duccini [52].

- The dimensions of the main table have the dimensions ($3m \times 3m$) made of Aluminium with a mass of (2 tons).
- It can be extended by providing additional parts of shaking table parts to have a dimension of ($6m \times 6m$) with a mass of (4 tons).
- The maximum displacement capacity of the table is ($\pm 125mm$) with a maximum velocity of ($0.75m/s$).
- The maximum acceleration without any extension is (8g) and (4g) empty with extension.
- Range of frequencies is (0-30 Hz).
- The capacity of the actuator is (250 kN).
- For the purpose of fixing the frame with the table, a base frame of channel sections were used so as not permits to the relative movements between the timber frame and table as shown in the (Fig. 6.3-b)
- The specimen of the house was designed as close as possible to reality with 2 doors and 4 windows such as they lie in the two sides of the plane of symmetry such that the loading of the table lies parallel to that plane so as to remove the possibility of torsion effects.
- The direction of the chosen movement activates the mode corresponding to the largest modal mass (proportion of the mass set in motion for a specific mode of the building).

a) Strip support in the corner

b) Fixing the sill plate to the base frame

c) Specimen of tested specimen of house showing the openings

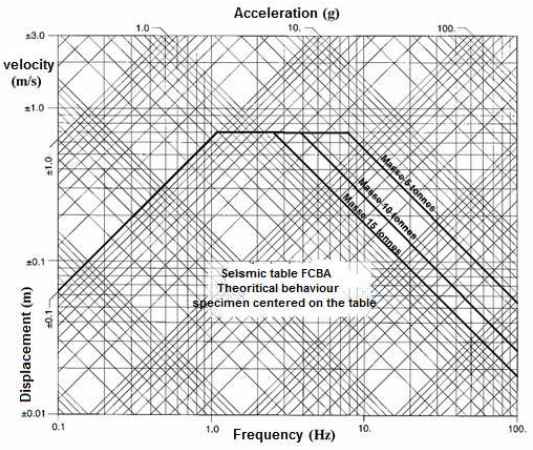

d) DVA Limitations of table as a function of the embedded mass.

Fig. 6.3: Installing and opening locations and capacity of shaking table test, Duccini [52].

6.4 Modeling of the 3D one storey house

The proposed models of bottom supports and the modelling of the behaviour of unit wall scale is to use as basic elements in the more complicated structures, for the seismic loadings and another horizontal and/or vertical service loads. This idea is to propose a finite element model by using some linear and nonlinear elements for the analysis of the structures made by main timber frame and infilled with some materials. This frame was proposed by the ReparH french program to suggests an enhanced performance of the Kay wall structures that are traditionally

constructed in Haiti as an optional cheap construction and effective structure to resists the future earthquakes. The multiscale analysis technique can be used for the modelling of the one or multistorey buildings.

6.4.1 Description of the model

From the connection and unit panel model we can build the house by using multiscale analysis as explained previously, see (Fig.5.1) in chapter 5. The concept of assemblage for all the components is to use linear and nonlinear elements to integrate the system with a minimum number of DOF and good accuracy requirements, this simplified model can be used for all types of vertical and horizontal load sources.

Roofing system

The roof of the Kay structures are relatively lightweight made by folded thin plates (sheet cover) rested on king post truss type, the dimensions of the latter are shown in (Fig. 6.4-a), this little mass of sheet cover was neglected in the analysis. As shown in (Fig. 6.4-b) the roof contains four beams at the corners with (10 cm width by 5 cm height section) for the reasons of increasing the diaphragm stiffness, these beams modelled as fixed ends. The four king post trusses connected together at the top by (5) purlins ($5 \times 5\, cm^2$) at each side modelled as a continuous beam and transversely by two extremes scissor-like trusses connected together by a bar with dimensions ($2.7 \times 10\, cm^2$). For all members, the ends were modelled as hinges except the four diaphgram beams.

Shear walls

The simple tested house has four shear walls and no internal walls exist, they have identical unit cells with the same dimensions as the shear wall model in (section 5.3.2), each one has a two diagonal nonlinear elements models all nonlinearities sources inside each panel. The idea is to separate the effects of the stiffness of the infilling and the two diagonal timber braces from the main frame. This idea is exactly as we used in the case of the shear wall by adding the main structural members. The main frame is constructed by big columns (posts) in the corners with the dimension of cross sections ($10 \times 10\, cm^2$) and all other interior posts have ($10 \times 5\, cm^2$), where the dimension ($10cm$) is uniform for all walls which represent the thickness of the walls. The roof system rests on four continuous beams with dimensions of ($10 \times 5\ cm^2$). The mid-height horizontal members are bar elements with ($10 \times 2.7\, cm^2$) dimensions. The openings in the walls have also a dimension consistent with the size of unit cell element, i.e. the dimensions of the windows is the same as the panel and the doors are twice of the panel as

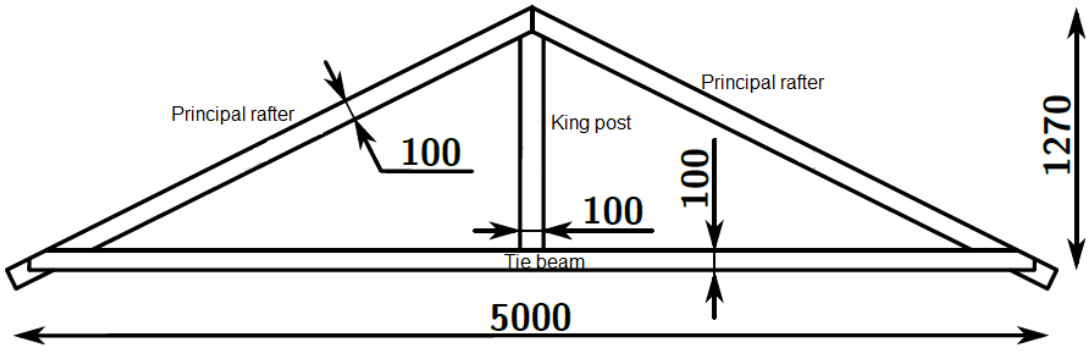

a) Roof king post truss dimensions

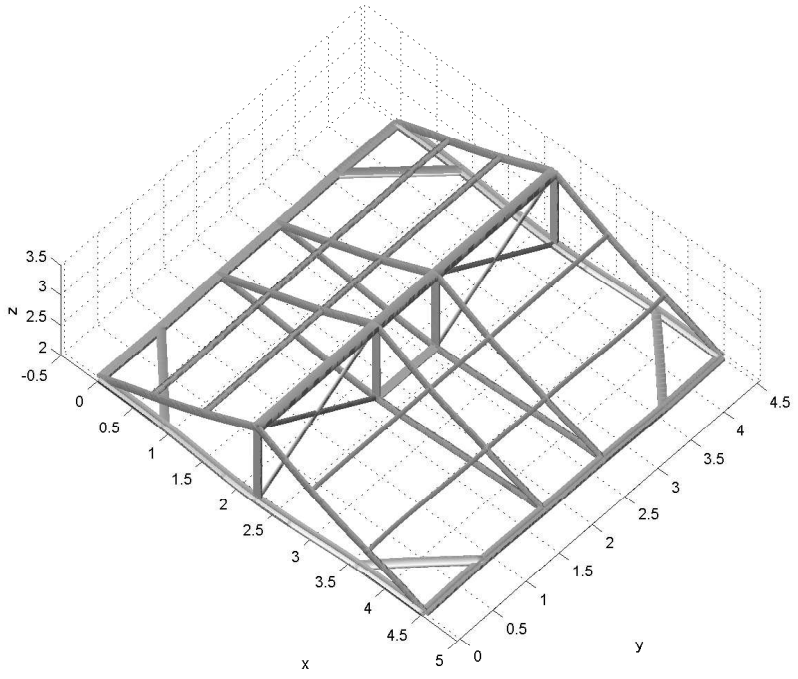

b) 3D assemblege of roof system.

Fig. 6.4: Modeling the roof.

shown in (Fig. 6.3-c). In terms of selected directions for the numerical model, the excitation of the shaking table is parallel the y-axis which is parallel to the axis of symmetry (yz-plane) in terms of both structural elements as well as the location of the openings. All the beams, columns, and bars timber members are considered as (C18) timber class with a modulus of elasticity ($E_{0,mean} = 9\,kN/mm^2$) and density of ($\rho_{mean} = 380\,kg/m^3$), EN 338, [55]. The bottom joints are modelled by 3D spring elements one for the axial tension and compression and two orthogonal for shear. The tested connections of scale 1 which are simulated by using Hysteretic constitutive law model and selecting their parameters according to normal bilinear for tension or compression and symmetric tangential shear deformation laws, as in (section 5.2). The ends of top continuous beams considered as pin joints at the top corners of the shear walls, furthermore as in the case of shear wall model, the mid-height of the posts are continuous and moment resisted sections whereas the two orthogonal nonlinear spring elements of infilling considered as bar elements so they have no shear resistance and can be considered from the structural point of view as bar elements.

6.4.2 Masses

The propagation of different (body and surface) seismic waves makes earthquake action on specific site by shaking the earth under foundation periodically. This is due to sudden motion along fractures in the earth crust called faults. The structure connects with the soil by a foundation, so the foundation will be shaken according to earth motion but the structure, as well as foundation, has an inertia and according to Newton's $1^{st.}$ law of continuity, the structure resists this motion according to this inertia. The inertia force of each DOF. in the structure is the product of the mass times the acceleration. Two types of masses are implemented in our model, consistent mass for all the timber structural elements of walls as well as roof system with a density of ($\rho = 380\,kg/m^3$) and a lumped mass distributed at each node of the shear walls to taking the account of infilling in three dimensions. The distribution of the masses at each node is considered by a factor of (0.25, 0.5, 0.75 and 1.0) part of the weight of each pannel of (150 kg), this distribution was illustrated by the same way of calculating the self-weight at each node according to its part of the infilling pannel mass as in the (Fig. 5.13) of (section 5.3.6). The only difference is that we have a factor of (0.75) due to the existing of openings which is not the case of the wall. The self-weight also taking into account in the analysis.
The distribution of the shared lumped mass (and of course the self-weight) at each node is shown in (Fig. 6.5).

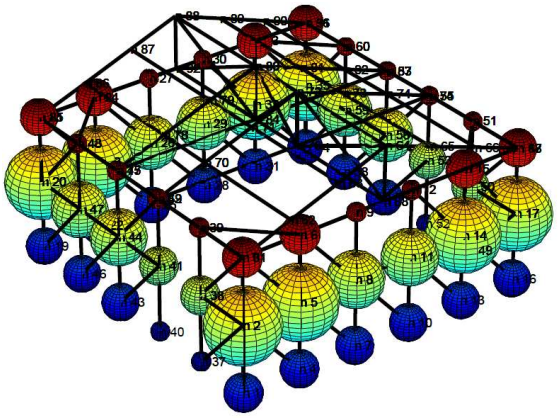

Fig. 6.5: Modeling of mass distribution of infilling materials

6.4.3 Modal analysis

The house was tested by the technique of experimental modal analysis (EMA) by subjecting the shaking table to a white noise signal with a rate of the small value of (0.5 mm root mean square (RMS) weighted $1/f^2$) corresponding directly to the value of the viscous damping rate to be selected for the dynamic numerical calculation, Vieux-Champagne, [135]. Indeed, for these small amplitudes, it can reasonably be considered that the house behaves elastically and that the value of ξ measured is not structural. By Rayleigh method, it will be possible to define a viscous damping rate equal to the average experimental ξ obtained from this test. The EMA technique can be performed by installing the structure on the table and applying the white noise for a period of time (say 60 seconds) and triaxial accelerometers fixed on the nodes of the structural model. The signal of the force measured by the load cell at the cylinder head as well as the acceleration signals at the different nodes of the frame are recorded. The AME has performed post-processing by calculating the frequency response functions (FRF) of the acceleration signals at the node with respect to the signal of the force. Then the modes are determined by the synthesis of these FRF by a CMIF curve (Complex Mode Indicating Function), Duccini [52], Vieux-Champagne, [135], and Allemang and Brown, [10].
The numerical fundamental frequency is (5.0 Hz) which corresponds the sway mode in x-direction as shown in (Fig. 6.6-a) and has an effective modal mass of (54.53%) shown in the (table 6.2). This mode was not appeared in the experimental modal analysis (EMA) because the shaking table is uni-directional imposing load machine in y-direction only, that is the first mode can not be evaluated experimentally.
The second mode of free vibration has a frequency of (5.2 Hz) with correspond-

ing normal modes shown in (Fig. 6.7-a) and a viscous damping ratio ($\xi = 5.2\%$) while the third mode has a frequency of (5.9 Hz) and a viscous damping ratio of ($\xi = 5.7\%$) with corresponding normal modes shown in the (Fig. 6.7-b). It is interesting to know that these two later experimental frequencies (2^{nd} and 3^{rd} modes) actually represents numerically one frequency (2^{nd} numerical mode) and the difference in the value of frequencies as well as the corresponding normal modes (shown in Fig. 6.7-a, b) is due to the practical reasons of construction of the two walls (front and back) which have a planes perpendicular to the direction of the loading of the shaking table by different properties (materials and construction method) so the structural characteristics of the two walls are different. This is proved by the numerical model which gives a corresponding second mode of vibration with frequency of (5.6 Hz) which is very close to the average value to the first two frequencies experimentals (5.55 Hz) with error of (0.9%), this proves the efficiency of the modeling of unit cell by using two croses inclined FE. braces instead of one horizontal spring element. This normal modes equivalent to a combination of the two latter experimental modes, and it has a corresponding effective modal mass of (77.34%) as illustrated in the (table 6.2).

The third experimental mode, has a frequency of (10.9 Hz) with a viscous damping ratio of ($\xi = 5.3\%$) and normal modes represents the sway of the trusses of roof system and shear deformation in the walls with some out of plane motion in the backward wall as shown in (Fig. 6.7-c), this mode is corresponding to the $14^{th.}$ numerical mode with a frequency of (10.5 Hz) with an error of (3.7%) and a corresponding effective modal mass of (9.43%), the depicted normal modes is shown in (Fig. 6.6-c), and again this error is as small as compared to the numerical value obtained by the previous study of (12.65 Hz).

The table (6.2) shows a comparison between these frequencies and corresponding experimental and numerical case. According to Vieux-Champagne, [135], the orientation of the roof was determined to obtain a minimum stiffness in the direction of the load of the house (North-South, or y-direction), however the numerically first mode of vibration was corresponding to the second horizontal direction (East-West, or x-direction), and this is due to the flexibility of the shear walls in x-direction due to the openings.

Tab. 6.2: Free vibration analysis of 3D house model.

Model	$Mode_1$, X-Direction	$Mode_2$, Y-Direction	$Mode_{14}$, Y-Direction
Present study	5.0	5.6	10.5
Vieux-Champagne, [135]	–	4.68	12.65
Experimental value by (EMA)	–	5.2, and 5.9	10.9
Effective modal mass %	54.53	77.34	9.43

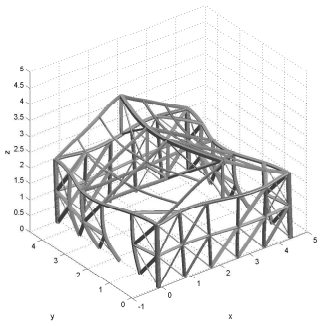

a) Mode 1 (front wall sway and out of plane), $f_2 = 5.0\,Hz$

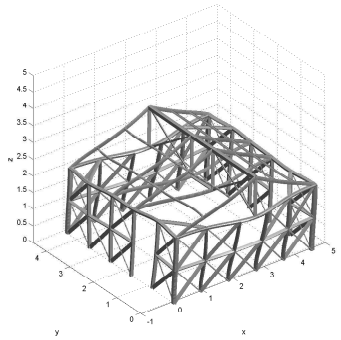

b) Mode 2 (corresponding to experimental $1^{st.}$ & $2^{nd.}$ mode), $f_2 = 5.6Hz$

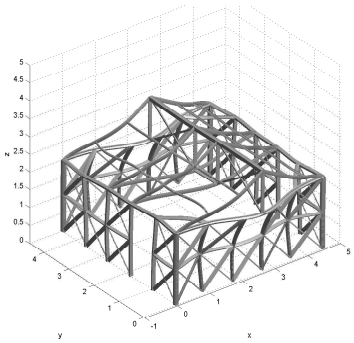

c) Mode 14 (corresponding to experimental $3^{rd.}$ mode), $f_3 = 10.5\,Hz$

Fig. 6.6: $1^{st.}$, $2^{nd.}$, and $14^{th.}$ normal modes of the proposed model.

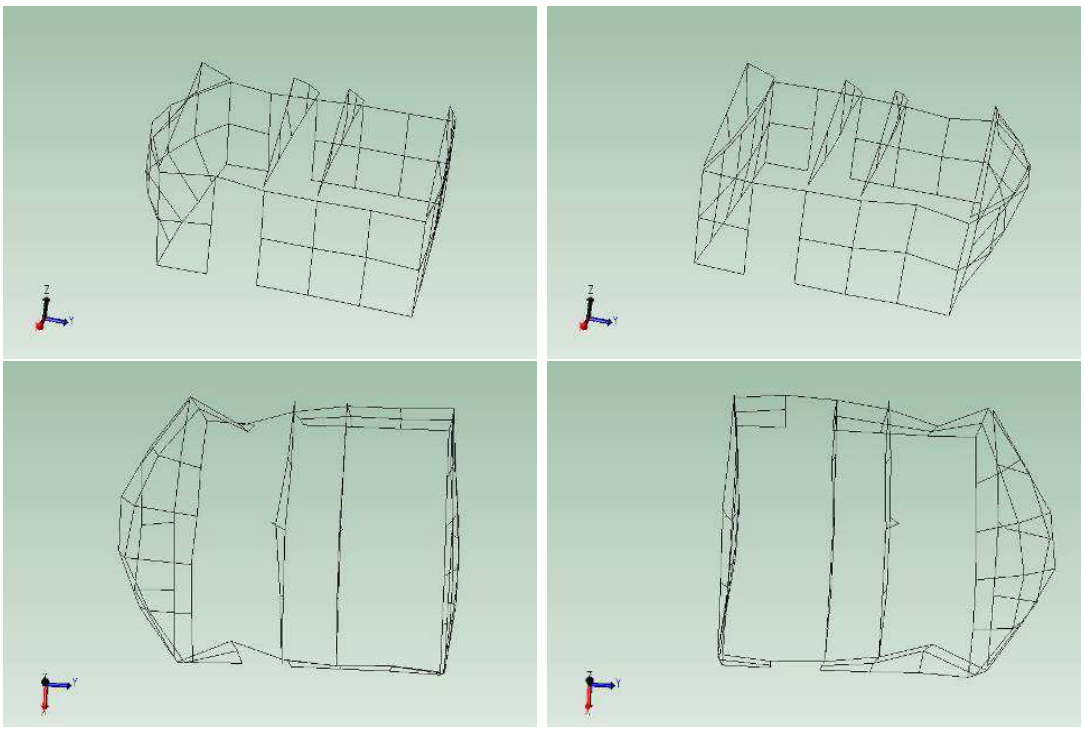

a) Mode 1 (front out of plane wall sway), $f_1 = 5.2\,Hz,\ \xi = 5.2\%$, side and top view

b) Mode 2 (backward out of plane wall sway), $f_2 = 5.9\,Hz$, $\xi = 5.7\,\%$, side and top view

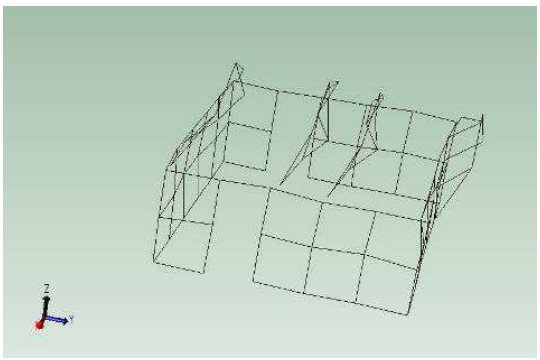

c) Mode 3 (wall and roof truss deformation), $f_3 = 10.9\,Hz$, $\xi = 5.3\,\%$, side view

Fig. 6.7: Normal modes by experimental modal analysis method, Duccini [52].

6.5 Proccedures of shaking table test

The shaking table test was performed by a step by step excitation for both the acceleration and displacement control as stated previously (see section 6.4.3), these steps are:

- Step 1: Deriving displacement control white noise intensity ($0.5\,mm\,RMS \times 1/f^2$) to evaluate free vibration analysis by EMA.
- Step 2: Subjecting initial Haiti 100% acceleration signal.
- Step 3: Repeat applying white noise.
- Step 4: Shaking the table by a factored acceleration signal in step 2 (Haiti 200%).
- Step 5: Reapplying the white noise.
- Step 6: Shaking the table by a factored acceleration signal in step 2 (Haiti 300%).
- Step 7: Reapplying the white noise.
- Step 8: Making a repairing [1] for the structure by repairing the infilling and fixing the steel strips in the top of the shear wall.
- Step 9: Reapplying the white noise.
- Step 10: Applying initial Guadalupe 100% acceleration signal.
- Step 11: Reapplying the white noise.
- Step 12: Applying the factored Guadalupe 390% acceleration signal.
- Step 13: Reapplying the white noise.

A detailed description of this EMA and shaking tests can be found by, Doccini, [52], and Vieux-Champagne, [135].

[1] After the first three tests carried out with the signal from Haiti and before the excitation of the building by the distant earthquake, a repair was carried out at the level of the deformed connections.

6.6 Time history analysis

The uni-directional shaking table enables us to test the house with respect to S-N direction which represents numerically the global y-axis. Different measuring instruments were used to assess the displacements and accelerations. The number of DOFs. are 464 with 84 nodes and 258 different types of elements. The obtaining of the output displacements in the time history analysis enables the measuring of the other parameters of the structure (strain, stress, etc.). From these data, it can be compared to numerical results and assess the numerical model. The quality of measuring the displacements for some points is a key at which can be chosen the selected sensor points. Registration of the accelerations allows the study of the structure in the frequency domain (measuring EMA for example). As a reminder, this type of analysis is the determination of natural frequencies, and associated mode shapes.

The structure of the house has been built on the platform of the shaking table and the table subjected to acceleration signal of Haiti (100, 200, 300%) and then by the signal of Guadaloupe (100, 390%). To obtain the output of the shaking test, some of the measuring instruments have been used to register the response of the frame to input accelerations. The measurement of some important nodes is shown in the (Fig. 6.8) for the accelerations and displacements.

6.6.1 Displacements measurements

Three types of instruments are used to acquire these parameters. The wire sensors (or potentiometric sensor) that measure the horizontal displacements, LVDTs. (Linear Variable Differential Transformers) which measure the vertical displacements as well as horizontal and speed cameras that record the movement in the plane of the shear wall.

- For the DWDS sensor (Draw Wire Displacement Sensor), there are twelve potentiometric displacement sensors. seven of them were positioned on the north side to obtain a measure for main nodes on the wall. Three sensors were however redundant: the DWDS1 (located on the south side) and that their ends DWDS2 were attached to each corner of the east facade. DWDS7 then measured the displacement head west wall to confirm the hypothesis that the structure is deformed symmetrically. The last sensor of the northern facade was DWDS12 ridge located of the house, to obtain data on the displacement of the roof. Finally, four sensors (DWDS8-11) were positioned at west side to measure out of plane deformations of the wall that could be induced by the transverse shear wall.

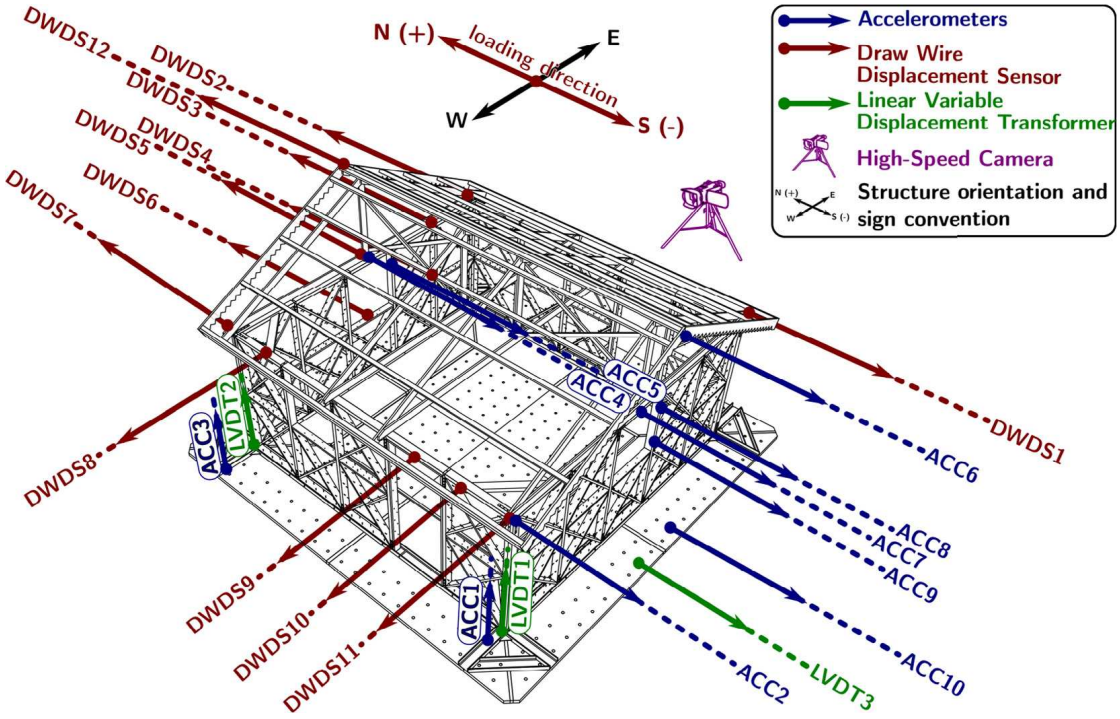

Fig. 6.8: Sensors of displacements and accelerations of tested frame

- LVDT Sensors: Two sensors of this type (RDP DCTH200AG) with a limit of ($\pm 50mm$) were used to quantify the uplift of the corner of the west facade columns.

In addition, a fast four cameras were installed and takes a video to make a digital image correlation, (DIC) analysis which is not included in this manuscript, one can see the results of Sieffert et al. [126].

6.6.2 Accelarations measurements

Accelerometers (ACC) Bruël & Kjaer Type 4574 were used to acquire the absolute acceleration at different nodes of the structure. The location of accelerometers can be shown in (Fig. 6.8) during shaking test. The ACC 10 provides accelerating of the table at which can be verified the input acceleration signal.

6.6.3 Validation of the numerical model

In structural dynamics, solving equation of motion can be evaluated by either in terms of time or in terms of frequency, this mapped picture because of the general

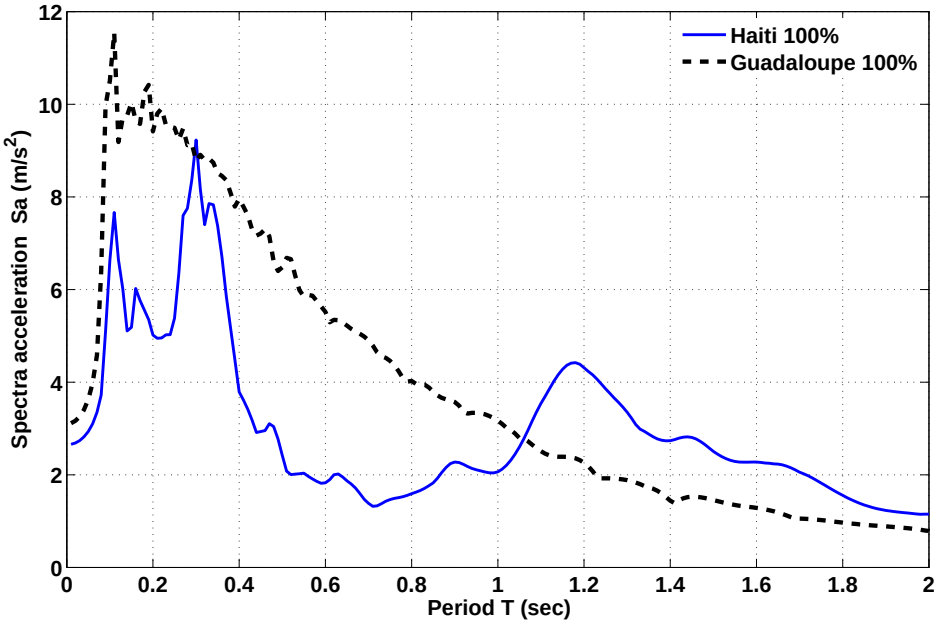

Fig. 6.9: Response spectrals of Haiti and Guadaloupe signals with 5% damping.

form of forces ($A.sin(2\pi.f.t + B)$) as input and also displacements (or velocity as well as accelerations) as output, where A: is the amplitude, f: the frequency, t, is the time instant, and B is the phase angle). So this term is two mutual variables, (time and frequency). The solution in the frequency domain yields complex numbers. The viscous damping ratio was used by Relaigh method was (1%), Xu and Dolan, [143]. The other choice is the solution in terms of time which called temporal analysis or time history analysis. The solution of the nonlinear (with stiffness time-dependent) equations of motion may be solved by Newmark's method (see section 3.2.1). In this section, the time history response of the house to the shaking of five different acceleration signals and compared the results to our FE. model as presented in previous sections.

To make a comparison between the two types of signals for a synthetic signal of Haiti and distant Guadaloupe, the response spectrum of each one is illustrated in the (Fig. 6.9). They show that for the Guadaloupe signal, the structures which have natural periods less than (1.0 s) are suffering to an amplification, whereas the amplification occurs for the structures of less than (0.5 s) and also for the natural periods between (1-1.5 s) for Haiti signal. This difference refers to the way of deriving synthetic acceleration time history signals.

6.6.4 Temporal response

For the case of the signals of Haiti, there are three shaking tests, the original signal Haiti 100% as in (Fig. 4.6) which is repeated with scale 2 and 3 times of the original signal, (200% and 300% respectively). The second Guadaloupe signal had been tested for the full-scale Guadaloupe 100% and 3.9 times, (Guadaloupe 390%) as follows:

- **Haiti** 100%: The relative displacements between the shaking table and that in the top node to study the response of the shear wall (DWDS1) is shown in (Fig. 6.10) for the non-factored signal (Haiti 100%). All the displacement signals in the direction of the actuator will be subtracted from the response of shaking table (signal LVDT3 in Fig. 6.8). In this curve it is difficult to make a comparison between the simulated numerical response and the experimental shaking table test due to the very noisy results and also due to the perturbation which had been occuring throw the experiment for the LVDT3 wire which subjected to free vibration, as a result it adds some addional spikes for each (5.3 seconds) time period with some frequencies which was, unfortunately, lie in frequency band range of the system (reach to sampling frequency 512 Hz), so it couldn't filtered out so as not to lose the original result data). The maximum relative displacement by experiment of shear wall corner was (-3.41 mm) while the numerical model gives a value of (3.89 mm) with error of (14.1%) and this appears to be big value as compared to the other signal errors due to small deformations which are affected by continuous noise and spikes amplitudes. The structure is near the linear elastic zone but the small value of deformation increases the sensitivity of the experimental results to the noise and spikes imperfection.

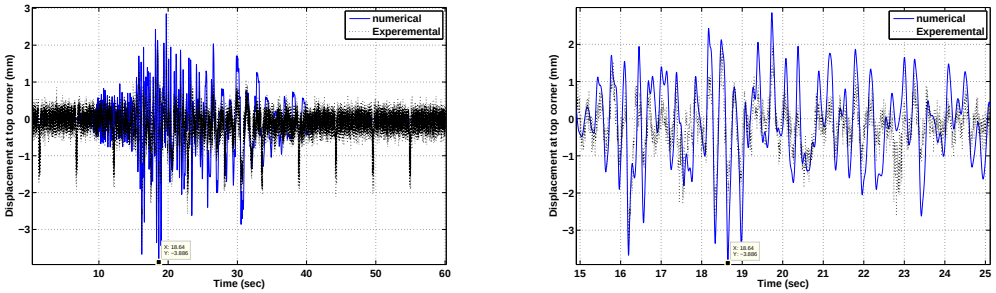

a) Time history of DWDS1 signal

b) Zooming in the DWDS1

Fig. 6.10: Relative displacements for top shear wall corner for Haiti 100%.

- **Haiti** 200%: The table was subjected to a second signal of two times the first, the response of the shear wall at top point DWDS1 is shown in the (Fig. 6.11) for the experimental and simulated relative displacements which shows acceptable error between the maximum experimental and numerical values.
  The maximum simulated value was (-7.56 mm) while the experimental value (-8.75 mm) with an error of (13.6% when the simulation starts from rest and no accumulated damage were used, in the case of accumulated damage the error was reduced to 7%) as shown in (table 6.3).

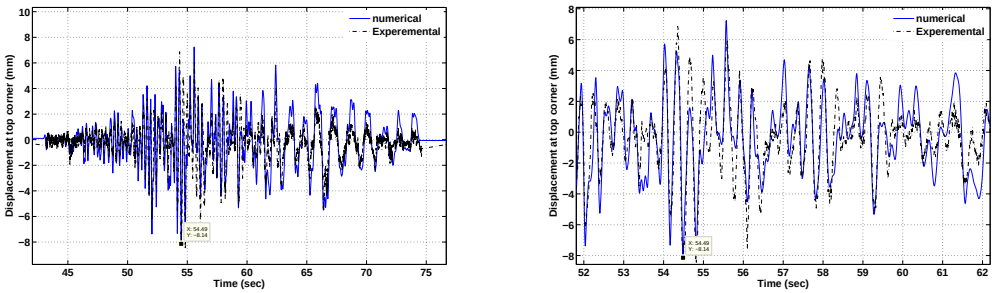

a) Time history of DWDS1 signal

b) Zooming in out the DWDS1

Fig. 6.11: Relative accumulated displacements for top shear wall corner for Haiti 200% after Haiti 100% displacement signal.

- **Haiti** 300%: In this case, the structure shows a nonlinearity and yields an error of (12.2% in direct simulation test and 3% in the case of accomulated loading case), as in (Fig. 6.12) between the maximum experimental displacement (-12.72 mm) and a corresponding maximum numerical values of (-11.17 mm, -12.34 mm for the two simulation cases). This first big error was reduced in the case of accumulated loading, so the initial numerical model for Haiti 300% does not reflect the real behaviour due to the damage after testing the previous shaking and white noise application according to the steps of EMA, as in (section 6.5). This error can be reduced if we make the analysis of accumulated signal time history for the Haiti three scales as shown in (Fig. 6.15-b) and table (6.3).

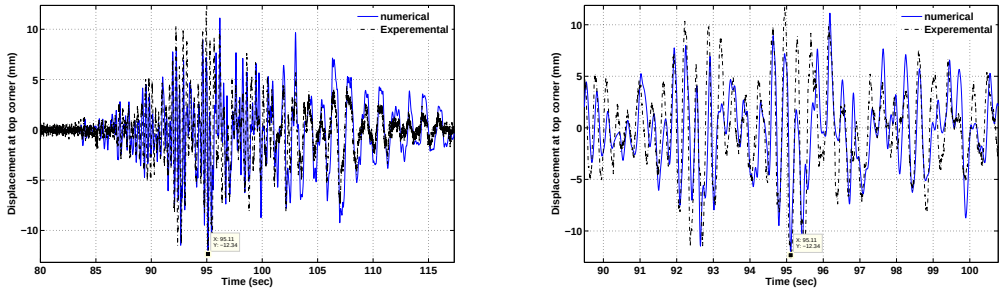

a) Time history of DWDS1 signal

b) Zooming in the DWDS1

Fig. 6.12: Relative accumulated displacements for top shear wall corner for Haiti 300% after Haiti 100% and 200% displacement.

- **Guadaloupe** 100%: The second distant acceleration records was subjected to the table after rehabilitation of the small damages after last acceleration and displacement excitations. The comparison for the displacements DSDW1 point, (Fig. 6.13) shows again big effect of the noise due to the small amplitudes as in the case of Haiti initial signal, the resulting errors is (21.9%, 41.9% for direct and accumulated loading respectively) between tested and simulated displacements. The reason of the latter big error is due to the fact that it can not be more make accumulated simulation because after Haiti 300% loading the structure was rehabilitated to return back its initial stiffness but the moderate error 21.9% shows that the rehabilitation process could not return back full original stiffness of the structure. This issue was emphasized by Duccini, [52].

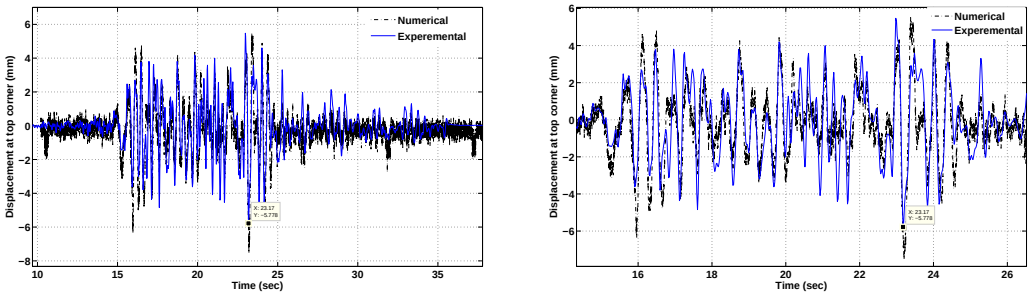

a) Time history of DWDS1 signal

b) Zooming in the DWDS1

Fig. 6.13: Relative displacements for top shear wall corner for Guadaloupe 100% from rest.

- **Guadaloupe** 390%: The last signal was the 3.9 times of Guadaloupe acceleration. The displacement at the top of the shear wall (DWDS1) was (-40.46 mm for testing result and -37.16 mm for numerical model response) with an error of (8.2%) as in (Fig. 6.14), this value will be increasing to (34.9%) if we make the comparison with total accumulated signal records, (Fig. 6.15). These results are validated and prove the efficiency of the numerical model and the actual evolution of the damage with respect to experimental test. The (Fig. 6.15-c) shows the time history response for Guadaloupe signals after repairing process which proves the actual behaviour of the structure according to the preparation process before of Guadaloupe signal application.

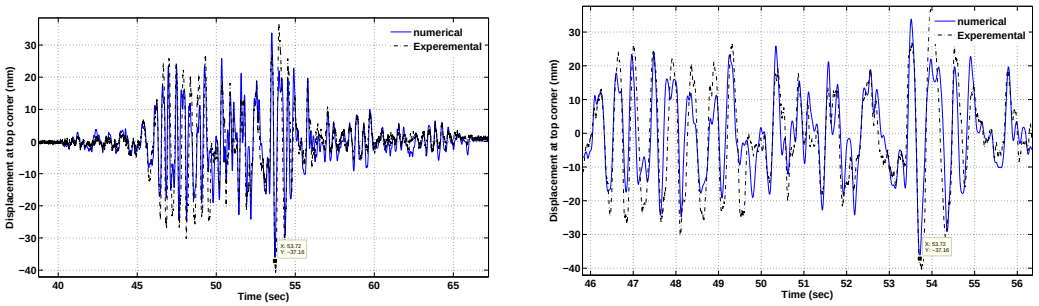

a) Time history of DWDS1 signal

b) Zooming in the DWDS1

Fig. 6.14: Relative accumulated displacements for top shear wall corner for Guadaloupe 390% after Guadaloupe 100% displacement signal.

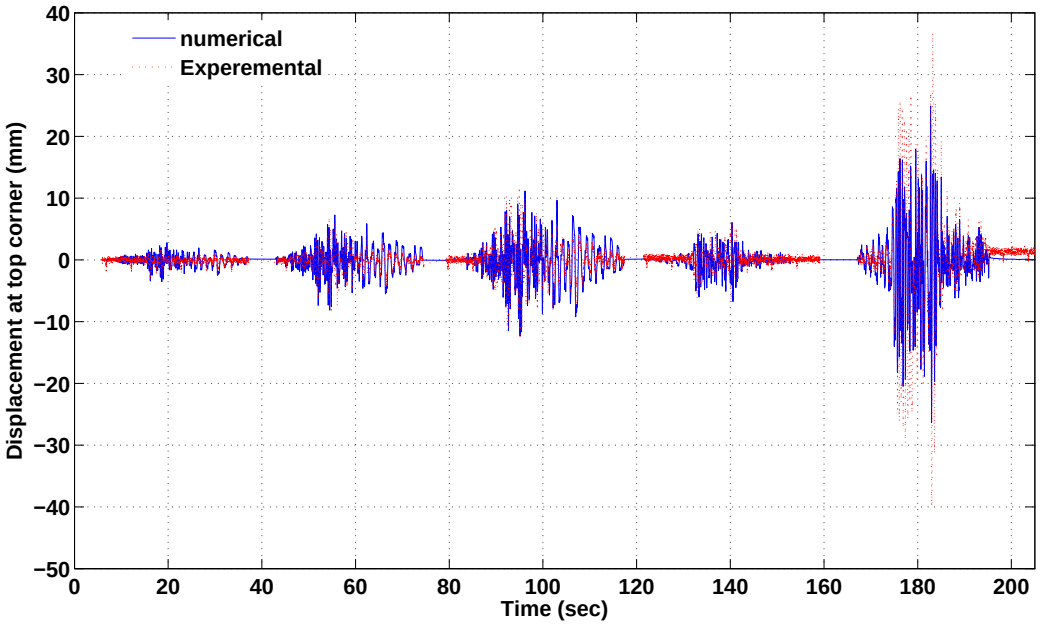

a) All signals

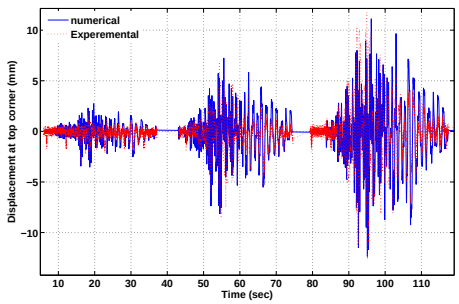

b) Haiti

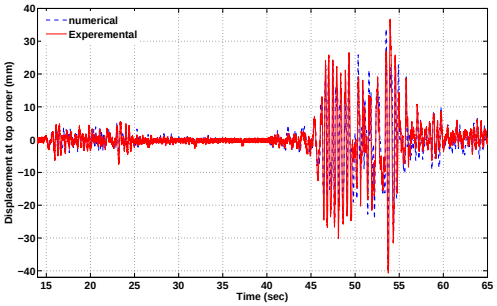

c) Guadaloupe

Fig. 6.15: Relative displacements DWDS1 response for all signals of accelerations

Table (6.3) shows a comparison of the displacements at top of the shear wall for all signals between experimental and numerical responses, it shows by the italic red colour the wrong values of successive or accumulated simulated damage which is not in the reality. To obtain accurate results, each signal (Haiti or Guadalupe) must simulate successively like in the experiments.

Tab. 6.3: Summary of maximum displacements at top shear walls.

Signal	Sign	Experimental (mm)	*Direct comparison**	Error %	Accumulated (mm)	Error %	Separate Accumulated	Error %	Macroelement model, [135]	Error %
Haiti	-	3.41	3.89	14.1	3.89	14.1	3.89	14.1	1.32	61.3
100%	+	2.22	2.85	28.4	2.85	28.4	2.85	28.4	1.60	27.9
Haiti	-	8.75	7.56	13.6	8.14	7.0	8.14	7.0	6.56	25.0
200%	+	6.89	6.64	3.60	7.24	5.1	7.24	5.1	7.86	14.1
Haiti	-	12.72	11.17	12.2	12.34	3.0	12.34	3.0	13.77	8.3
300%	+	12.17	10.78	11.4	11.12	8.6	11.12	8.6	18.21	49.6
Guadaloupe	-	7.40	5.78	21.9	4.30	***41.9***	5.78	21.9		
100%	+	4.35	5.29	21.6	2.41	***44.6***	5.29	21.6		
Guadaloupe	-	40.46	22.27	***45.0***	26.34	***34.9***	37.16	8.2		
390%	+	36.80	24.12	***34.5***	24.92	***32.3***	33.73	8.3		

* Direct comparison: Means make a comparison of the numerical results without taking into account the accumulated damage throw the test.

6.7 *Hysteresis laws*

The seismic resistance and good performance of the structures based on the behaviour of some structural parameters, these are basically stated as ductility and sources of dissipated energy. The relation-ship between the displacement DWDS1 and developed shear force of the shear wall below such point in the y-direction as well as total shear force of structure are shown in (Fig.6.17) and (Fig.6.16) for Guadaloupe and Haiti signals respectively. These dissipation of energy are clear by the area enclosed by each hysteresis curves. The total shear force curves shows the small value of yield displacements (less than 1 mm) this premature nonlinearity comes from different sources of the composite structure of traditional buildings that are mensioned above and as we know for all of these components they have already themselves high material nonlinearity as well as the combination of them which increase the nonlinearity behaviour. This behaviour permits the structure to dissipate the energy from the small deformation level which helps to formation structural damping of the system and this will explain the high capacity of the system for energy dissipation. The sources of this dissipation come from the friction between infilling weak materials themselves as well as the contact friction between infilling and surrounding timber frame elements.
The evaluating of the stiffness of these nonlinear constitutive laws is so difficult, so for the nonlinear behaviour structures, the effective stiffness may be another optional choice, eg. Sieffert et al. [126], Chopra and Goel, [35]. It is simply defined by the ratio of force to the displacement for some ductility or displacement level, table (6.4) shows these values which are illustrated as (force-displacements pairs)

of each acceleration signal in the (Figs. 6.16, and 6.17).
The total shear force curves were compared to the experimental results of digital image correlation (DIC) by Vieux-Champagne et al., [138] and Sieffert et al. [126], good results were obtained as illustrated in the rignt side of (Figs. 6.16 and 6.17) and table (6.4).

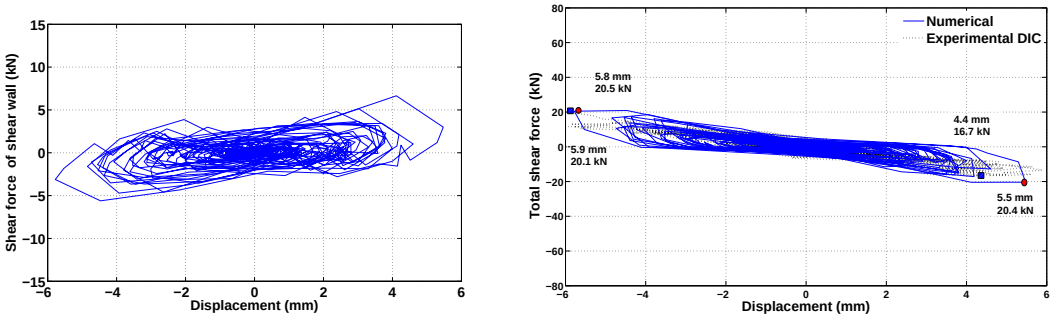

Guadaloupe 100 signal.

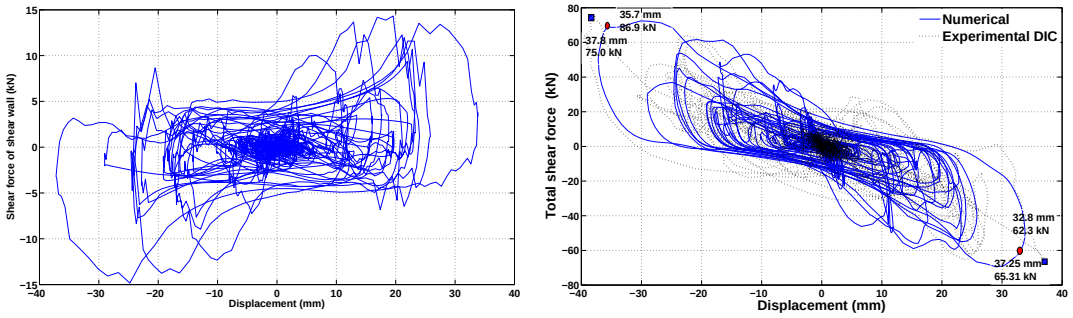

Guadaloupe 390.

Fig. 6.16: Relationships between shear force of (a) one shear wall, (b) total shear force vs. Top corner shear wall displacement DWDS1, Guadaloupe signals.

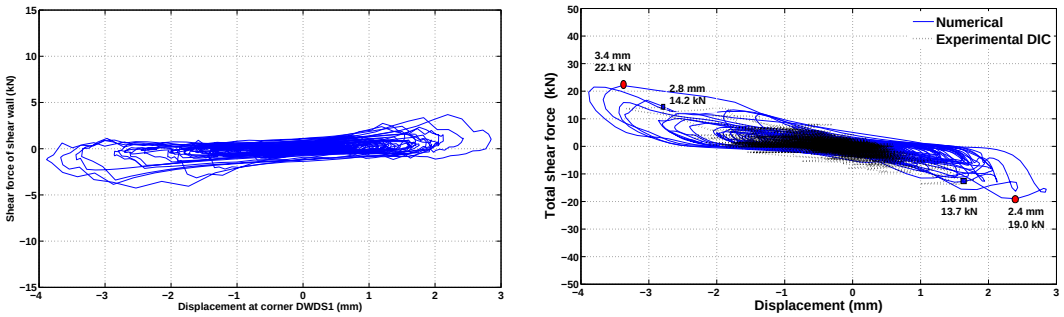

Haiti 100 signal.

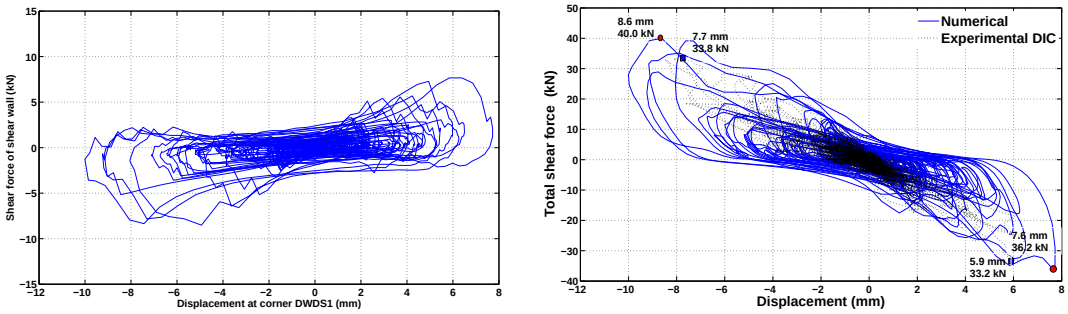

Haiti 200 signal.

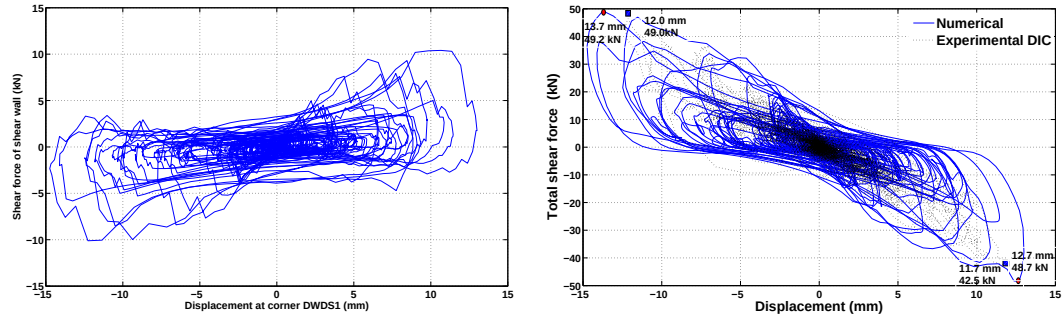

Haiti 300 signal.

Fig. 6.17: Relationships between shear force of (a) one shear wall, (b) total shear force vs. Top corner shear wall displacement DWDS1, Haiti signals.

Tab. 6.4: Effective stiffness of total shear force (point selected for maximum force value).

Signal	δ_+ (mm)	$Force_-$ (kN)	δ_- (mm)	$Force_+$ (kN)	K_- (kN/mm)	K_+ (kN/mm)	$K_{ave.}$ (kN/mm)	$K_{ave.}$ Exp. [138] –	*Error* (%)
Haiti 100%	2.40	19.00	3.40	22.10	7.92	6.50	7.21	6.82	5.74
Haiti 200%	7.60	36.20	8.60	40.00	4.76	4.65	4.71	5.00	6.01
Haiti 300%	12.60	48.70	13.70	49.20	3.83	3.59	3.71	3.86	3.76
Guadaloupe 100%	5.50	20.40	5.80	20.50	3.71	3.53	3.62	3.60	0.57
Guadaloupe 390%	32.80	62.30	37.80	75.00	1.90	1.98	1.94	1.87	3.91

6.8 *Torsion effect*

We mentioned recently that the actuator of the shaking table is applying the loading in the direction parallel to the plane of symmetry of the house model, so the temporal response of each two conjugate DOF. wrt. the plane of symmetry are identicals. This is true in the (S-N y-direction) excitation but not for the (E-W x-direction). To discover the torsion effect which is very important factor because the earthquake comes usually in randomly inclined angle, it must test the responses for the signals which are not pass through the vertical plane of symmetry or that are not passe throw center of rigidity and center of gravity of the buildings simultaneously. To do this, a comparison between the displacement in the x-axis at the S-W corner in the top of shear walls (the points at Fig. 6.18) and the other corner (N-W) at top of the shear wall (point d). The latter figure and table (6.5) show the maximum displacements of the corners top shear wall nodes and so the horizontally deformed plane of these points, these maximum deformations occurred at a time period of (23.61 sec.). It is evident that the torsion effect can be neglected due to the existing of the four diaphragm corner members and according to a maximum rotation angle of (0.5922°=0.0103 radians). These results are for un accumulated of the maximunm signal of guadaloupe 390%.

6.9 *Pushover analysis*

This type of nonlinear static analysis is used to find a rapid approximate estimation of the behaviour of the structure w.r.t. any seismic signal. The objective as mentioned in (sec. 5.4) is to find the performance point which can be found graphically as the intersection point of ADRS (acceleration displacement response spectrum) which defines for a specified acceleration signal and damping ratio (elastic response spectrum) the force and corresponding displacement undergoes by the structure during seismic loading. As we mentioned recently it can be evaluated

Tab. 6.5: Maximum displacements in the case of lateral non-symmetric loading x-direction.

Point	$\delta_x\,(mm)$	Time	$\delta_y\,(mm)$	Torsion angle θ
a	-44.11	23.61	-0.13	0.5546 °
b	-44.04	23.61	0.22	0.5633 °
c	-46.22	23.61	0.18	0.5922 °
d	-46.29	23.61	-0.11	0.5848 °

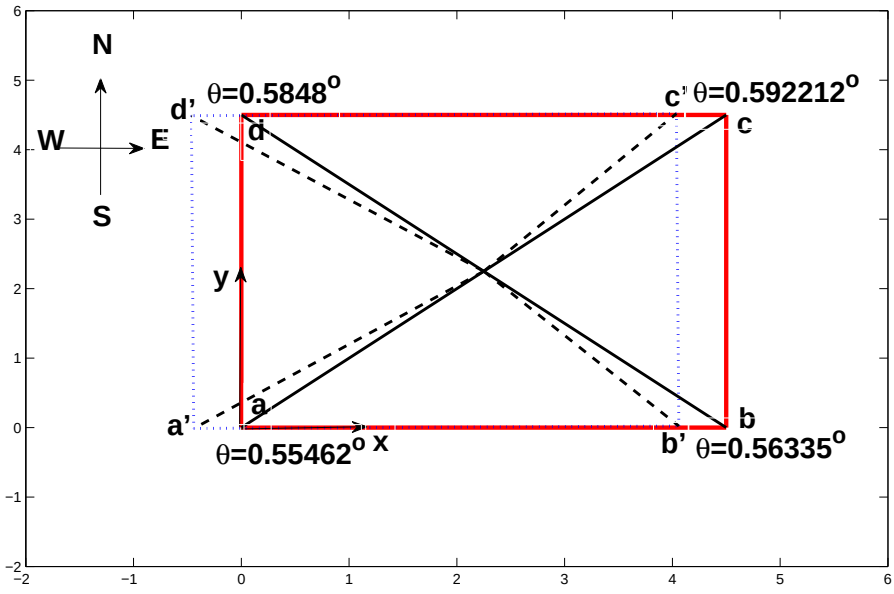

Fig. 6.18: Torsion occurs due to loading in x-direction.

from a superposition of capacity (shear force-displacement) and demand curve (response spectrum) in ADRS format. The target displacement can be considered as an estimation of the global displacement (equivalent SDOF) by the structure which is expected to experience in a design earthquake. The tested house is one storey structure, so each storey in the literature will be replaced by a node, i.e. the shear force of the capacity curve will be obtained by the mass at each node multiplied by the first mode shape value (second mode of the system for the loading in the direction of table actuator, y-direction). This means that the capacity force is the summation of inertia forces in a specified direction. The method of EC8 code, [65] which proposed by Fajfar, [56] based on a basic assumption that the displacement shape of normal modes does not change through the structural response to a ground motion. The reason of the assumption of elasto-plastic relationship (post-yield stiffness equal to zero) in Fajfar N2 method is that the reduction factor R_μ is defined as the ratio of the required elastic strength to the yield resistance, the neglecting of the moderate hardening (as in the procedure of FEMA-440, [40]) had been incorporated in the demand curve and it has not a significant effect on displacement demand, Fajfar, [56]. Pushover method states that the response of the structures in not depends on time, so this is not true especially for the structures that are affected by higher modes. This disadvantage can be overcome (or at least decrease) by choosing two different loading pattern distribution and envelope the results, Fajfar, [56] and also the problem of formation of the plastic hinge which may be not controlled by the analysis.

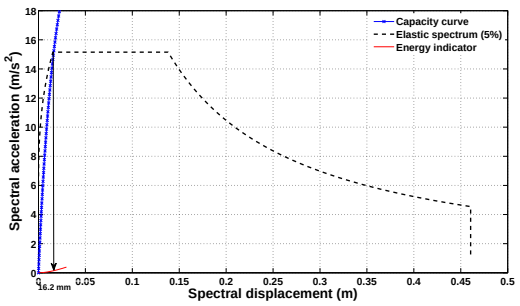

b) PGA=2.65 m/s^2

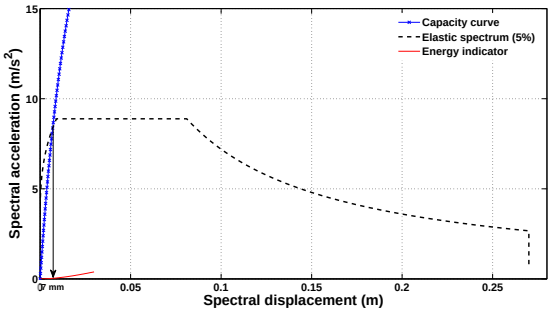

c) PGA=3.09 m/s^2

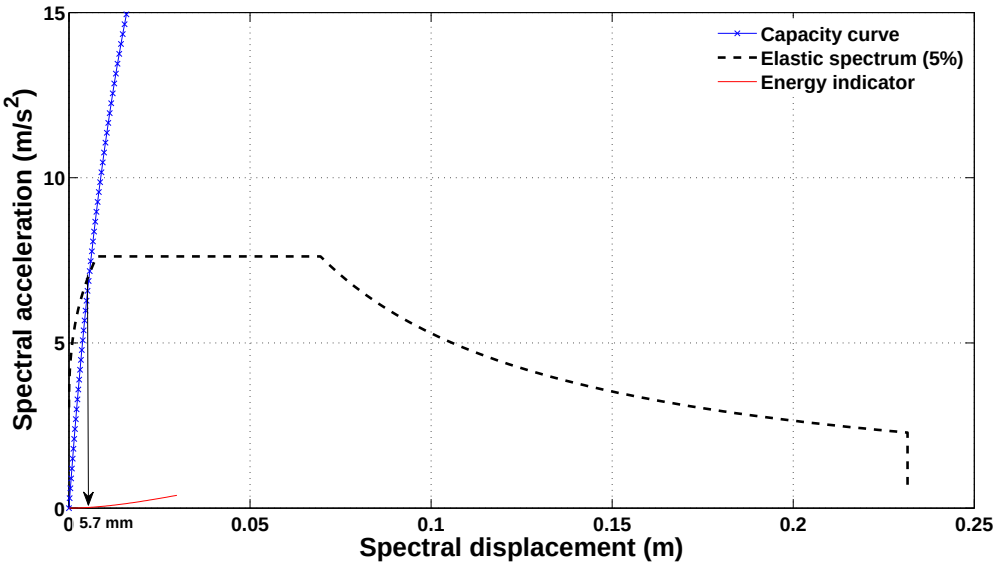

a) PGA=5.27 m/s^2

Fig. 6.19: Pushover analysis by the method of Eurocode EC8 for different values of PGA.

(Fig. 6.19) shows the pushover analysis in terms of ADRS format and shows that the good performance of the traditional timber frames which can resists the signal of PGA=5.27 m/s^2 which is equal to the 200% of the Haiti synthetic signal within the elastic range. It shows also that the capacity curve of the structure meets with the demand curve in the acceleration sensitive zone ($T \leqslant T_B$), T is the natural period and T_B is the minimum period in the plateau of response spectrum curve as in the EC8, [65] as mensioned in the free vibration analysis.

6.10 Two storey Building

In this section the numerical model will be applied to two storey building which represent the example of traditional timber framed in 'Fig. 6.20).
The sill plate in the first (earth) floor is rested on a plain concrete or masonry foundation by the same way as in the one storey house (see Fig. 5.2). As in the house one storey, the walls consist of vertical trusses connected by diagonal St. Andrew's crosses and horizontal planks. The crosses and the planks are fixed with nail connections to the vertical posts (Figure 5.9). Also as in the case of one storey house.
Between the first and the second story, a horizontally continuous beam separates the vertical post of the second story from the one of the first story. Similar to the metal connection at the bottom of the house, the lower and the upper post are connected by a metal strip at both sides of the wall (Fig. 6.21). At the corners, one metal strip for each of the two horizontal directions was installed.
The ceiling system was design so that the main girders consist each of two parallel beams which are attached to the lower vertical posts with six bolts. In this case and to avoid tearing failure the required width for the girders were modified to (20 cm instead of 10 cm). For fire protection and sound insulation, a gypsum plasterboard and a 15 cm thick layer of light hemp concrete is optional. Onto this, wooden boards are used as floor.
The roof is the same as that of one storey house and the roof trusses are parallel to the girders of the ceiling. The four stiffner elements in the corners are used for the two floor and roof levels.

Fig. 6.20: Sample of two storeys building in Haiti.

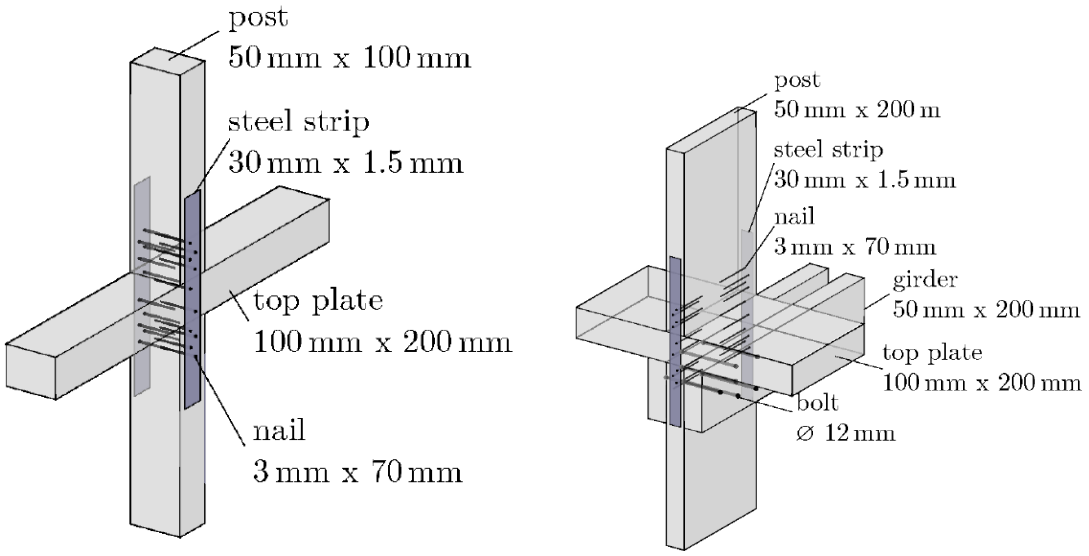

a) Dimensions of continous beam and connecting posts

b) Dimensions of middle girder with continous beam and connecting posts

Fig. 6.21: Detailed dimensions of the wall girder connection in the floor level with steel strip connections

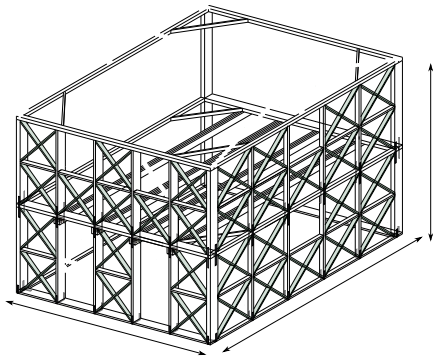

Fig. 6.22: Modeling of the two storeys school building.

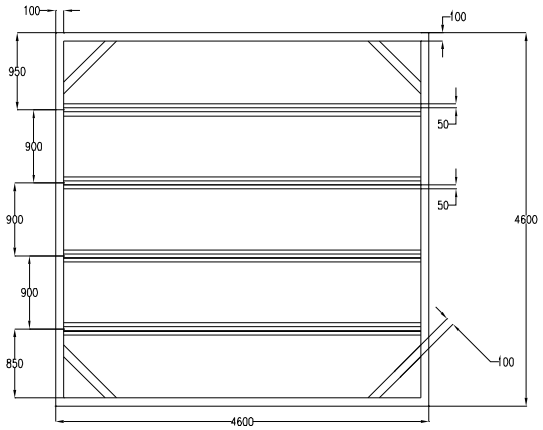

Fig. 6.23: Roof system details for the two storeys school building.

6.10.1 Modelling of the structure

As we mensions in the wall and house scale the nonlinearity source of the structure are concentrated in the connections as well as the unit pannel scale which comes from the interaction of the shear resistance of nails with respect to wood medium and the steel strip and the composite substructure of the timber braces and infilling.

Finite elements and constitutive law

In the simulation, linear and non linear elements are used together, the timber-framed structure and the infill is represented by non-linear truss elements, as it's shown in (Fig. 6.24). Totally, the building is modelled with 418 elements and 734 degrees of freedom.
The modeling were performed by the same way of one stroey house by choosing the same beam, bar as well as nonlinear emlements.
For the shear wall (with diagonals and infill) it is supposed that the vertical resistance of the connection in the wall compared to the single metal strip connection is not influenced by the infill. The shear resistance however increases significantly because of the infill. This is again caused by the friction between the infill and the horizontal beams and the deformation resistance of the infill. Moreover, the diagonals resist against a horizontal displacement of the post and therefore also

increase the shear resistance of the connection compared to a single metal strip. For timber framed structures, the most amount of the dissipative energy phenomena are concentrated in the joints.

To model of the metal strip connection between the first and the second story (see Fig. 6.21-b and Fig. 6.21-a)), the same non-linear element as for the metal strip connection at the bottom) is used. This approximation is justified by the similarity of both connections, namely the same number of nails as well as the same type of metal strip which gives same shear resistance from the nails.
Every opening in the wall such as doors and windows is created by removing the diagonal non-linear elements in the respective cell.

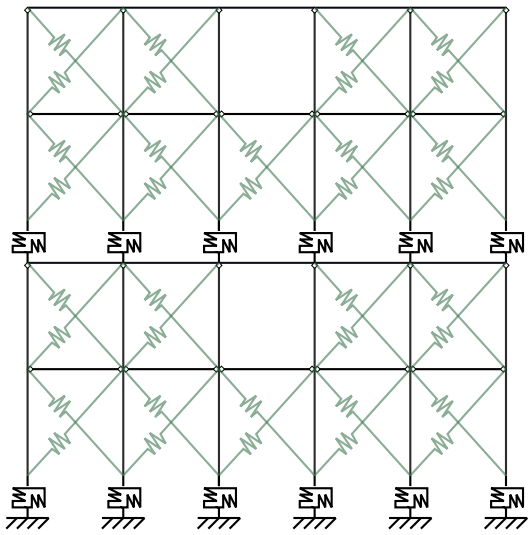

Fig. 6.24: Modeling of the xz-plane shear wall.

6.10.2 Distribution of masses

In the modeling by the FEM method, all masses (like in the stiffness values) are concentrated in element nodes. This is due to the basic definition of the masses which is the force required to gives a specified DOF unit acceleration, Paz, [110]. Compared to the light timber frame structure, the mass of the masonry infill predominates the total mass. As mensioned above this mass is equally distributed to the four nodes of the respective square. (Fig. 6.25) shows the building with the masses of the walls concentrated to the element nodes. The volume of a sphere is equivalent to the mass at the node. Each two nodes which are connected by a

metal strip (see Fig. 6.24) have identical coordinates. Therefore, the masses of the two nodes are added and combined in one sphere for this figure. In the simulation, each of the two nodes connected by a metal strip has its own mass depending on adjacent filled squares as in the previous two scales.
For dynamical loading, the mass of the ceiling has a significant influence on the behaviour of the building. As mentioned above, a wooden support structure combined with gypsum plasterboard and a light hemp concrete infill is chosen. As calculated in (Fig. 6.25-a), the self-weight of the ceiling onto one girder is (61 kg). This additional mass is very small compared to the mass of the wall and can be therefore neglected. Instead, the influence of a heavier slab with a (7 cm) concrete screed layer is simulated, which corresponds to a mass of (600 kg) per girder. The mass of the ceiling is transferred to the lower vertical posts by the four girders. Considering the mass of the ceiling, (Fig. 6.25-b) shows a significant increase of the masses.

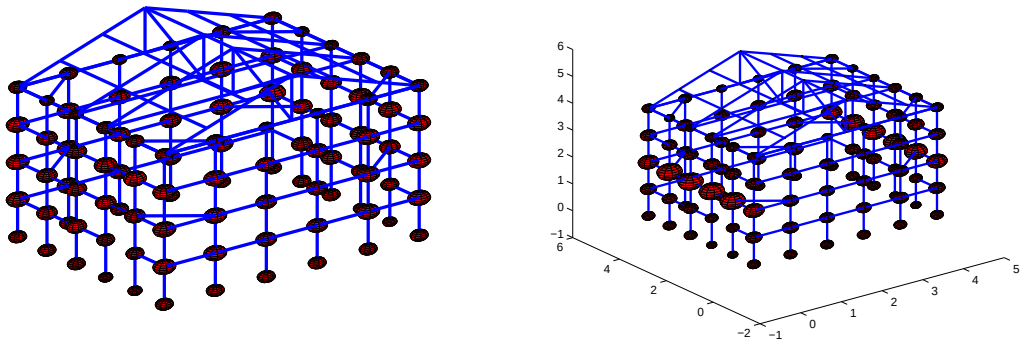

a) Lumped mass distribution without ceiling mass.

b) Lumped mass distribution with ceiling mass.

Fig. 6.25: Lumped mass distribution of two storey building.

Boundary Conditions

(Fig. 6.26) gives an overview about the setting of the boundary conditions. The horizontal timber foundation beam at the bottom (sill plate) of the house is considered as rigidly mounted. As a consequence, it can be replaced by multiple single fixation points at the connection points to the vertical posts. At these mounts, all translatory movements and all rotations are set to zero. The bottom nodes of the timber frame structure are connected by metal strips to these mounts. The resistance of the metal strip is separated into a shear and a normal (vertical) one.

Therefore, a relative displacement between the fixed mounts and the bottom nodes in horizontal and vertical direction is allowed (in the plane of the wall). As the rotational resistance of the steel strip is not modelled due to lack of experimental information about $M - \theta$ relationships, is is not taken into account, the connected diagonals and vertical posts are hinged to the bottom nodes and can rotate. The rotational resistance of the metal strip is included in the total shear resistance of the wall. A rotation around the horizontal axis of the plane is possible. In the corners, the boundary conditions for both shear walls are combined.
For the nodes connected by the metal strips between the first and the second story, in general the same conditions are applied. However, as none of the nodes is fixed in any direction, only a kinematic relation between the nodes connected by a metal strip can be specified. The displacement orthogonal towards the wall is identical for two connected nodes.

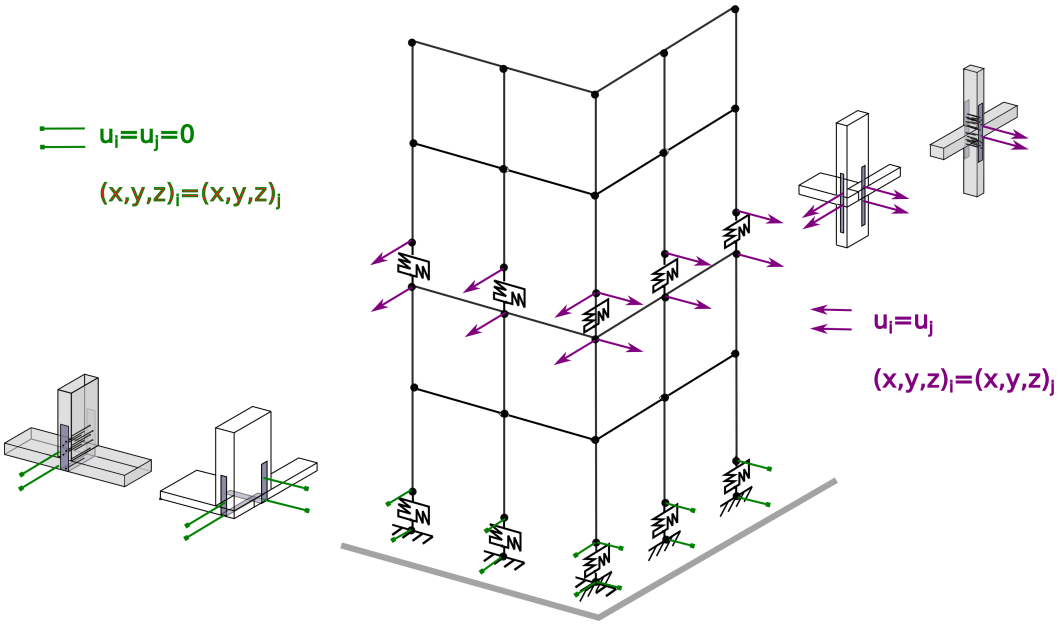

Fig. 6.26: Boundary conditions of two storeys building.

Tab. 6.6: Simulations for the two-storied building

N°	Direction of acceleration [−]	Force of acceleration [%]	Mass of the slab [kg per beam]
1	y	100	-
1a	y	100	600
2	y	200	-
2a	y	200	600
3	y	300	-
3a	y	300	600
1-x	x	100	-
2-x	x	200	-
3-x	x	300	-

6.11 Displacements and Forces

Some parameters were studied for the scale of two storey building as the existing of masses of floor and the direction of loadings. The fundamental frequencies of the two storey frame are (3.3, 3.7 Hz for the x, y direction of motion respectively without added masses of the concrete floor, these values will reduces to 2.3, 3.5 Hz if we taking the mass into account). Table (6.6) gives an overview about the simulations which were run for the two-stories building. In the following discussion, *shear walls* and *front walls* will be differentiated. The walls parallel to the direction of acceleration of haiti for three different scales are termed as *shear walls*; the walls which are orthogonal to the direction of acceleration are *front walls*.
Fig. (6.27) illustrates the decisive nodes for forces and displacements. For an acceleration in y-direction, the nodes represent:

- At node (a), the tensile reaction force in vertical direction is maximal. The vertical displacement in the metal strip connection under tensile load is decisive for the resistance of the connection.
- At nodes (b) and (c), the maximum horizontal displacement in y-direction is measured. With this values, the drift of the shear wall can be calculated.
- Nodes (d) and (e)
  For the front wall, the total orthogonal displacement toward the wall is studied.
  For the acceleration in the x-direction, the represented nodes are:

- Node (h): The tensile reaction force in the vertical direction is maximal. The vertical displacement in the steel strip connection under tensile force is decisive for the resistance of the connection.
- Nodes (i) and (j): The maximum horizontal displacement in x-direction is measured. With this values, the drift of the shear wall can be calculated.
- In the nodes (f) and (g), the total orthogonal displacement towards the wall is studied.

The maximum values of displacements and forces at these decive nodes for an acceleration in y-direction are shown in the (table 6.7) and for the acceleration in the x-direction are illustrated in the (table 6.8).

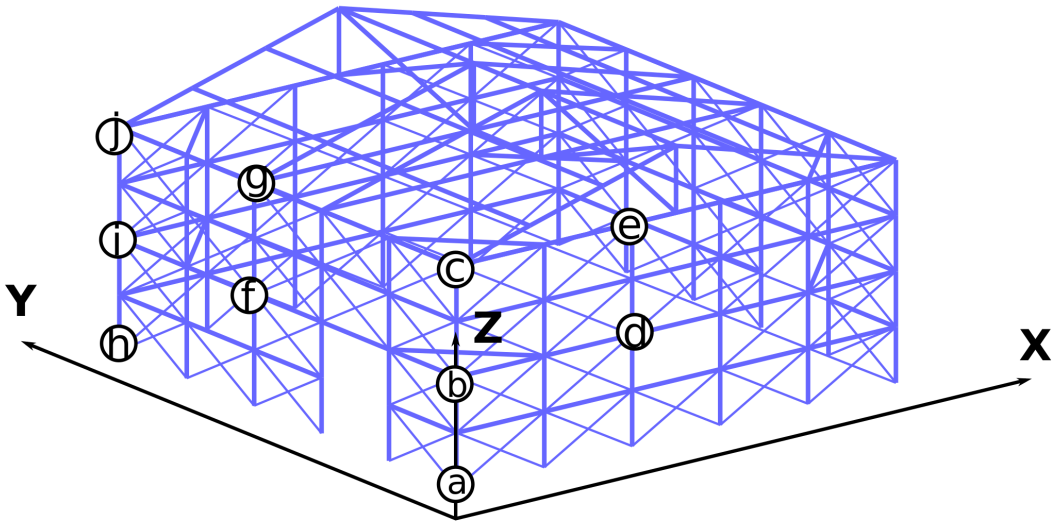

Fig. 6.27: Some selected decisive nodes for the calculation of forces and displacements.

In the table (6.7) reccognize the big effect of the added mass for the floor of second storey on the vertical force at the corner (node a) by the increasing of

Tab. 6.7: Maximum values of forces and displacements for an acceleration in y-direction.

Simulation			1	1a	2	2a	3	3a
a	F_{tens}	$[kN]$	2.67	4.53	6.29	6.15	7.11	7.50
	u_z	$[mm]$	1.11	1.47	3.19	3.03	4.63	4.83
b	u_y	$[mm]$	7.45	9.43	18.06	21.77	27.05	29.59
	drift shear wall	[%]	0.38	0.47	0.90	1.09	1.35	1.48
c	Δu_y	$[mm]$	2.26	2.64	5.20	5.30	7.50	7.15
	drift shear wall	[%]	0.11	0.13	0.26	0.27	0.38	0.36
d	u_y	$[mm]$	9.49	13.25	26.66	27.37	38.57	36.74
	drift shear wall	[%]	0.48	0.66	1.33	1.37	1.93	1.48
e	Δu_y	$[mm]$	8.66	4.65	5.40	9.22	9.66	12.1
	drift shear wall	[%]	0.43	0.23	0.27	0.46	0.48	0.61

Tab. 6.8: Maximum values of forces and displacements for an acceleration in x-direction.

Simulation			1-x	2-x	3-x
h	F_{tens}	$[kN]$	3.63	5.40	7.30
	u_z	$[mm]$	0.91	2.26	4.66
i	u_x	$[mm]$	4.13	9.60	17.98
	drift shear wall	[%]	0.21	0.48	0.90
j	Δu_x	$[mm]$	2.60	5.25	6.96
	drift shear wall	[%]	0.13	0.26	0.35
f	u_x	$[mm]$	13.24	16.12	40.00
	drift shear wall	[%]	0.66	0.81	2.00
g	Δu_x	$[mm]$	0.15	3.76	-13.05
	drift shear wall	[%]	0.01	0.19	-0.65
b	Δu_x	$[mm]$	5.00	8.80	13.30
	drift shear wall	[%]	0.25	0.44	0.67
c	Δu_x	$[mm]$	2.20	4.40	3.10
	drift shear wall	[%]	0.11	0.22	0.16

(70%) for the (100%) acceleration, which is not the case of the (200% and 300%) signals, the reason is the big value of forces due to the inertial forces will make the structure to be more flexible by decreasing the stiffness of the unit cell element which will decrease the possibility of rocking rigid body motion and activate the shear deformation of the shear walls. There is almost moderate effect for the additional mass on the drift values for different acceleration scales.
That is the added mass of the floor will be neglected for the simulations of accelerations in the x-axis as in the table (6.8). The torsion effect due to the non symmetric deformed shape in the x-direction acceleration indicated by the differences between either the (nodes (b), (i) in the floor level as well as nodes (c), (j) in the roof level). This effect can be calculated roughly (without taking into account the deformations in the y-direction) by the difference between each pairs at each level divided by the length of the conected wall between them (line $\overline{bi}$ and $\overline{cj}$) as shown in (Fig. 6.27). These values are:

- For the floor level, the rotation angle (in radians) was 0.019, -0.018, -0.1 % for 100%, 200%, and 300% respectively.
- For the roof level, the rotation angle (in radians) was -0.009, -0.019, -0.084 % for 100%, 200%, and 300% respectively.

The permissible value of eccentricity that stated at Eurocode 8 (EC8, [65]) as the location of the center of masses is ±5% at each storey, and the above values of rotations are so far, so the structure has no need to design for the torsion, knowing that this comment is also correct for the case on one storey building as depicted in (Fig. 6.18).

6.12 Verifying damage criteria

To evaluate the resistance of the timber-framed structure, a failure criterion mais be determined. For the building, the steel strip supports at the bottom of the house are supposed to be the controlling element for the failure of the structure. This connection resists high compression forces but will fail under tensile stress. The maximum tensile stress due to the horizontal seismic load is imposed onto the bottom supports at the corners of a shear wall (node a). Consequently, this maximum tensile force during the dynamic loading is compared to the maximum tensile resistance of a static tensile test for the connection in scale 1, (sec. 5.2). The relation between the tensile force and the vertical displacement for the connection with nails according to static tests is shown in (Fig. 6.28-b). The maximum tensile force was identified with (11 kN), which is equivalent to a vertical uplift displacement of (11 mm). To respect a certain safety, the static maximum potential tensile force must be reduced to get a maximum permitted tensile force.

A reference value for this force can be found via a maximum permitted drift of a storey. Based on Eurocode 8 in paragraph 4.4.3, the drift is limited to 1% for damage limitation.
The relation between the drift and the vertical displacement for a static horizontal force is simulated. The load is applied in the same time at the top of the two shear walls. As shown in (Fig. 6.28-a), the drift limit of 1% corresponds to a vertical displacement in the bottom steel strip of (3.64 mm). This value leads to a tensile force of (5.76 kN) for the two-storey house (Fig. 6.28-b).
This maximum permitted tensile force reach to 52% of the maximum static potential force of the steel strip. Therefore, a sufficient safety is included in the failure criterion. If one compares the results in (table 6.7 and table 6.8) with this limit force, it can be seen that the two-storey building with a light-weight slab or with a thin concrete slab also resists for the 100% acceleration signal. The maximum value of the tensile force in the steel strip is lower than the limit criterion (5.76 kN). This gives the proof of the seismic-resistant behavior of a filled timber-framed structure with two-storey in accord with Eurocode 8. At an increased seismic level (200% and 300% signal), the tensile force in the steel strip exceeds the limit criterion. Let's note that with these signals, the tensile force in the steel strip are still lower that the maximum experimental value (11 kN). The maximum tensile force in the steel strip is obtained for the thin concrete slab and 300% signal and it equates to 68% of the maximum static potential force. Then the two-storey building should be not collapsed even at this high level of ground motion signal.

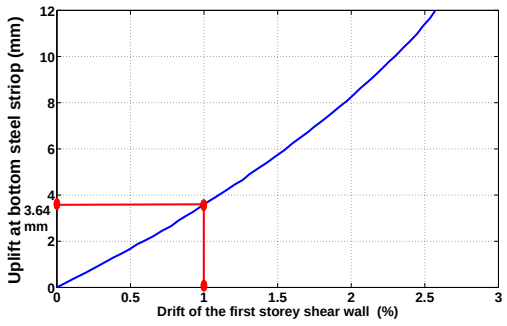

a) Drift of the first storey shear wall vs. vertical displacement at steel strip connection

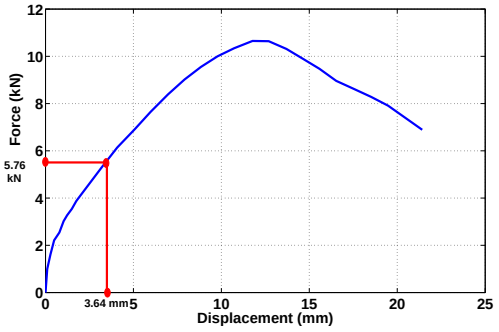

b) Tensile force displacement relation of steel strip connections

Fig. 6.28: Evaluation of damage criteria of the buildings by earthquake loading.

6.13 Conclusions

In this chapter, the dynamic analysis of the scale three of full 3D timber frame structures with infilling was performed for one and two storeys buildings modelled according to the results of the 1^{st} and 2^{nd} scales of connection and unit wall respectively under some restrictions (same material and dimensions). Two types of acceleration signals were used to validate the model with experimental shaking table tests, a synthetic signal of Haiti and a distant signal of Guadaloupe acceleration records. The results show the ability of the proposed model to simulate the real complicated physical phenomenon of the composite material by a simpler structural representation of linear and nonlinear finite elements. This was verified by comparing the experimental free and forced vibration analysis. The nonlinear infilling effects were idealised by a truss nonlinear element by using constitutive law according to Hysteretic constitutive law model and their masses were lumped into each node. The second source of nonlinearity was the connections in the base of one storey as well as the joints between the posts of the 1^{st} and 2^{nd} storeys. The model shows also good results in terms of accumulated loading steps for different values of acceleration (PGA). The composite structure shows a premature nonlinearity in the small level of strains. No considerable torsion effect for both one and two storeys frames. The pushover analysis shows that the signals of Haiti 100% and 200% and Guadalupe 100% stays in the linear range and no plasticity was occurred. Also the damage criteria was tested and the structure was safe for the 100% Haiti signal according to EC8, the 200%, 300% Haiti fails according to safety service criteria but not collapsed according to the resistance of the bottom connection which was the crucial element for the collapse requirements.

7. CONCLUSION AND RECOMMENDATIONS

The analysis and the behaviour of the traditional buildings of timber frame structures subjected to earthquake loading can be summarised and many conclusions could be observed and some suggestions for the next work in the future as:

7.1 Conclusions

1- A new nonlinear numerical FEM model was proposed for the analysis and design of the modified Kay frame structures which composed of main timber frame, the walls contain similarities unit cells with some specified dimensions and provided by two diagonal Saint's Andrew braces and connection system of steel plates with proper nails dimensions.
2- Many types of traditional buildings show a good performance against the seismic loadings due to some designed characteristics, and there are many of them distributed around the world which show a resistance to the seismic strong motion, this performance comes usually from the existing of the timber members which provides a flexibility to the integrated system and distribute the forces through the different elements safely.
3- The experimental works show the high efficiency of the vertical loads to increase the resistance of such structures.
4- There are many sources of the dissipated energy in the different types of traditional timber frames with infilling which are the main reason for the good performance of seismic resistance, which can be evaluated in terms of area enclosed by the force-displacement curve of the cyclic pseudo analysis, but the main sources of the modified Kay structure type which is used in our study are:

- The contact friction between the infilling and the surrounding timber members (main columns and beams and horizontal and inclined braces).
- Due to the weakness of the morter and the mechanical properties of the clay, cracks in the infilling materials are occurred due to the cohesion between the clay material and the adhesion between the rocks and surrounding morter. These two effects were simulated implicitly in the constitutive law of the two diagonal unit cell element which is used in the analysis of wall and building analysis.

- Slip off of the nails that connect the joints in the middle and top connections except that connects the foundation and at the floor level which connects (in the multi-storey buildings) posts et every two successive stories. This effect was neglected and modelled as a hinge connection.

- The friction between the infilling and the horizontal beam of the foundation (sill plate), this effect was taken into account by increasing the shear resistance as well as stiffness of the bottom connections (scale 1) by 10%.

- Big amount of energy dissipation occurs in the bottom and inter-storey connections, therefore, a nonlinear FE. model was implemented in this study by using experiments for the tangential shear and normal deformations which represents this force-slip relation and corresponding energy dissipation. This energy comes from pulling out the nails due to shear forces applied in the plane of the cross-section of the nails and also with a little effect of contact friction between the steel plate and both nails as well as timber member contact area.

So the nonlinearity is taking into account directly in the connections and indirectly in the two diagonal panel element. These FE. models are modeled according to Hysteretic constitutive law and verified with laboratory monotonic and cyclic tests for specified design of material and dimensions.
5- A multi step analysis technique was used to develpe a calibrated numerical model based on experimental results for each scale.
6- The simlified 3D-model of buildings of traditional timber masonry structures gives a good results as compared to the shaking table tests, This model comopund of bottom support nonlinear model, two nonlinear diagonal spring set model for infilling and braces, and main structure of linear Bernouli's 3D-beam and bar elements.
7- Pushover analysis was performed in addition to the dynamic analysis for the wall and one storey buildings.
8- The out of plane deformations in the parallel to loading directions was the source of damage in the one storey house according to the experements, this effects did not taking into account in this study because the objective of the study is to discover the effects of seismic loads to shear walls and due to lack of experements in this direction. So for practical purposes i propose to providing a plastic thin sheets to cover the walls to decrease the out of plain rocks separation.
9- Analytical computaion shows that there is no significant effect to torsion for both one and two storey buildings, this is due to the existing system of diaphragm of diagonal beams at each corner.
10- The behaviour of the structures is significantly depending of the behaviour on bottom connections, that is the modes of failur is mainly depend on the connections

and the relation-ships between the shear and normal resistance of the connections and according to these relation the mode of failures of the structures is controled and also the force resistance as well as ductility of the global system.

7.2 Recommendations for the future work

Of course no job without defects, so to continue in this field and collect more informations for the traditional buildings to implement the results to national codes of these type of buildings some of studies may be added to go in deep for the behaviour of these structures for the static and dynamic imposing loading including seismic loading:

7.2.1 Experimental recommendations

In addition to the previous experimental tests in the literature, there are some points does not studied or not studied briefly, so according to some difficulties in our work some experiments needs as:

1- Many small parts of rocks of infilling were droped in the normal to excitation plane throw the shaking table tests of one storey house model, which is the only remarkable damage in the test so a shaking table tests are required for the out of plane deformations with some parametric studies like covering by thin plastic sheets or any other restriction tools to decrese the out of plane droping parts.
2- As we mensioned above the shear tests of the connections and the resulted constitutive law (force-slip relation-ships) did not takes into account some of the physical phenomena as:

- The two braces members which were connected to the joints and participate to the resistance of some tangential horizontal force and re-distribute it to the other elements of the wall, this force could not be impelemented directly in the simple FE. model or at least the participation of the connection and the conjugate braces (in the case of middle posts only) can not be assured according to this simplification.

- Also the shear slip value will be decreases in the case of taking the braces into account.

- The existing of the infilling provides confinement and then decrease the slip value as well as increasing the shear force resistance and of cource the stiffness.

As a result it is very interested to repeat the shear test of the connection for the shear by taking into account the existance of braces as well as infilling.

3- The constitutive law for the middle and top joints (moment-rotation relashioships) can be tested to study the dissipated energy and the effect of end moments and angle of rotations at these joints.
4- Changing the aspect ratio of the plan of the speciment and two storey shaking table tests to check the torsional effects for non regular structures.
5- Changing the dimensions as well as the construction materials of the shear walls to develope a different constitutive laws for the behaviour of different cases.
6- We can repeat the previous tests on flexible base to taking into account the soil structure interaction.
7- The test of shear of connections can be used to measuring the the moment-rotation law for the bottom joints also (as in point 3 above) by measuring the arm of the moment from location of the tangential applied load to the center of ordered nails.

7.2.2 Numerical recommendations

1- To study the effect of out of plane in the normal to loading direction wall, a model of equivalent shear wall model is required or a local numerical study of the contact between rocks and morter or using contact friction model (may be based on mohr-columb model) to study the effect of friction between infilling and surrounding timber members.

2- Propose a general relation-ships for constant material but for different diamensions of the unit wall scale acording to the experements in the point (5) of previous section, (7.2.1), the only study in the literature of Kouris and Kappos, [93] and derive a mathematical rule(s) for the different materials and/or dimensions to verify the results of the authors.

3- The effects of soil structure interaction can be studied according to the tests in point (6) in the previous section.
4- Develope a new constitutive law for the moment-theta relation-ships for the moment DOF. (θ_x, θ_y, θ_z) according to availability of experimental data.
5- Adding another degrees of freedom e.g. transverse shear in the two orthogonal direction to axial (or/and) adding moment capability in one or more rotational DOF of the hysteresis spring (Hysteretic constitutive model). This modifications of adding more DOF could be derived from aditional experimental tests.

BIBLIOGRAPHY

[1] R. . Langenbach. Learning from the past to protect the future: Armature crosswalls. Journal of Engineering Structures, 30:2096–2100, 2008.

[2] E 2126. Standard Test Methods for Cyclic (Reversed) Load Test for Shear Resistance of Vertical Elements of the Lateral Force Resisting Systems for Buildings. International Organization for Standardization, 2009.

[3] FEMA Agenct. Prestandard and Commentary for the Seismic Rehabilitation of Buildings : FEMA-356. Fedral Emargency Manegement Agency, ASCE, 2000.

[4] N. Ahmad, Q. Ali, and M. Umar. Simplified engineering tools for seismic analysis and design of traditional dhajji-dewari structures. Bulletin of Earthquake Engineering, 10:1503–1534, 2012.

[5] N. Ahmed, Q. Ali, and Umar M. Seismic vulnerability assessment of multistory timber braced frame traditional masonry structures. Advanced materials research, 601:168–172, 2013.

[6] A. AKAN. Some observations on traditional on the seismic behaviour of traditional timber structures in turkey. Master's thesis, middle east technical university, 2004.

[7] A. H. Akhaveissy. Finite element nonlinear analysis of high-rise unreinforced masonry building. Latin American Journal of Solids and Structures, 9:547–567, 2012.

[8] Y. D. Aktas, U. Akyuz, A. Turer, B. Erdil, and N. S. Guchan. Seismic resistance evaluation of traditional ottoman timber-frame hımıs¸ houses: Frame loadings and material tests. Earthquake Spectra, 30, 4:1711–1732, 2014.

[9] Q. Ali, T. Schacher, Ashraf M., Alam B., Naeem A., N. Ahmad, and M. Umar. In-plane behavior of the dhajji-dewari structural system (wooden braced frame with masonry infill). Earthquake Spectra, 23 No. 3:835–858, 2012.

[10] R. J. Allemang and D. L. Brown. A complete review of the complex mode indicator function (cmif) with applications. In Structural Dynamics Research Laboratory, Mechanical, Industrial and Nuclear Engineering, University of Cincinnati, *http : //www.sdrl.uc.edu/sdrl/referenceinfo/documents/papers*, 2005.

[11] ATC-40. Seismic evaluation and retrofit of concrete buildings, Volume 1. Applied Technology Council, ATC-40, California seismic safety commission, November 1996.

[12] J. F. AUDEFROY. Haiti: post earthquakes lessons learned from traditional construction. ENVIRONMENT and URBANIZATION, International Institute for Environment and Development, 23, 2:447–462, 2011.

[13] A. Ayoub. Seismic analysis of wood building structures. Journal of Engineering Structures, 29:213–223, 2007.

[14] T. Baber and M. Noori. Random vibration of degrading, pinching systems. Journal of Engineering Mechanics, ASCE, 111, 8:1010–1026, August 1985.

[15] T. Balendra, S. Suyanthi, K. H. Tan, and A. Ahmed. Seismic capacity of typical high-rise buildings in singapore. THE STRUCTURAL DESIGN OF TALL AND SPECIAL BUILDINGS, 22:1404–1421, 2013.

[16] N. Barbacci, R. Langenbach, S. Kelley, P. Sparks, K. Rowell, M. Hammer, and O. J. Julien. The preservation of gingerbread style houses in Haiti. Rapport of Mission after the Earthquake of January 2010, WORLD MONUMENTS FUND, Repport in French, 2011.

[17] K. J. Bathe. Finite Element Procedures. Prentice Hall,Pearson Education, Inc., 2006.

[18] C. Boudaud. Analyse de la vulnérabilité sismique des structures à ossature en bois. Ph.d. thesis, Université Joseph Fourier, France (in french), 2012.

[19] C. Boudaud, L. Daudeville, J. Baroth, and S. Hameury. Multiscale modelling of timber frame structures under seismic loads. In XII International conference on computational plasticity, fundamentals and applications COMPLAS XII, pages 1–12, 2013.

[20] J. Branco, P. Cruz, M. Piazza, and H. Varum. Modelling of timber joints in traditional structures. In International Workshop on Earthquake Engineering on Timber Structures, volume 1, pages 1–15, 2006.

[21] J. BRANCO, P. CRUZ, M. PIAZZA, and H. VARUM. Modelling of timber joints in traditional structures. In International Workshop on (Earthquake Engineering on Timber Structures), Coimbra, Portugal, pages 1–15, November 2006.

[22] J. N. Brune. Tectonic stress and spectra of seismic shear waves from earthquakes. Journal of Geophysical research, 75-26:4997–5009, September 1970.

[23] BS. BS 5268-2 Structural use of timber, Part 2: Code of practice for permissible stress design, materials and workmanship. BSi, 2002.

[24] F. Carbajal, G. Ruiz, and Schexnayder C. J. Quincha construction in peru. Practice Periodical on Structural Design and Construction ASCE, 10(1):56–62, 2005.

[25] R. Cardoso, M. Lopes, and R. Bento. Seismic evaluation of old masonry buildings. In 12^{th} European Conference on Earthquake Engineering, volume 463, 2001.

[26] M. Causevic and S. Mitrovic. Comparison between non-linear dynamic and static seismic analysis of structures according to european and us provisions. Bull Earthquake Eng, springer press., pages –, July 2010.

[27] A. CECCOTTI, P. FACCIO, M. NART, SANDHAAS C., and P. SIMEONE. Seismic behaviour of historic timber frame buildings in the italian dolomites. In 15^{th} International symposium Istanbul and Rize (Turkey), pages 1–16, September 2006.

[28] A. CECCOTTI, P. FACCIO, M. NART, and P. SIMEONE. Seismic behaviour of wood framed buildings in cadore mountain region - italy. In 13^{th} World Conference on Earthquake Engineering, Vancouver, B.C., Canada, volume Paper No. 4011, 2004.

[29] A. Ceccotti and H. J. Karacabeyli. Validation of seismic design parameters for wood-frame shearwall system. Can. J. Civ. Eng., 29:484–498, 2002.

[30] A. Ceccotti and M. Nart. Seismic behaviour of historic wooden-frame buildings-drain 3d modeling with florence hysteresis model. In The $14^{th.}$ World Conference on Earthquake Engineering October, Beijing, China, 2008.

[31] A. Ceccotti and C. Sandhaas. A proposal for a standard procedure to establish the seismic behaviour factor q of timber buildings. In WCTE, world conference on timber engineering, 2010.

[32] A. Ceccotti, C. Sandhaas, and M. Yasumura. Seismic behaviour of multi-story cross-laminated timber buildings. In Proceedings of the International Convention of Society of Wood Science and Technology and United Nations Economic Commission for Europe – Timber Committee, Geneva, Switzerland, pages 1–14, October 2010.

[33] A. Ceccotti and A. Vignoli. A hysteretic behavioural model for semi rigid joints. Eurepean earthquake engineering., 1989.

[34] A. Chopra. Dynamics of Structures. Prentice-Hall International Series in Civil Engineering and Engineering Mechanics, 2007.

[35] A. K. Chopra and R. K. Goel. Evaluation of nsp to estimate seismic deformation: Sdf systems. JOURNAL OF STRUCTURAL ENGINEERING, ASCE, 126(4):482–490, APRIL 2000.

[36] A. K. Chopra and R. K. Goel. Capacity demand diagram methods based on inelastic design spectrum. Erthquake spectra, 15(4):56–62, November, 1999.

[37] I. P. Christovasilis and A. Filiatrault. Two-dimensional numerical framework for the nonlinear static and dynamic analysis of light-frame wood structures. In WCTE, world conference on timber engineering, 2010.

[38] Ying H. Chui, Chun. Ni, and L. Jiang. Finite element model for nailed wood joints under reversed cyclic load. Journal of Structural Engineering, ASCE, 124:96–103, January 1998.

[39] M. Collins, B. Kasal, P. Paevere, and G. Foliente. Three-dimensional model of light frame wood buildings i model description. JOURNAL OF STRUCTURAL ENGINEERING, ASCE, 2005.

[40] Applied Technology Council. IMPROVEMENT OF NONLINEAR STATIC SEISMIC ANALYSIS PROCEDURES. Federal Emergency Management Agency, FEMA-440, ATC-55 project, June 2005.

[41] C. Cuadra, T. Saito, and C. Zavala. Dynamic characteristics of traditional adobe quincha buildings in peru. In In Proceedings of the 15 th World Conference on Earthquake Engineering, Lisbon, Portugal, volume Paper No. 2653, 2012.

[42] F. Cuny. Improvement of rural housing in Haïti to withstand hurricanes. Intertect dallas., 1982.

[43] M. A. Dar and S. Ahmad. Traditional earthquake resistant systems of kashmir. International Journal of Civil and Structural Engineering Research, 2(2):86–92, 2015.

[44] L. Daudeville, L. Davenne, N. Richard, and N. Kawa. Etude du comportement parasismique de structures à ossature en bois. Revue française de génie civil, in french, 2(6):651–665, February 1998.

[45] D. D'Ayala and N. Quinn. In-plane experimental testing on historic quincha walls. In SAHC2014 – 9^{th} International Conference on Structural Analysis of Historical Constructions, Mexico City, Mexico, pages 1–12, 2014.

[46] H. Diskaya. Damage assessment of 19_{19} century traditional timber framed structures in istanbul. In From Material to Structure-Mechanical Behaviour and Failures of the Timber Structures, ICOMOS IWC-XVI International Symposium–Florence, Venice and Vicenza, 2007.

[47] M. Dogan. Seismic analysis of traditional buildings: Bagdadi and himis. The Open Construction and Building Technology Journal, 11:35–45, 2010.

[48] A. Dogangun, O. Iskender, R. Livaoglu, and R. Acar. Traditional wooden buildings and their damages during earthquakes in turkey. Journal of Engineering Failure Analysis, 13:981–996, 2006.

[49] J. Dolan. The dynamic response of timber shear walls. Phd. thesis, University of British Columbia, Vancouver, BC, Canada., 1989.

[50] J. D. Dolan and R. O. Foschi. Structural analysis model for static loads on timber shear walls. Journal of Structural Engineering, ASCE, 117:851–861, January 1998.

[51] M. Dorn, K. de Borst, and J Eberhardsteiner. Experiments on dowel-type timber connections. Journal of Engineering Structures, 47:67–80, 2013.

[52] J. C. Duccini. Essais sismiques de mur et maison à ossature bois pour Haiti Projet REPARH, Rapport d'essais, Projet REPARH, No. 403/13/604,. FCBA, Université Joseph Fourier, Report in French, 2013.

[53] B. DUJIC and R. ZARNIC. Method for modelling dynamic response of timber frame building. In Structural building components association, 2004.

[54] EU. Eurocode Commetee. Eurocode 5: Design of timber structures - Part 1-1: General-Common rules and rules for buildings, BS EN 1995-1-1:2004. European Committee for Standardization Provided by IHS under license with CEN, 2004.

[55] EU. Eurocode Commetee. Structural timber, Strength classes. EUROPEAN COMMITTEE FOR STANDARDIZATION COMITE EUROPÉEN DE NORMALISATION EUROPÄISCHES KOMITEE FÜR NORMUNG, December 2009.

[56] P. Fajfar. A nonlinear analysis method for performance based seismic design. Earthquake spectra, 16(3):573–592, August 2000.

[57] G. J. Ferreira, M. J. Teixeira, A. Dutu, F. A. Branco, and A. M. N. Goncalves. Experimental evaluation and numerical modelling of timber-framed walls. Experimental Techniques, Society for Experimental Mechanics, 38:1–9, July 2012.

[58] H. Filiatrault, A. Isoda and B. Folz. Hysteretic damping of wood framed buildings. Journal of Engineering Structures, 25:461–471, 2003.

[59] G. Foliente. Hysteresis modeling of wood joints and structural systems. Journal of Structural Engineering, 121:1013–1022, 1995.

[60] G. C. Foliente. Hysteresis modeling of wood joints and structural systems. Master's thesis, Virginea Polytechnic Institute and State University, 1993.

[61] G. C. Foliente. Stochastic Dynamic Response of Wood Structural System. Ph.d. thesis, Faculty of the Virginia Polytechnic Institute and State University, 1993.

[62] B. Folz and A. Filiatrault. Seismic analysis of woodframe structures. i: Model formulation. JOURNAL OF STRUCTURAL ENGINEERING, ASCE, 130:1353–1360, 2004.

[63] B. Folz and A. Filiatrault. Seismic analysis of woodframe structures. ii: Model implementation and verification. JOURNAL OF STRUCTURAL ENGINEERING, ASCE, 130:1361–1370, 2004.

[64] M. Fonseca. Reabilitacao de edificios pombalinos, analise experimental de paredes de frontal. Master's thesis, universidade tecnica de lisboa, in Portuguese, 2010.

[65] European Committee for Standardization. EN 1998-1 Eurocode 8: Design of structures for earthquake resistance Part 1: General rules seismic actions and rules for buildings. European Committee for Standardization, 2004.

[66] R. Foschi. Modeling the hysteretic response of mechanical connections for wood structures. In World Conference of Timber Engineering, Whistler, 2000.

[67] K. Gatto and C. M. Uang. Effects of loading protocol on the cyclic response of woodframe shearwalls. Journal of Structural Engineering, ASCE, 129:1384–1393, OCTOBER 2003.

[68] G. Gonzalez and J. Gutierrez. Structural performance of bamboo bahareque walls under cyclic load. J. Bamboo and Rattan, 4(4):353–368, 2005.

[69] S. Grange. Modélisation simplifiée 3D de l'interaction sol-structure : application au génie parasismique. Ph.d. thesis, Institut Polytechnique de Grenoble (in french), 2008.

[70] A. Gubana, A. Frangipane, and G. Tomasi. A simplified procedure for evaluation of traditional timber framehouse seismic response. In World Conference on Timber Engineering, WCTE Auckland New Zealand, session 27, 2012.

[71] P. Gulkan and R Langenbach. The earthquake resistance of traditional timber and masonry dwellings in turkey. In 13^{th} World Conference on Earthquake Engineering Vancouver, B.C., Canada, volume Paper No. 2294, 2004.

[72] J. Gutierrez. Structural Adequacy of Traditional Bamboo Housing in Latin America, National Laboratory for Materials and Structural Models. Civil Engineering Department, University of Costa Rica, TECHNICAL REPORT No.19, 2000.

[73] J. Gutierrez. Notes on the seismic adequacy of vernacular buildings. In 13^{th} World Conference on Earthquake Engineering Vancouver, B.C., Canada, volume Paper No. 5011, 2004.

[74] D. Habineza, M. Rakotondrabe, and L. G. Yann. Multivariable generalized bouc- modeling, identification and feedforward control and its application to multi-dof piezoelectric actuators. In Proceedings of the 19^{th} World Congress, The International Federation of Automatic Control Cape Town, South Africa., pages 10952–10958, August, 2014.

[75] T. H. Hanks and H. Kanamori. A moment magnitude scale. JOURNAL OF GEOPHYSICAL RESEARCH, 84-B5:2348–2350, 1979.

[76] Stephen H. Hartzell. Earthquakae aftershock as green's functions. Geophysical research letters, 5-1:1–4, 1978.

[77] G. He, L. Xie, X. Wang, J. Yi, L. Peng, Z. Chen, P. J. Gustafsson, and R. Crocetti. Shear behavior study on timber-concrete composite structures with bolts. BioResources, Timber-concrete structures, PEER-REVIEWED ARTICLE, 11-4:9205–9218, 2016.

[78] K. Hicyilmaz. Dhajji Dewari Affordable seismically resistant and sustainable housing. ARUP, 2011.

[79] K. Hicyilmaz, T. Wilock, C. Izatt, J. Da Silva, and R. Langenbach. Seismic performance of dhajji dewari. In WCEE, LISBOA, volume 15, 2012.

[80] Y. Hu, B. Davison, I. Burgess, and R. Plank. Multi-scale modelling of flexible end plate connections under fire condition. JOURNAL OF SCIENCE AND TECHNOLOGY Applied Sciences and Engineering, 4:88–101, 2010.

[81] T. J. R. Hughes. The Finite Element Method - Linear Static and Dynamic Finite Element Analysis. Prentice Hall, Englewood Cliffs, NJ, 1987.

[82] J. Humbert. Caracterisation du comportement des structures bois assemblages metalliques sous sollicitations sismiques. Ph.d. thesis, Université Joseph Fourier, France, 2010.

[83] J. Humbert, C. Boudaud, J. Baroth, S. Hameury, and L. Daudeville. Joints and wood shear walls modeling i : constitutive law, experimental tests and fe model under quasi-static loading. Engineering Structures, 65:52–61, 2014.

[84] T. Joffroy. Reconstruction Haiiti after Earthquake of January 2010. CRAterre-ENSAG, Repport in French, 2014.

[85] T. Joffroy. Re-constuire Haiti après le séisme de janvier 2010. CRAterre-ENSAG, November 2014.

[86] A. Jorissen and M. Fragiacomo. General notes on ductility in timber structures. Journal of Engineering Structures, 33:2987–2997, 2011.

[87] J. P. Judd. Analytical modeling of wood-frame shear walls and diaphragms. Master's thesis, Brigham Young University, 2005.

[88] A. J. Kappos, G. G. Penelis, and C. G. Drakopoulos. Evaluation of simplified models for lateral load analysis of unreinforced masonry buildings. Journal of Structural Engineering, ASCE, 128 (7):1–8, July 2002.

[89] E. Karacabeyli and A. Ceccotti. Quasi-static reversed-cyclic testing of nailed joints. In XIn Proceedings of the 29th CIB-W18 Meeting, Universität Karlsruhe, Karlsruhe, Germany, pages 29–7, 1996.

[90] C. Karakostas, V. Lekidis, T. Makarios, T. Salonikios, I. Sous, and M. Demosthenous. Seismic response of structures and infrastructure facilities during lefkada, greece earthquake of 14/8/2003. Journal of Engineering Structures, 27:213–227, 2005.

[91] E. KOPANOU and M. L. MORETTI. Earthquake resistant unreinforced masonry buildings. In Second European Conference on Earthquake Enineering and Seismology, Istanbul, pages 1–10, August 2014.

[92] L. A. S. Kouris and A. J. Kappos. Detailed and simplified nonlinear models for timber framed masonry structures. Journal of Cultural Heritage, 13:47–58, 2012.

[93] L. A. S. Kouris and A. J. Kappos. A practice oriented model for pushover analysis of a class of timber framed masonry buildings. Journal of engineering structures, 75:489–506, 2014.

[94] R. Langenbach. The earthquake resistant mud and brick architecture of kashmir (of taq and dhajji dwarii) adobe. In Proceedings, International Conference on Earthen Architecture, Las Cruces, New Mexico, Getty Conservation Institute, 1990.

[95] R. Langenbach. Preventing pancake collapses: Lessons from earthquake-resistant traditional construction for modern buildings of reinforced concrete. In International Disaster Reduction Conference (IDRC), Davos, Switzer land ICCROM: Integrating traditional knowledge systems and cultural heritage into risk management, volume 1, pages 1–44, 2005.

[96] R. Langenbach. From opus craticium to the chicago frame: earthquake resistant traditional construction. International Journal of Architectural Heritage, Taylor & Francis Group, LLC, 1:29–59, 2007.

[97] M. Li, F. Lam, R. O. Foschi, S. Nakajima, and T. Nakagawa. Seismic performance of post and beam timber buildings i: model development and verification. Journal of Wood Science, 58:20–30, 2012.

[98] M. Lopez, J. Bommer, and P. Mendez. The seismic performance of bahareque dwellings in el salvador. In 13^{th} World Conference on Earthquake Engineering Vancouver, B.C., Canada, volume Paper No. 2646, 2004.

[99] G. Magenes and G. M. Calvi. In-plane seismic response of brick masonry walls. EARTHQUAKE ENGINEERING AND STRUCTURAL DYNAMICS, John Wiley & Sons, Ltd., 26:1091–1112, 1997.

[100] G. Magenes and D. Fontana. Simplified non-linear seismic analysis of masonry buildings. In In Proceedings of the fifth International Masonry conference, London, volume Proceedings 8, pages 190–195, 1998.

[101] T. Makarios and M. Demosthenous. Seismic response of traditional buildings of lefkas island, greece. JOURNAL OF ENGINEERING STRUCTURES, 28:264–278, 2006.

[102] H. Meireles, R. Bento, S. Cattari, and S. Lagomarsino. A hysteretic model for frontal walls in pombalino buildings. Bulletin of Earthquake Engineering, 10(5), 2012.

[103] H. Meireles, R. Bento, S. Cattari, and S. Lagomarsino. Seismic assessment and retrofitting of pombalino buildings by fragility curves. 15 WCEE LISBOA 2012, pages 1–10, 2012.

[104] H. A. Meireles, R. Bento, S. Cattari, and S. Lagomarsino. Formulation and validation of a macro element for the equivalent frame modelling of internal walls in pombalino buildings. In 15 WCEE LISBOA 2012, 2012.

[105] W. Munoz, M. Mohammad, A. Salenikovich, and P. Quenneville. DETERMINATION OF YIELD POINT AND DUCTILITY OF TIMBER ASSEMBLIES. IN SEARCH FOR A HARMONISED APPROACH, engineered wood products association, 2008.

[106] Phillip J. Paevere, Greg C. Foliente, and Bo Kasal. Load sharing and redistribution in a one story woodframe building. Journal of Structural Engineering ASCE, 129:1275–1284, 2003.

[107] W. Pang and D. Rosowsky. Beam-spring model for timber diaphragm and shear walls. Structures and Buildings, 163(SB4):227–244, 2010.

[108] W. Pang, D. Rosowsky, S. Pei, and W. Van de Lindt. Evolutionary parameter hysteretic model for wood shear walls. JOURNAL OF STRUCTURAL ENGINEERING, ASCE, 2007.

[109] P. Paultre. Dynamics of Structures Theory and applications to earthquake engineering. John Wiley and Sons, Inc., 2011.

[110] M. Paz and W. Leigh. INTEGRATED MATRIX ANALYSIS OF STRUCTURES Theory and Computation. KLUWER ACADEMIC PUBLISHERS, 2001.

[111] E. Poletti and G Vasconcelos. Seismic behaviour of traditional halftimbered wall: cyclic tests and strengthening solutions. Journal of Heritage Conservation, 129:1275–1284, SEPTEMBER 2003.

[112] H Prautzsch, W. Boehm, and M. Paluszny. Bézier and B-Spline Techniques. Springer-Verlag Berlin Heidelberg GmbH, Mathematics and Visualization, 2002.

[113] C. Qing, Y. Zhi, and P. J. Wu. Experimental study on seismic characteristics of typical mortise and tenon joints of chinese southern traditional timber frame buildings. Science China Technological Sciences, 54(9):2404–2411, 2011.

[114] L. F Ramos and P. B. Lourenco. Modeling and vulnerability of historical city centers in seismic areas: a case study in lisbon. Journal of Engineering Structures, 26:1295–1310, 2004.

[115] K. H. Reineck. Examples for the Design of Structural Concrete with Strut and Tie Model. International SP.208, ACI-ASCE, 2002.

[116] N. Richard. Approche multi-échelles pour la modélisation des structures en bois sous sollicitations sismiques. Ph.d. thesis, L'ECOLE NORMALE SUPERIEURE DE CACHAN (in french), 2001.

[117] N. Richard, L. Daudeville, Prion H., and F. Lam. Timber shear walls with large openings: Experimental and numerical prediction of the structural behaviour. Can. J. Civ. Eng., 29:713–724, 2002.

[118] N. Richard, M. Yasumura, and L. Davenne. Prediction of siesmic behaviour of wood framed shear walls with openings by pseudodynamic test and fe model. The Japan Wood Research Society, 49:145–151, 2003.

[119] C. Rossi and F. Russo. Ancient Engineers Inventions, Precursors of the Present. History of Mechanism and Machine Science, Volume 33, Springer, 2^{nd} edition, 2017.

[120] G. Salerno, F. Geremia, E. Pagano, M. Zampilli, N. Ruggieri, and S. Stellacci. The Masonry Timber Framed Load Bearing Structure of "Baraccato" System: A Numerical Model. Historical Earthquake-Resistant Timber Framing in the Mediterranean Area, Lecture Notes in Civil Engineering, HEaRT, Vol.(1), (205-213), Springer, 2015.

[121] C. K. Sansorny, F. Courboulex, M. Bour, and N. Deschamps. A two-stage method for ground-motion simulation using stochastic summation of small earthquakes. Bulletin of the Seismological Society of America, 95-4:1387–1400, 2005.

[122] P. Schadle and A. Blab. Earthquake behaviour of modern timber construction systems. In WCTE, world conference on timber engineering, 2010.

[123] M. D. Shah, A. N. Desai, and S. B. Patel. Performance based analysis of r.c.c. frames. In National Conference on Recent Trends in Engineering and Technology, May, 2011.

[124] V .R. Shah and R. Tayyibji. The kashmir house its seismic adequacy and the question of social sustainability. In The $14^{th.}$ World Conference on Earthquake Engineering October, Beijing, China, 2008.

[125] Mir Z. Shams. Multi scale modeling of particle reinforced concrete throw finite element analysis. Master's thesis, University of Wisconsin Milwaukee, 2016.

[126] Y. Sieffert, F. Vieux-Champagne, S. Grange, P. Garnier, J. C. Duccini, and L. Daudeville. Full-field measurement with a digital image correlation analysis of a shake table test on a timber-framed structure filled with stones and earth. Journal of Engineering Structures, 123:451–472, 2016.

[127] W. Stewart. The seismic design of plywood sheathed shear walls. Ph.d. thesis, University of Canterbury., 1987.

[128] T. Takeda, M. A. Sozen, and N. N. Neilson. Reinforced concrete response to simulated earthquakes. OHBAYASHI-GUMI Technical Research Report No.5, 1971.

[129] E. T. Theohari and H. Mouzakis. A post-byzantine mansion in athens. the restoration project of the timber structural elements. In World Conference of Timber Engineering, WCTE, 2010.

[130] S. Tobriner. Wooden architecture and Eathquakes in Istanbul, A reconnaissance report and commentary of the performance of wooden structures in the Turkey eartquakes of 17 August and 12 november 1999. United Nations Center For Regional Development, 2000.

[131] R. Tomasi and T. Sartori. Mechanical behaviour of connections between wood framed shear walls and foundations under monotonic and cyclic load. Journal of Construction and Building Materials, 44:682–690, 2013.

[132] UBC. Uniform Building Code. International Conference of Building Officials, 1997.

[133] J. W. Van de Lindt, S. Pei, H. Liu, and A. Filiatrault. Three-dimensional seismic response of a full-scale light-frame wood building: Numerical study. JOURNAL OF STRUCTURAL ENGINEERING, ASCE, pages 56–65, JANUARY 2010.

[134] G. Vasconcelos, E. Poletti, E. Salavessa, A. Jesus, P. Lourenço, and P. Pilaon. In-plane shear behaviour of traditional timber walls. Engineering Structures, 56:1028–1048, 2013.

[135] F. Vieux-Champagne. Analyse de la vulnérabilité sismique des structures à ossature en bois avec remplissage. Ph.d. thesis, Université Joseph Fourier, France (in french), 2014.

[136] F. Vieux-Champagne, S. Grange, Y. Sieffert, L. Daudeville, A. Ceccotti, and A. Polastri. Experimental analysis of seismic resistance of shear wall in traditional haitian houses. In 15 WCEE, LISBOA, volume 15, 2012.

[137] F. Vieux-Champagne, S. Grange, Y. Sieffert, P. Garcia, C. Faye, J. Duccini, and L. Daudeville. Numerical analysis of timber frame structures with infill under seismic loading. Not puplished paper.

[138] F. Vieux-Champagne, Y. Sieffert, S. Grange, C. N. Belinga, E. Bertrand, J. C. Duccini, C. Faye, and L. Daudeville. Experimental analysis of a shake table test of timber-framed structures with stone and earth infill. Earthquake Spectra, Earthquake Engineering Research Institute, 33-3:1075–1100, August 2017.

[139] F. Vieux-Champagne, Y. Sieffert, S. Grange, A. Polastri, A. Ceccotti, and L. Daudeville. Multi scale snalysis of timber-framed structures filled with earth and stones. In XII International conference on computational plasticity, fundamentals and applications COMPLAS XII, pages 431–440, 2013.

[140] F. Vieux-Champagne, Y. Sieffert, S. Grange, A. Polastri, A. Ceccotti, and L. Daudeville. Experimental analysis of seismic resistance of timber-framed structures with stones and earth fill. Engineering Structures, 69:102–115, 2014.

[141] E. Vintzileou and P. Touliatos. Seismic behaviour of the historical structural system of the island of lefkada, greece. Structural Studies, Repairs and Maintenance of Heritage Architecture IX , WIT Transactions on The Built Environment, WIT Press, 83:291–300, 2005.

[142] M. W. White and J. D. Dolan. Nonlinear shear wall analysis. Journal of Structural Engineering, ASCE, 21 (11):1629–1635, November 1995.

[143] J. Xu and D. Dolan. Development of a wood-frame shear wall model in abaqus. JOURNAL OF STRUCTURAL ENGINEERING, ASCE, 135:977–984, 2009.

[144] J. Xu and D. Dolan. Development of nailed wood joint element in abaqus. JOURNAL OF STRUCTURAL ENGINEERING, ASCE, 135:968–976, 2009.

[145] N. Yamaguchi, E. Karacabeyli, C. Minowa, N. Kawai, K. Watanabe, and I. Nakamura. Seismic performance of nailed wood-frame shear walls. In World Conference on Timber Engineering, Whistler Resort, British Columbia, Canada, 2000.

[146] M. Yasumura, T. Kamada, Y. Imura, M. Uesugi, and L. Daudeville. Pseudodynamic tests and earthquake response analysis of timber structures ii: two-level conventional wooden structures with plywood sheathed shear walls. The Japan Wood Research Society, 52:69–74, 2006.

[147] M. Yasumura and S. Yasui. Pseudodynamic tests and earthquake response analysis of timber structures i: plywood-sheathed conventional wooden walls with opening. The Japan Wood Research Society, 52:63–68, 2006.

[148] R. R. Youngs, S. J. Chiou, W. J. Silva, and J. R. Humphrey. Strong round motion attenuation relationships for subduction zone earthquakes. Seismological research letters, 68-1:58–73, 1997.

[149] Z. Yue. A study on traditional chinese wood joint differences as a supplement for wood structure code. In SHATIS'11 International Conference on Structural Health Assessment of Timber Structures-Lisbon, Portugal, June 2011.

Appendices

Appendix A

HYSTERESIS LAWS

There are many laws of hysterical behaviour used in the literature. Each one of them are already discussed in Chapter 3 section (3.4.1).

1. Foschi model (2000):

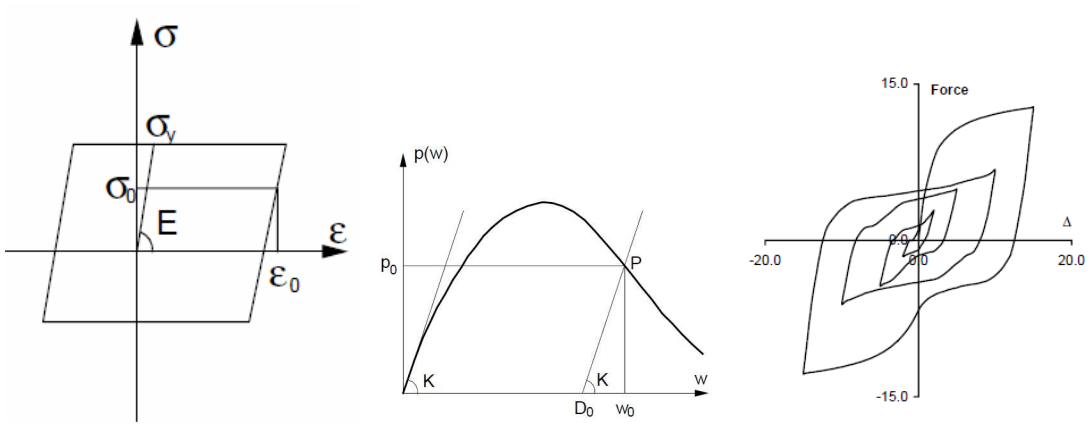

a) Elasto-plastic for steel nails. b) Constitutive law for timber. c) Resulted hsteresis.

Fig. A.1: Foschi hysteresis model.

2. Ayoub model (2007):

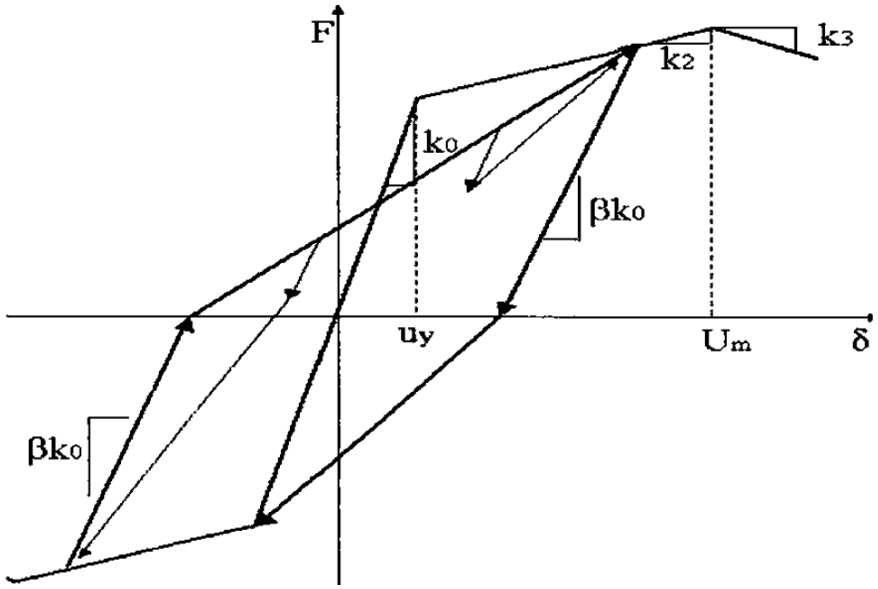

Fig. A.2: Clouph model.

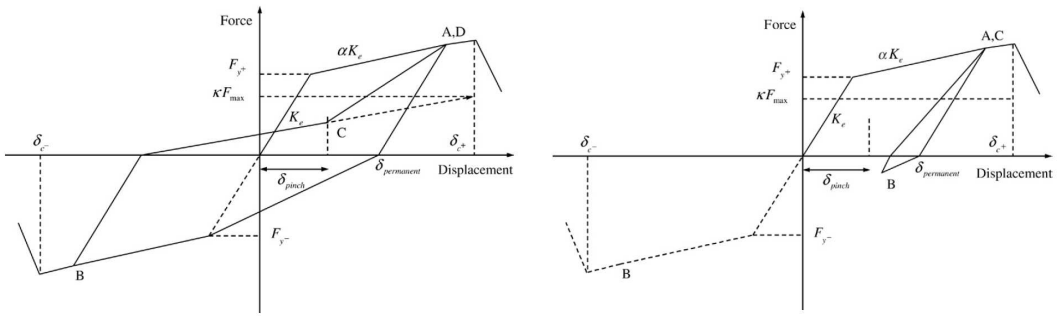

a)Full cycle. b) Part of the cycle.

Fig. A.3: Modified Clouph model.

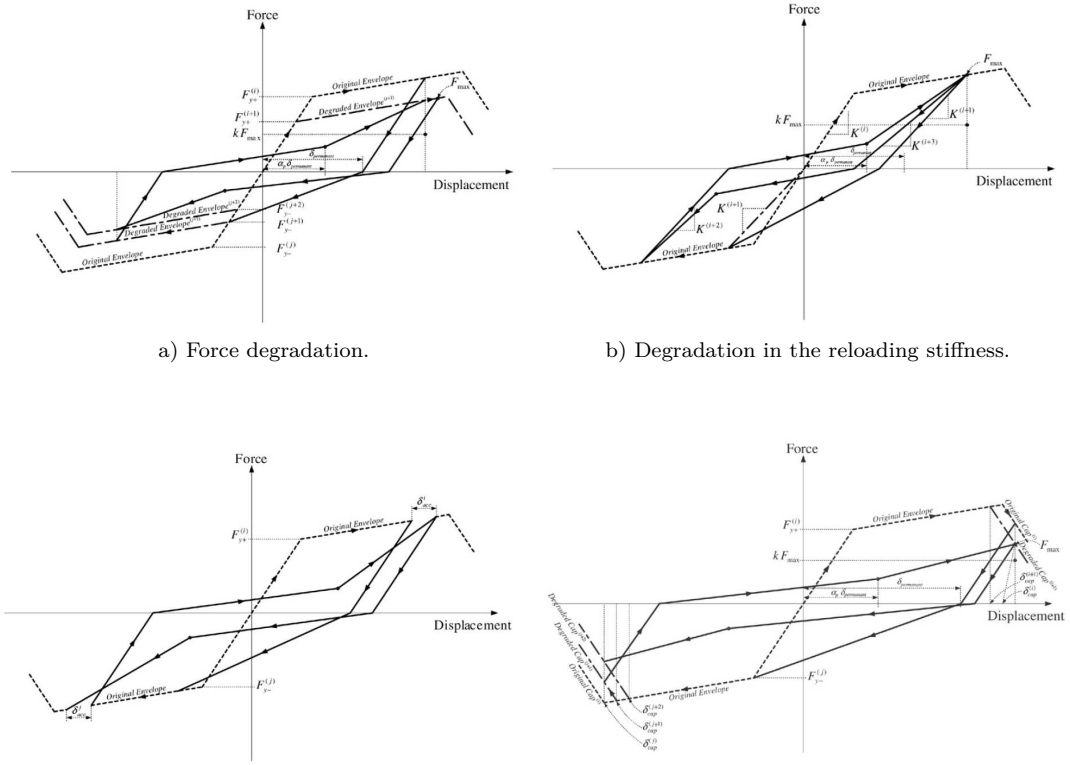

a) Force degradation.

b) Degradation in the reloading stiffness.

c) Degradation in the loading stiffness.

d) Cap degradation.

Fig. A.4: Ayoub hysteresis model.

3. Evolutionary Parameter Hysteretic Model (EPHM) (2007):

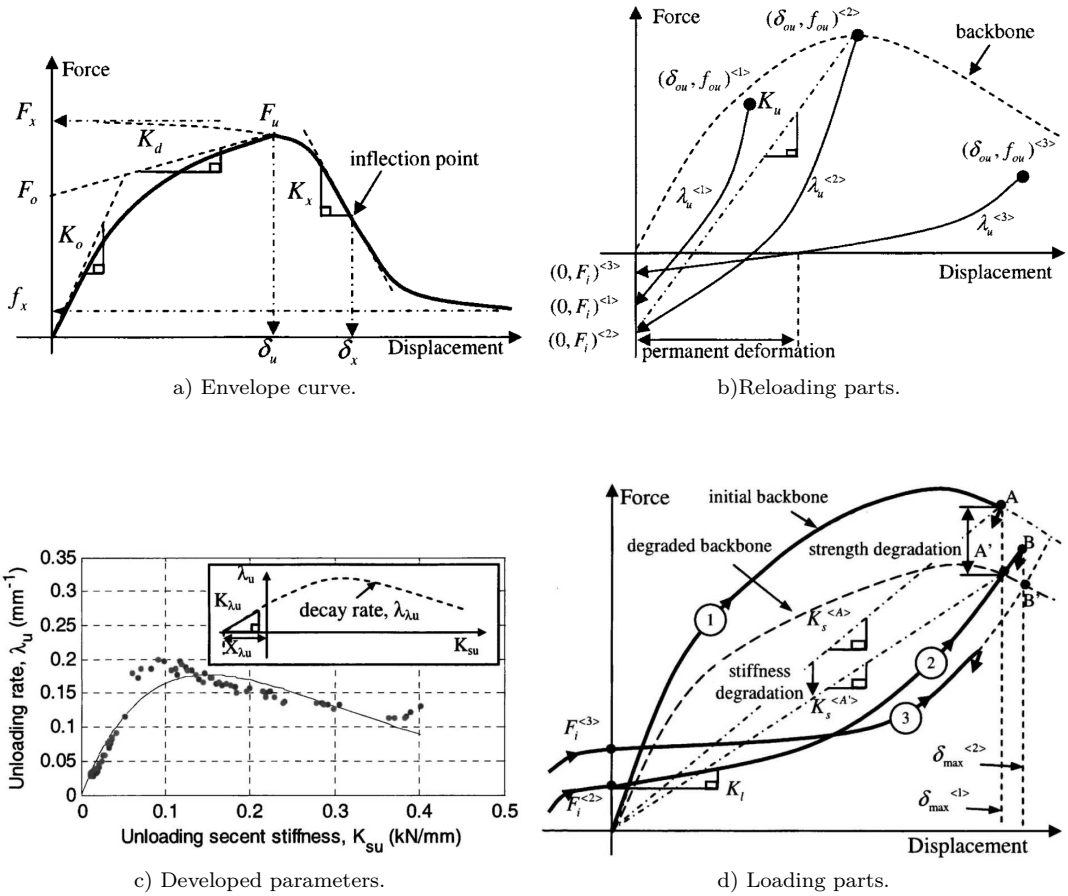

a) Envelope curve. b)Reloading parts.

c) Developed parameters. d) Loading parts.

Fig. A.5: EPHM model.

4. Q-Hyst model (1979):

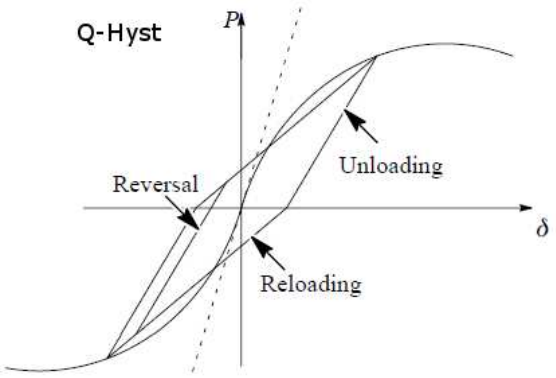

Fig. A.6: Q-Hysteresis model.

5. Stewart model (1987):

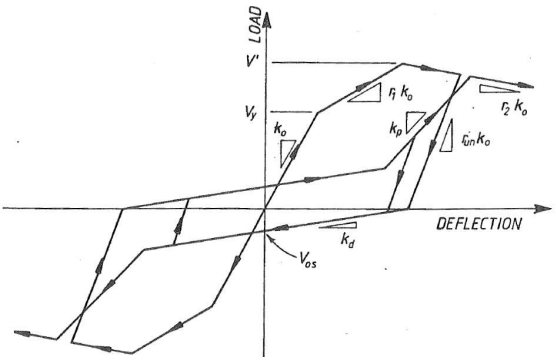

Fig. A.7: Stewart hysteresis model.

6. Q-Pinch (2005):

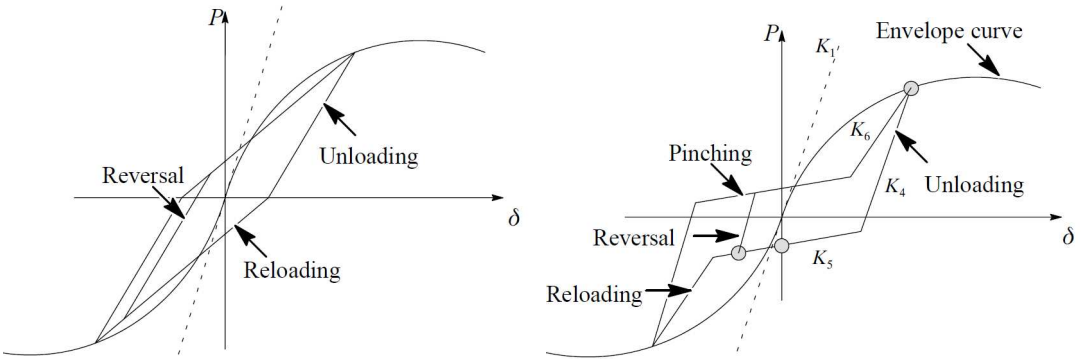

a) Small amplitude hysteresis. b) Large amplitude hysteresis.

Fig. A.8: Q-Pinch hysteresis model

7. Ceccotti (1989):

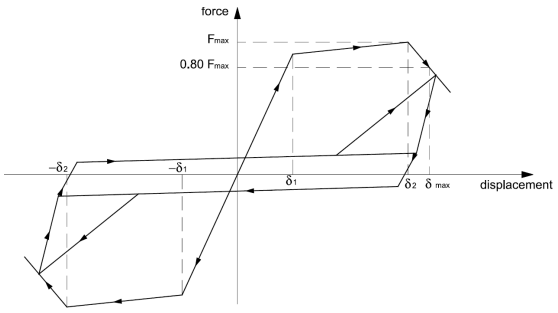

Fig. A.9: Ceccotti model.

8. Collins (2005):

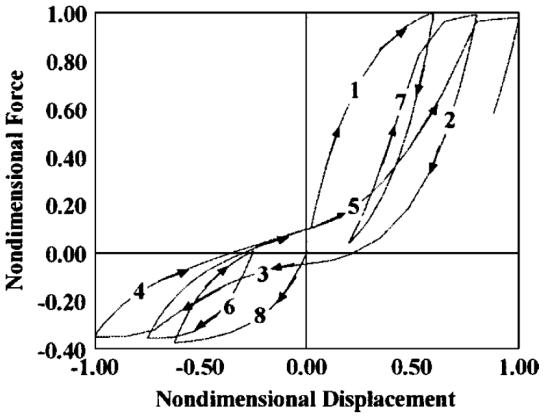

Fig. A.10: Collins model.

9. Dolan model (1991):

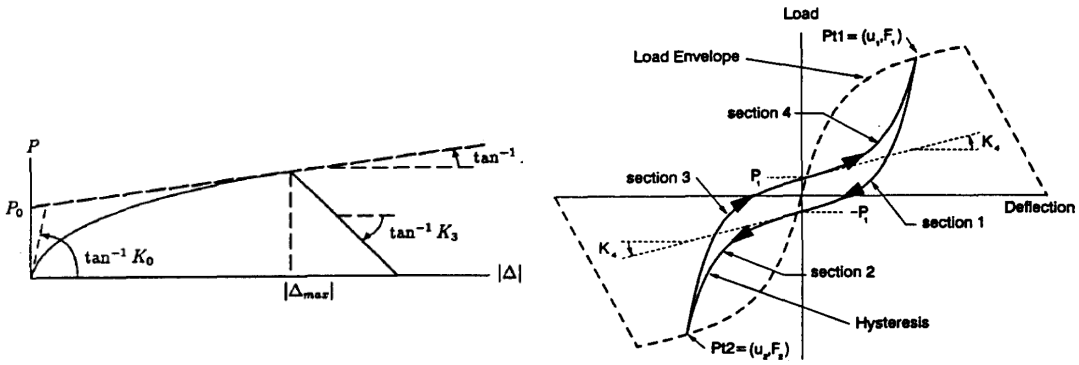

a) Monotonic curve. b) Cyclic curve.

Fig. A.11: Dolan model.

10. Folz model (2001):

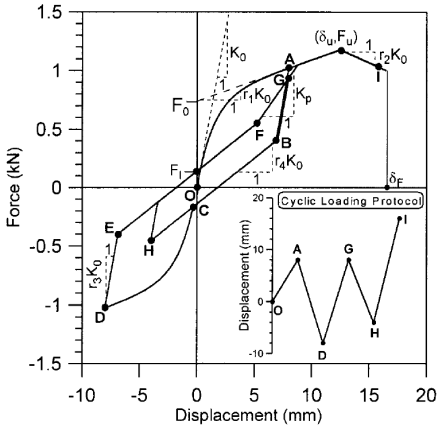

Fig. A.12: Folz model.

11. Humbert (2010):

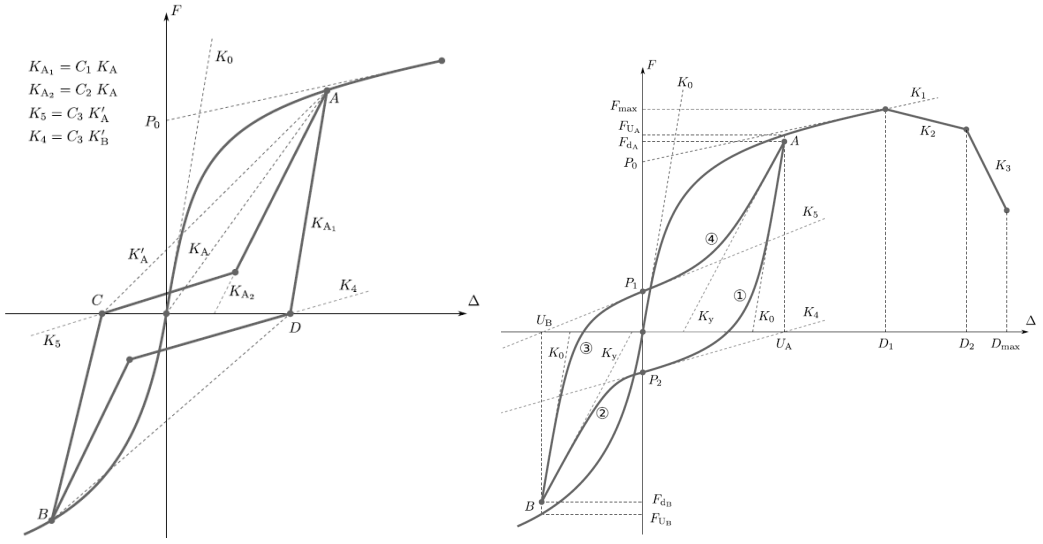

a) Yasumura hysteresis model. b) Richard hysteresis model.

Fig. A.13: Original versions of Humbert hysteresis model.

12. Bouc Wen Baber Noori (BWBN)(1985):

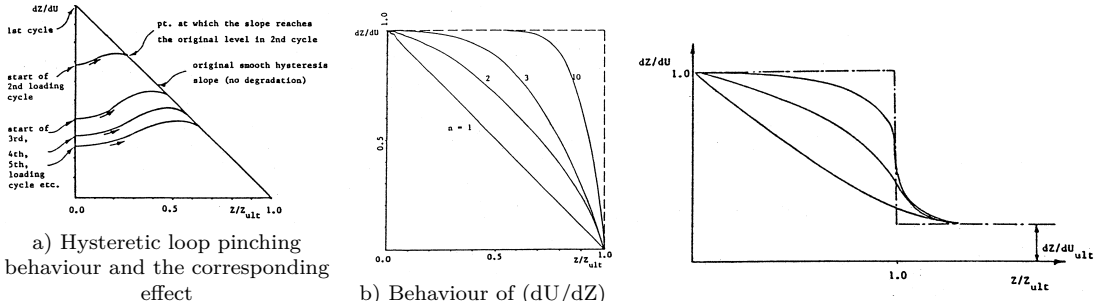

a) Hysteretic loop pinching behaviour and the corresponding effect on the variation of (dU/dZ) versus Z.

b) Behaviour of (dU/dZ) versus Z for smooth hsteresis model.

c) Cyclic dependent postyield restoring force.

Fig. A.14: Some BWBN parameters, Baber and Noori, [14].

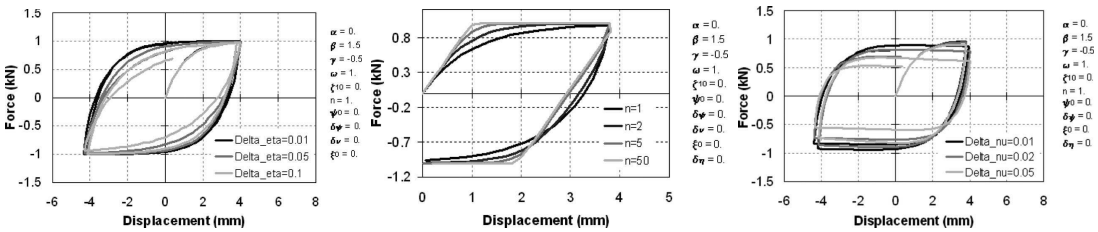

a) Effect of (δ_n) on the shape of hysteresis.

b) Effect of (n) on the shape of hysteresis.

c) Effect of (δ_v) on the shape of hysteresis.

Fig. A.15: Some modification on BWBN parameters by Xu and Dolan, [144] for timber applications.

Appendix B

BÉZIER CURVES

Bézier polynomials are parametric curves originaly developed by the French engineer Pierre Béezier for use in computer-aided design (CAD) in the automotive industry. They were developed in order to defne smooth curves, i.e. displaying natural-looking rounded shapes. This abstract property made them fairly popular from a visual point of view, most notably for use in CAD and vector graphics. However, they hold also many other advantages. Bézier curves are defined in the 2D space using a set of points called the control points of the curve. By manipulating these control points one can change not only the starting and ending points of the curve, but also its visual smoothness, which is defined mathematically as its curvature. The higher curvature, the sharper the curve will appear, meaning its curve will look making (sharp turns) like a curved road usually does. The points of a Bézier curve are defined as barycenter[1] of the control points. As a result the curve holds the major benefit to be invariant under anffine transformations such as translations, rotations and scaling. Indeed affine transformations preserve barycenters. Thus transformation of the curve simply resumed to a transformation of its control points, making Bézier curve rather simple to use from a theoretical point of view too.

B.1 Definition

Formally a Bézier polynomial is a parametric curve B(t) of the parameter ($t \epsilon R$) defined by its degree n and a set of (n + 1) control points $P_0, ..., P_n$. The definition is given by Equation (B.1) using binomial coefficients. Because B(0) = P_0 and B(1) = P_n the curve runs through the first and last control points, so-called endpoints. Intermediate control points $P_0, ..., P_{n-1}$ however are usually not part of the curve itself; instead they control the curvature. This actual property often leads one to restrict its defintion of the curve to the interval [0;1]. The associated arc of curve is thus bound by P_0 (t = 0), and P_n (t = 1), respectively denoted as the (**starting**

[1] In geometry the term "barycenter" is a synonym for (centroid), in astrophysics and astronomy, barycenter is the center of mass of two or more bodies which are orbiting each other.

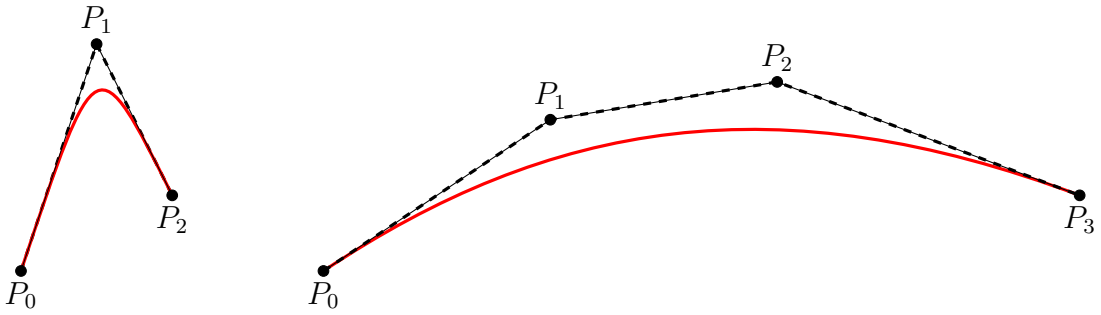

Fig. B.1: Two examples of Bézier polynomial curves with associated control points P_i. Left : second-order polynomial, right: third-order polynomial.

point) and the **ending point**. A common disadvantage of language however references this arc as the full Bzéier curve. Since most properties are only relevant on the [0;1] interval, we will comply with this common abuse of language. Except where stated otherwise, the term Bézier curve thus references in the following the arc of curve defined for t ϵ [0;1].

$$\forall \epsilon R \qquad B(t) = \sum_{i=0}^{n} \binom{n}{i} t^i (1-t)^{n-i} P_i \qquad where \qquad \binom{n}{i} = \frac{n!}{(n-i)!.i!} \quad \text{(B.1)}$$

B.1.1 Properties of Bézier curves

1. **Property 1** Endpoint interpolation property
   The curve begins at P_0 and ends at P_n.

2. **Property 2** Collinearity property
   The curve is a straight line if and only if all the control points are collinear.

3. **Property 3** Convex hull property
   The curve lies within the convex hull of the control points, so-called the Bézier polygon.

4. **Property 4** Upcasting property
   Every degree n Bézier curve is also a degree m curve for any m > n.

5. **Property 5** Endpoint tangents property
   The start (end) of the curve is tangent to the first (last) section of the Bézier polygon.

Several definitions and properties are introduced here. First we recall the previously stated (Property 1) so-called endpoint interpolation property, which derives directly from the formal definition. In a same way since the curve is defined a barycenters of the control points we can easily deduce the collinearity property (Property 2). Then we define the Bézier polygon as the convex hull of the control points $P_0, ..., P_n$. This polygon is used to define the convex hull property (Property 3), again deriving directly from the barycentric definition. The upcasting property states that every Bzéier curve is also a Bézier curve of higher degree. The recursive demonstration is straightforward using the formal definition. Finally the endpoint tangents property simply states that endpoint tangents are equal to the $[P_0, P_1]$ and $[P_{n-1}, P_n]$ segments. These properties are referenced in the following to address critical issues in using Bézier curves to define our behavior law.

B.2 Application of Bézier curves in the constitutive laws

We now want to use a Bézier curve to define a smooth curve representing a branch of our behavior law. Since we use generalized coordinates, this branch is defined in the displacement-force axes. Let S = (d_S, F_S) and E = (d_E, F_E) be respectively the starting and ending control points, with respective slope tangents K_S and K_E (Figure B.2). The endpoints define in these axes a bounding box delimited by their coordinates. Intuitively we would like to define the curve from S to E as either a straight line, a convexe parabolic-like function or as represented as concave parabolic-like function. Finally for convenience the curve should lie within the bounding box. This last objective is easily achieved using the convex hull property (Property 3) provided that the control points themself lie within the bounding box. In order to choose the appropriate degree n for the curve, we look at boundary conditions. The intuitive solution is to use a third degree Bézier curve with four control points: two endpoints and two intermediate control points defining the direction of the endpoint tangents. In our problem, this polynomial curve describes the relation between the displacement and the force. When implementing a behavior law into a

nite element code one should write a procedure to determine at a given timestep i the force Fi = F(di) given a displacement di predicted from the Newton algorithm or equivalent methods. As a consequence, a parametric curve B(t) = (d(t), F(t)) can not be used directly. Instead given a displacement di one should first determine the associated parameter t_i by solving the equation d(t_i) = d_i, then compute the associated force F_i = F(t_i). Choosing a 3^{rd} degree Bézier curve thus implies finding the roots of the 3^{rd} degree polynomial Q(t) = d(t) - d_i, which is not an easy task. For this reason we would like to simplify this problem by lowering the degree of

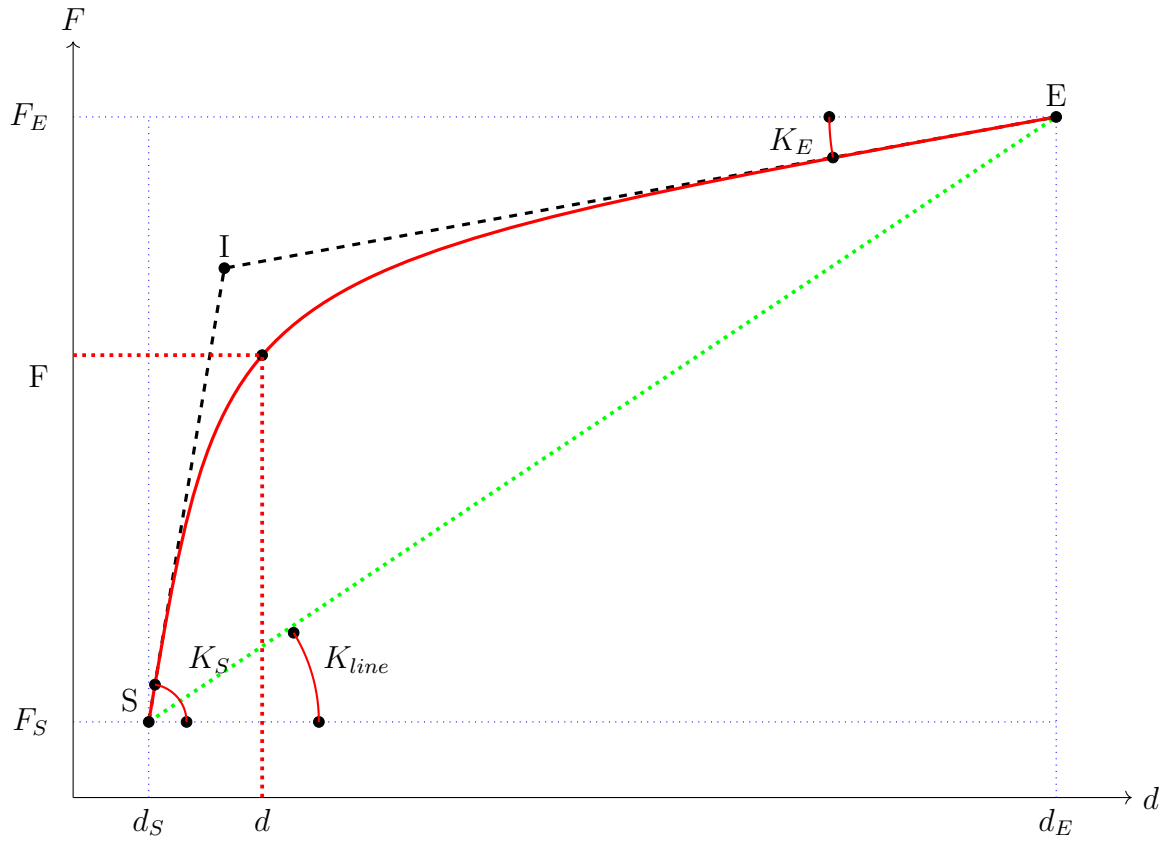

Fig. B.2: Use of a 2^{nd} degree of Bézier curve to define the evolution of the force F function in terms of the displacement d between a starting point S and an ending point E.

the curve. Moreover since we do not only want straight lines the degree n must be at least 2. In the end we would like to investigate the n = 2 possibility. This solution would be convenient because the associated root-finding operation resume to computing the discriminant of a quadratic equation.

$$B(t) = (1-t)^2.P_0 + 2.t.(1-t)P_1 + t^2.P_2 \tag{B.2}$$

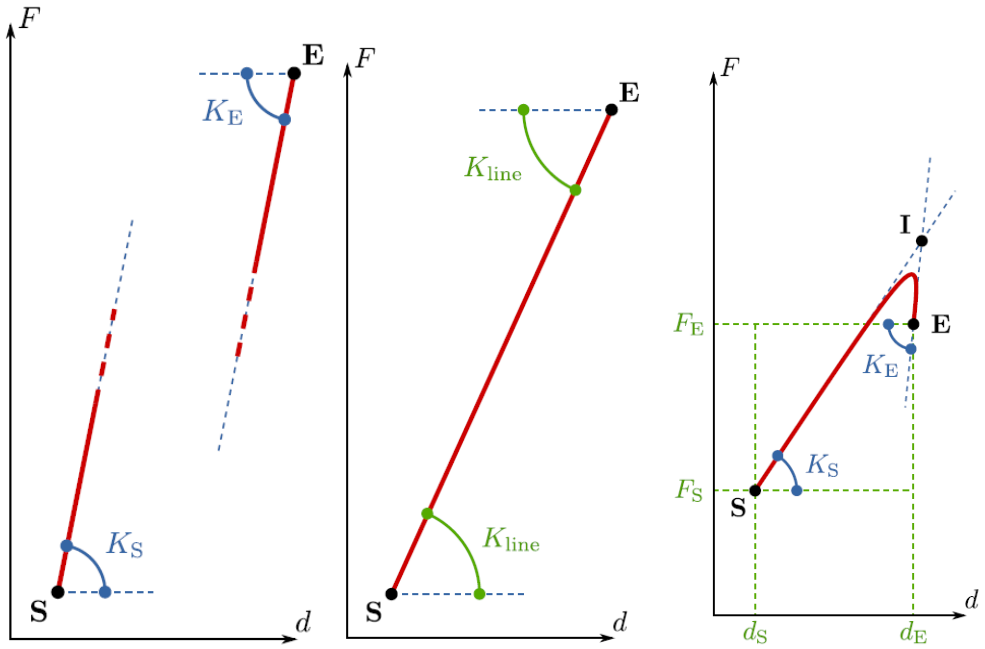

a) Parallel endpoint tangents. No intersection to define I.

b) Straight line joining endpoints.

c) Intermediate control point I outside of the bounding box.

Fig. B.3: Degenerate cases occuring when using a 2^{nd} degree of Bézier curve to define the evolution of the force F function of the displacement d., [82]

Let us have a look at a 2^{nd} degree of Bézier curve. The formal definition given in Equation ((B.1)) is simplified into Equation ((B.2)). From the endpoint tangents property (Property 5) we can state that this curve is tangent to both the $[P_0,P_1]$ and $[P_1,P_2]$ line segments. Now with an inverse reasoning given two endpoints and their associated tangents the position of P_1 is uniquely defined, provided that these tangents have an intersection. In fact if the endpoint tangents are parallel, one can show that the 2^{nd} degree of Bézier polynomial cannot be used. The other degenerated case where the tangents merge corresponds to the straight line case. First we can immediately deal with this simple case. Indeed a straight line is 1^{st} degree of Bézier and, thanks to the upcasting property (Property 4) is also an order of n^{th} degree of Bézier curve for any n > 1. The collinearity property (Property 4) thus implies that this line can be defined as any n^{th} order of Bézier (n > 1) having all its intermediate control points on the [S, E] segment. Associated values for the endpoint slopes are thus limited to the single value K_{line} (Equation (B.3)). Then we look at the cases where the curve is not a straight line. This implies that the order n of the curve is at least equal to 2. Thus there is at least

one intermediate control point I (Figure B.2). Since this control point can not be on the [S,E] segment, otherwise the curve is a straight line, it falls down to be either above or below, while being constrained to lie into the bounding box.

$$\kappa_1 = K_{line} \times K_{line} \tag{B.3}$$

$$\kappa_2 = [K_{line}, +\infty] \times [0, K_{line}] \tag{B.4}$$

$$\kappa_3 = [0, K_{line}] \times [K_{line}, +\infty] \tag{B.5}$$

$$(K_S, K_E) \in \kappa_1 \cup \kappa_2 \cup \kappa_3 \tag{B.6}$$

Figure (B.2) shows the case where point I is above the segment. Associated values for the slopes are defined by Equation (B.(B.4)). The symetrical case where it is under the segment corresponds to Equation (B.(B.5)). In the end the (KS;KE) couple must be in one of those sets, as stated by Equation (B.(B.6)).

Figure (B.3) presents some cases avoided by use of the previous restrictions: parallel tangents without intersection (Figure B.3-a), meeting tangents with an infinity of intersections (Figure B.3-b), and slopes on the same side as the linear limit Kline pushing the intersection point I outside of the bounding box (Figure B.3-c). While case (b) can be dealt with in a simple way, other cases must be avoided because of their complexity (case (c)) or even total impossibility to define the curve (case (a)). For complex cases, we prefer dividing the problem into smaller problems and define simpler curves complying with the previous de

nition. As a consequence, we demonstrated that a 2^{nd} Bézier curve can be used to define a branch of a force/displacement behavior law, provided that the slopes of the endpoint tangents remain in some limits specified by Equation (B.B.6). Although Bézier polynomials could be enough for our application, by lowering the degree to n = 2, we lost the ability to control the shape of the curve. Thus we decided to use a generalized version called rational Bézier curves. This choice was motivated by the possibility to control quite precisely the curvature of the function without changing the control points and thus the endpoint tangents. Rational Bézier curves are formed by associating a weight ω_i to each control point P_i. This weight has no significance by itself but instead should be viewed as the relative importance of the control point it is associated to with reference to

the other control points. Hence multipliying all weights by a fixed quantity does not change a rational Bézier curve. This property appears when looking at the formal definition of a second order rational Bézier curve (Equation ((B.7))), where the denominator aims at normalizing the expression. One should note that this definition does not constrain the value of ω_i. In fact the curve is defined for $\omega_i \in \mathbb{R}$. However for negative values the convex hull property (Property 3) is not verified. As a consequence we restrict the values of the weights to the [0, +1] interval.

The weights can be adjusted to fit a particular shape without changing neither the starting and ending points nor their tangents. The result of changing only the weight $\omega_1 = \omega_I$ of the intermediate control point $P_1 = I =$ of a degree-2 2^{nd} curve is presented in Figure B.7. This adaptabibility is particularly appreciable for the implementation into a

nite element code as the control points are fully defined by the origins and tangents derived from the physical mandatory parameters of the model, while the shape of the curve can be deformed using weights given as optional law parameters. Default unit values for the weights correspond to a (non-rational) 2^{nd} curve as defined previously. It produces a smooth natural-looking curve. By changing the weights the user can deform this curve for increased precision when fitting experimental data. Alternatively a degenerated first order curve (straight line can be easily obtained by nullifying the intermediate weight ($\omega_1 = 0$) without any other change.

$$B(t) = \frac{(1-t)^2.\omega_0 P_0 + 2t.(1-t).\omega_1.P_1 + t^2.\omega_2 P_2}{(1-t)^2.\omega_0 + 2t.(1-t).\omega_1 + t^2.\omega_2} \tag{B.7}$$

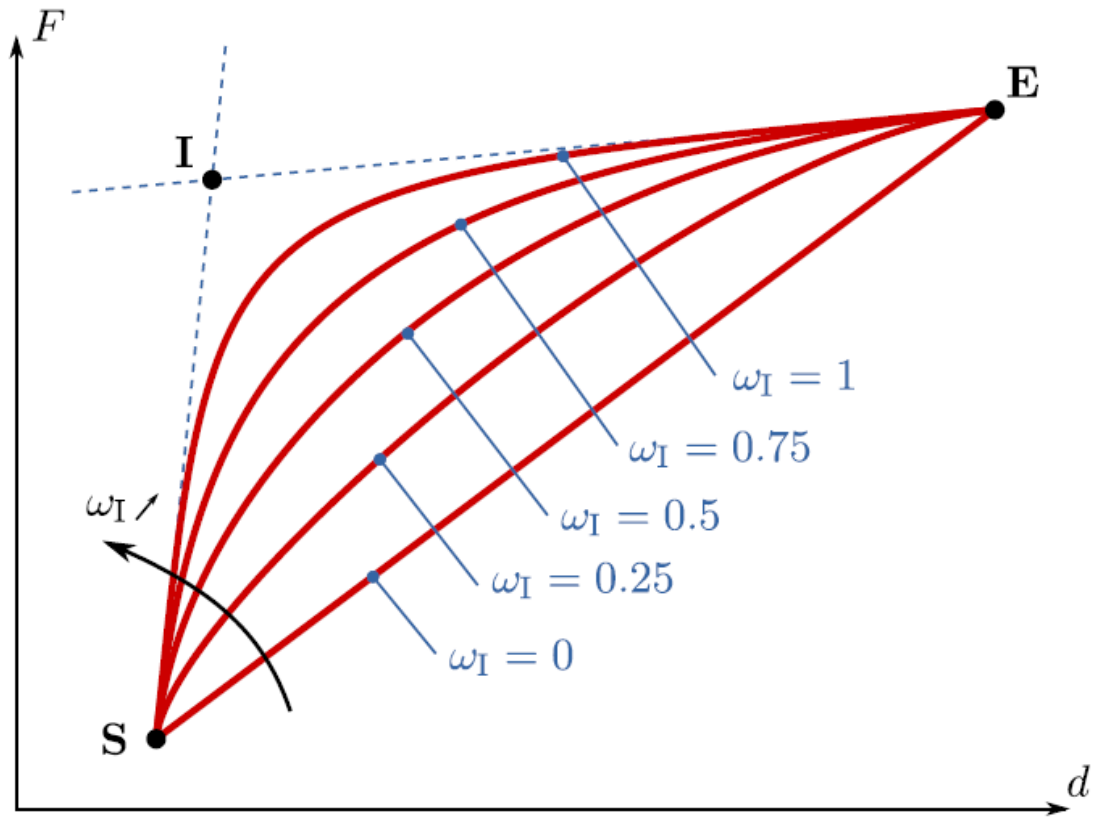

Fig. B.4: Effect of the weight ω_I of the intermediate control point I of a 2^{nd} degree of Bézier curve with unit endpoint weights $\omega_S = \omega_E = 1$.